Experimental Investigation of Bubble Behaviours in Domestic Heat Pump Water Heating System

A thesis submitted for the degree of

Doctor of Philosophy

By

Jianbo Qin, M.Sc.

Department of Mechanical, Aerospace and Civil Engineering

College of Engineering, Design and Physical Sciences

Brunel University

July 2018

Abstract

The growing awareness of global warming potential has internationally aroused interest and demand in reducing greenhouse gas emissions produced by human activity. Each year, the UK consumes a significant amount of energy for residential and industrial space heating and domestic hot water production. At present, gas boilers are mostly installed in the domestic water heating which contributes significantly to excessive CO_2 emissions and consumption of primary energy resources. However, air-source heat pump system has higher performance efficiency comparing to the traditional gas boiler, which can reduce the carbon dioxide emission and the usage of primary energy resources. The coefficient of efficiency of the heat pump can be range from 2 to 4.5 in various situations. The market shares of heat pump have been predicted to increase in the coming years to meet the requirement of the European Union Commission. There were about 22,000 heat pumps set up in the UK with 18 percent growth comparing to 2016 as reported by BSRIA. A range from 0.6 to 5.7 million heat pumps are estimated by the National Grid to be set up by 2030 to increase the energy efficiency of the UK. Although the energy efficiency of the heat pump is extremely high, there is still a space for improvement in air-source heat pump water heating system. The performance of the heat pump water heating system can be further enhanced if the dissolved gases in its hot water circuit can be efficiently discharged. The undissolved bubbles can stack in a specific position of the radiator, which would cause the cold spot. This could immensely reduce the efficiency of the heat pump water heating system. To avoid this happening, the bubble behaviors in the heat pump water heating system need to be extensively investigated. The better understanding of the bubble behaviors in an air-source heat pump water heating system can contribute to the design of an air evacuation valve and heat pump piping systems. In this thesis, the effects of various heat pump hot water side parameters on gas microbubble diameters and bubble productions were measured and analyzed by varying different experimental conditions. Correspondingly, a summarized conclusion has been presented to predict the gas microbubble's diameter distributions and volumetric void fraction distributions at different operating conditions. These parameters include various system pressures, water flow rates, and saturation ratios.

In this thesis, the main results showed that larger average bubble diameter is at the higher water flow rates at heat pump exit. At 2.2 bar condition, when system water flow rate increased from 800 l/h to 1150 l/h, the average bubble diameter increased from 0.086 mm to 0.108 mm. Moreover, the average bubble diameters increase along with the decrease in system pressures. At 1000 l/h condition, when system pressure increased from 2.2 bar to 2.7 bar, the average bubble diameter decreased from 0.100 mm to 0.087 mm. At 850 l/h condition, when system pressure increased from 1.7 bar to 2.5 bar, the average bubble diameter decreased from 0.101 mm to 0.081 mm. In addition, the average bubble diameters slightly increase along with the increase in saturation ratio. Besides, a prediction equation for the bubble diameter distribution in the water pipe was proposed. At SR 1.15 and 2.5 bar condition, when water flow rate increased from 900 l/h to 1100 l/h, volumetric void fraction decreased from 2.25 E-05 to 4.83 E-06. However, at 1000 l/h and SR 1.15 condition, when system pressure increased from 2.2 bar to 2.7 bar, volumetric void fraction decreased from 2.16 E-05 to 3.78 E-06. It is found that the highest city main saturation ratio was achieved at 1.07 at the specific environmental condition.

Author's Declaration

This research project has been accomplished according to the guidance of Prof. Yunting Ge and Prof. Savvas Tassou. The content presented in this thesis is own work of the author except where references are given.

I have not submitted this thesis for another degree or award to any other institution.

Jianbo Qin

Date: 23th July 2018

Acknowledgements

Initially, I would like to express my appreciation to my supervisor, Prof.Yunting Ge and Prof. Savvas Tassou for the invaluable assistance they provided to me throughout this project and for giving me the opportunity of taking part in such an exciting subject. This effort would not have been completed without their unfailing guidance and their substantial support.

I would also like to express my gratitude to Ing. A.G. Lamers from the Spirotech b.v. for his invaluable guidance and patience throughout this project.

Additionally, I would like to thank Dr. Ali Shefik from Cyprus International University for his valuable assistance during the execution of the experiments. I would also like to express my gratitude to Costas Xanthos for his help in patience. Besides, I would like to thank the Brunel University London and Spirotech b.v., the Netherlands for supporting this research work.

I wish to express my gratitude to my family, who even though I am far away from home, they support me.

Finally, I would like to express my gratefulness to my friend, Fanchao Meng for his remarkable patience and support during this project.

Table of Contents

Table of Figures

List of Tables

Nomenclature

C_{gas}	Actual dissolved gas mole fraction present in the bulk fluid	(-)
C_{sat}	Maximum gas mole fraction at system condition	(-)
d_b	Diameter of the gas bubble	(mm)
D_p	Length of each pixel	(mm)
D_{ball}	Dimensions of the ball	(mm)
D_{image}	Dimensions of the picture	(mm)
D_{focal}	Distance between the camera lens and the focal plane	(mm)
H	Henry's law proportionality constant	(atm)
P_v	Vapour pressure	(bar)
P	System pressure	(bar)
P_g	Partial gas pressure	(bar)
P_{ball}	Pixels of picture	(-)
P_{image}	Pixels of the image	(-)
Q	System heating load	(kW)
Re	Reynolds number	(-)
Sr	Saturation ratio = Ca/Cm	(-)
T_1	Condenser inlet temperature	(°C)
T_2	Supply water temperature	(°C)
T_s	Supply water temperature	(°C)
T_w	Desired supply water temperature	(°C)
T_3	Outdoor air temperature	(°C)
T_4	Evaporator temperature	(°C)
T_5	Return water temperature	(°C)
T_6	Condenser outlet temperature	(°C)
V_b	Volume of bubble	(mm^3)
T_{tgm}	Total gas measurement temperature	(°C)
$V_{gas\ bubble}$	Total volume of all the gas bubbles in the sample investigated	(mm^3)
V_{water}	Volume of the water in the sample investigated	(mm^3)

V_w	Volumetric flow rate	(Litre / Hour)
W	Weber number	(-)

Greek Symbols

α	Shape parameter (-)
β	Scale parameter (-)
μ	Location parameter (-)
ν	Kinematic viscosity, (m^2/s)
ρ	Density of liquid (kg / m^3)
ε_{sample}	Volumetric void fraction of the sample investigated (-)

Abbreviations

BV	Ball Valve	
AAV	Automatic Air Vent	
HX	Heat Exchanger	
SV	Solenoid Valve	
EFM	Electromagnetic Flow Meter	
WMS	Water Main Supply	
EV	Expansion Vessel	
OH	Outlet of Heat Pump	
IH	Inlet of Heat Pump	
SG	Sight-glass	
EPSRC	Engineering and physical sciences research council	
Fps	Frame per second	
TGM	Total gas measurement	
CAD	Computer aided design	
SR	Saturation ratio	
HP	Heat Pump	
PHE	Plate heat exchanger	
TGM	Total gas measurement	
DOF	Depth of focal plane	mm
FR	Water Flow Rate	
LS	Lowest Saturation	
EP	Effect of Pressure	
EF	Effect of Flow Rate	
ES	Effect of Saturation Ratio	
CM	City Main Water	
RT	Return Side Test	
VF	Bubble Void Fraction	

List of Appendices

List of Formulas and Equations

Chapter 1 Introduction

"There is no energy crisis, only a crisis of ignorance."

(R.Buckminster Fuller, 1968)

1.1 Context of the project

Each country has a responsibility to put forth the effort to solve the real existence of the global warming crisis, which is damaging the global environment. Despite the reserve of conventional fossil fuels such as oil and coal continue to decrease the demand for energy experiences sharp growth. As the greenhouse gas emission generated from the conventional fossil fuels is one of the main contributors to the climate changing and global warming, the need for energy-saving technologies is more urgent than ever. European Union countries have adopted European Union Energy Efficiency Directive, which requires all Member States to introduce a programme of regular energy audits for large enterprises, in order to perform the obligations of the Kyoto Protocol and reduce their emission of ozone-depleting substances in 2002 (EU, 2002). Besides, based on the article 8 of the EU Energy Efficiency Directive, the 'Energy Savings Opportunity Scheme' (ESOS) is an approach proposed by the UK Government to identify energy saving recommendations in July 2013 (DECC, 2013). Furthermore, the European commission has decided to achieve 20 percent energy efficiency of Europe by 2020 and 30 percent energy efficiency of Europe by 2030 as introduced in its Energy Efficiency Directive. (The European Commission, 2016) The growing awareness of global warming potential has internationally aroused interest and demand in reducing greenhouse gas emissions produced by human activity. Almost 50 percent energy of the European Union was used for heating and cooling the residential and industrial building as introduced by the European Commission (The European Commission, 2018). In the European residential field, 79 percent of energy is consumed by heating space and residential hot water (The European Commission, 2018).

Under such a background as described in the preceding paragraph, improving the building heating efficiency is an essential approach to improve the energy efficiency of the European Union. Besides, a good understanding of bubble behaviours in the heat pump water heating system can contribute to improving the efficiency of deaeration

equipment. Therefore, the reason of this research is to investigate bubble behaviours to optimise domestic heat pump water heating system.

1.2 Aims and objectives

The principal aim of this project is to experimentally investigate the bubble behaviours in the domestic air-source heat pump water heating system.

The broad objectives of the project include:

- To study and improve existing experimental methods of investigating bubble behaviours from previous PhD projects.
- To investigate the lowest saturation ratio that can be achieved by keeping the system run.
- To investigate the bubble size distribution in horizontal pipe at the exit of an air-source heat pump water heating system.
- To investigate the bubble volumetric void fraction distribution in horizontal pipe at the exit of an air-source heat pump water heating system.
- To determine the relationship between bubble average diameter and the system pressure.
- To determine the relationship between bubble average diameter and the fluid flow rate.
- To determine the relationship between bubble average diameter and the saturation ratio.
- To determine the relationship between bubble volumetric void fraction and the system pressure.
- To determine the relationship between bubble volumetric void fraction and the fluid flow rate.
- To determine the relationship between bubble volumetric void fraction and the saturation ratio.
- To investigate the bubble behaviours in horizontal pipe at the inlet of an air-source heat pump water heating system.

1.3 Structure of the thesis

This thesis mainly consists of six chapters which follows sequence of the adopted methodology. The introduction of each chapter is briefly presented below:

Chapter 1: This chapter introduces the context, aims & objectives and the structure of the project.

Chapter 2: In this chapter, a literature review is presented, which includes brief working principle of the heat pump system. Furthermore, the gas bubble behaviours reviewed. Finally, the solubility of gases in the water is explained.

Chapter 3: The methodology and design of the test facility are described in this chapter. The air-source heat pump, the camera system, test rigs and instruments are illustrated. Moreover, the methodology of experiment is also explained.

Chapter 4: The experimental procedure based on the order is described. The results of the experiment are illustrated and discussed.

Chapter 5: The bubble production in the return pipe to heat pump has been introduced, and the relationship between bubble production and system pressure drop is explained.

Chapter 6: The conclusion of the analysis is presented, and some recommendations are proposed for further development.

1.4 Achievements

The main achievements of this research project are the research reports for the Spirotech Limited to improve the air-vent products in the heat pump water heating system. Besides, some research results were published in open literature. A new journal paper is prepared to submit for summarising the findings in this research project.

1.4.1 Journal paper

Qin, J., Jiang, X. and Ge, Y. (2017) 'Experimental investigation of gas bubble diameter distribution in a domestic heat pump water heating system', Energy Procedia. Elsevier, 123, pp. 361–368. doi: 10.1016/J.EGYPRO.2017.07.270.

1.4.2 Conference paper

Qin, J., Ge, Y. (2015) 'Experimental Investigation of Bubble Behaviours in a Heat Pump Water Heating System', 14th UK Heat Transfer Conference 2015, Edinburgh (Sept 7 – Sept 8, 2015)

Qin, J., Jiang, X. and Ge, Y. (2017) 'Experimental Investigation of Gas Bubble Behaviours in a Domestic Heat Pump Water Heating System', ICEFM 2017: 19th International Conference on Experimental Fluid Mechanics Zurich, Switzerland.

Chapter 2 Literature Review

2.1 Introduction

Now, more gas boilers are installed than heat pumps by residents in the UK, which contributes to excessive carbon dioxide emissions and consumption of the conventional fossil fuels (Vorushylo *et al.*, 2018). However, if these gas boilers could be replaced by heat pumps, which have higher performance efficiency, a significant saving of carbon dioxide emissions could be achieved (Shuxue *et al.*, 2018). A department of the UK government, called Renewable Heat Incentive, supports the promotion of heat pumps in the UK, which guaranteed 19p per kWh to domestic buildings for 7 years and 9p per kWh to the commercial buildings for 20 years with using heat pumps. (The Renewables First, 2018). Nevertheless, the progress is still slow to meet the target of the ten percent of the heating energy delivered by renewable sources by 2020 (Vorushylo *et al.*, 2018). The cost performance of heat pumps has potential to be further improved to meet the consumers' expectations. The consumers can break even with at least the Coefficient of Performance of heat pumps reached three comparing to gas boilers by considering the price difference between electricity and gas (The Renewables First, 2018). This demand causes many further researches of the heat pump in various aspects. The studies of heat pumps have obtained many achievements and heat pumps continue to be improved such as the commercial carbon dioxide heat pump applications (Nawaz *et al.*, 2017). The improvement of refrigerants of heat pumps is an effective way to increase the performance of heat pumps. And the heat pump combined with the clean energy generator is a solution as well (Wu *et al.*, 2018). Furthermore, the cost performance of the consumers could be improved by avoiding the cold spots in the heat pump water heating system. The cold spots in the water heating system are caused by the trapped gas bubbles in some positions of the pipe lines. These gas bubbles dissolve in the water at the condition of low water temperature. And gas bubbles separate out from water in the circumstances of the high-temperature on the condenser wall of heat pumps. In addition, gas bubbles can also separate from water at the position of low pressures of the system.

Two-phase bubbly flow behaviours in the heat pump domestic water heating system had not been investigated thoroughly, which affects the energy efficiency of the heat

pump system. At present, most published literature focus on the fundamental bubble generation on the flat heat transfer wall and the flow regime of the bubbly flow with injected bubbles. There are few literatures studying bubbly two-phase flow in heat pump water heating system.

A numerical study of the bubble collision and coalescence in the micro-channel has been conducted by (Liu, Wang and Palm, 2017) as shown in Figure 2.1. They reported there are three stages of bubbles in micro-channel, which are the sliding stage, merger stage and post-merger stage. The bubbles keep growing in micro-channel until they are big enough to reach the bubbles on the opposite wall. They also conclude detachment diameters of the bubbles are affected by the mass flux and the heat flux. A larger bubble detachment diameter can be found at a lower mass flux or a higher wall heat flux condition. Liu found that the bubbles merge earlier at low Reynolds numbers. This phenomenon could significantly affect the bubbly two-phase flow at the heat pump exit. (Liu, Wang and Palm, 2017)

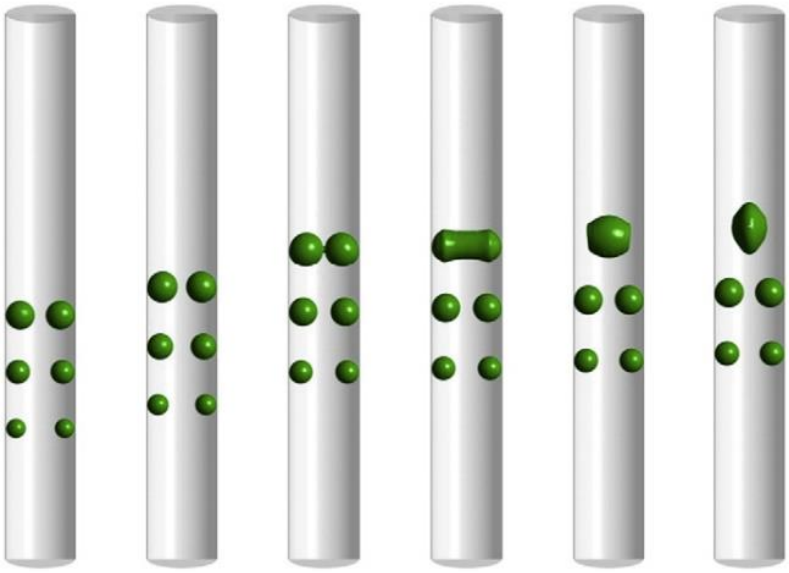

Figure 2. 1 Bubbles collision and coalescence in micro-channel (Liu, Wang and Palm, 2017)

(Kong *et al.*, 2018) studied the flow regimes of the horizontal two-phase flow. There are mainly three flow regimes, Bubbly Flow, Plug Flow and Slug Flow, involved in water heating system, in which the water is the dominant phase. Figure 2.2 illustrates the flow regimes with various superficial velocities of the water and the gas. Kong

reported the effect of the pipe diameter on the flow regime (Kong et al., 2018). The flow regime transitions are the essential research in the two-phase flow. In Figure 2.2, j_f represents superficial fluid velocity and j_g represents superficial gas velocity.

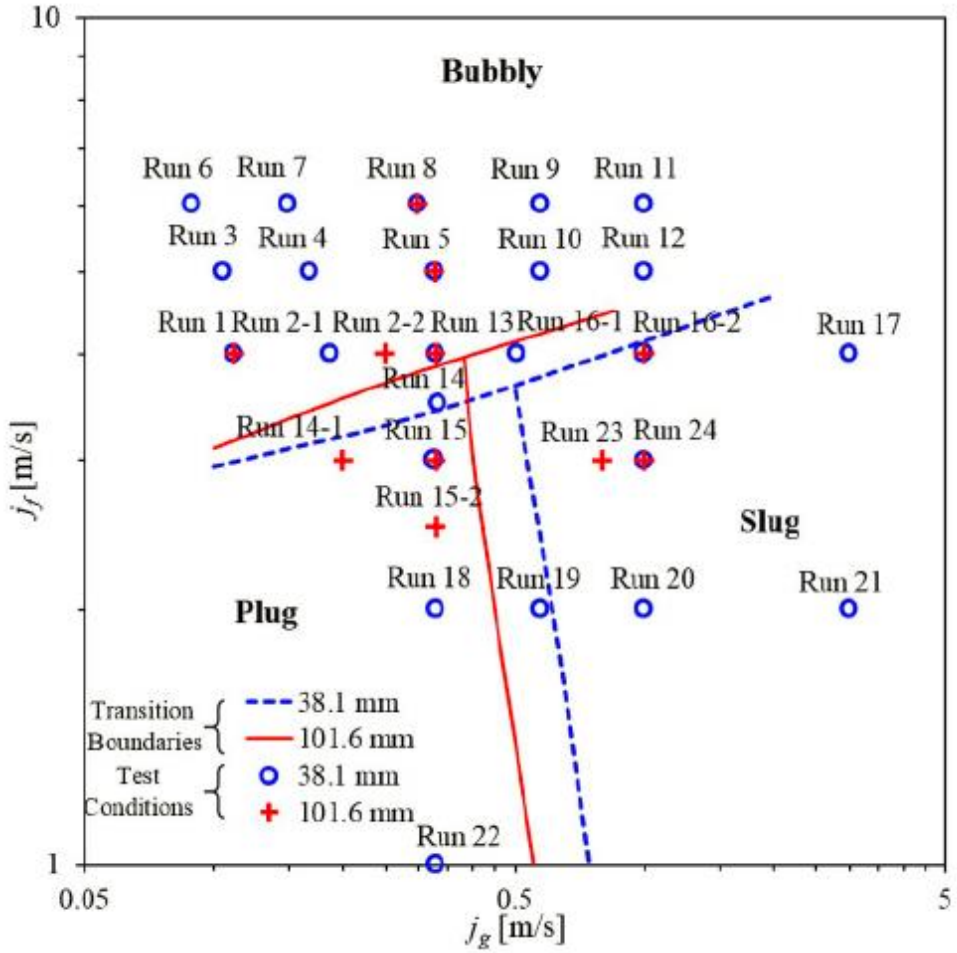

Figure 2. 2 Flow regimes of the horizontal two-phase flow in 38.1 mm and 101.6 mm pipes (Kong *et al.*, 2018)

Therefore, a literature review has been presented in this thesis to understand the significance of studying bubble behaviours in the heat pump water heating system, the solubility of nitrogen in the water, the bubble formation and the flow regime of the two-phase horizontal flow.

2.2 Heat pump system

2.2.1 Introduction

Studying the bubble behaviours in a heat pump system contributes to improving the energy efficiency of heat pump system, which helps popularizing heat pump systems. The importance of the heat pump systems is introduced by (Chua, Chou and Yang, 2010), who reviewed heat pump systems and stated the enormous potential to boost the energy efficiency by extracting energy from other sources in many fields such as industry, residence and commerce. Hence, the understanding of the applications and researches of the heat pump system is essential for this thesis. This section is going to introduce the fundamental of the heat pump and the prospection and researches of the heat pump system.

2.2.2 The fundamental of heat pump system

Along with the support of the European government and the increase of the energy efficiency, the instalments of all kinds of heat pump systems have been increasing during recent years (Desideri, Proietti and Sdringola, 2009). Heat pump system consists of evaporator, condenser, expansion valve and compressor, which are main four core components in common heat pump systems as shown in Figure 2.3 (The Renewables First, 2018). The working principle of the heat pump system is transferring heat from the low-grade energy to higher-grade energy in the opposite direction compared to the spontaneous heat flow by using a few electricity with high energy efficiency (Wallerand *et al.*, 2018). The conventional categories of heat pump system for space heating are air-source heat pump system, ground-source heat pump system, water-source heat pump system. Nowadays, some other heat sources of heat pump system have gained increasing attention such as waste heat (low-grade energy) and solar energy as reported by (Miglani, Orehounig and Carmeliet, 2018), (Mohanraj *et al.*, 2018) and (Wallerand *et al.*, 2018). However, as the best equipment to increase the energy efficiency in residential and industrial fields and save the carbon dioxide emissions, there are still some areas of the heat pump system that need to be improved such as the refrigerant aspect and the waste heat recovery aspect (Liu *et al.*, 2018; Wang *et al.*, 2018).

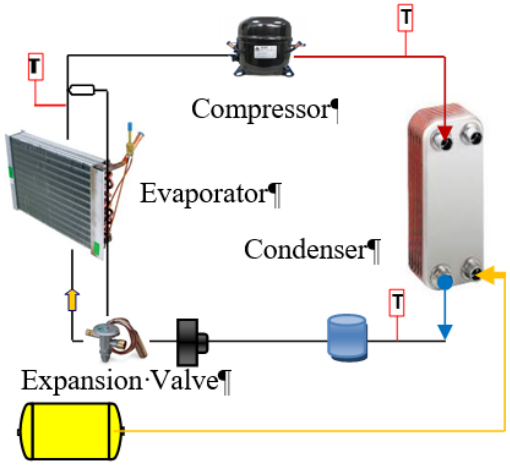

Figure 2. 3 The working principle of heat pump unit

2.2.3 Gas bubbles in heat pump systems

In the residential and industrial fields, gas bubbles always generate in the water loop of closed heat pump water heating system causing the rapidly reduction of the heating efficiency. The water loop of heat pump system is introduced in the methodology. In the water loop, some gas bubbles dissolve into the water in returning piping again. And the low-temperature water has the ability to absorb more quantity of gas than the high-temperature water (Hefter and Tomkins, 2003a).

To discharge bubble production in hot water circuit of heat pump system, passive deaerators are widely installed in the heat pump water heating systems(Hefter and Tomkins, 2003a). There are many journal papers about subcooled boiling and two-phase bubbly flow through microchannel but the data and theoretical scientific models to predict two-phase flow characteristics in heat pump water heating system in open literature are limited at present. At present, the performance of the deaerators installed into heat pump water heating systems is still lower than expected. Besides, the guidance of the design of passive deaerators in domestic heat pump system are limited by the gap of the study in this field.

Bubble diameters detached from the surface of a heat exchanger has been studied and discussed by many researchers (Dean, 1944; Winterton, 1972; Blander and Katz, 1975;

Jones, 1999; A.M. Fsadni, Ge and Lamers, 2011; Yin, Jia and Xu, 2015; Hoang *et al.*, 2016). Dean (Dean, 1944) reported the study of the formation of bubbles in a supersaturated liquid. Winterton (Winterton, 1972) proposed the bubble detachment model in the aspect of mechanical analysis. As reported by(Jones, 1999), he found the insufficient of the classical nucleation models developed by (Blander and Katz, 1975) and discussed bubble generation in low supersaturated liquid. (Fsadni, Ge and Lamers, 2012) extends Winterton's theoretical model to other shapes of ducts and reported the bubble detachment diameters in a domestic gas boiler central heating system. Their work contributes to the design of gas deaerators in a gas boiler water heating system. (Yin, Jia and Xu, 2015) achieved experimental investigation on sub-cooled boiling flow on a flat wall of a microchannel. They reported the bubble slides on the horizontal heat transfer wall until it slid to the end of channel. There are two sliding stages of a bubble on a horizontal flat wall, one is the slow sliding stage and the other is the accelerated sliding stage. They also reported the characteristics of the bubble in two stages are significantly different. The diameter of the bubble in slow sliding stage was constant while it in accelerated stage decreased along with the increase of the velocity. (Hoang *et al.*, 2016) obtained a mechanistical model for predicting the maximum diameter of attached bubble nucleating in a sub-cooled flow boiling.

There are many other researchers have studied bubble diameters detached from the heat transfer wall. This knowledge can be used in most industry area such as designing a heat exchanger. But there is still a gap in knowledge in the bubble production at heat exchanger exit of heat pump system for discharging gas bubbles. This is because of the involving of turbulent flow in a plate heat exchanger. Experimental investigations of gas-liquid turbulent flow characteristics inside a plate heat exchanger have been conducted by some researchers such as (Vlasogiannis *et al.*, 2002; Tsai, Liu and Shen, 2009; Nilpueng and Wongwises, 2010). Strong turbulent flow affects bubble diameter detached off the plate heat exchanger. (Abdelmessih, Hooper and Nangia, 1972) considered the bubble collapse and the effect of fluid velocity but the heat exchange wall is still smooth which is different from the plate heat exchanger which is investigated in the air-source heat pump system.

(Abdelmessih, Hooper and Nangia, 1972) experimentally investigated two-phase flow in the corrugated gap created by two adjacent plates of a PHE. Polyurethane was used

to caste the plates instead of standard stainless-steel, which is normally used for the majority of heat exchanger plates, to achieve the visualized two-phase flows. They observed three different flow regimes which are bubbly flow, film flow and slug flow respectively. They also studied the pressure drop in a PHE and had a comparison between the predicted pressure drop and the experimental data. As reported by (Bonjour, Clausse and Lallemand, 2000), the coalescence phenomenon during boiling on a vertical heated wall is presented. The heat fluxes were varied, and the wall was superheated at various temperatures. Besides, they reported the coalescence phenomenon caused a decrease in the bubble frequency. (Bonjour, Clausse and Lallemand, 2000) experimentally investigated the sub-cooled flow boiling of the refrigerant in a vertical PHE with a chevron angle of 60 degree. They report that, particularly at low mass flux and high saturation temperature, boiling curves change significantly during onset of nucleate boiling. Furthermore, the boiling hysteresis phenomenon is significant when the refrigerant mass flux is low and sub-cooled boiling is affected significantly by the mass flux of the refrigerant. Boiling hysteresis is an adverse phenomenon, preventing high heat flu system from thermal stabilization, characterized by a boiling curve variation at an increase and decrease of heat flux density. However, this hysteresis phenomenon does not exist on water-side of plate heat exchanger in heat pump water heating system, as the maximum temperature of heat transfer wall is lower than 100 degrees Celsius. In addition, the heat transfer coefficient had been improved slightly by increasing the inlet sub-cooling and saturation temperature. There is a gap of knowledge over the experimentally studying the effect of bubble coalescence phenomenon at water-side heat exchanger. The research of Bonjour etc. at refrigerant side provide a guess that bubble coalescence phenomenon causes a decrease in bubble frequencies.

The effect of buoyancy on bubble nucleation and flow, which is at water loop, is concerned with bubble behaviours in sub-cooled flow boiling in a domestic water heating system and it has been investigated by many researchers such as (Pamperin and Rath, 1995; Zhang *et al.*, 2015). (Zhang *et al.*, 2015) extensively studied the effect of buoyancy in dynamics. They claim the effects of buoyancy are not particular concerned with microscopic cavitation bubbles, while the effects of the buoyancy on the large bubbles are essential, but the effects are still important to understand the bubble flow distribution in the pipe. (Pamperin and Rath, 1995) studied the effect of buoyancy on

bubble nucleation and reported the effect of buoyancy on the size of nucleated bubbles weakens with the increase of Weber number (*W)*.

The bubbles easily stack at some positions of pipes to cause cold spots of radiators. This phenomenon causes poor water circulation which leads to parts of the heating area do not achieve heating requirements (Lu, Fernández and Tryggvason, 2005). The gas bubbles seriously affect the practical heating effect of the heat pump system. Those gas bubbles flow through pipe works of heat pump system causing noise (RENSEN, LUTHER and LOHSE, 2005). The noise is extreme loud while the bubbles flowing through uncovering fin system. As a result of this phenomenon, the sleep quality of the home users is affected seriously by the noise of the heat pump system. The bubbles mainly contains nitrogen, but still have some oxygen and other corrosive gases (Leith and Thompson, 1960). These corrosive gases in the piping of the heat pump system can lead to the equipment of the system to corrode including the terminal heat sink and the heat equipment. This problem causes substantial economic losses in lack of protective methods. A good understanding of bubble behaviours in heat pump heating system could optimise heat pump system. And consequently, as an environment-friendly equipment, an optimised heat pump water heating system would have significant environmental benefits.

2.2.4 Summary

This section provides some up-to-date insights of the heat pump system developments. Gas bubbles reduce the heating efficiency of heat pump heating system by forming cold spots in radiators. The broad prospect of the heat pump water heating system proves the significance of studying the bubble behaviours in heat pump water heating system. A further development of the heat pump technologies is the vital approach to meet the energy efficiency required by the European policies. Optimised heat pump system has the enormous potential to reduce the carbon dioxide emissions in most application environments.

2.3 The solubility of gases in the water

2.3.1 Introduction

The study of the solubility of gases is a vital fundamental subject, which is used in many disciplines widely. The present project uses the knowledge of the solubility of gases in the water. The solubility of gases in water has been studied experimentally since the 19th century, which describes the ability of the gas, as a solute, dissolving in water under specific temperature and pressure (Battino and Clever, 1966). (Fogg, 2003) introduced the solubility of gases, as the solute, rest with many aspects such as the nature of the gases, chemical and physical of the solvent, partial pressure of the gases, the temperature and the involvement of substances. In another way, (Wilhelm, Battino and Wilcock, 1977) reported the solubility of the gas represents the saturated status, in which the concentration of the gas is steady at specific conditions. A good understanding of the solubility of gases in water is important for controlling experimental conditions and analysing the experimental results.

2.3.2 Henry's law

There are two methods to express the solubility of gases. One method is representing the solubility by using the volume of gases dissolved in the solvent at specific conditions, and the other one is representing the solubility by using the mole fraction to the solvent (Hefter and Tomkins, 2003b). The mole fraction method has been very common, which is calculated by using the moles of solute over the moles of the solvent at specific conditions. In present project, the solute is mainly the nitrogen, and the solvent is the water.

Henry's Las is proposed by the English chemist, William Henry, to describe the solubility of gases, based on the comprehensive experimental investigations in the 19th century. (Henry, 1803) reported there is a relationship between the solubility of the gases in the solvent and the partial pressures of them at the area which is contacting the solvent. However, Henry did not describe the relationship between the solubility of gases and the pressure in the mathematical language. There are some restrictions of Henry's law, which limit the working condition of it. Henry's law only can work, when the system pressure is low and there is no chemical reaction between the solute and the

solvent (Staudinger and Roberts, 1996). Moreover, the highest system pressure is 2.7 absolute bars and the there is no chemical reaction between the nitrogen and the water, in the present project. Hence, the henry's law can be used in the present study.

(Perry, Green and Maloney, 1997) introduced Henry's law in the mole fraction method as shown in Equation 2.1.

$$C_{gas} = \frac{P_g}{H} \tag{2. 1}$$

In Equation 2.1, C_{gas} represents the mole fraction of the actual dissolved gas in the liquid (-), P_g represents the partial pressure of the gas (atm) and H represents the Henry's proportionality constant (bar).

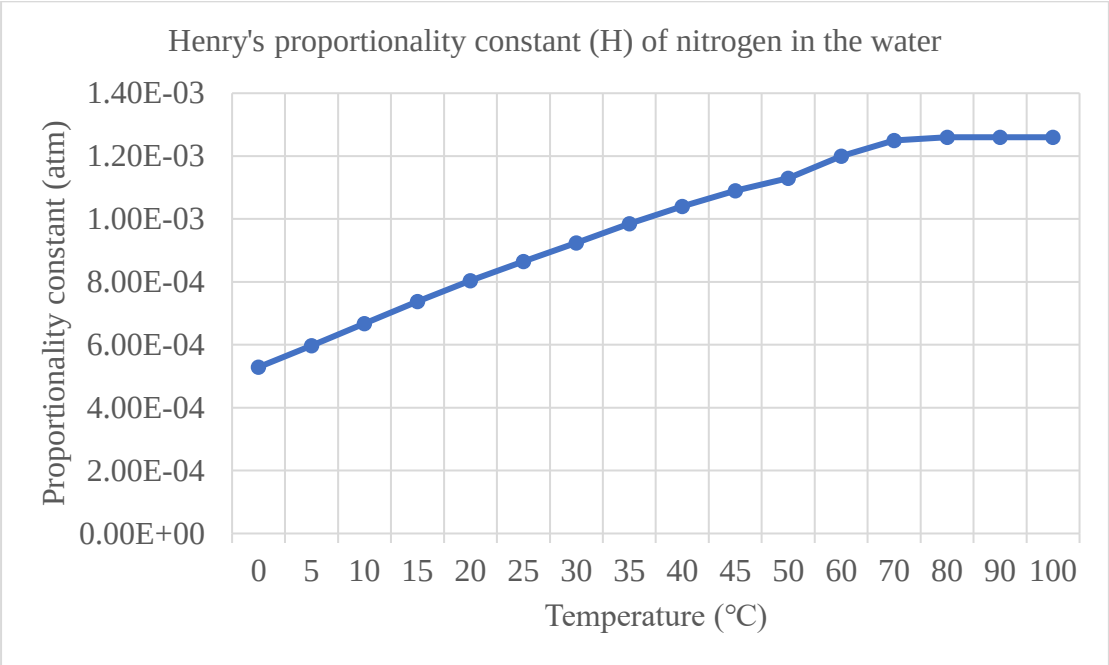

Figure 2. 4 Henry's proportionality constant (H) of nitrogen in the water

Figure 2.4 illustrates the relationship between Henry's proportionality constant of the nitrogen and the temperature, which is reported by (Perry, Green and Maloney, 1997). This figure can be used to calculate the mole fraction of dissolved gas in the water in the present project. In equation 2.1, Henry's proportionality constants (H) can be found in Figure 2.4 at different temperatures.

2.4 Bubble behaviours in gas boiler water heating system

There is a gap in knowledge of bubble behaviours in domestic heat pump water heating system. However, Dr. Fsadni and Dr. Shefik did researches of bubble behaviours in domestic gas boiler water heating system (Fsadni, 2012; Shefik, 2015). The knowledge of their research can be used to compare to the study of heat pump system.

Dr. Fsadni reported water flow rates has the largest effect on detachment average bubble diameter from the primary heat exchanger wall. Average bubble diameters decrease along with increases in water flow rates. It is also stated that heat flux and pressure have shown marginal effects on bubble sizes. In his experiment, saturation ratios did not result in any effect on bubble sizes. Furthermore, Dr. Fsadni reported bubble production rates to increase along with increases in heat flux, saturation ratios, and water flow rates. On the contrary, bubble production rates decrease along with increases of system pressures. (Fsadni, 2012)

Dr. Shefik reported bubble production and void fractions increase along with the temperature, boiler heating load, and saturation ratio escalate. On the contrary, bubble production and void fractions reduce along with increases in system pressure and water flow rate. Furthermore, he stated there was not a clear relationship between average bubble diameters and system parameters, except for the water flow rate. It is reported that bubble sizes at boiler exit decreases along with water flow rates increase. (Shefik, 2015)

2.5 Summary

This chapter introduced the fundamental of the heat pump system. Several key findings, which is related to current study, of journal papers in open literature are introduced. The solubility of gases in the water is reviewed, which is used for calculation in current study. The bubble behaviours in gas boiler heating system are introduced.

The thorough understanding of bubble behaviours in heat pump water heating system contributes to filling the gap of knowledge in open literature. The knowledge could

improve predicting the bubble behaviours in pipelines, guidance to heat pump system operation conditions, and designing air-vents with higher efficiency.

Chapter 3 Methodology and Design of the Test Facility

3.1 Introduction

The gas-water two phase flow characteristics in a domestic air-source heat pump central heating system has not been well investigated as described in the preceding sections. Effects of system pressures, water flow rates and saturation ratios on gas-water two phase flow, need to be investigated thoroughly.

A small size simulative air-source heat pump central heating system was designed and constructed to achieve the requirements and objectives set by Spirotech b.v., the Netherlands and Brunel University London. The data acquisition equipment was installed to monitor the conditions of the system for control and evaluation purposes.

This chapter consists of seven sections that detail the test facility and the methodology was used in this project. First section provides a brief introduction of this chapter. Second section details the construction of the test facility which includes mechanical, image acquisition, control and monitoring systems. Third section describes the image analysis techniques. Fourth section introduces the experimental run conducted to achieve the objectives. Fifth section explains the equations used for calculation in the project. In addition, the sixth section introduces the experimental uncertainty. Finally, the seventh section sums up this chapter.

3.2 Test facility

The test facility has been designed to investigate gas bubble behaviours in a domestic central heating system powered by air-source heat pump. The test facility includes mechanical setup, image acquisition system, control system and monitoring system. This section describes these systems in detail.

3.2.1 Mechanical setup

The mechanical part, experimental setup, consists of four main modules; Air-source heat pump module, sight-glass module, cooling system module and buffer vessel

module. The schematic diagram of the experimental setup is shown in Figure 3. 1. In Figure 3. 10, the city main water injection valve is shown, which is used to inject the working water to the heating system, control the system working pressure and offset the system water losses.

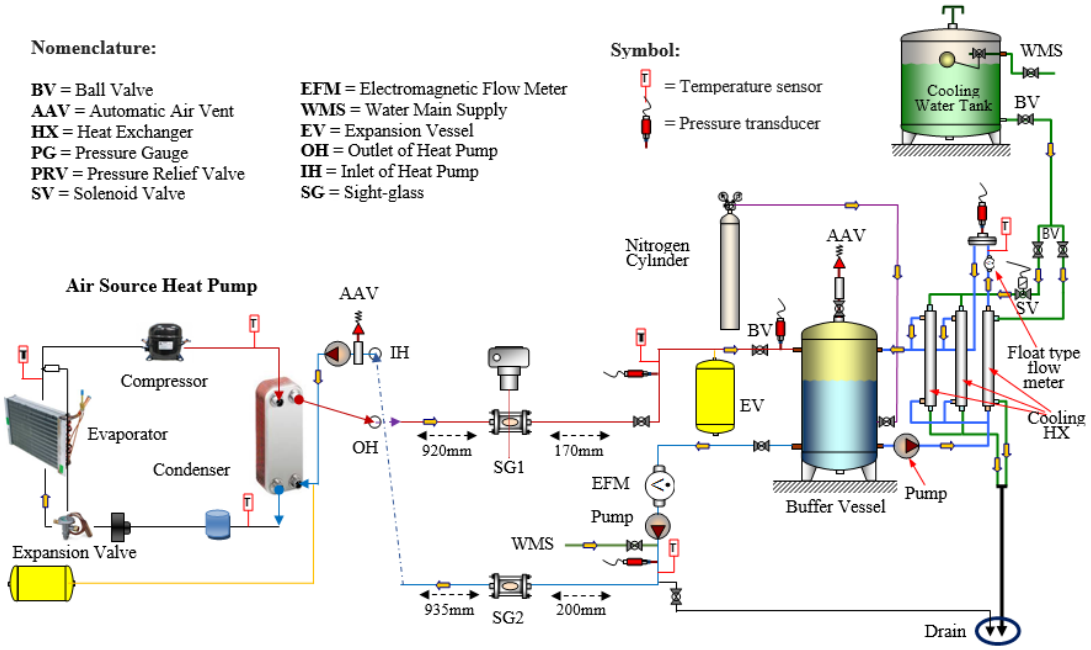

Figure 3. 1 Schematic diagram of experimental setup

3.2.1.1 Air-source heat pump

The air-source heat pump water heating unit is provided by Kingspan Limited and it is connected to 22 mm BSP copper tubing which supplies the buffer vessel.

Figure 3. 2 Air-source heat pump

Figure 3.2 shows the image of air-source heat pump provided by Kingspan. The detail of the heat pump is shown in the Table 3.1.

Table 3. 1 Kingspan air-source heat pump specification

Brand	Kingspan
Model	KHP0004
Serial	07AVI08451
Maximum supply water temperature	60℃
Maximum water pressure	300 kPa
Capacity	5.8 kW
Refrigerant	R410A (1350g)
COP	3.0

The heat pump was selected to study the potential gas bubble behaviours in a domestic water heating system due to its popularity worldwide and the space of the system energy efficiency to improve. (Song *et al.*, 2018) The manufacturer's maximum flow temperature is set at 60℃. However, the compressor cannot keep work on its highest

frequency, and it will shut down after working on the target of 60 ℃ supplying water for a period. In the test run, 55℃ was chosen as the supply water temperature. 55 ℃ is the highest temperature that the heat pump system can maintain with no compressor shut down. As shown in the Figure 3.1, the air-source heat pump is mainly consisted of compressor, plate heat exchange (condenser), evaporator and expansion valve.

The heat pump system is installed outside and connected to piping system through the drilled hole across the wall. The drilled hole across the wall is horizontal and makes sure the pipe can directly connect to the plate heat exchanger outlet.

3.2.1.2 Sight-glass

There are two sight-glasses horizontally installed on the supply and return position respectively as shown in Figure 3.1 and 3.3. As that has been showed in the Schematic Diagram of Heat Pump System, the SG1 is positioned 920 mm from Outlet of Heat Pump and 170 mm from the pipe bend, and SG2 is positioned 935 mm from Inlet of Heat Pump and 200 mm from the pipe bend. They were designed by Fsadni (Ge, Fsadni and Wang, 2013) and developed by Shefik (Shefik, 2015). Sight-glasses are the key component of the test setup providing the possibility to investigate the bubble diameter. Figure 3.4 illustrates the top view of the sight-glass case which is mounted on the flange. There is another hole on the bottom of the sight-glass allowing the light provided by the light-source to reach the high-speed camera. Inside the aluminium case, two 3 mm glass was glued on the case at the top and bottom side. Silicone was injected into the gap between the flange and the aluminium case to prevent the water leaking.

Figure 3. 3 Sight-glasses

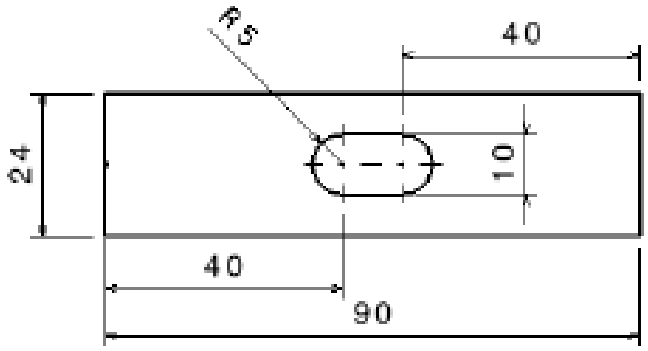

Figure 3. 4 Sight-glass aluminium case (Shefik, 2015)

Figure 3.5 illustrates the CAD model of the sight-glass details the design in different views. Two pieces of copper pipe were mounted on the outer side of the flange. During the test, light-source was fixed underneath the central of the sight-glass and the high-speed camera was installed above the central of the sight-glass. Sight-glass was cleaned every three months to make sure there is no incrustation on the inner surface of the glasses. Bubble filming and data acquisition are introduced in the section 3.2.2 Image acquisition.

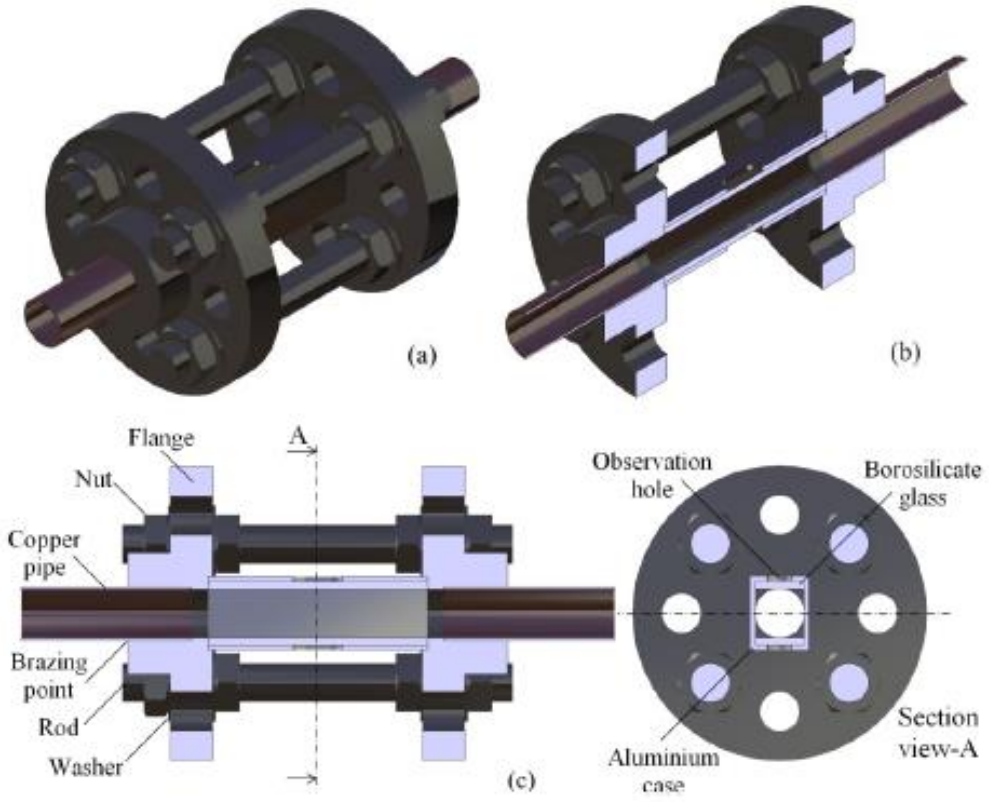

Figure 3. 5 CAD model of the Sight-glass (Shefik, 2015)

3.2.1.3 Buffer vessel

Figure 3.6 shows the yellow water tank which is used as buffer vessel in the simulative domestic water heating system. The system water is heated and stored in the vessel. The capacity of the buffer vessel is about 40 Litres. It is connected to the total gas measurement equipment and three heat exchangers which is used as a simulative heating load. The total gas measurement equipment is introduced in the 3.2.4 data logging system. Three heat exchangers have been installed as a cooling system to make the heat pump working continuedly which is introduced in the next section. There is an automatic air vent installed on the buffer vessel which exhausts majority gas precipitated from water. The circulation pump lets the water run through the heat exchangers and the total gas measurement equipment from the buffer vessel.

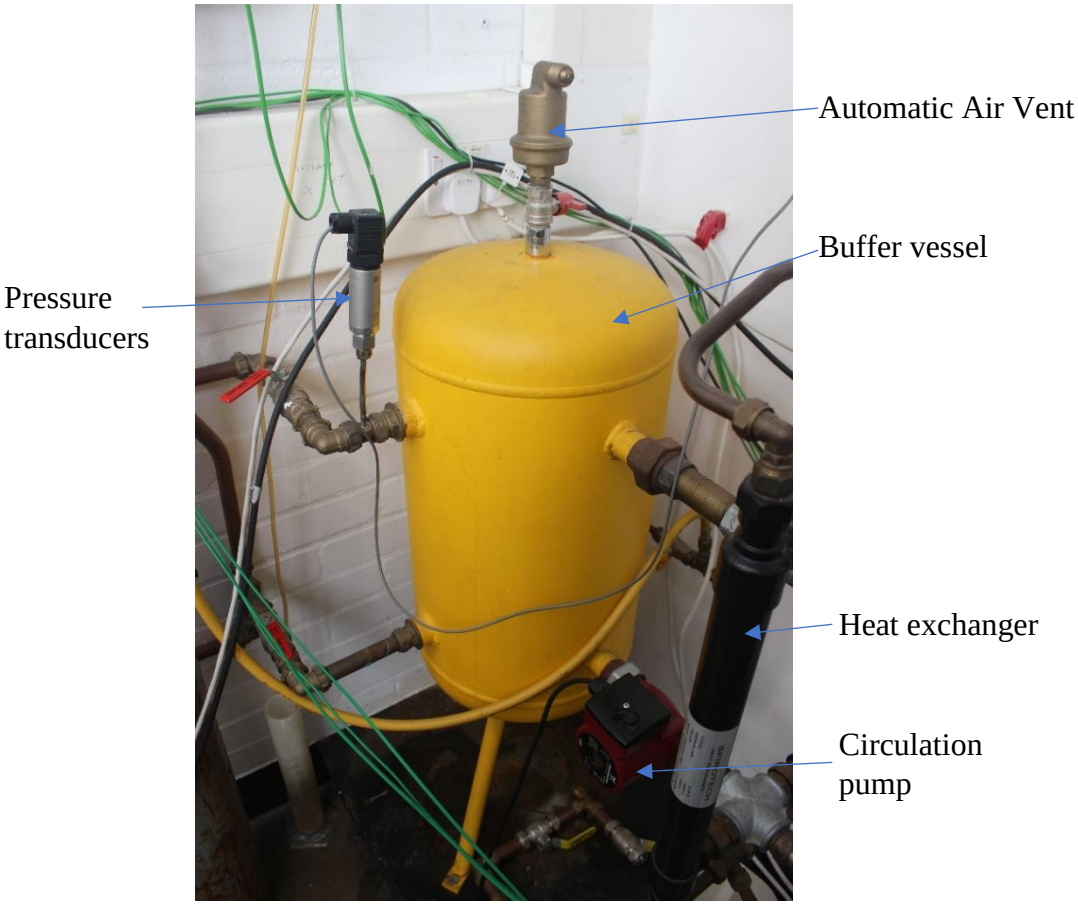

Figure 3. 6 Buffer vessel

Figure 3. 7 Nitrogen gas cylinder

A nitrogen gas cylinder is connected to the buffer vessel and can inject nitrogen into it to achieve supersaturated water as shown in Figure 3.7.

3.2.1.4 Cooling system

Figure 3.8 shows three tube heat exchangers connected to the buffer vessel and total gas measurement equipment. They are connected to the mains water supply to achieve cooling function. The cooling system is a separate loop from the primary water loop. The control method of the cooling system is introduced in 3.2.3 control system section.

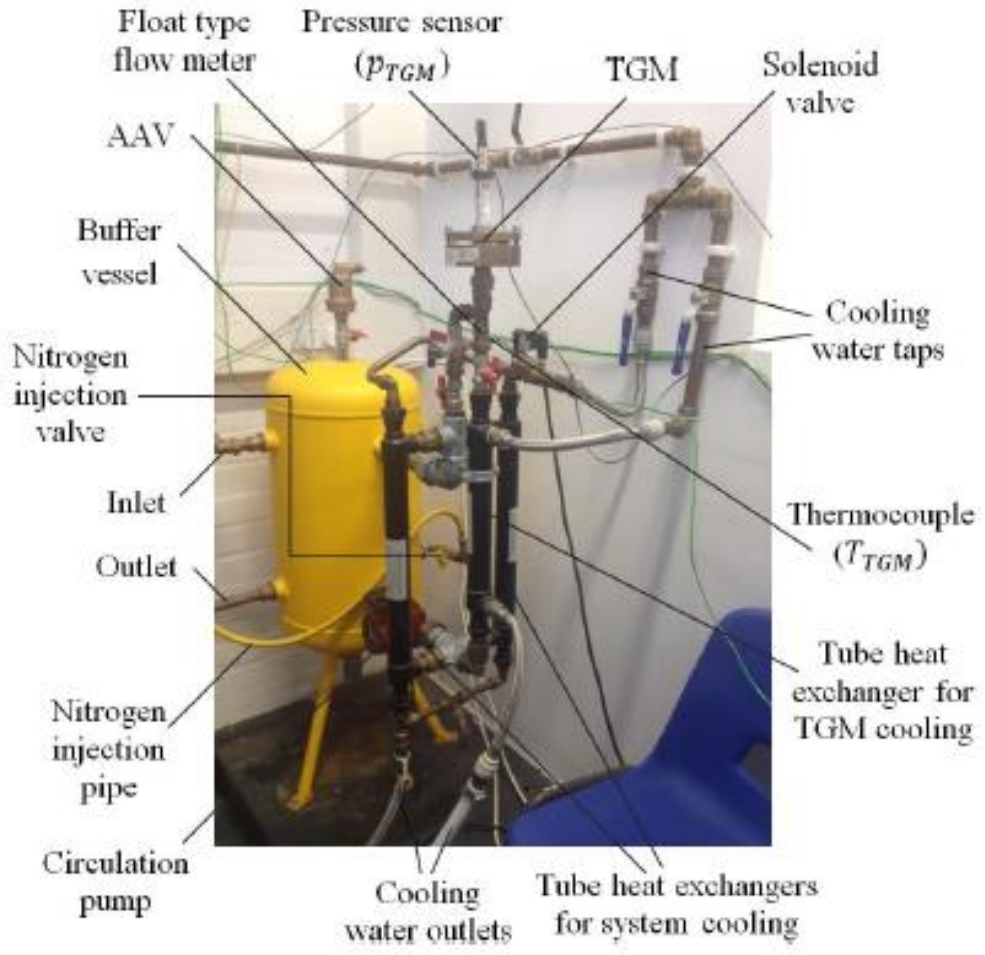

Figure 3. 8 Tube heat exchanger and total gas measurement (Shefik, 2015)

3.2.1.5 Other equipment

There is an expansion vessel installed on the supply position of the pipe as shown in Figure 3.9. The function of it is reducing the system pressure fluctuation and vibration while system water temperature fluctuates. The electromagnetic flow meter is installed on the return position of the pipe as shown in Figure 3.9.

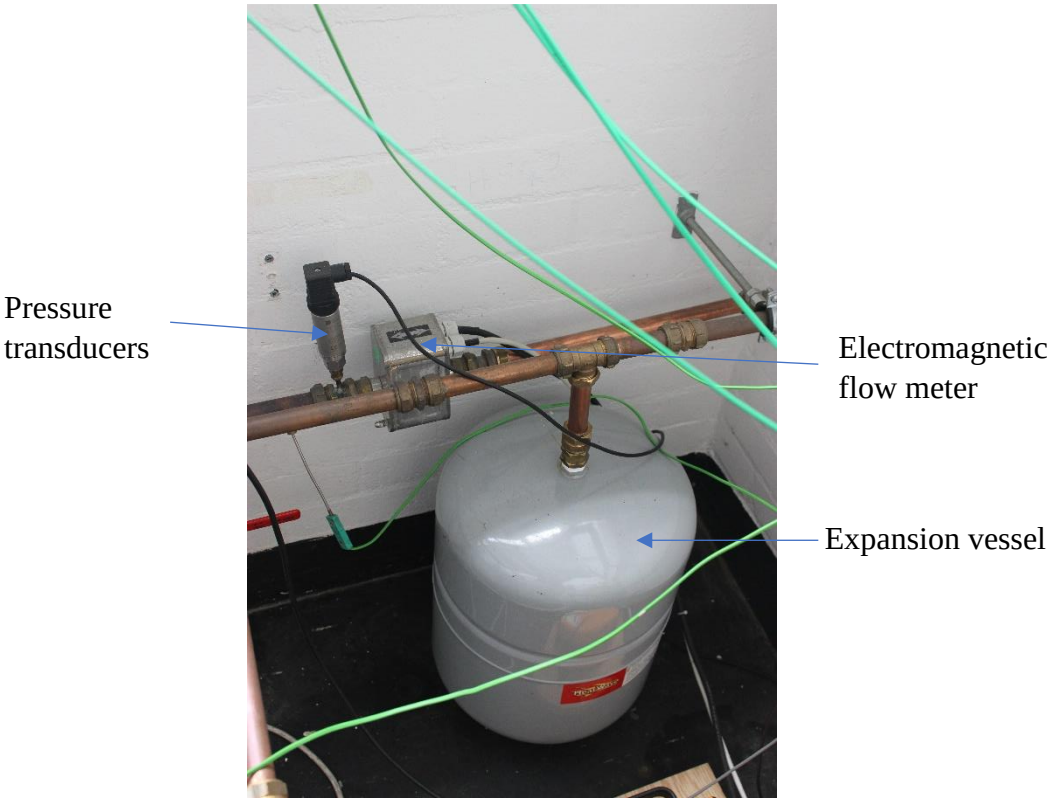

Figure 3. 9 Picture of expansion vessel

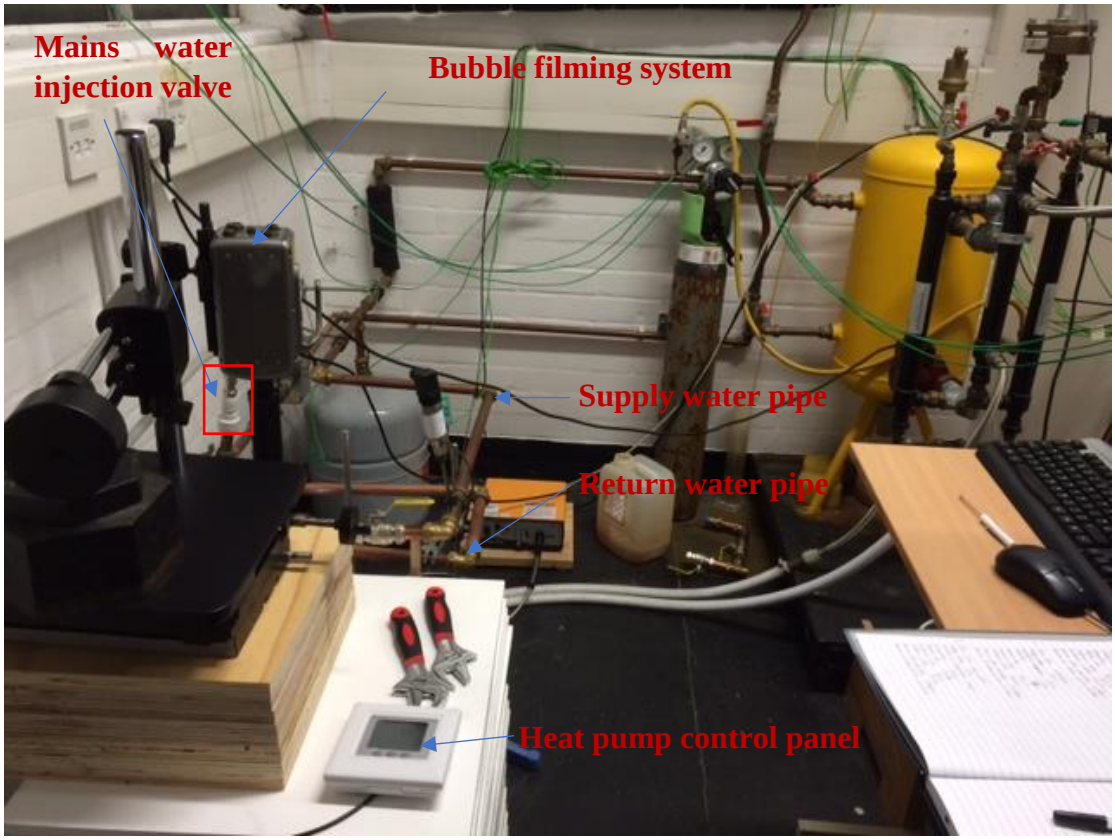

Figure 3. 10 Picture of test facility

Figure 3.10 shows the panorama of the test facility. The water charging of the water primary system is by using the city main water injection valve. Main water can come into the primary system by opening the valve and water system pressure can be set by control the amount of water injected into the system.

3.2.2 Image acquisition

The bubble measurement system consists of the high-speed camera, light-source and data logging software. Figure 3.11 illustrates the bubble measurement system in a straightforward way. Number one in Figure 3.11 is the light-source fixed underneath the horizontal sight-glass (number two). Number three is the high-speed camera which is connected to the computer (number five). Image data logging system is introduced in section 3.2.2.3 data logging system. One camera focal plane is shown as the number six in the figure. Number four is the microscope lenses. This section introduces the function of these units respectively.

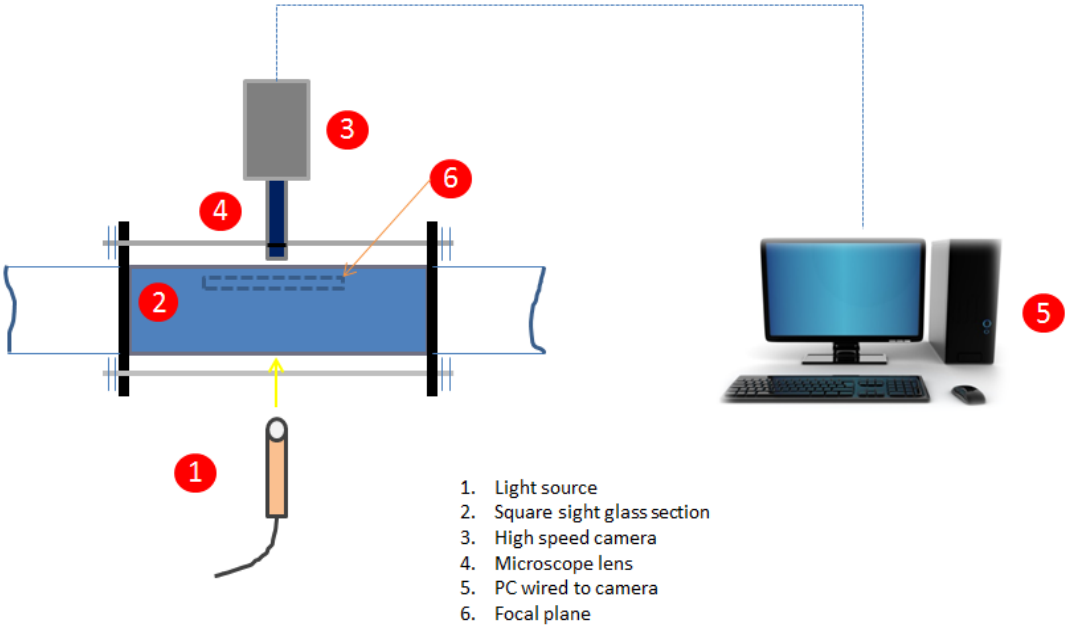

Figure 3. 11 Bubble measurement system

3.2.2.1 High-speed camera

The high-speed camera used in the test is Phantom V5.1 Digital High-Speed Camera which is provided by the EPSRC. The specifications of the high-speed camera are

shown in the Table 3.2. This high-speed camera is sponsored by EPSRC. It provides the ability to track bubbles and analyse the bubble behaviours in the horizontal pipe in the simulative domestic air-source heat pump water heating system.

Table 3. 2 Phantom V5.1 Digital High-Speed Camera Specifications (Phantom, 2007)

8-bit CMOS sensor composed of 1024 x 1024 pixels / colour or monochrome
1200 frames per second full resolution /up to 95,000 fps maximum
Continuously Adjustable Resolution in 64 x 4-pixel increments
2400 ISO/ASA monochrome 600 ISO/ASA colour sensitivity equivalency
Global on-chip shuttering to 2 microseconds
PIV - Particle Image Velocimetry (standard)
4 Gigabytes DRAM
IRIG-B timing capture modulated or unmodulated /IRIG lock w/phase shift
Continuous video output: RS-170 (NTSC, PAL)
Range data input
Automated multiple session recording for remote unmanned operation
Gigabit Ethernet or RS232 control
Size: 4.3 x 4.0 x 9.5 inch (HWD)
Weight: 3.2kg
Power: 1.5 Amp
Mounting: 1/4-20 inch and four 10-32 threaded hole pattern in base and top
Mounting Axis: Any position

Figure 3.12 illustrates the high-speed filming at the return position of system. The camera is fixed on the 3-axis base which allows it moving subtly between two sight-glasses as shown in Figure 3.13. Figure 3.13 also illustrates the working method of 3-axis camera base. This 3-axis base contributes in the ability to investigate the bubbly flow at supply and return position in one test run at different saturation ratios.

Figure 3. 12 Phantom V5.1 Digital High-Speed Camera

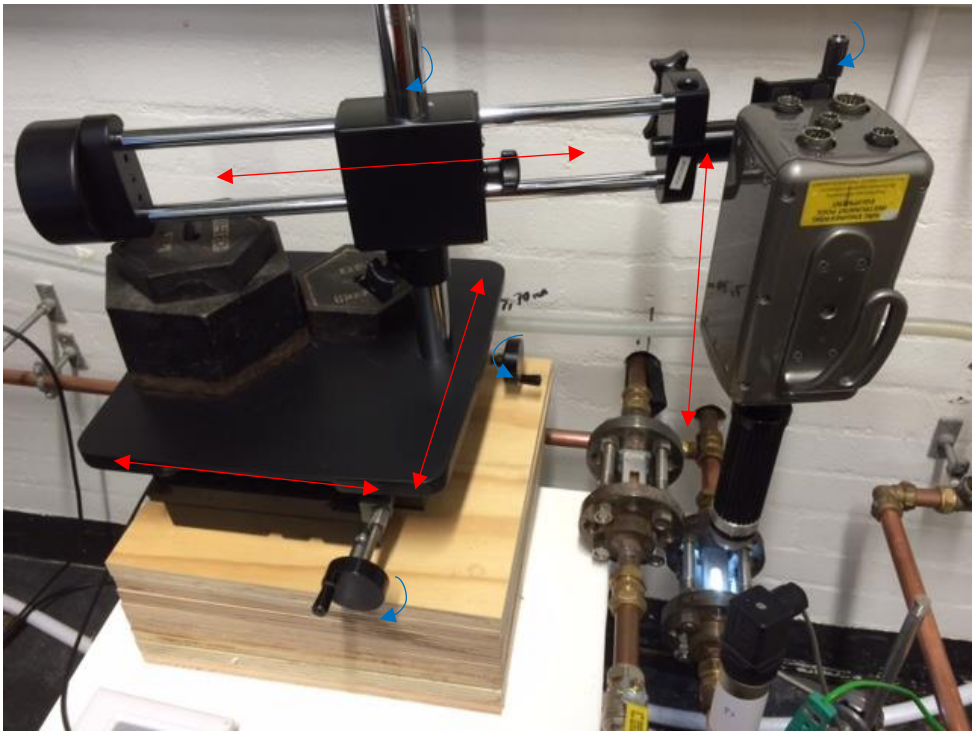

Figure 3. 13 3-axes camera base

The camera and lens were set as shown in Table 3.3 by considering the objectives and requirements of the test.

Table 3. 3 Camera and lens settings

Camera used	Phantom V5.1 High Speed Camera
Zoom	Leica Monozoom 7
Amplifier	3.0x
Objective used	2.0x
Zoom level	1x
Resolution	768x768
Sample rate	30 FPS
Exposure time	20µs
EDR exposure	1µs
Post trigger	1p

Two-minutes image filming had been achieved for each focal plane at one test run to investigate bubbly flow in a period. Hence, there is a big demand for computer hard drive space. 30 frames-per-second is a reasonable filming speed considering the supply water speed to avoid one bubble had been captured two times. The amplifier and objective were set to film clear micro-bubble in the sight-glass.

3.2.2.2 Light-source

One light-source is used to provide enough bright illumination to high-speed camera for capturing bubbles. Figure 3.14 presents the light-source used in the test. It comes with high-speed camera. There is a rotary knob on it to control the level of illumination. The light-source calibration was done before every set of tests by analysing the images taken by the high-speed camera.

Figure 3. 14 Light-source

3.2.2.3 Image data logging software

The camera is connected to a lab computer by using the Phantom Control Software, which is for Phantom totally digital high-speed cameras, as shown in Figure 3.15. As Table 3.3 presents, resolution is 768 * 768 pixels.

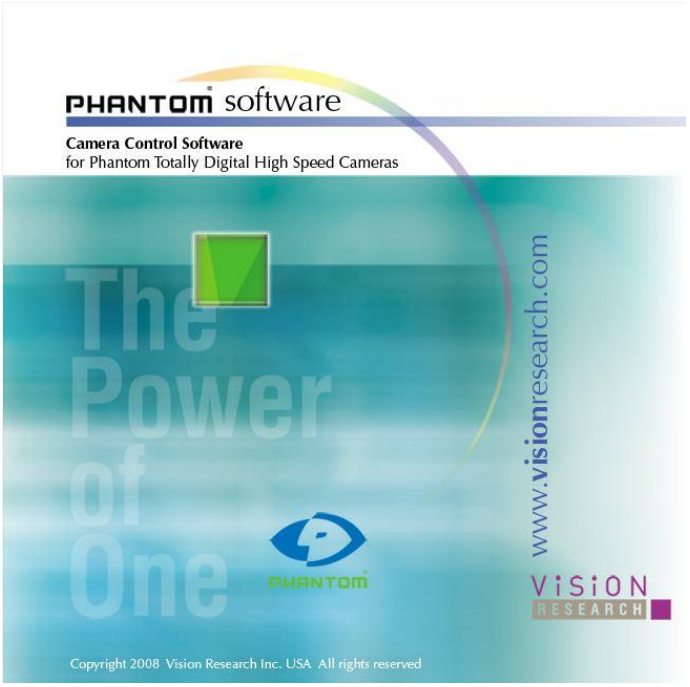

Figure 3. 15 Cine viewer application, image data logging software

And sample rate is 30 Fps, exposure time is 20 μs, EDR exposure is 1 μs and post trigger is 1 picture.

3.2.3 Control system

The automatic control system in this project includes heat pump control and cooling load control. Most bubbles generate in the condenser of the air-source heat pump. To investigate the bubbly flow, heat pump should be set to work continually. Two methods had been conducted. One is to use dry contact and choose the highest heating climate curve and another one is to cool down the water in the system.

3.2.3.1 Heat pump control

Figure 3.16 shows how the user control panel is connected to the printed circuit board of the air-source heat pump. User control panel can be used to set the target indoor temperature and heating climatic curve as shown in Figure 3. 17.

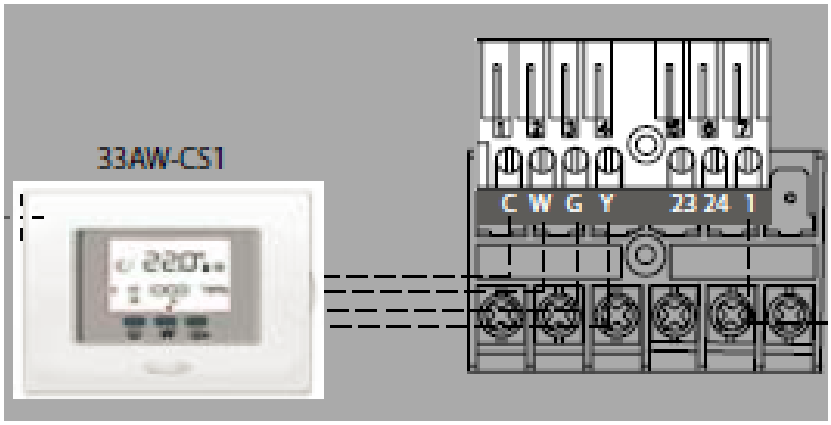

Figure 3. 16 Heat pump user control panel connection (Kingspan, 2014)

In each test run, 38℃ is set as the target indoor temperature which is also the highest temperature user can set.

Figure 3.17 shows the heating climatic curve that this air-source heat pump can provide. Curve 1 to 3 are used for under floor heating with lower supply water temperature. Curve 4 to 6 are used for fan coil heating with higher supply water temperature. Curve 6 was chosen by using control panel. The maximum supply water temperature of this operation curve is 60℃. By using curve 6, desire experimental supply water temperature, 55 ℃, can be achieved.

This heating climatic curve is affected by outside air temperature. Hence, the sensor of outside air temperature is fixed in an ice box. The reading value of the sensor is around 0 ℃. This method keeps the compressor work on the highest frequency. As a result, the

wall temperature of the plate heat exchanger is maintained at the highest value that this heat pump can achieve.

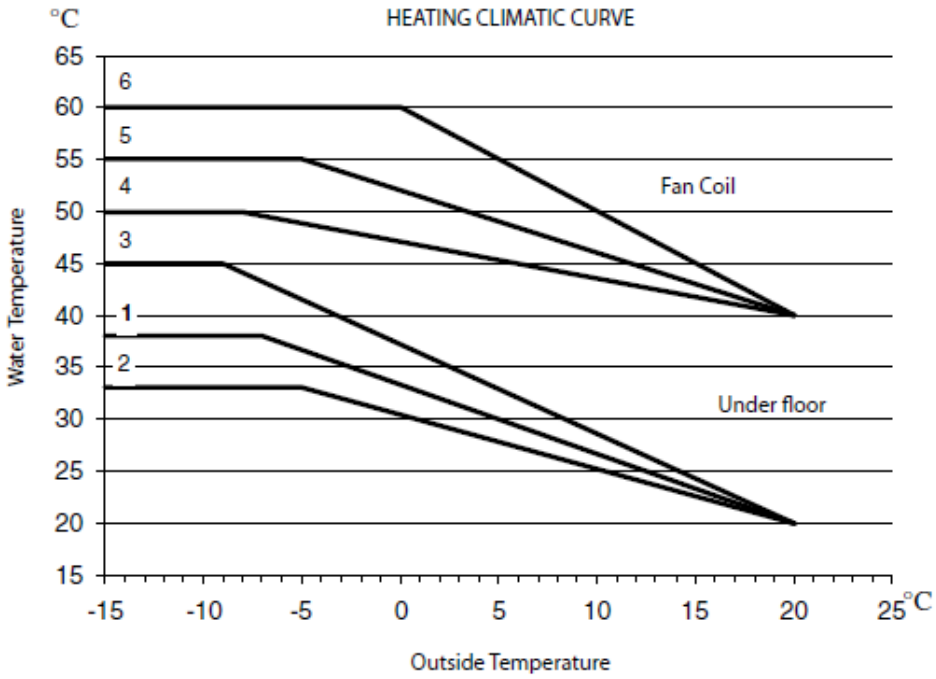

Figure 3. 17 Heating climatic curve (Kingspan, 2014)

3.2.3.2 Cooling load control

A cooling control formula is added into the LabVIEW code. This control method is a kind of PID control (proportional–integral–derivative control). It is used to maintain the supply water temperature at a certain value without unwanted fluctuation. Formula 3.1 presents this cooling system control formula, in which T_w is the wanted supply water temperature, x is time (3 samples per second) and T_s is the real-time actual supply water temperature.

$$T_w + 0.5 \times \left|\sin(\frac{\pi x}{6})\right| < T_s$$

Formula 3. 1 Cooling system control formula

When this inequality exits, the cooling system is turned on. The cooling system is an independent cycle. The control of the cooling system is conducted by the solenoid valve as shown in the Figure 3.19. When the solenoid valve is turned on, the cooling system is working and reducing the water temperature in the buffer vessel by three heat

exchangers as shown in Figure 3. 1.

Figure 3.18 illustrates the working method of the control method. The pink dash line represents the T_s and the red curve represents the converted T_w. As pink dash line is higher than red curve, which means the real-time supply water temperature is higher than the wanted supply water temperature, the solenoid valve is open. In Figure 3.18, (a) and (b) represent the solenoid valve on/off signal at different real-time supply water temperature. In another way, cooling system opens longer when the temperature difference between T_w and T_s is bigger.

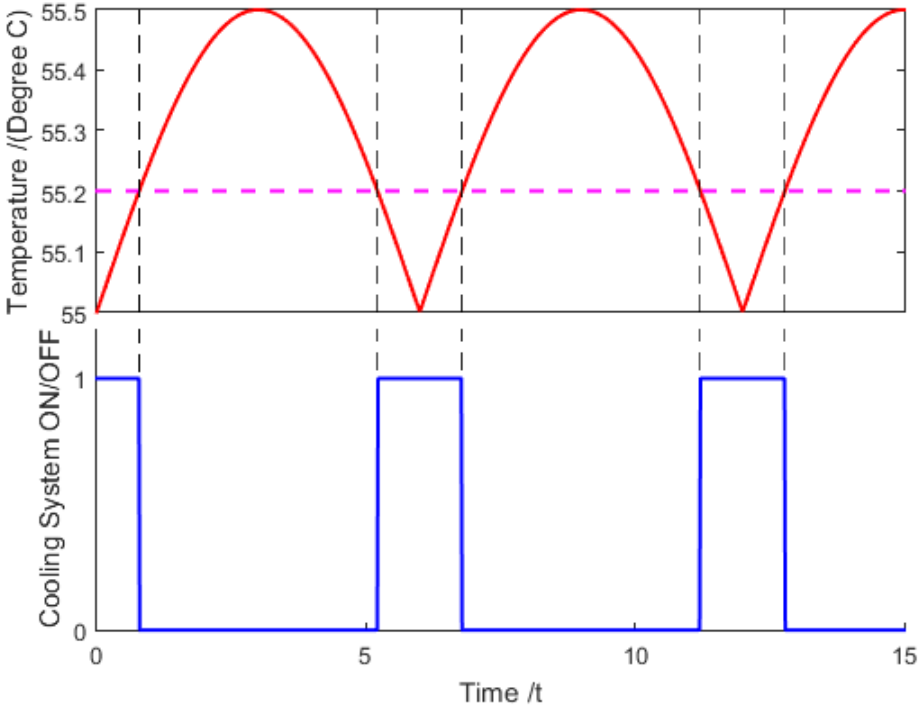

(a)

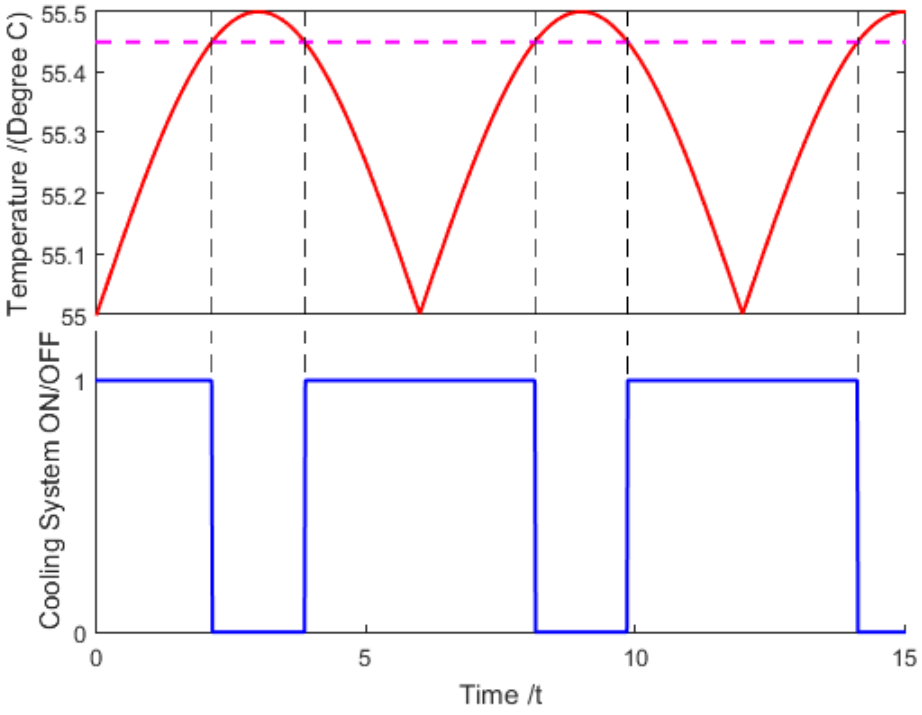

(b)

Figure 3. 18 Cooling system control method

Figure 3. 19 Solenoid valve

Solenoid valve is connected to the National instrument data acquisition equipment and controlled by the LabVIEW programme which is introduced in the next section.

3.2.4 Data logging system

This section introduces the equipment and software used for data logging. Section 3.2.4.1 presents the temperature and pressure sensors. And section 3.2.4.2 and 3.2.4.3 introduce the national instruments data acquisition equipment and LabVIEW software. In addition, section 3.2.4.4 illustrates the total gas measurement equipment. Furthermore, section 3.2.4.5 shows the flow meter. Finally, section 3.2.4.6 introduces the calibration.

3.2.4.1 Temperature and pressure sensors

Seven stainless steel sheathed K-type thermocouples and three pressure transducers are installed along the piping in air-source heat pump unit and domestic water heating system. Figure 3.20 illustrates how the pressure transducers are mounted on the pipe. These are industrial level pressure transducers of which the serial number is PTX 7517. As shown in Figure 3.1, the pressure transducers are installed at the heat pump exit, heat pump inlet and the buffer vessel inlet. The working range of the pressure transducers is between 0 and 10 bars and the temperature of the system should be at the range from - 40℃ to 100℃ (Druck, 2014). It contains two wires. Current output of the pressure transducer is from 4 mA to 20 mA. The pressure transducers measure total pressures at specific positions respectively.

Figure 3.21 illustrates the installation of K-type temperature thermocouples. Figure 3.1

has shown the positions of 6 thermocouples. The other one is used to investigate the

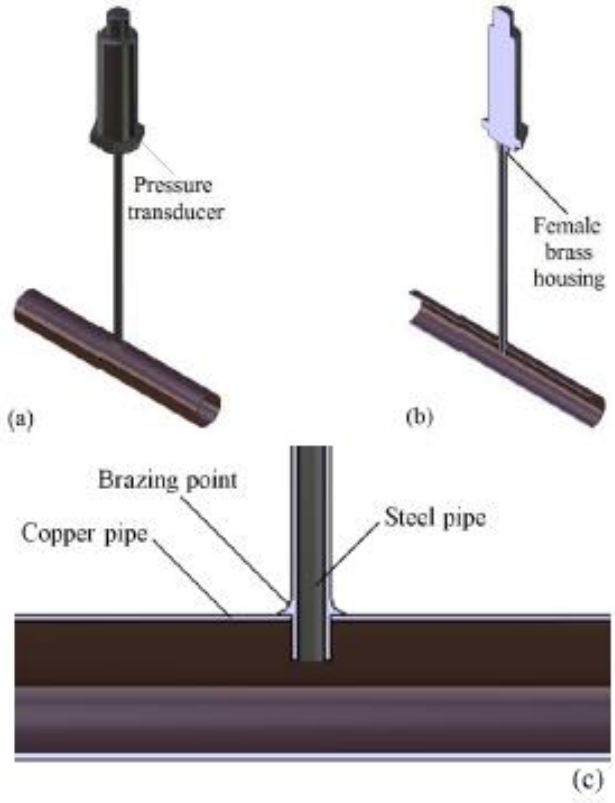

Figure 3. 20 CAD model of the pressure transducer (Shefik, 2015)

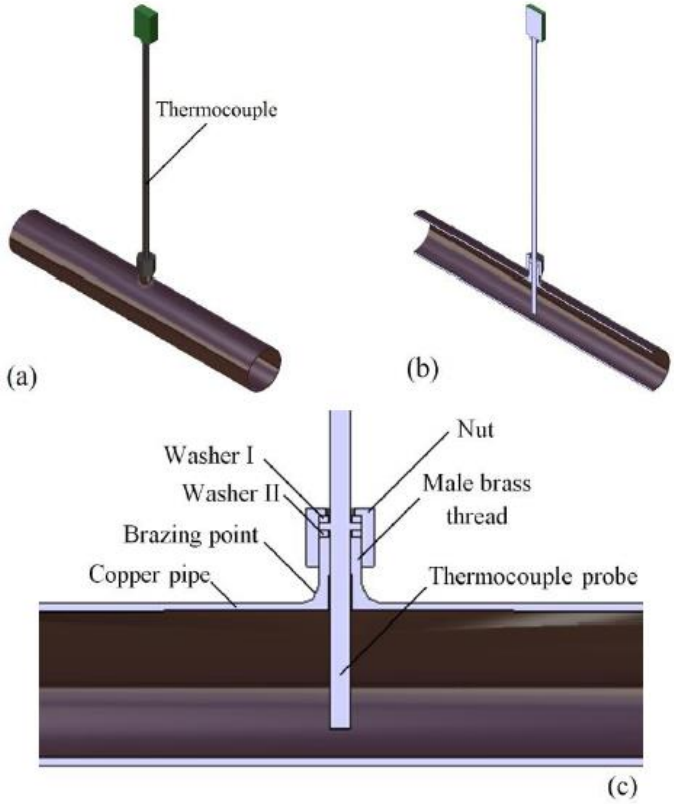

Figure 3. 21 CAD model of the K-type thermocouples (Shefik, 2015)

outdoor air temperature. The positions of heat pump exit, heat pump inlet and total gas measurement equipment where are installed thermocouples to monitor temperature. The other three thermocouples are installed in the air-source heat pump unit outdoor. In the heat pump unit, the temperatures of compressor exit, plate heat exchanger exit, and the evaporator have been measured by them respectively.

3.2.4.2 NI Data Acquisition

All the signals from the transducers, thermocouples and electromagnetic flow meter are collected by the National Instrument cDAQ-9172 chassis and NI9211, NI9203, NI9481 data modules as shown in Figure 3.22. This chassis can be loaded with maximum 8 modules and recognizes analogue and digital signals with USB connection (National Instruments, 2008). There are four modules are installed in this project which are NI-9211, NI-9203 and NI-9481 respectively.

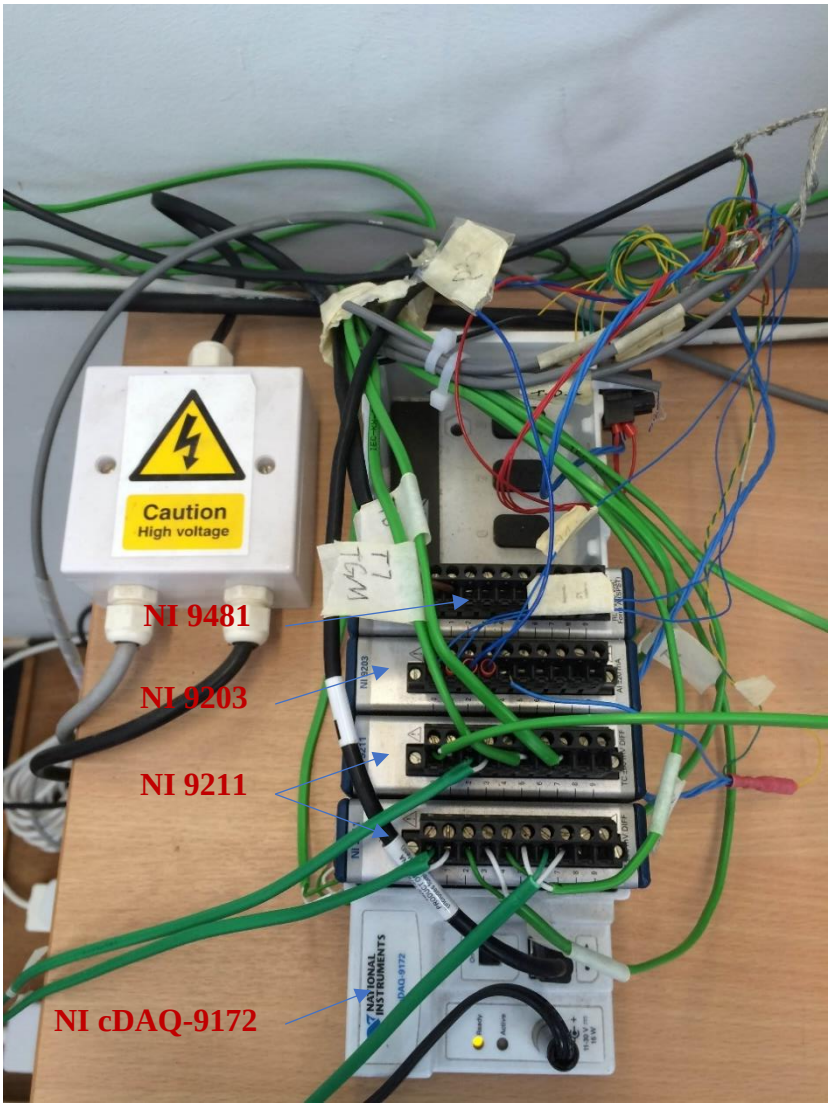

Figure 3. 22 NI data acquisition chassis with modules

Green cables stand for the temperature thermocouples and blue cables stand for the pressure transducers. The NI-9211 module receives signals from temperature thermocouples and the NI-9203 module receives signals from the pressure transducers and the electromagnetic flow meter. The NI-9481 module is connected with the solenoid valve signal cable to control the cooling system as discussed in section 3.2.3.2.

3.2.4.3 LabVIEW

A programmed LabVIEW code used to collect and save the signals. It was also used to control the system water supply temperature by controlling the cooling system as shown in the Figure 3.23. All the signals were calibrated, and the calibrating equations are programmed in the LabVIEW software.

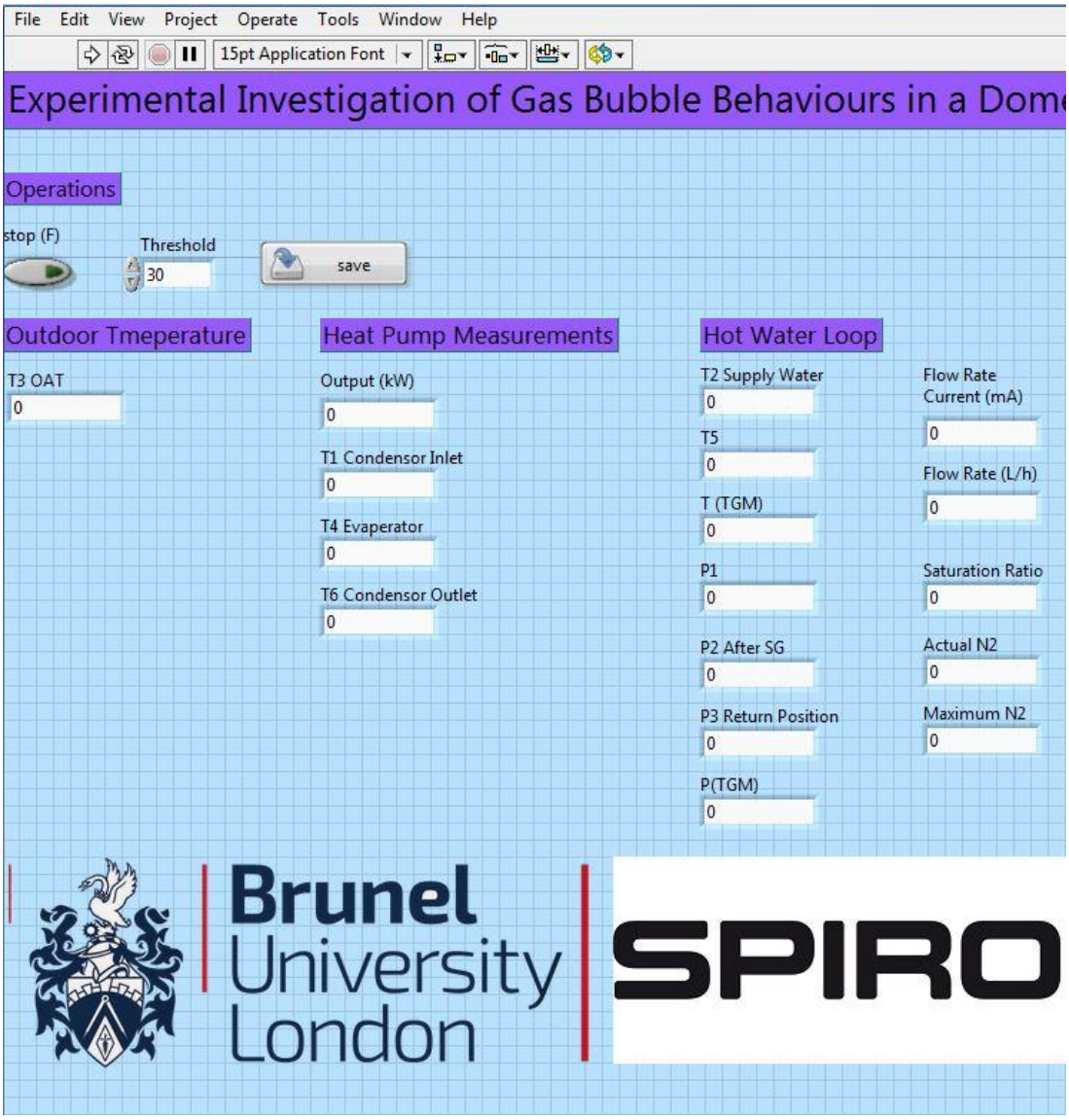

Figure 3. 23 Programmed LabVIEW user interface

The names of each value have been introduced in the nomenclature. In the user interface, there are mainly four parts: threshold temperature, outdoor temperature, heat pump measurement and hot water loop measurement. The T_1 represents the temperature of the condenser inlet, which is also named as the plate heat exchanger inlet. The T_2 represents the temperature of heat pump exit, which is also named as the temperature of supply water. The T_3 represents the temperature of the outdoor air temperature. The T_4 represents the temperature of the evaporator of the heat pump. The T_6 represents the temperature of the condenser outlet, which is also named as the refrigerant temperature of the condenser exit. The T_5 represents the temperature of the heat pump inlet, which is also named as the return water temperature. In addition, the T_{tgm} represents the temperature of the total gas measurement equipment. Moreover, the P_1 stands for the

pressure of the buffer vessel inlet. The P_2 stands for the pressure of the heat pump exit, which is named as after-sight-glass pressure as well. Furthermore, the P_3 stands for the pressure of the return position, which is named as heat pump inlet as well. Finally, the P_{tgm} represents the pressure of the total gas measurement. The detail of the block programme design is presented in Appendix II.

3.2.4.4 Total gas measurement

Working temperature of the total gas pressure monitoring system is between 20 and 45 °C. As shown in Figure 3.24, the system consists of a pressure transducer, semi-permeable silicone membrane and a two-hole tube sheet which allows water to go through the holes and have a contact with the silicone membrane. The partial gas pressure is calculated through the subtraction of the relevant water vapour pressure from the total gas pressure.

3.2.4.5 Flow meter

An electromagnetic flow meter is used to measure system fluid flow rates as shown in Figure 3.25. This flow meter, 500 series, is from Litremeter Company. It can work at the conditions of fluid temperature ranging from -20 to 160 ℃ and system pressure reaching to 1600 Kilopascals (Litremeter, 2010). This flow meter is located at the heat pump inlet position as shown in Figure 3.1.

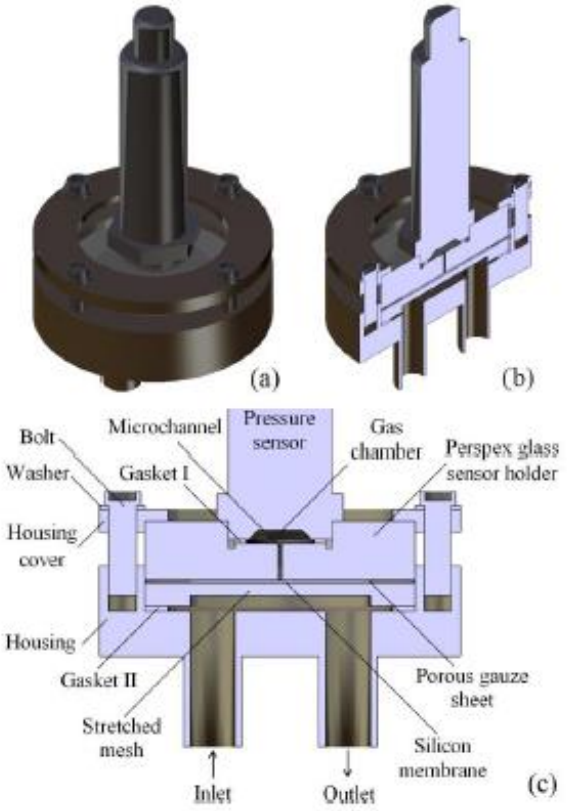

Figure 3. 24 Total gas measurement equipment (Shefik, 2015)

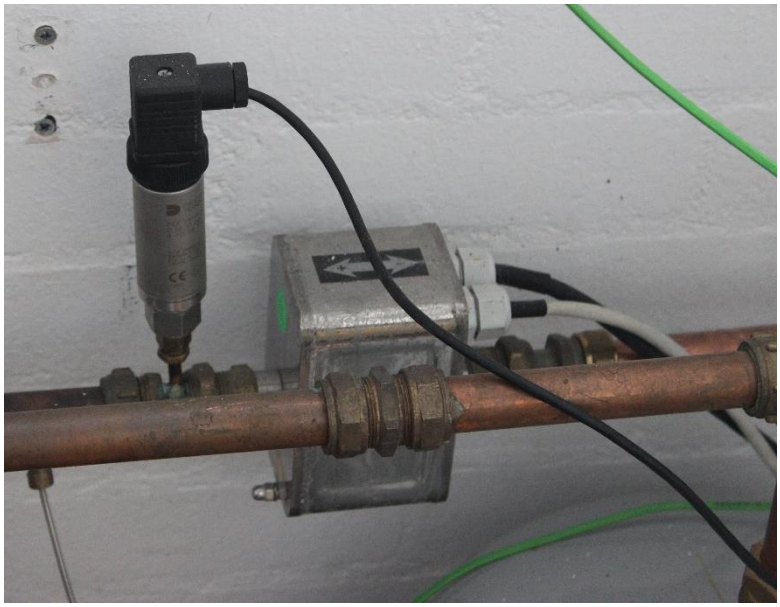

Figure 3. 25 500 series electromagnetic flow meter

3.2.4.6 Calibration

The temperature thermocouples and pressure transducers installed in this air-source heat pump water heating system have been calibrated by using the methods of the water bath and the dead weight to enhance the accuracy of the data logging. The flow meter company, Litre Meter Limited, has calibrated the electromagnetic flow meter used in this project and provided the calibrated the calibration data for the tester (Shefik, 2015).

Figure 3.26 has shown the calibration equation for the T1 condenser inlet temperature. Nine different temperatures were tested to increase the accuracy of the calibration equation. The x-axis represents the original temperature recorded by the temperature thermocouple at a specific actual temperature. The y-axis represents the actual temperature maintained by the water bath equipment. After several tests, the relationship between the temperature of the temperature thermocouple data logging and the accurate and actual temperature has been found. Then the calibration equation has been presented.

This calibration equation was used in the LabVIEW programme to calibrate the raw data of the thermocouple, and make sure the final recorded data is accurate. All the other calibration equations for other sensors have been presented in Appendix III.

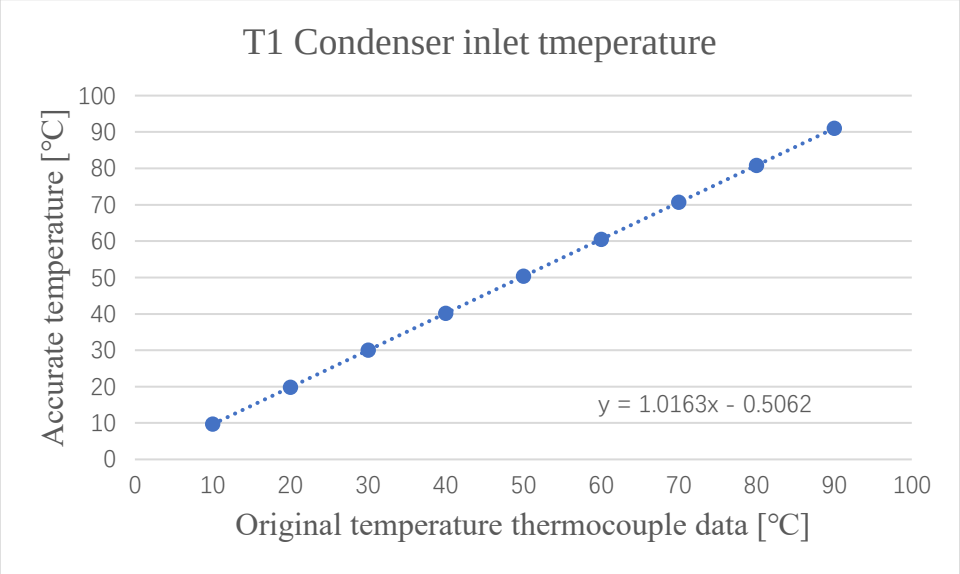

Figure 3. 26 Calibration equation for T1 condenser inlet temperature

3.2.4.7 TGM Assembly

Saturation ratio of bulk fluid in the system is a very important value to understand bubble behaviours in heat pump water heating system. This value is calculated by $C_{gas-act}/C_{gas-max}$ (according to P_{tgm}, T_{tgm}, P_{supply} T_{supply}). P_{tgm} is achieved by reading from TGM.

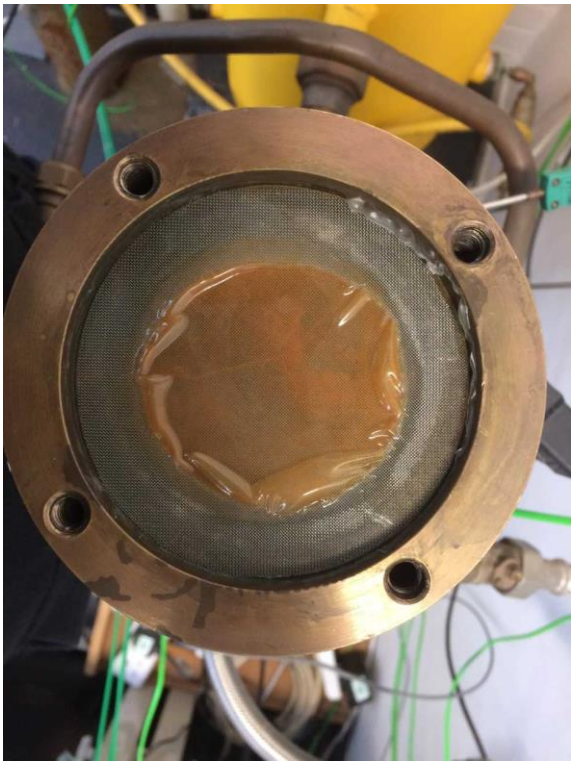

Figure 3. 27 Membrane in TGM

However, the TGM requires exceptionally high assembling skills to work correctly. The most frequent problem is caused by different pressures at four different screws of the flange of TGM. As shown in Figure 3.27, the membrane is in the middle of the TGM, and there are four screws at the rim of the TGM. The membrane can prevent water going through to reach the pressure sensor of the TGM. The uneven pressures of four screws of the flange affect the reading of the pressure sensor of the TGS. This problem can lead to the wrong interpretation of the saturation ratios. And the false value of the saturation ratio would cause wrong conclusions about bubble behaviours in the heat pump water heating system. This problem has been solved by using torque wrench as shown in Figure 3.28. The best value, 10 NM, of the torque wrench, has been found by proceeding several experiments. By using this torque wrench, the pressure readings of the TGM are more accurate comparing to without it.

Figure 3. 28 Torque wrench

3.3 Image process

The bubble images, captured by the Phantom V5.1 camera, were saved in the laboratory computer. And these images needed to be processed to achieve the digital data. Hence, the image process is a vital part of this project as all the image files are converted to the raw digital data during this process. The Phantom control software saves the bubble images in the 'Cine' format as shown in the section 3.2.2.3. An efficient and accurate method is needed to analyse the mass of data. In this project, a MATLAB programme, used to conduct the bubble images processing, is developed by Collette Baptiste with the help of Dr. Hongying Meng, Prof. Yunting Ge, Ali Shefik, Jianbo Qin and Asim Jan (Baptiste, 2015). This MATLAB code improved by Xianghua Jiang and Jianbo Qin. This programme can only analyse the '.avi' format files. Hence, the original data was converted to the 'Avi' format by the Phantom Cine Viewer application as shown Figure 3.29.

Figure 3. 29 Cine Viewer Application

Figure3.30 shows an example of the processed bubble image. The clear bubble, which is in the depth of the focal plane, is recognized by the programme. This section is going to provide an introduction of the image process in three parts. These three parts are the MATLAB programme, calibration of the size of the picture and the depth of the focal plane respectively.

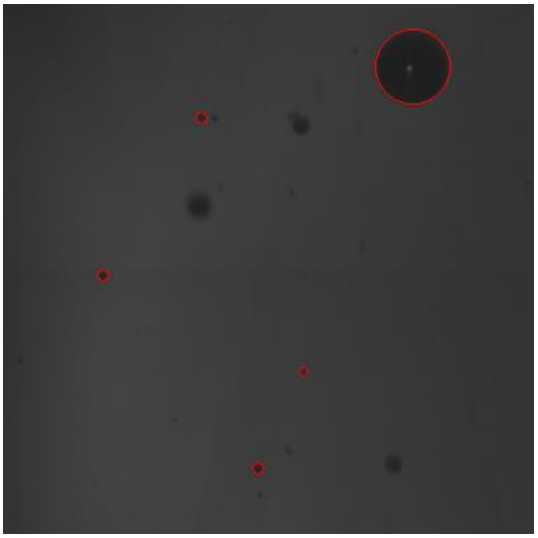

Figure 3. 30 Recognized bubbles by the programme

3.3.1 The MATLAB programme

The MATLAB programme as described in the preceding section is attached in the Appendix IV. The user interface of the MATLAB has been shown in Figure 3.31. The functions of this programme include output plot option, bubble tracking, change filters and other options. It can process several files in a row by clicking the 'all file' button. The results of the bubble numbers, bubble diameters and volumetric void fraction are written in the excels. Figure 3.32 has shown the result of removing the background of the bubble images. The background of the bubble images is calculated by summing all the images to compute an average image, which does not affect the recognition of the blurred and non-blurred bubbles. In Figure 3.32, the left one is the original picture and the right one is the picture after background removed. The dirt particles and stains on the sight glass are motionless. Hence, they are treated as the background during the image processing and thus removed. After removing the background of the images, the blurred bubbles need to be removed which affects the accuracy of the data. Bubbles are blurry when they are not in the focal plane. The Sobel Filter, a blurring filter, is used in the program to do the edge detection which determines in or out of focus. During the images processing, the image was reduced to half ratio of the original size to increase the computing time and efficiency of the analysis.

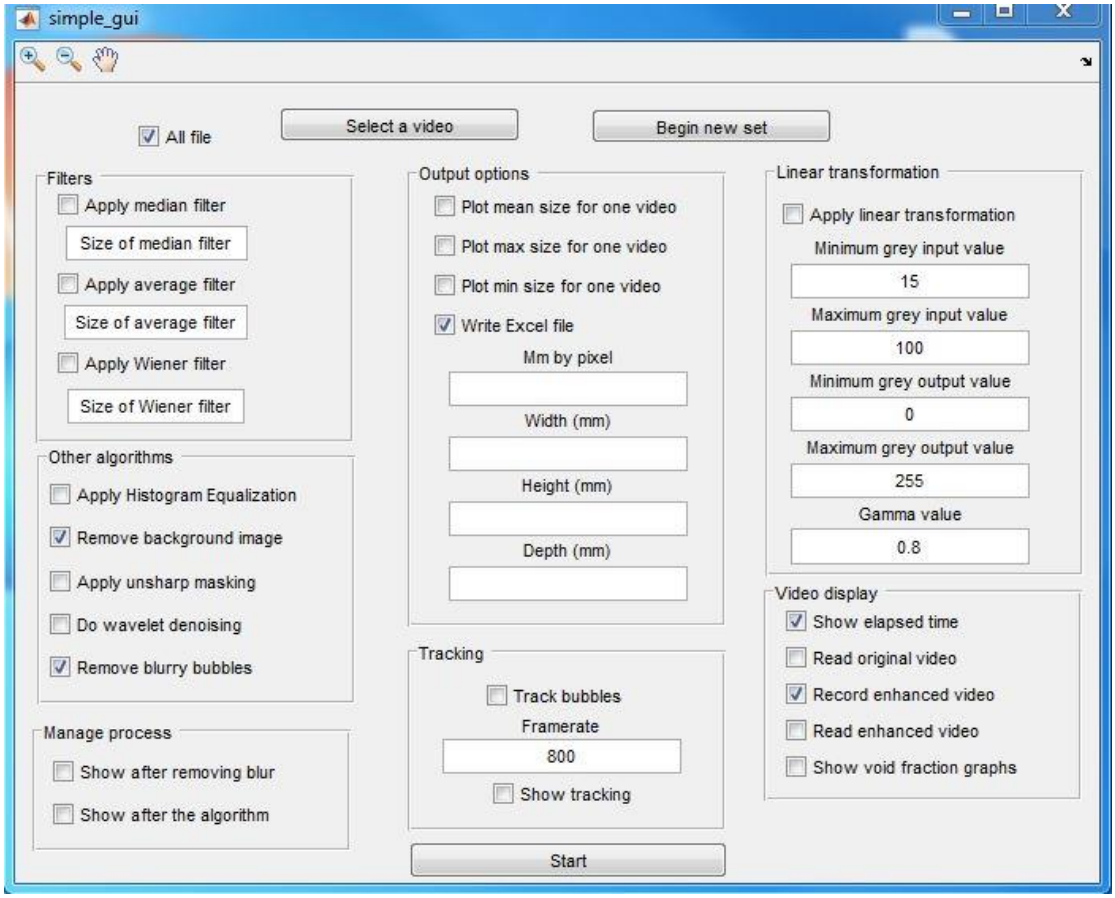

Figure 3. 31 The MATLAB programme user interface

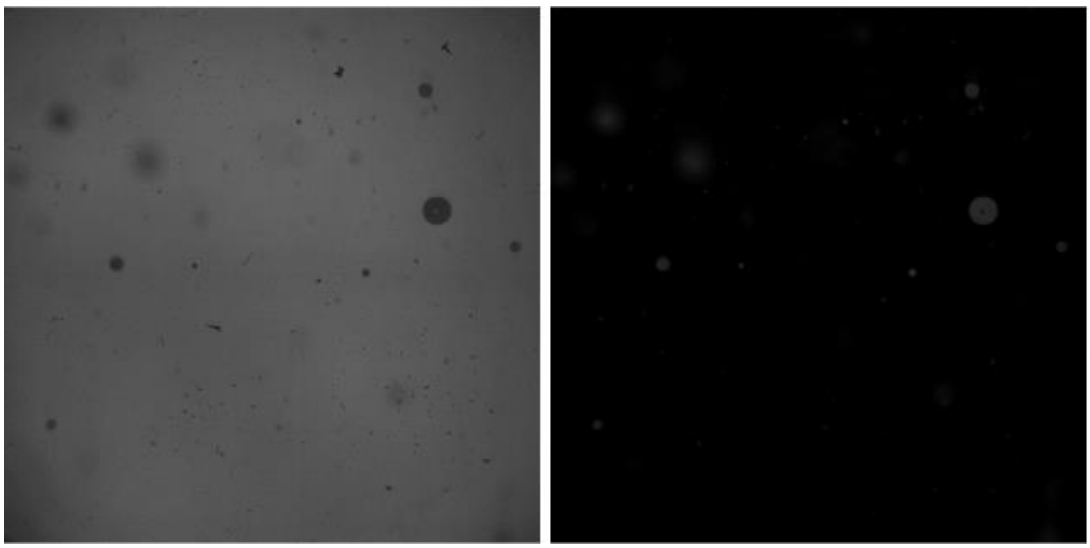

Figure 3. 32 Removing background of the bubble image

3.3.2 Calibration of the size of the bubble image

The calibration is an essential task for image processing. The resolution of the image ($P_{picture)}$ is 768 * 768 pixels in the camera settings. In order to investigate the actual size of the whole image, a calibration test was conducted. A bag of metal balls had been provided by the Spirotech Limited as shown in Figure 3.34. The diameter of the metal balls is 2 mm with the absolute uncertainty of 0.00254 mm, which is described by the manufacture (Simply Bearings Ltd, 2010).

A metal bubble was located on the sight-glass (D_{ball} = 2 mm), and a test film was taken. The original image has been in Figure 3.33. The metal ball's pixel size, $P_{ball,}$ was measured. Hence, the actual dimension of the image can be calculated based on Equation 3.1.

$$D_{\text{image}} = P_{\text{image}} \times \frac{D_{\text{ball}}}{P_{\text{ball}}} \quad \textbf{(3. 1)}$$

Based on all the information, the actual dimension of the image is 4.2 mm * 4.2 mm. And the size of one pixel is 0.0055 mm. As the error of the metal ball is smaller the size of one pixel, the calibration is acceptable. These values are used in the calculation of the other parameters in the following sections. Furthermore, the minimum diameter of the bubble that can be identified is 0.05 mm in this project by using the experimental method and equipment.

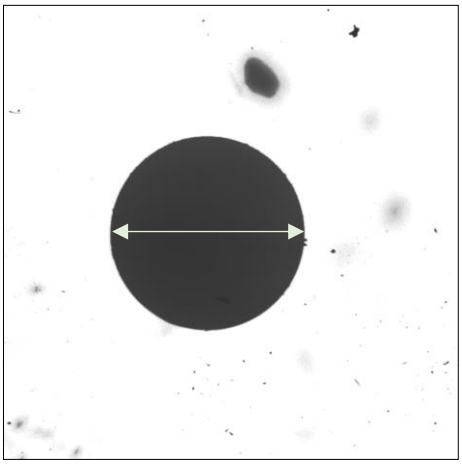

Figure 3. 33 Calibration of the size of the picture; Figure 3. 34 Metal balls

3.3.3 Depth of the Focal Plane measured

Five focal planes were measured as shown in Figure 3. 35. The actual dimension of the cross-section of the pipe is 20 mm x 20 mm. However, the measurement of the camera shows that the distance between the bottom of top glass and the top of bottom glass of sight-glass device is close to 14 mm. The reason of this phenomenon is due to the light refraction. During the test, the focal plane depths measured of the 1st, 2nd, 3rd, 4th and 5th layer is 1 mm, 2 mm, 5mm, 8 mm and 11 mm respectively. These lengths represent the distances of the high-speed camera moving from the bottom of the top glass.

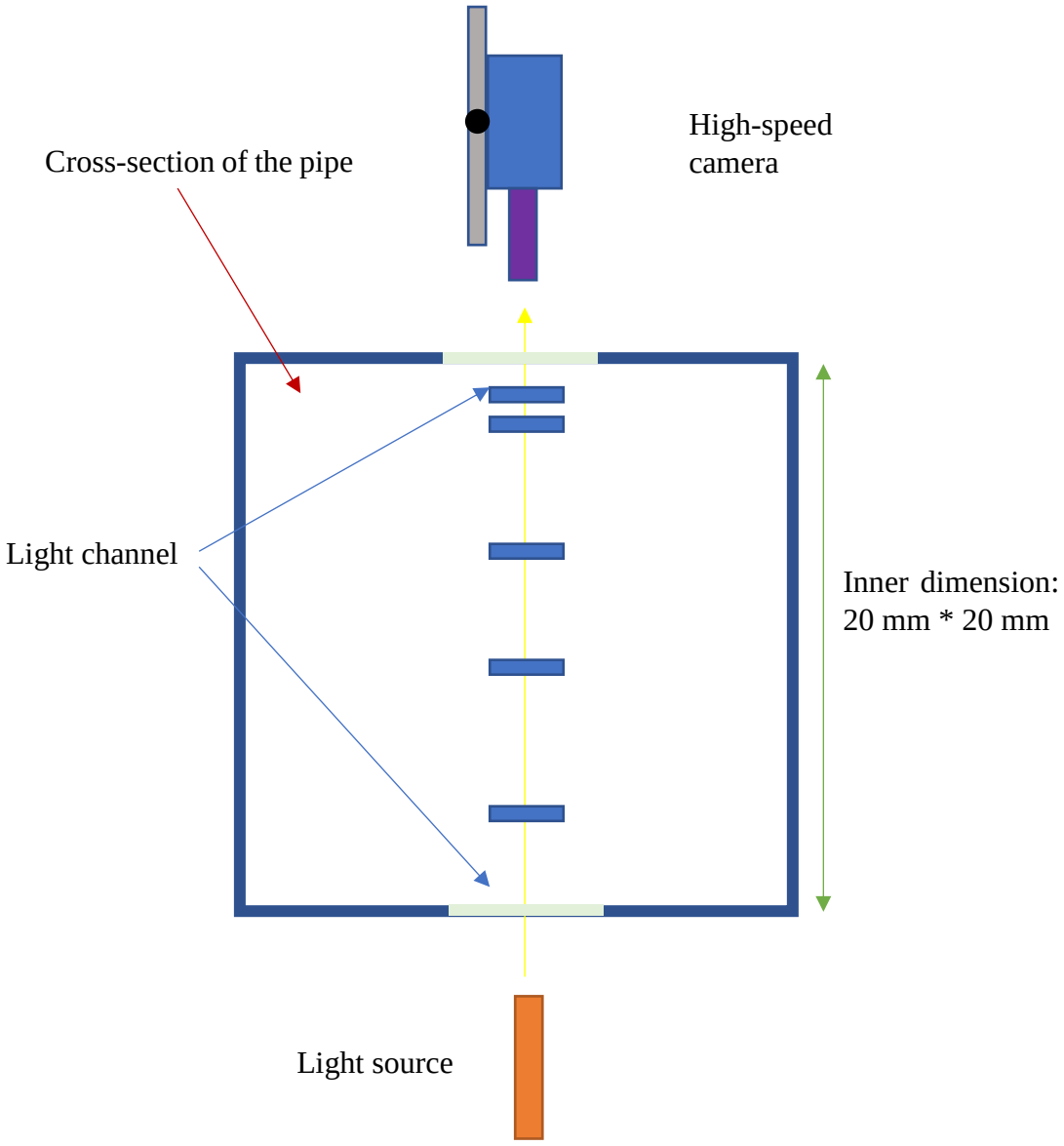

Figure 3. 35 Depth of focal plane measured (Cross-section of the pipe)

The apparent total depth of the sight-glass affected by the light refraction has been studied in Shefik's thesis (Shefik, 2015). However, the apparent depth of each focal plane has not been discussed by Dr.Shefik. This gap has been filled.

This section is going to discuss the effect of the light refraction on the depth of focal plane measured and calculate the actual depth of DOF measured. In Equation 3.2 to 3.5, Θ indicates an angle.

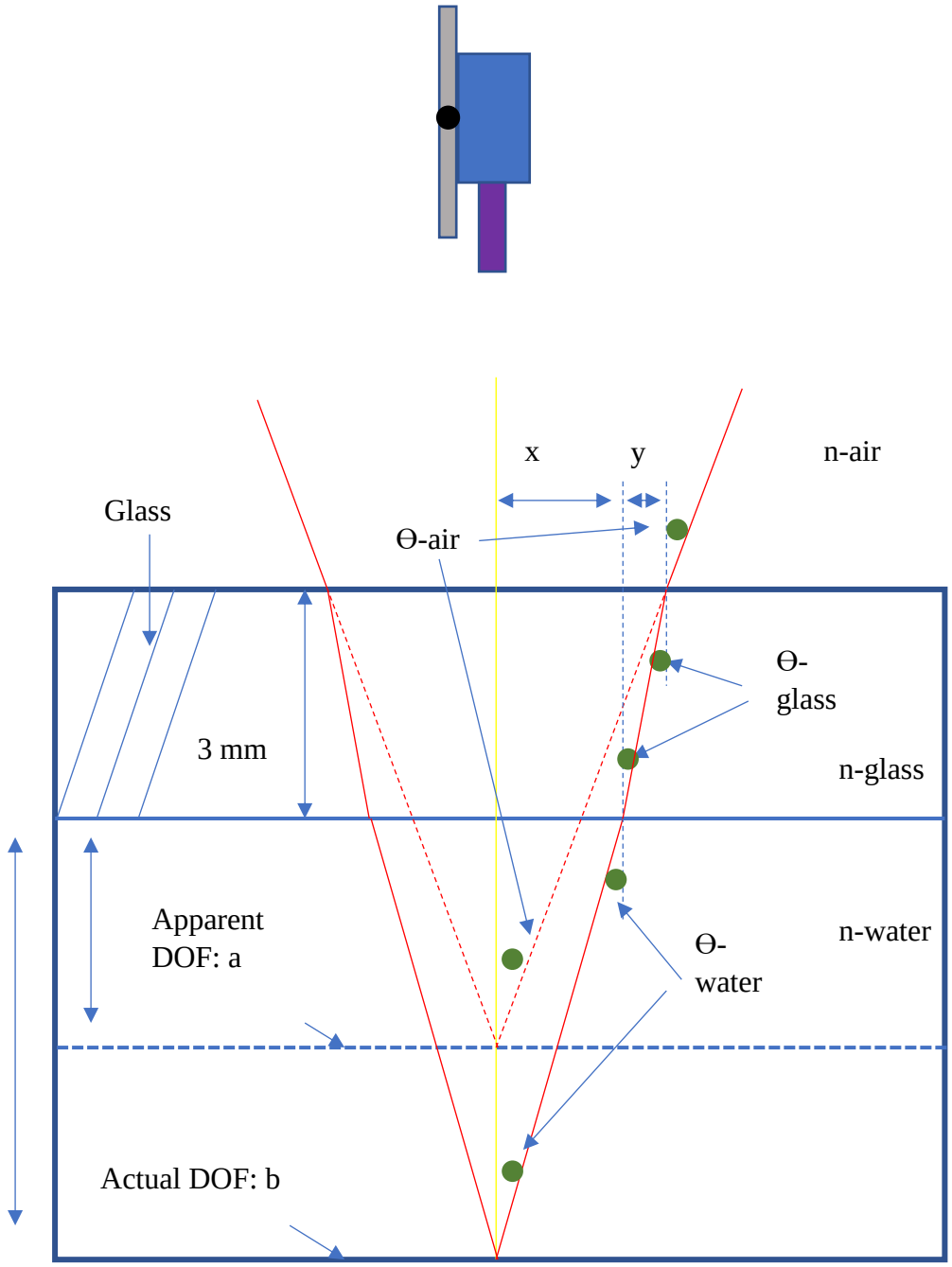

Figure 3. 36 The effect of the light refraction on the DOF

According to the Snell's Law the following equation 3.2 can be summarised (Nassar, 1994). In Equation 3.2 to 3.5, the parameters of the equations are identified in Figure 3.36. And n represents the refractive index.

$$n_{air}sin\theta_{air} = n_{glass}sin\theta_{glass} = n_{water}sin\theta_{water}$$

(3. 2)

In order to find out the relationship between the apparent DOF and actual DOF, the following mathematical proceedings have been done.

$$tan\theta_{air} = \frac{x+y}{3+a}$$
$$tan\theta_{glass} = \frac{y}{3}$$
$$tan\theta_{water} = \frac{x}{b}$$

(3. 3)

Equation 3.3 has shown the sine of each angle. In this project, the angle of incident is very small. Hence, the angle of refraction is very small as well. Then, an assumption can be made based on this information that tanϴ=sinϴ.

$$\frac{n_{water}}{n_{glass}} = \frac{sin\theta_{glass}}{sin\theta_{water}} = \frac{tan\theta_{glass}}{tan\theta_{water}} = \frac{by}{3x}$$
$$\frac{n_{water}}{n_{air}} = \frac{sin\theta_{air}}{sin\theta_{water}} = \frac{tan\theta_{air}}{tan\theta_{water}} = \frac{b(x+y)}{x(3+a)}$$

(3. 4)

By combining Equation 3.2 and Equation 3.3, Equation 3.4 is obtained. By using the mathematical skills to arrange the Equation 3.4. The relationship between actual DOF and apparent DOF is obtained as Equation 3.5.

$$Actual\ DOF = b = \frac{N_{water}(3+a)}{N_{air}} - \frac{3N_{water}}{N_{glass}}$$

(3. 5)

Therefore, a table has been made to illustrate the relationship between the actual DOF and apparent DOF as shown in Table 3.4.

Table 3. 4 Depth of focal plane table

D-apparent (mm)	D-real (mm)
1	3
2	4
3	5
4	7
5	8
6	9
7	11
8	12
9	13
10	15
11	16
12	17
13	19
14	20

The apparent depth of focal is equal to the distance of the high-speed moving from the bottom of the top glass. The actual depth of focal plane measured can be found in Table 3.4. The 1 mm, 2mm, 5mm, 8mm and 11 mm depth of focal planes are corresponding to the 3 mm, 4mm, 8mm, 12mm and 16 mm respectively.

In addition, the view angle of camera can be obtained by using Equation 3.6

$$\theta = 2\arctan\left(\frac{D_{image}}{2D_{focal\ distance}}\right) \quad \textbf{(3. 6)}$$

In Equation 3.6, $D_{\text{focal distance}}$ is the distance between the camera lens and the focal plane, and D_{image} is dimensions of the image. The results of tan Θ and sin Θ are approximate as the value of Θ is very small.

3.3.4 The obtainment of the depth of field

As shown in Figure 3.37, when observing from a set of lenses, the scene of the object would appear acceptably sharp only in the area near the focal length of the lenses. This distance, from the upper side of the sharp area to the lower side, is called the depth of field (DOF).

Figure 3. 37. Depth of field when observing text through lenses (Cambridge in Colour, 2018)

Referring to the theory of DOF, the DOF can be expressed by equation 3.7.

$$D_{\mathrm{DOF}} \approx \frac{2NCU^2}{f^2} \tag{3. 7}$$

In Equation 3.7, N --F-number of lens; C --Circle diameter of confusion (on image, mm) In optics, Circle of confusion is a spot caused by a corn of light which may blur the picture; U --distance to focus plane (in object space, mm); f --Focal length of lens, mm.

When camera has been set up, these parameters are also fixed, and DOF is fixed consequently. Hence, we can measure DOF by detecting the critical position where the image turns from sharp to blurred, or vice versa.

To obtain the DOF of the high-speed filming system, a DOF measurement system has been designed and arranged as shown in Figure 3.38. The bubbles are in the water and

stick to the side glass wall. The material of the side wall is same with the sight-glass (3 mm glass). The critical position can be found by continuously adjusting subject distance (the distance from camera lens to the bubble).

As shown in Figure 3.38, the light source and sight-glass filled with water were fixed on the table. And high-speed Camera was fixed on the slider. The screw pitch was marked with angles and measured. When the slider moves, pictures of various positions can be captured and marked. All these images are going to be analysed by MATLAB programme. According to the results, the DOF was calculated based on the range of sharp bubbles which are recognised by programme. Hence, the depth of focal plane can be obtained by measuring the distance of two critical positions. 11 identical experiments were carried out to get a mean value of DOF with the standard error of mean, as shown in Table 3.6.

By conducting this test, initially, the camera should be adjusted in a place very close to the bubble, where the image, could be judged by eye, is blurred. The movement of the camera towards a direction closing to the bubble leads to the image becoming sharper and more precise. When the bubble is first identified as a sharp one by the MATLAB program, it represents the lower critical position of DOF has been found. And keep moving the camera until the bubble is finally identified as a blurred bubble again. And this represents the last sharp position is the upper critical position of DOF.

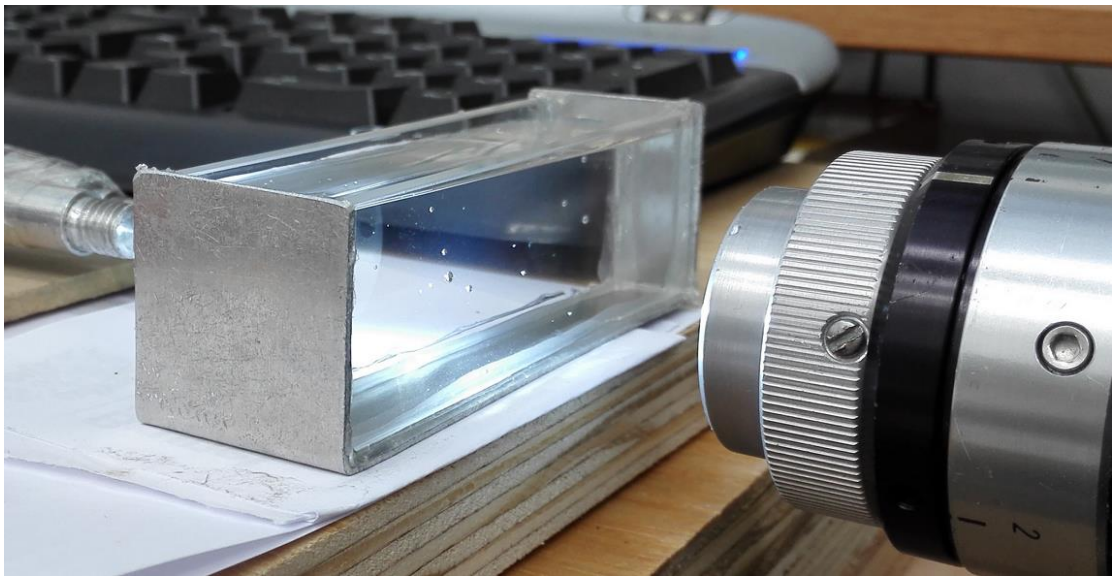

Figure 3. 38. DOF Measurement Test

Figure 3.39 shows the bubble series images taken from a lower position to a higher position, which illustrates that a series of continuously bubbles gradually change from blurred to sharp, and back to blurred again.

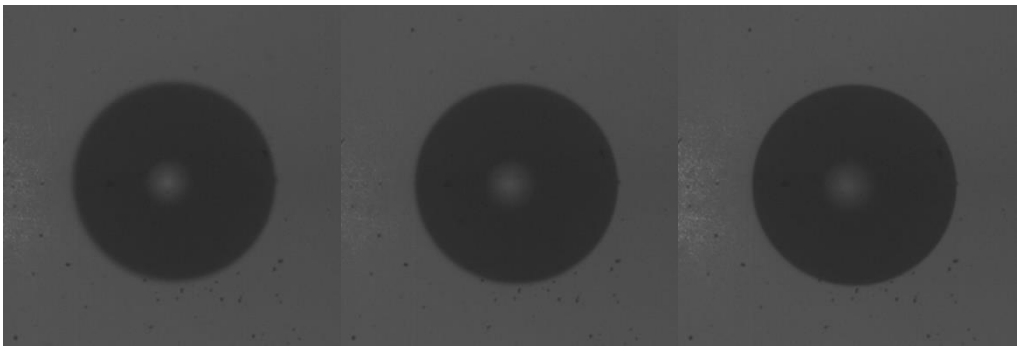

(a) (b) (c)

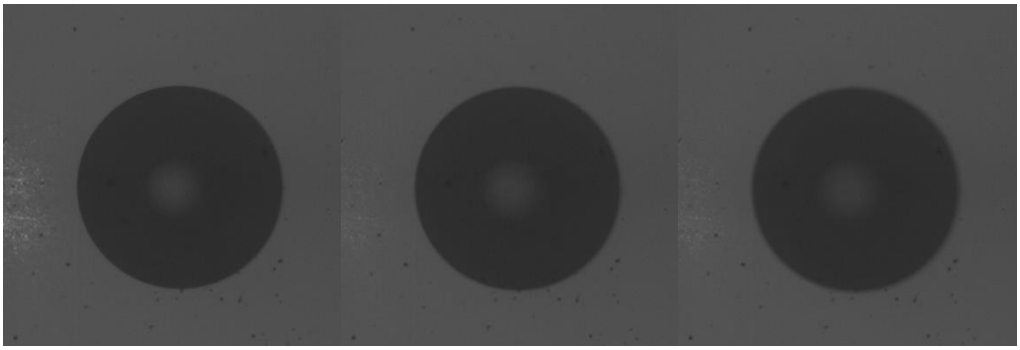

(d) (e) (f)

Figure 3. 39. Image of a bubble with continues changes of subject distance

Figure 3.40 shows the images near the critical position, in which image A is identified as a blurred one and the image B is identified as a sharp one.

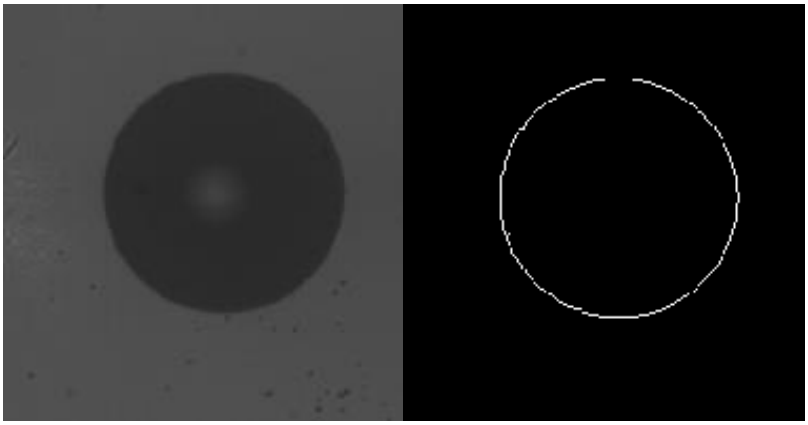

(a) Image A **(b) Processed image of image A**

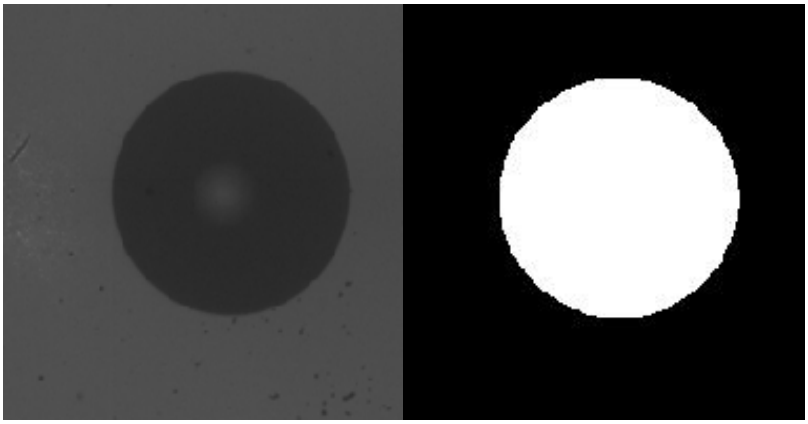

(c) Image B **(d) Processed image of image B**

Figure 3. 40 Two images near the critical position and after procession

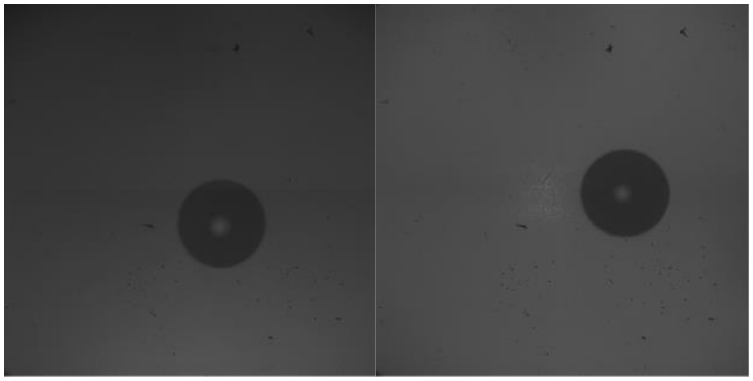

Figure 3. 41 Bubble Attached at Glass Wall

Table 3. 5 Experimental result of DOF measurement

Index	DOF /(mm)	Index	DOF /(mm)
1	**0.6647**	**6**	**0.6008**
2	**0.6967**	**7**	**0.5049**
3	**0.5688**	**8**	**0.6647**
4	**0.5369**	**9**	**0.5049**
5	**0.6008**	**10**	**0.6967**
11	**0.6647**	**Average**	**0.6095 ± 0.022**

As shown in Table 3.5, the average result of DOF is calculated as 0.6095mm, and the standard error of mean is 0.022 mm. The repeat tests have been conducted, and the result of the depth of focal plane is accurate.

3.4 Experimental methodology

3.4.1 Introduction

To conduct the aim and objectives as described in the preceding chapters, an elaborate experimental methodology is introduced in this chapter. Section 3.4.2 introduces the test procedures during the experiment. Section 3.4.3 explains how to achieve the lowest saturation ratio. Section 3.4.4 presents how to investigate the effect of system pressure on the bubble size and production at the heat pump exit. A summary test conditions carried out at the heat pump exit has been shown in Table 3. 6. In addition, section 3.4.5 presents how to investigate the effect of system water flow rate on the bubble size and production at the heat pump exit. Finally, section 3.4.6 introduces the test to investigate the bubble production in return pipe to heat pump.

A summary of the test conditions conducted has been shown in Table 3.6. In total, there are about eight series tests have been conducted to achieve specific aims. In Table 3. 6, superficial water velocities are calculated by using water flow rates over the cross-sectional area of the pipe. The series 1-LS investigated the lowest saturation ratio of the water in the system. The series 2-EP investigated the effect of system pressures at water flow rate 1000 l/h on bubble diameters. The series 3-EP investigated the effect of system pressures at water flow rate 850 l/h on bubble diameters. The series 4-EF investigated the effect of water flow rates at system pressure 2.5 bar on bubble diameters. The series 5-EF investigated the effect of water flow rates at system pressure 2.2 bar on bubble diameters. The series 6-ES investigated the effect of saturation ratios on bubble diameters.

Table 3. 6 Summary of the test conditions

Test series	Water flow rate (l/h)	Superficial water velocity (m/s)	Pressure at heat pump exit (abs-bar)	Temperature at heat pump exit (℃)	Saturation ratio (-)
1-LS	1000	0.88	2.5	55	1.20-1.00
2-EP	1000	0.88	2.2-2.7	55	1.15-1.00
3-EP	850	0.75	1.7-2.5	55	1.15-1.00
4-EF	800-1100	0.71-0.97	2.5	55	1.15-1.00
5-EF	800-1150	0.71-1.02	2.2	55	1.15-1.00
6-ES	800-1100	0.71-0.97	2.2-2.7	55	1.15-1.00
7-CM	1000	0.88	2.4	55	1.07-1.00

8-RT	800-1100	0.71-0.97	2.2-2.5	55	1.15-1.00
9-VF	850-1100	0.75-0.88	2.2-2.7	55	1.15-1.00

The series 7-CM investigated the highest saturation ratio of the city main water in the system without nitrogen injection. The series 8-RT investigated the bubble production in the return position. The series 9-VF investigated the void fraction at various conditions. The results are going to discuss in each section respectively.

3.4.2 Test procedures

In this section, the experimental procedures based on the order are described. The focal plane investigated are set by controlling the adjustable slider manually. The experimental procedure is not very complicated but incredibly time-consuming. One day can only investigate one test condition due to the complex of the experiment. A detailed introduction of experimental procedure has been organised. In this way, it is easy to follow the experimental procedure and avoid the happening of mistakes. The following example shows the process for each test.

Test Procedure

Step 1: Decide next experimental conditions
➢ Inject or release water to increase or decrease system pressure
Step 2: Inject nitrogen into buffer vessel.
➢ The amount of nitrogen is quantitative
➢ Increase the pressure of system to a specific value
Step 3: Open circulating pump
➢ Enhance the dissolution of nitrogen gas
Step 4: Wait 9 hours
➢ Wait for the process of dissolution of nitrogen gas
Step 5: Open LabVIEW program
➢ Check all conditions
Step 6: Put the sensors of heat pump system into cold environment
➢ Put the sensor of outdoor unit into ice box (0 ℃)
➢ Put the sensor of indoor control panel into ice box (5 ℃)
Step 7: Close circulating pump
Step 8: Open buffer vessel circulating pump

Step 9: Open valves of TGM
➢ Check the accuracy of TGM
Step 10: Set up camera system
➢ Fix and open the position of light source
➢ Power on the camera and open the Phantom 663 software
➢ Fix the focal plane of camera
➢ Calibrate camera settings
➢ Make a testing record and check the quality of video
Step 11: Power on heat pump system (7 kW)
Step 12: Set target temperature 38 ℃ at UI control panel
Step 13: Set target supply temperature 55 ℃ at LabVIEW
Step 14: Adjust water flow rate by using buffer vessel inlet valve (1 flow rate each day)
Step 15: When temperature of TGM reaches 30 ℃
➢ Open cooling system for TGM
Step 16: Open AAV to release gas from buffer vessel
➢ Make sure system pressure drops slowly
Step 17: When all conditions reach target values
➢ Start to record data and videos
Step 18: Save data and videos in the order
➢ Convert video file format from *. Cine into *. AVI
➢ Use MATLAB self-code program analysing pictures
Step 19: Power off heat pump system
Step 20: Close camera system
Step 21: Cool down the system temperature below 30 ℃
Step 22: Close the valves of TGM

After the data measurement, the post processing is taken to calculate the results and make the result visualization. The data was recorded by computer as described in section 3.2.4.

3.4.3 Lowest saturation ratio investigation

There is no such investigation on the lowest saturation ration in public literature. One of the main objectives is to know is there bubble production in the air-source heat pump water heating system. Hence, this test has the priority to be designed and conducted first. If there is bubble production in the heat pump water heating system, it means the dissolved gas in the water come off. Therefore, the lowest saturation ratio can be

achieved by running the heat pump system continuedly till there is no gas come off.

The lowest saturation ratio leads to the design of other experimental conditions. As illustrated in Table 3.7, The designed water flow rate is 1000 l/h. The Superficial water velocity is 0.88 m/s. The pressure at the heat pump exit is 2.5 abs-bar. The saturation ratio is going to be measured and recorded during the test.

Andrew and Ali have achieved the lowest saturation ratio 0.4 at gas boiler water heating system (Shefik, 2015). The comparison of the lowest saturation ratio between the gas boiler and heat pump can help the air-vent industry design their products.

Table 3. 7 Test condition for the lowest saturation ratio investigation

Water flow rate (l/h)	Superficial water velocity (m/s)	Pressure at heat pump exit (abs-bar)	Temperature at heat pump exit (℃)	Saturation ratio (-)
1000	0.88	2.5	55	1.20-1.00

3.4.4 The effect of the system pressure on the bubble size and production at heat pump exit

There is an effect of the system pressure expected on the bubble behaviours in the heat pump water heating system as this effect is presented in Ali's thesis (Shefik, 2015). Hence, serious test conditions are designed to investigate the effect of the system pressure as shown in Table 3.8.

During the tests, it is essential to make sure all the conditions are fixed on the same value except the system pressures. There are two series of tests have been conducted which are 2-EP and 3-EP respectively. The EP represents effect of pressures. The reason of 1000 l/h and 850 l/h used to investigate the effect of pressures is these water flow rates are close to the actual flow rate applied. And various pressures were investigated to find out the effect based on the requirements of the company, Spirotech.

Table 3. 8 Test conditions for investigating the effect of the system pressure

Test series	Water flow rate (l/h)	Superficial water velocity (m/s)	Pressure at heat pump exit (abs-bar)	Temperature at heat pump exit (℃)	Saturation ratio (-)

2-EP	1000	0.88	2.2	55	1.15-1.00
2-EP	1000	0.88	2.35	55	1.15-1.00
2-EP	1000	0.88	2.5	55	1.15-1.00
2-EP	1000	0.88	2.7	55	1.15-1.00
3-EP	850	0.75	1.7	55	1.15-1.00
3-EP	850	0.75	1.9	55	1.15-1.00
3-EP	850	0.75	2.1	55	1.15-1.00
3-EP	850	0.75	2.3	55	1.15-1.00
3-EP	850	0.75	2.5	55	1.15-1.00

In the 2-EP series, the water flow rate is set at 1000 l/h, which represents the superficial water velocity is 0.88 m/s. The superficial water flow rate is an essential factor which contributes the flow regime with superficial gas flow rate in the two-phase bubbly flow. It has not been studied intensively in the horizontal pipe in the open literature, and a few tests have been done in high superficial speed region which is not suitable for the air-source heat pump water heating system. And the pressures at the heat pump exit are set as 2.2, 2.35, 2.5 and 2.7 abs-bar respectively. These pressures are the variable factors in this series test. Furthermore, the temperature at the heat pump exit is set as 55 ℃ which is a simulative value with the domestic hot water condition. The saturation ratio is in the range from 1.15 to 1.00. The bubble images have been recorded at the conditions of four saturation ratios which are 1.15, 1.10, 1.05 and 1.00 respectively.

In the 3-EP series, the water flow rate is set at 850 l/h, which represents the superficial water velocity is 0.75 m/s. And the pressures are set as 1.7, 1.9, 2.1, 2.3 and 2.5 abs-bar. In addition, the temperature at heat pump exit is set as 55 ℃. The saturation ratios change from 1.15 to 1.00 as well.

After the data processing, the comparison of results at these test conditions can illustrate the effect of the system pressures on the bubble behaviours.

3.4.5 The effect of system water flow rate on the bubble size and production at heat pump exit

The water flow rate supposed to be another factor affects the bubble flow behaviours in the air-source water heating system (Fsadni, Ge and Lamers, 2012). Therefore, two series test conditions are designed to study the effect of the system water flow rate on

the bubble behaviours as shown in Table 3.9.

Table 3. 9 Test conditions for investigating the effect of the system water flow rate

Test series	Water flow rate (l/h)	Superficial water velocity (m/s)	Pressure at heat pump exit (abs-bar)	Temperature at heat pump exit (℃)	Saturation ratio (-)
4-EF	800	0.71	2.5	55	1.15-1.00
4-EF	850	0.75	2.5	55	1.15-1.00
4-EF	900	0.80	2.5	55	1.15-1.00
4-EF	950	0.84	2.5	55	1.15-1.00
4-EF	1000	0.88	2.5	55	1.15-1.00
4-EF	1050	0.93	2.5	55	1.15-1.00
4-EF	1100	0.97	2.5	55	1.15-1.00
5-EF	800	0.71	2.2	55	1.15-1.00
5-EF	900	0.80	2.2	55	1.15-1.00
5-EF	1000	0.88	2.2	55	1.15-1.00
5-EF	1100	0.97	2.2	55	1.15-1.00
5-EF	1150	1.02	2.2	55	1.15-1.00

In 4-EF series, the pressure at heat pump exit is set as 2.5 abs-bar. And the temperature at heat pump exit is 55 ℃. As this series tests are designed to study the effect of the system flow rate, the system water flow rates are variable factors. Hence, the system water flow rates are set as 800, 850, 900, 950, 1000, 1050 and 1100 l/h. The superficial water velocities are 0.71, 0.75, 0.80, 0.84, 0.88, 0.93 and 0.97 m/s respectively. Four saturation ratios, 1.15, 1.10, 1.05 and 1.00, are the filming conditions as well.

In 5-EF series, the system water flow rates are set as 800, 900, 1000, 1100 and 1150 l/h respectively. The superficial water velocities are 0.71, 0.80, 0.88, 0.97 and 1.02 m/s respectively. In this series, the system pressure is set as 2.2 abs-bar to study the effect of the water flow rate at different system pressures. The two series tests can make sure to achieve the accurate the relationship between the bubble behaviours and the water flow rates.

After the data processing, the comparison of results at these test conditions can illustrate the effect of the water flow rates on the bubble behaviours.

3.4.6 The effect of the saturation ratio

As discussed in the Ali's thesis, the saturation ratio is proved to affect the bubble production in the gas boiler water heating system (Shefik, 2015). Hence, the saturation ratio is expected to affect the bubble production in the heat pump water heating system. A series of test results are summarised to find out the effect of the saturation ratio on the bubble behaviours as shown in Table 3.10.

Table 3. 10 Test conditions for investigating the effect of the saturation ratio

Test series	Water flow rate (l/h)	Superficial water velocity (m/s)	Pressure at heat pump exit (abs-bar)	Temperature at heat pump exit (℃)	Saturation ratio (-)
6-ES	800-1100	0.71-0.97	2.2-2.7	55	1.15-1.00

The higher the saturation ratio, the higher the bubble production is supposed to be. The comparison of the results can identify the assumption. In addition, the relationship between the bubble average diameter and the saturation ratio can be found.

3.4.7 Bubble production in return pipe to the heat pump

Bubble production in the heat pump inlet is another aim of this project. There is no information published in open literature about the bubble production in the return pipe to the heat pump. Considering the bubble generation principle, it is interesting to find out whether there is bubble production in the heat pump inlet as the pressure of heat pump inlet is lower than the heat pump exit. The bubble generation principle in the heat pump water heating system is explained in the section 4.2. The test conditions are shown in Table 3.11.

Table 3. 11 The test conditions for investigating the bubble production in the return pipe

Test series	Water flow rate (l/h)	Superficial water velocity (m/s)	Pressure at heat pump exit (abs-bar)	Temperature at heat pump exit (℃)	Saturation ratio (-)

8-RT	800-1100	0.71-0.97	2.2-2.5	55	1.15-1.00

3.4.8 City main water test

For industrial interests, a test has been done to find out the highest saturation ratio with filling the city main water at 10 ℃ outdoor temperature. The test conditions are shown in Table 3.12.

Table 3. 12 The test conditions for investigating the highest saturation ratio of the city main water with 10 ℃ outdoor temperature

Test series	Water flow rate (l/h)	Superficial water velocity (m/s)	Pressure at heat pump exit (abs-bar)	Temperature at heat pump exit (℃)	Saturation ratio (-)
7-CM	1000	0.88	2.4	55	1.07-1.00

This test provides the insight of the actual working condition of the air-source heat pump water heating system.

3.5 Data reduction

As described in the objectives of this thesis, to study the bubble behaviours in the domestic air-source heat pump water heating system, there are some parameters used for investigation. However, these parameters cannot be investigated immediately. These parameters such as saturation ratio, bubble volume, volumetric void fraction and superficial flow rate are calculated. This section presents how these parameters are calculated.

3.5.1 Saturation ratio

The saturation ratio is an important parameter for studying the bubble behaviours in the two-phase flow. It represents the degree of the gas dissolved in the water in this project. The Equation 3.8 is used to calculate the saturation ratio, which is defined by Jones et al. (Jones, Evans and Galvin, 1999).

$$\mathrm{Sr} = \frac{C_{gas}}{C_{sat}} \tag{3. 8}$$

In Equation 3.8, the C_{gas} is the actual dissolved gas mole fraction present in the bulk fluid; The C_{sat} is the maximum mole fraction at saturation conditions.

Dry air consists of 78% Nitrogen, 21% Oxygen and 1% others (Moumouni and Galupa, 2018). The oxidation process in the system leads to iron oxide and hydrogen gas. Hence, Nitrogen is the dominant gas in the closed loop heat pump water heating system. Andrew has proofed this phenomenon in his thesis (Fsadni and Ge, 2012). Hence, the property of Nitrogen is used to represent the properties of the dissolved gas in the study. The C_{gas} and C_{sat} are needed to be calculated to get the saturation ratio at specific conditions.

Equation 3.9 is used to calculate the actual dissolved gas mole fraction, C_{gas}, which is known as the Henry's Law (Perry, Green and Maloney, 1997).

$$C_{gas} = \frac{p_g}{H} \tag{3. 9}$$

In Equation 3.9, the P_g (pa) is the partial gas pressure, which can be calculated by the following Equation 3.10: The H is calculated based on the T_{TGM}, which represents the Henry's law proportionality constant.

Lubetkin introduced that the total gas pressure P_{TGM} is equal to the sum of vapour pressure P_v and partial pressure of gas P_g as shown in Equation 3.10 (Lubetkin and Blackwell, 1988).

$$Total\ Gas\ Pressure\ P_{TGM} = Vapour\ pressure\ P_v + Partial\ pressure\ of\ gas\ p_g$$

(3. 10)

The total gas pressure P_{TGM} can be measured by the pressure transducer. The vapour pressure P_v can be calculated based on the temperature of the liquid. Hence, the partial gas pressure P_g can be obtained by using P_{TGM} subtracts the P_v.

Equation 3.11 can be obtained by combining Equation 3.8, Equation 3.9 and Equation 3.10. Equation 3.11 is used to calculate saturation ratios.

$$SR = \frac{Actual\ air\ mole\ fraction}{maximum\ air\ mole\ fraction} = \frac{\frac{P_g}{H_{T_{TGM}}}}{\frac{P_{sat}}{H_{T_{sg}}}} = \frac{\frac{P_{TGM} - f_1(T_{TGM})}{f_2(T_{TGM})}}{\frac{P_{sg} - f_1(T_{sg})}{f_2(T_{sg})}}$$

(3. 11)

$$f_1 = 3.15232721856732 \times 10^{-14} \times x^6 + 3.66127774257229 \times 10^{-11} \times x^5 + 1.84328324132066 \times 10^{-9} \times x^4 + 3.08107798385748 \times 10^{-7} \times x^3 + 1.35040050608382 \times 10^{-5} \times x^2 + 4.49924430427018 \times 10^{-4} \times x + 6.0991293371444 \times 10^{-3}$$

(3. 12)

$$f_2 = ((2.32758222502898 \times 10^{-11} \times x^6 - 4.99871071662009 \times 10^{-9} \times x^5 + 3.93484457905657 \times 10^{-7} \times x^4 - 2.08339008800351 \times 10^{-5} \times x^3 + 1.51929463299894 \times 10^{-4} \times x^2 + 1.3994852081214 \times 10^{-1} \times x + 5.28392426835126) \times 1000) \times 1.01325$$

(3. 13)

In Equation 3.11, T_{sg} is the temperature at heat pump exit position, and P_{sg} is the pressure at heat pump exit position. Besides, P_{TGM} is the pressure of the TGM (Total Gas Measurement), and T_{TGM} is the temperature of the TGM. Equation 3.12 is used to

calculate the vapour pressure at specific temperature, and Equation 3.13 is used to calculate the Henry's constant at specific temperature. Therefore, all the equations involved in the calculation of the saturation ratio have been introduced in this section.

3.5.2 Bubble volume

The bubble volume is calculated based on the bubble diameter provided by the MATLAB programme. There are two situations for the calculation of the bubble volume. As shown in Figure 3.42, the bubbles could be in or out of the focal plane, and the bubble could be in the focal plane with a larger diameter than the depth of the focal plane.

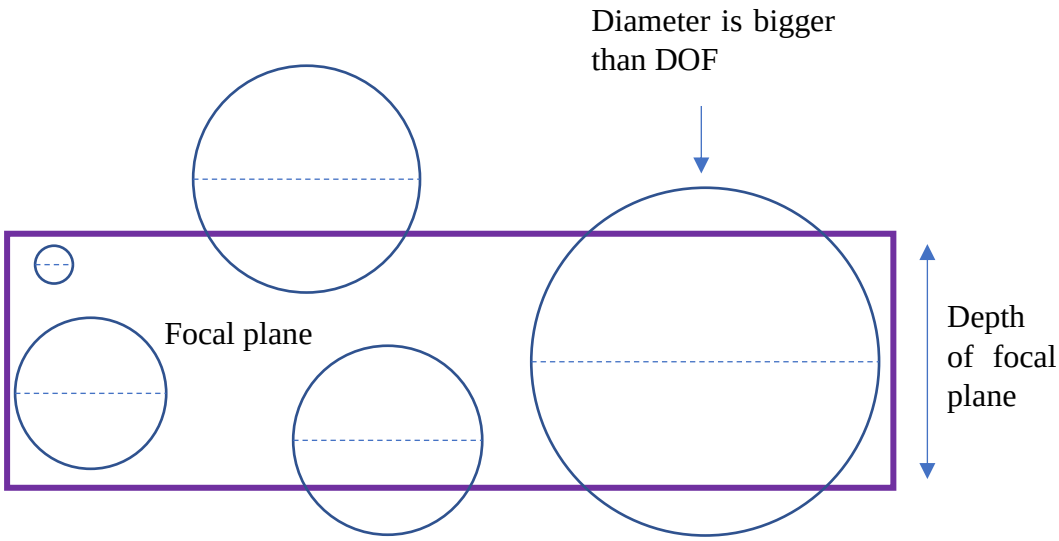

Figure 3. 42 Gab bubbles go through the focal plane

First, when the bubble is in the focal plane with a smaller diameter than the depth of the focal plane, the bubble volume can be calculated by using Equation 3.14.

$$V_b = \frac{1}{6}\pi {d_b}^3 \quad \textbf{(3. 14)}$$

In the second situation, when the bubble is in the middle of the focal plane with a bigger diameter than the depth of the focal plane, the bubble volume can be calculated by using

Equation 3.15 which is proposed by Ali (Shefik, 2015).

$$V_b = DOF \times \frac{\pi}{6} \times \left(\frac{3{d_b}^2}{2} - \frac{3DOF^2}{2} + DOF^2\right)$$

(3. 15)

3.5.3 Volumetric void fraction

The volumetric void fraction is another essential derived parameter to express the bubble production at specific test condition. In the two-phase bubbly flow, the volumetric void fraction represents the volume of the minority phase over the volume of the majority phase as shown in Equation 3.16.

$$\varepsilon_{sample} = \frac{V_{gas\ bubble}}{V_{water}}$$

(3. 16)

In Equation 3.16, the ε_{sample} represents the volumetric void fraction of the sample investigated, the $V_{gas\ bubble}$ represents the total volume of all the gas bubbles in the sample investigated, and the V_{water} represents the volume of the water in the sample investigated.

3.6 Uncertainty Analysis

In engineering experiments, errors exist inevitably in all measurements (Taylor, 1997). These errors of sensors and parameters cannot be avoided in most situations. It should be ensured all the errors are at a minimal level and can be calculated (Taylor, 1997). As described in Taylor's book, errors consist of bias errors and random errors (Taylor, 1997). In this project, the bias errors are repeatable and come from the sensors. The random errors of the repeated tests can be calculated by using the standard error of the mean. The bias errors of the derived parameters can be calculated as introduced in the section. The random errors are nonredundant, and the best method to find the true value is repeated measurement. This section is going to introduce the bias errors of the sensors and the resultant parameters. The standard error of the mean method was used for the repeated tests, which is shown in Appendix V.

Sometimes, errors of resultant parameters depend on more than one factor. For example, a resultant value C is calculated from X_1, X_2, X_3 till to X_n as shown in Equation 3.17.

$$C = f(X_1, X_2, X_3, \dots, X_n)$$

(3. 17)

In the case of $C = X_1 \times X_2$, the deviation of C (δC) can be obtained by using Equation 3.18.

$$\delta C = \frac{\partial C}{\partial X_1}\delta X_1 + \frac{\partial C}{\partial X_2}\delta X_2$$

(3. 18)

In Equation 3.18, δX_1 and δX_2 are the deviations of X_1 and X_2 respectively. The partial derivative $\frac{\partial C}{\partial X}$ represents the differentiating C with respect to X. The law of propagation of the uncertainty can be obtained by squaring the Equation 3.18 and take the average of δX_1 and δX_2 as shown in Equation 3.19 (Taylor, 1997).

$$(\delta C)^2 = (\frac{\partial C}{\partial X_1})^2 {\delta X_1}^2 + (\frac{\partial C}{\partial X_2})^2 {\delta X_2}^2 + 2\frac{\partial C}{\partial X_1}\frac{\partial C}{\partial X_2}\overline{\delta X_1 \delta X_2}$$

(3. 19)

In the case of X_1 and X_2 are uncorrelated, the $\overline{\delta X_1 \delta X_2}$ is zero. Hence, the Equation 3.20 is obtained when there are n factors in the equation of the C.

The Equation is used to calculate the combination of individual errors as shown in Equation 3.20. In this formula, d_c represents the absolute uncertainty of C, dx_1 represents the absolute uncertainty of X_1 and $\frac{\partial C}{\partial X_1}$, differentiating C with respect to X_1, represents the influence coefficient of X_1. The influence coefficient provides the ability to emphasize some main factors and ignore the others. (Taylor, 1997)

$$d_c = \sqrt{(\frac{\partial C}{\partial X_1})^2 {dx_1}^2 + (\frac{\partial C}{\partial X_2})^2 {dx_2}^2 + \cdots + (\frac{\partial C}{\partial X_n})^2 {dx_n}^2}$$

(3. 20)

The relative uncertainty of C (R_c) can be calculated by dividing C at both sides of the

Equation 3.20 as shown in Equation 3.21.

$$R_c = \sqrt{\left(\frac{X_1}{C}\frac{\partial C}{\partial X_1}\right)^2 \left(\frac{d_{x_1}}{X_1}\right)^2 + \left(\frac{X_2}{C}\frac{\partial C}{\partial X_2}\right)^2 \left(\frac{d_{x_2}}{X_2}\right)^2 + \cdots + \left(\frac{X_n}{C}\frac{\partial C}{\partial X_n}\right)^2 \left(\frac{d_{x_n}}{X_n}\right)^2} \quad \textbf{(3. 21)}$$

The uncertainty values of measured of derived parameters have been summarised in Table 3.13. The uncertainty values of measured parameters are obtained during the calibration process. The relative uncertainty of the sensors is calculated based on the maximal difference between the fit line and the line of the calibrated actual conditions. The uncertainty values of derived parameters are calculated by using Equation 3.21 relative uncertainty calculation.

The details of the relative uncertainty of the derived parameters are introduced in the following sections respectively.

Table 3. 13 Summarised uncertainty values

Measured/derived parameter	Instrument category	Uncertainty (%)
T1	K-type_Thermocouples	± 0.37
T2	K-type_Thermocouples	± 0.31
T3	K-type_Thermocouples	± 0.34
T4	K-type_Thermocouples	± 0.34
T5	K-type_Thermocouples	± 0.25
T6	K-type_Thermocouples	± 0.19
T_{TGM}	K-type_Thermocouples	± 0.20
P1	DRUCK_PTX_7500	± 0.44
P2	DRUCK_PTX_7500	± 0.53
P3	DRUCK_PTX_7500	± 0.51
P_{TGM}	Keller_PAA_35S	± 0.27
Water flow rate	Euromag_Electromagnetic_Flowmeter_500	± 0.81
Bubble diameter	MATLAB Programme	± 1.01
Bubble volume	MATLAB Programme	± 3.02
Saturation ratio	LabVIEW	± 3.12

3.6.1 Bubble diameter

The MATLAB programme can distinguish the bubble in or out of the focal plane. It also can count the pixels inside the bubble. Hence, the bubble diameter can be calculated by using Equation 3.22. The length of the pixel is calibrated as described in the preceding section.

$$Bubble\ diameter\ d_b = D_p \times N_p$$

(3. 22)

In Equation 3.22, the D_p represents the length of a pixel, and N_p represents the number of pixels of the bubble diameter.

The absolute uncertainty of the bubble diameter can be calculated by applying Equation 3.20 as shown in Equation 3.23.

$$d_b = \sqrt{(\frac{\partial d_b}{\partial D_p})^2 (dD_p)^2 + (\frac{\partial d_b}{\partial N_p})^2 (dN_p)^2}$$

(3. 23)

The Equation 3.24 is derived from Equation 3.23 by calculating the differentiation.

$$d_b = \sqrt{(N_p)^2 (dD_p)^2 + (D_p)^2 (dN_p)^2}$$

(3. 24)

Hence, the relative uncertainty can be derived by dividing d_b on both side of Equation 3.24 as shown in Equation 3.25.

$$R_b = \sqrt{(\frac{dD_p}{D_p})^2 + (\frac{dN_p}{N_p})^2}$$

(3. 25)

In Equation 3.25, the $\frac{dD_p}{D_p}$ represents the relative uncertainty of the size of the pixel. As described in the previous section, the size of the bubble image is calibrated by the metal

ball. The size of the metal ball is 2 mm ± 0.00254 mm, which is provided by the manufacturer. Hence, the relative uncertainty of the pixel is ± 0.127%. Besides $\frac{dN_p}{N_p}$ is the relative uncertainty of the number of pixels of the diameter of the bubble. Sometimes, the shapes of the gas bubbles are irregular, which leads to the uncertainty. This value is found out to be ±1% by analysing the bubble data.

The relative uncertainty of bubble diameter can be calculated by substituting the relative uncertainty of the pixel and the relative uncertainty of the number of pixels into Equation 3.25 as shown in Equation 3.26.

$$R_{bubble\ diameter} = \sqrt{(0.127\%)^2 + (1\%)^2} = 1.008\% \quad \textbf{(3. 26)}$$

3.6.2 Bubble volume

As introduced in the preceding section, the bubble volume is calculated by using Equation 3.14. The absolute uncertainty of the bubble volume can be got by substituting Equation 3.14 into Equation 3.20 as shown in Equation 3.27.

$$d_{bubble\ volume} = \sqrt{\left(\frac{\partial V_b}{\partial d_b}\right)^2 (d_{d_b})^2} \quad \textbf{(3. 27)}$$

Equation 3.28 is obtained by calculating the differentiation in Equation 3.27.

$$d_{bubble\ volume} = \sqrt{\left(\frac{\pi {d_b}^2}{2}\right)^2 (d_{d_b})^2} \quad \textbf{(3. 28)}$$

Hence, the relative uncertainty of the bubble volume can be calculated by dividing Equation 3.28 by Equation 3.14 as shown in Equation 3.29.

$$R_{bubble\ volume} = \frac{\sqrt{\left(\frac{\pi {d_b}^2}{2}\right)^2 (d_{d_b})^2}}{\frac{1}{6}\pi {d_b}^3} = 3 \times \left(\frac{d_{d_b}}{d_b}\right) = 3 \times 1.008\%$$
$$= 3.024\%$$

(3. 29)

As shown in Equation 3.29, the relative uncertainty of the bubble volume is ±3.024%

3.6.3 Saturation ratio

The saturation ratio is calculated by using Equation 3.11. The relative uncertainty of the saturation ratio can be calculated by using the same method as the preceding derived parameters. The summarised equation is introduced in this section, and the process of calculating is not going to be presented as the complex calculating.

The absolute uncertainty of the C_{gas} is calculated as shown in Equation 3.30.

$$d_{C_{gas}} = \sqrt{\left(\frac{\partial C_{gas}}{\partial P_{TGM}}\right)^2 (d_{P_{TGM}})^2 + \left(\frac{\partial C_{gas}}{\partial P_v}\right)^2 (d_{P_v})^2 + \left(\frac{\partial C_{gas}}{\partial H}\right)^2 (d_H)^2}$$

(3. 30)

Relative uncertainty of C_{gas} can be derived by calculating the differentiation in Equation 3.30 and dividing by C_{gas} as shown in Equation 3.31.

$$R_{C_{gas}} = \sqrt{(\frac{d_{P_{TGM}}}{P_v - P_{TGM}})^2 + (\frac{d_{P_v}}{P_v - P_{TGM}})^2 + (\frac{d_H}{H})^2}$$

(3. 31)

In an equivalent way, the relative uncertainty of the amount of the dissolved gas at saturated condition can be derived as shown in Equation 3.32.

$$R_{C_{sat}} = \sqrt{(\frac{d_{P_2}}{P_{v2} - P_2})^2 + (\frac{d_{P_{v2}}}{P_{v2} - P_2})^2 + (\frac{d_H}{H})^2}$$

(3. 32)

Hence, the relative uncertainty of the saturation ratio can be derived by using Equation 3.31 as shown in Equation 3.33.

$$R_{SR} = \sqrt{(\frac{d_{C_{act}}}{C_{act}})^2 + (\frac{d_{C_{sat}}}{C_{sat}})^2}$$

(3. 33)

3.7 Summary

This chapter introduced the brief test equipment, data logging and processing information, the fundamental theory used in this project and the test conditions to achieve the aims of this project. This chapter provides the insight of how to conduct the two-phase horizontal bubbly flow tests and how to convert the video data to the digital data. First, the function of the mechanical parts of the test rig is explained. Second, the data logging system is introduced in detail. Thirdly, the image process method is presented in several sections which include the MATLAB programme, calibration of the size of the bubble image, depth of the focal plane measured and the obtainment of the depth of field. The MATLAB programme code is attached in the appendix. The light refraction in the filming system is illustrated in the figure. Besides, the experimental methodology is provided. The effects of the several parameters are investigated in the air-source heat pump water system. Furthermore, the calculations of the several parameters are introduced including the saturation ratio, bubble volume, void fraction and superficial flow rate. Finally, the uncertainties of the derived parameters are discussed and calculated.

Chapter 4 Results and discussion

4.1 Introduction

The test conditions presented in the experimental methodology has been achieved and this chapter is going to introduce and discuss the experimental results. There are three parameters might affect the gas bubble two-phase horizontal flow behaviours in the air-source domestic water heating system and these parameters are varied in the experiment to study the effect of each parameter. The investigated parameters include system fluid flow rate, system pressures and system saturation ratios. Both the bubble average diameters and bubble void fractions at various conditions are investigated. The bubble production behaviour has proved the theoretical analysis in Figure 4.3.

It should be mentioned that the number of processed images is in a large quantity. And the differences between processed images are bubble numbers that recognized. Therefore, representative processed images are presented in Appendix VI.

This chapter is organised as follows; First, section 4.2 introduces the typical experimental conditions achieved. Second, section 4.3 illustrates the lowest saturation ratio achieved by keep running the heat pump system. In addition, section 4.4 presents and discusses the bubble size characteristics and section 4.5 talks about the bubble void fraction characteristics. Besides, section 4.6 discusses the bubble production rate, and section 4.7 introduces the city main water test. Finally, section 4.8 discusses the flow regime of two-phase horizontal flow and section 4.9 summaries this chapter.

4.2 Typical experimental conditions achieved

This section briefly introduces the typical experimental conditions achieved during one test. The temperatures and pressures measured by the sensors are plotted in Figure 4.1. The saturation ratio is shown in the figure as well.

Figure 4. 1 shows the experimental conditions from 50 minutes to 310 minutes, which is suitable to conduct the test. The locations of these sensors can be found in Figure 3.1. The purple line represents the water temperature of the heat pump exit, which is set at

55 ℃ in purpose. The blue line represents the water temperature of the heat pump inlet, which is around 48 ℃. This temperature is affected by the heat pump capacity and the cooling system load. The light red line represents the pressure of the heat pump exit, which is around 2.5 bar. This pressure is adjustable by injecting or releasing the water of the test system. The dark green line represents the pressure of the buffer vessel, which is around 2.15 bar. The light blue line represents the pressure of the heat pump inlet, which is around 2.05 bar. The dark red line represents pressure of the total gas measurement equipment, which is decreasing along with the experimental time. This is due to the gas comes off the water and flows off from the system through the air-vent. According to the equation of the saturation ratio, the decrease of pressure of total gas measurement results in the reduction of saturation ratio. The orange line represents the temperature of the total gas measurement, which is around 30 ℃. This temperature is in the range of its working temperature. The grey line represents the actual gas dissolved in the water. The yellow line represents the saturated condition of the dissolved gas in the water. The light green line represents the saturation ratio, which decreases from 1.17 to 1.0.

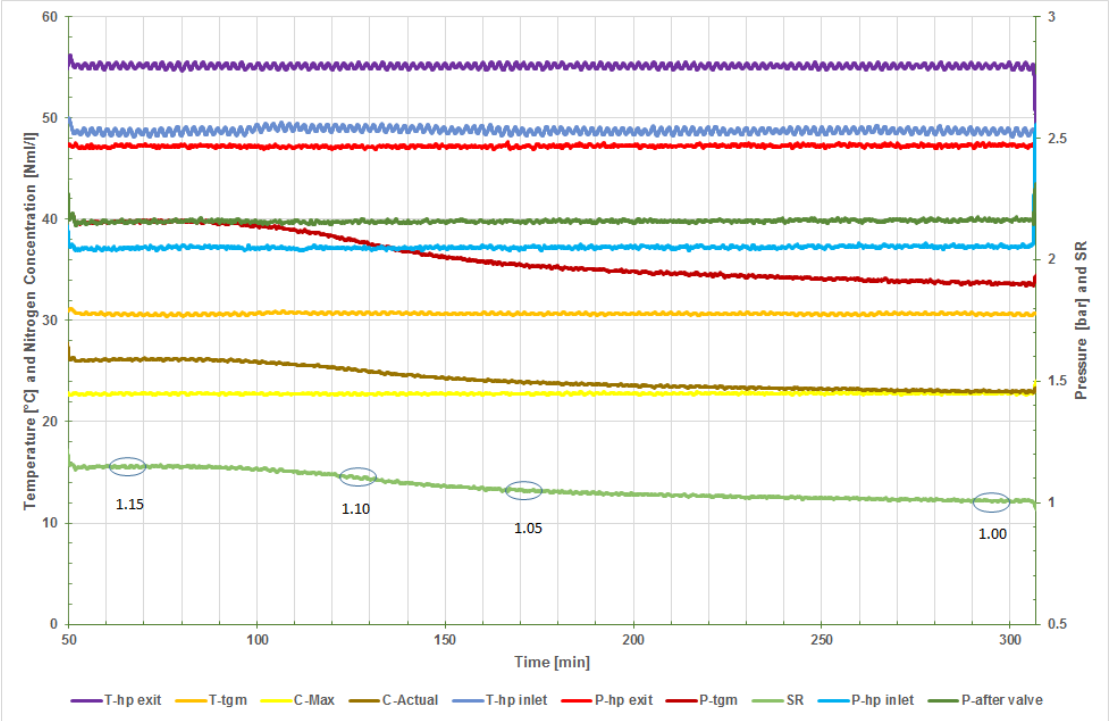

Figure 4. 1 Typical experimental conditions

There are four circles in the figure highlight when the films were taken at specific saturation ratios. There are four saturation ratios have been investigated which are 1.15,

1.10, 1.05 and 1.00 respectively. These saturation ratios stand for the supersaturated water conditions. As explained in the section 4.2, due to the low wall temperature of the plate heat exchanger of the heat pump, the undersaturated condition does not need to be investigated, which means no bubble exist.

4.3 Lowest saturation ratio achieved by keeping the system run

The lowest achievable saturation ratio of the air-source heat pump water heating system is an essential information for this project. This value leads to the design of experimental conditions. The system was maintained to keep running about 9 hours till to the stabilization of the value of saturation ratios. As illustrated in Figure 4.2, the lowest SR at supply position (SG1) achieved is around 1. As the decreasing trend shown in Figure 4.2, saturation ratios would take longer time to reach lower than one. The test cannot run for longer time as the limitation of the open-time of the laboratory. However, this lowest saturation ratio is verified by all the experiments achieved. There is no more bubble as the saturation ratio reached lower than one, which means the saturation ratio cannot decrease due to no gas bubble come off from the water.

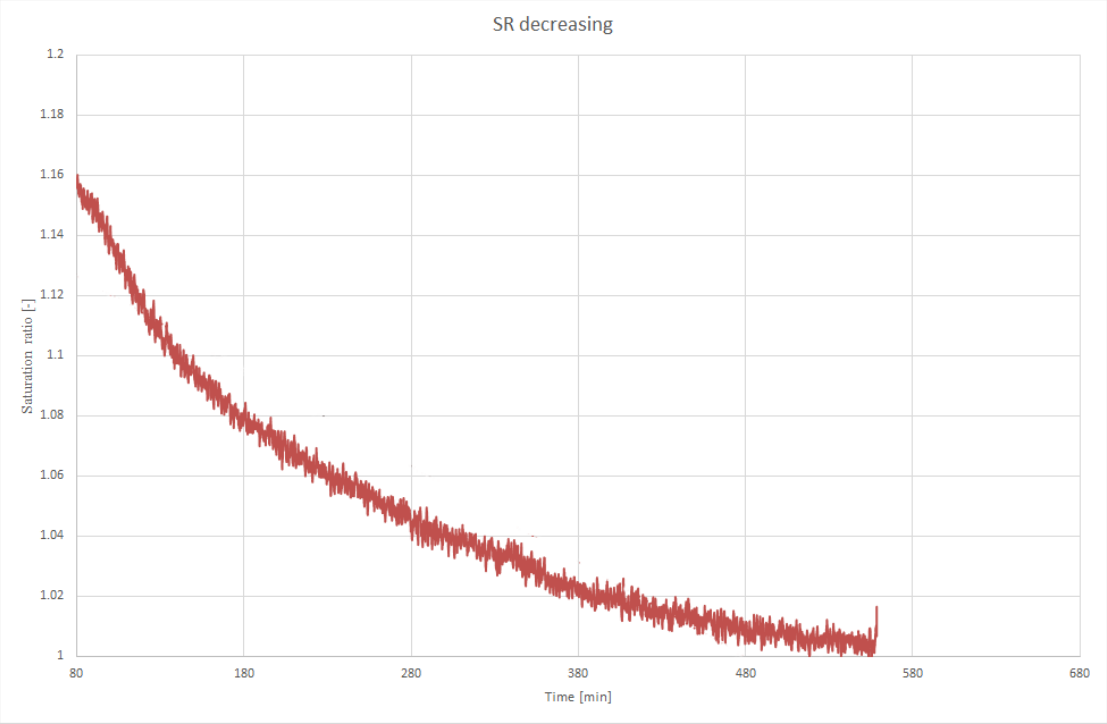

Figure 4. 2 Lowest saturation ratios achieved by keeping the system run

The lowest saturation ratio depends on the wall temperature of the plate heat exchanger of the air-source heat pump. This is different from the gas boiler which can let SR keep decreasing.

It is essential to compare the wall temperature between the heat pump and gas boiler, which can help understand the differences in bubble production between a gas boiler and a heat pump. The flame temperature of Methane (natural gas) in air is 1950 °C/3542 °F. The refrigerant goes into the plate heat exchanger at around 90 °C. The following figure illustrates 0 ml N2 can dissolve in the water if the temperature is more than 130 °C at 2.5 bar.

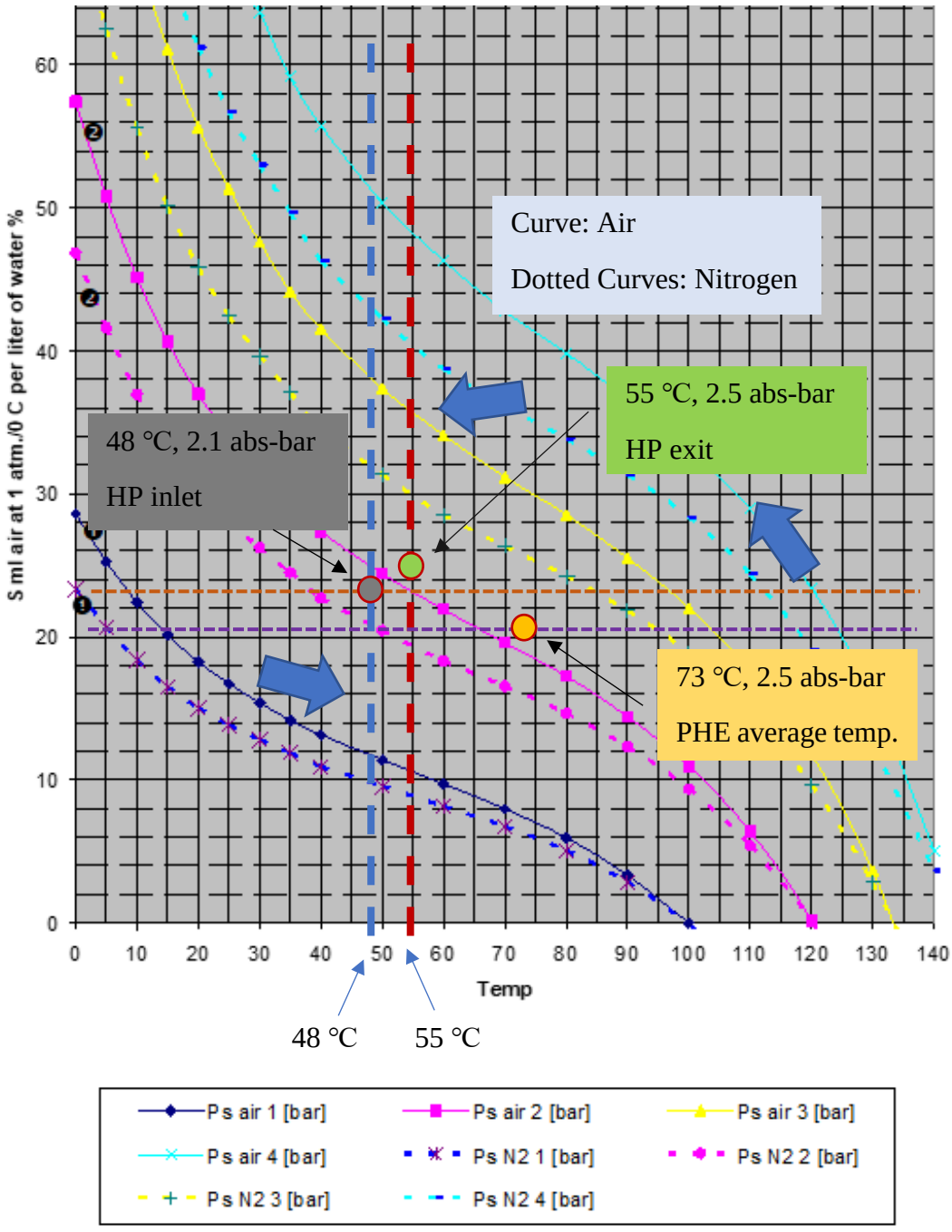

Figure 4. 3 Air and Nitrogen dissolution data

In another way, there would be gas bubble production at the heat transfer wall in gas boiler even though the actual dissolved gas in water is 10 ml per litre, which is a very low value. But at the same condition, there would not be gas bubble production because the highest temperature is about 90 °C which is smaller than 115 °C. (10 ml/litre: 115 °C) In addition, the effects of sub-cooled boiling in gas boiler is uncertain. The steam bubble my speed up the gas bubble production. But there is no sub-cooled boiling in heat pump system.

As illustrated in Figure 4.3, the situation at the wall of the plate heat exchanger in the heat pump, the situation at heat pump inlet and the situation at the heat pump exit have been shown. The water in the system goes through these positions in the directions as the arrow shows. When the actual N_2 dissolved in the water more than max N_2 at these three positions, the gas bubble generation would happen at each position.

The temperature thermocouple is fixed on the surface of the refrigerant pipe of the heat pump rather than installing a temperature thermocouple inside the pipe to avoid causing other factors affect the bubble production. Hence, the reading value of the refrigerant plate heat exchanger inlet is not the average temperature inside the micro channel of the plate heat exchanger. There is a way to estimate the average wall temperature between the refrigerant and water channels in the plate heat exchanger by checking the air and nitrogen dissolution chart (see Figure 4.3). The actual dissolved N2 and the pressure and temperature conditions affect the gas bubble production at certain time. When there is no more bubble production or SR stop decreasing, it reflects the actual dissolved gas is equal to the max dissolved gas in the water. When SR is 1, the actual dissolved gas is about 23 ml/litre. Therefore, the average heat transfer wall temperature should be more than, but close to 73 °C.

4.4 Bubble diameter characteristics

Bubble diameter characteristics is an essential part of this project. The experimental methodology was proposed to investigate the bubble diameter behaviours at the heat pump exit. As shown in Figure 4.4, several test conditions had been achieved to study the bubble diameter behaviour. Bubble diameter in the piping system at the heat pump exit could be affected by several factors such as system pressure, system water flow rate and system water flow rate. This section is going to study and discuss the effects of these factors respectively. First, section 4.4.1 presents the effect of system pressures. Second, section 4.4.2 introduces the effect of system water flow rates. In addition, section 4.4.3 illustrates the effect of the system saturation ratios. Finally, section 4.4.4 presents the bubble diameter distribution at the heat pump exit and proposes the prediction function of bubble diameter distribution at heat pump exit.

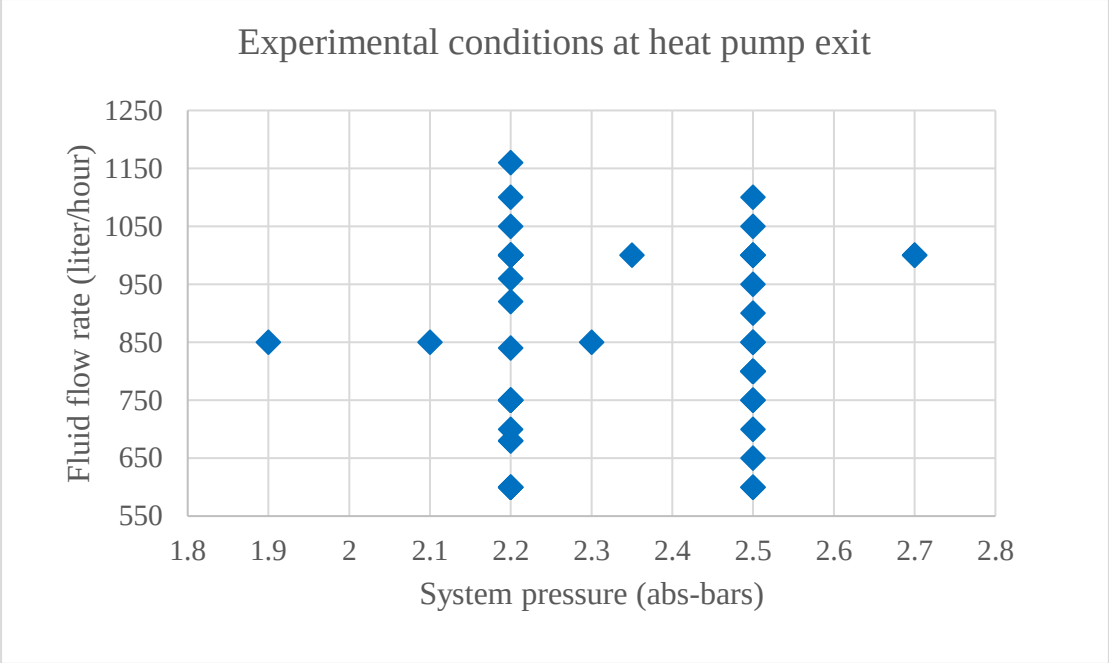

Figure 4. 4 The experimental conditions investigated on heat pump exit position

4.4.1 Effect of system pressures

The effect of system pressures is tested in two series investigations which are at 1000 l/h and 850 l/h respectively. The codes of the two series are 2-EP and 3-EP as described in the methodology. Figure 4.5 illustrates the relationship between the average bubble diameter and the heat pump exit pressure at 1000 l/h. In this series of tests, the system pressures were set at 2.2, 2.35, 2.5 and 2.7 absolute bars respectively. At the heat pump exit, the temperature of the supply water is 55 ℃. The standard error of mean is calculated to represent the uncertainties of the average bubble diameters at each test condition. The data of uncertainties is attached in Appendix I.

As shown in Figure 4.5, the average bubble diameters of four pressures are around 0.09 mm. This value is smaller than the 0.12 mm of the average bubble diameter in the gas boiler water heating system (Shefik, 2015). The effect of the exit pressure in the gas boiler system is reported by (Shefik, 2015) that there is no significant effect on the average bubble diameter. In another way, the average bubble diameters at different system pressures are quasi-constant in the gas boiler system.

However, Figure 4.5 shows that the average bubble diameters decrease along with the increase of the heat pump exit pressure. This trend is identical with the result of Fsadni

in the gas boiler system (A. M. Fsadni, Ge and Lamers, 2011). Both trends are achieved in the supersaturated water conditions. But, as reported by (Shefik, 2015), the saturation ratio was undersaturated. This is could be the reason of the different trend.

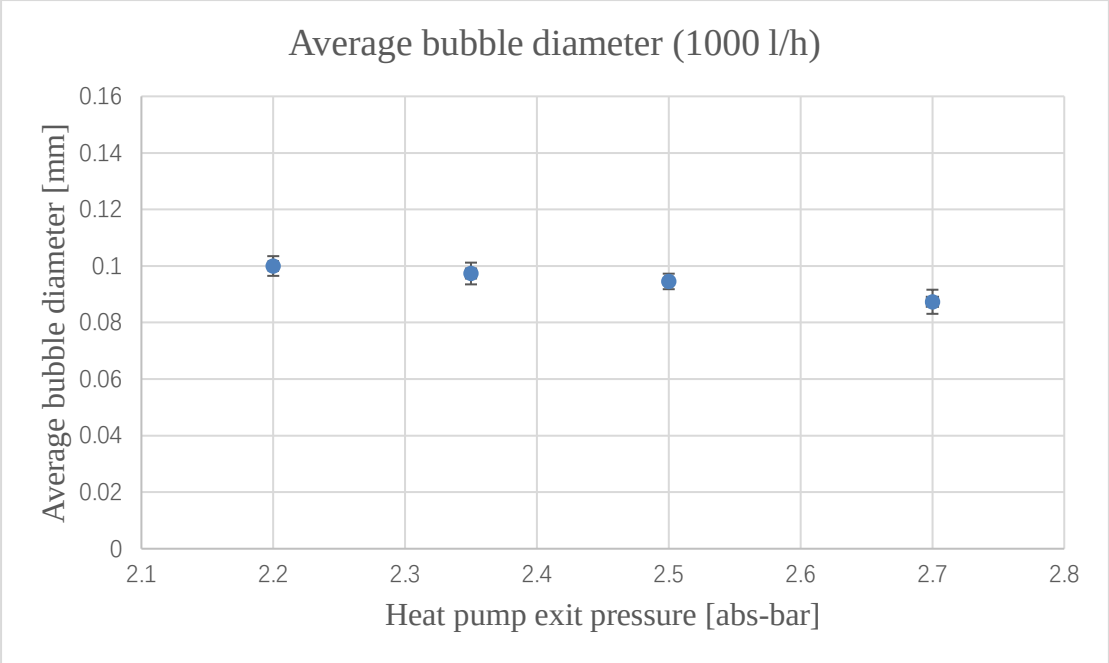

Figure 4. 5 The effect of the pressure on the average bubble diameter at 1000l/h

Besides, as reported by (Prodanovic, Fraser and Salcudean, 2002), in the subcooled boiling, the relationship between the average detachment diameter and the system pressure is same with the finding of this project.

The relationship between the average bubble diameter and the exit pressure is validated by another series of tests as shown in Figure 4.6.

Figure 4.6 illustrates the relationship between the average bubble diameter and the heat pump exit pressure at 850 l/h. In this series of tests, the system pressures were set at 1.7, 1.9, 2.1, 2.3 and 2.5 absolute bars respectively. At the heat pump exit, the temperature of the supply water is 55 ℃ as well. The relationship between the two axes at 850 l/h is investigated to identify the accuracy.

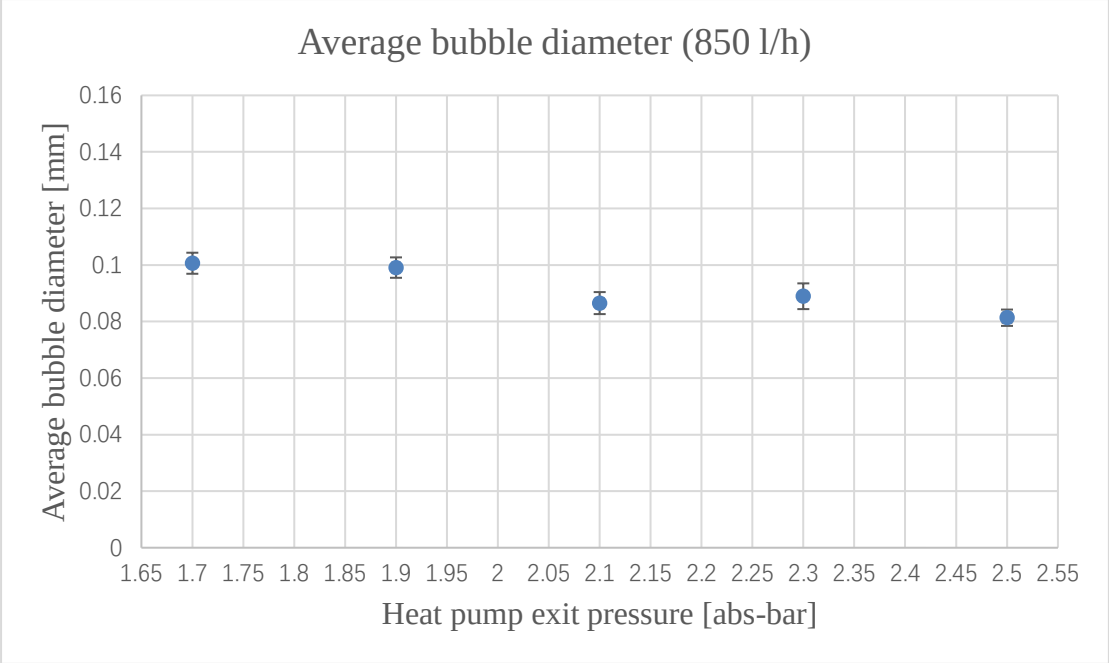

Figure 4. 6 The effect of the pressure on the average bubble diameter at 850l/h

Figure 4.6 presents the average bubble diameter of five pressures at 850 l/h is around 0.9 mm. But, without considering the two low pressures, 1.7 bar and 1.9 bar, the average diameter of the rest reduces to 0.085 mm.

With the trends as shown in two figures, a conclusion can be made that the increase of the exit pressure results in the decrease of the average bubble diameter.

4.4.2 Effect of system water flow rate

The effect of system water flowrates is tested in two series investigations which are at 2.5 absolute bars and 2.2 absolute bars respectively. The codes of the two series are 4-EF and 5-EF as described in the methodology. The temperature of the supply water is 55 ℃ at the exit of the heat pump, which is controlled by the cooling system as introduced in chapter three.

Figure 4.7 illustrates the relationship between the average bubble diameter and the water flow rate at 2.5 absolute bars. In this series of tests, the system water flow rates were set at 800, 850, 900, 1000,1050 and 1100 l/h respectively. The uncertainties of the measurements are represented by the standard error of mean, which is shown as the

error bars in Figure 4.7. The data of these uncertainties are presented in Appendix I.

As shown in Figure 4.7, the average bubble diameters of seven water flow rates are around 0.09 mm. This value is smaller than the minimum bubble diameter of all test conditions in the gas boiler water heating system (Shefik, 2015).

As introduced by (Shefik, 2015), there is no significant relationship between the average bubble diameter and the water flow rate due to the effect of the 90-degree bend near the sight-glass. However, the relationship between the average bubble diameter and the water flow rate is investigated by (A.M. Fsadni, Ge and Lamers, 2011) as well, who reports that the average bubble diameter decreases along with the increase of the water flow rate. Fsadni's find is identical with the results of the single bubble boiling test on the flat heat exchanger wall. The researches of the boiling on the flat heat exchanger wall have been investigated by many researchers in the laboratory conditions, in which (Zeng *et al.*, 1993) reported that the average bubble diameter decreases along with the increase of the water flow rate. But, as shown in Figure 4.7, there is a clear trend that the average bubble diameter increases along with the increase of the water flow rate at the heat pump exit. This relationship between the average bubble diameter and the water flow rate is caused by the effect of the bubble collision and coalescence in the micro-channels and the 90-degre bend in the supersaturated water. As reported in the newest research by (Lee, Devahdhanush and Mudawar, 2018), the increase of the bubble size and the decrease of the bubble number in the smooth micro-channel are filmed by the camera. Lee's study proves the existence of the bubble collision and coalescence. In Lee's test, the bubbly two-phase flow develops to be the saturated boiling (Lee, Devahdhanush and Mudawar, 2018). Hence, Lee's research provides the reason to the trend in Figure 4.7. Figure 4.7 summarises the relationship between the average bubble diameter and the system flow rate at heat pump exit which is not at the plate heat exchanger in the heat pump.

This investigating position chosen is intended to study the bubble behaviours at the heat pump exit to improve the design of the deaerator equipment. The fins of the plate heat exchanger increase the chance of the bubble collision and coalescence in the micro-channel. Furthermore, the higher water flow rate results in the higher Reynolds number in the micro-channel of the plate heat exchanger, which boosts the turbulence level.

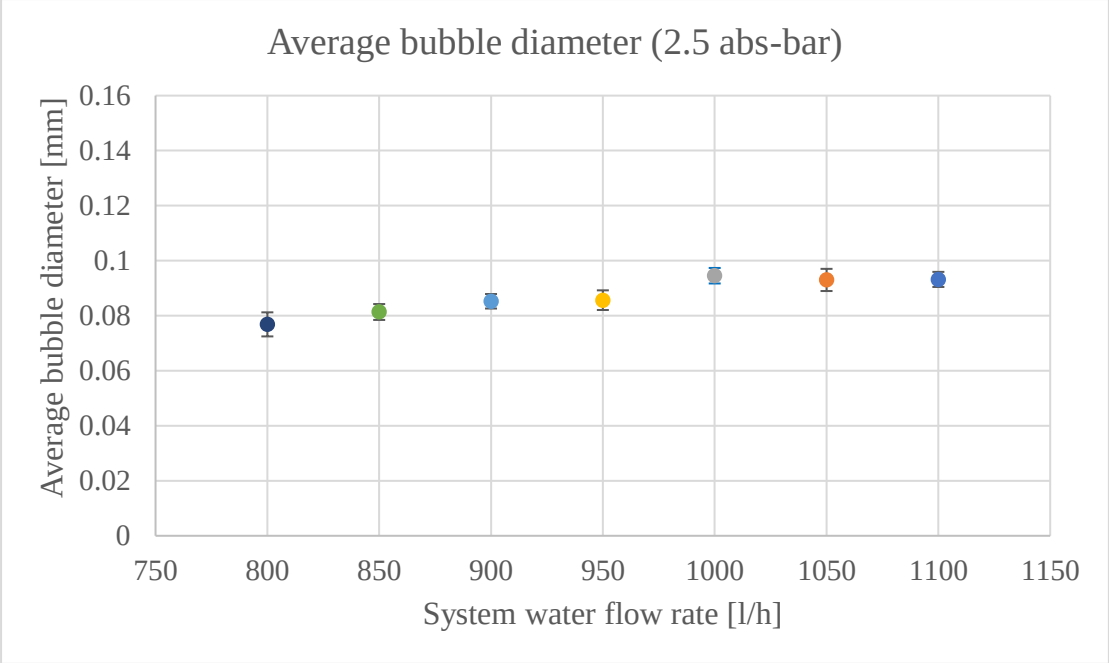

Figure 4. 7 The effect of the water flow rate on the average bubble diameter at 2.5 absolute bar

Figure 4.8 illustrates average bubble diameter at different saturation ratios. Totally, four saturation ratios, 1.15, 1.10, 1.05 and 1.00 are presented. At each water flow rate, the high saturation ratio tends to have bigger average bubble diameter as shown in Figure 4.8. This trend accounts to the effect of the bubble collision and coalescence as there are more bubbles at the higher saturation ratio, which is going to be intruded in the following sections

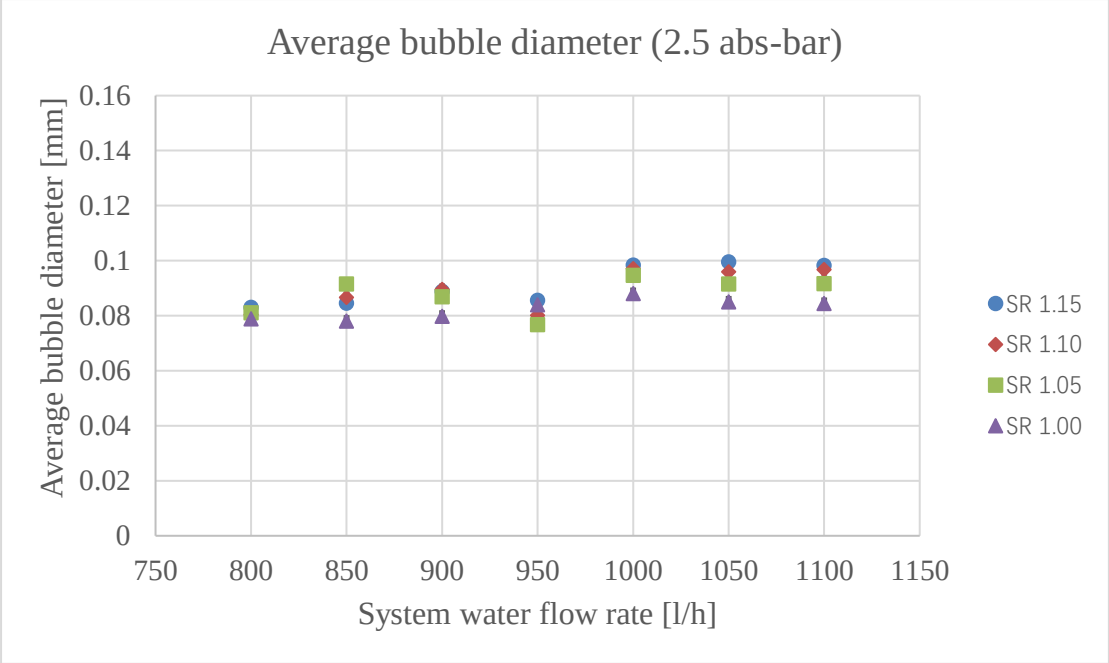

Figure 4. 8 The effect of the water flow rate on the average bubble diameter at 2.5 absolute bar in four saturation ratios

The flow regime changes with the increase of the water superficial flow rate. In Figure 4.8, from 800 l/h to 950 l/h, which is from 0.71 m/s to 0.84 m/s representing by using superficial velocity, the relationship between the average bubble diameter and saturation ratio is not clear as there is a huge number of bubbles to participate in the collision and coalescence with low turbulence level resulting in the irregular results. However, from 1000 l/h to 1100 l/h, which is from 0.88 m/s to 0.97 m/s representing by using superficial velocity, the trend is clear that the higher the saturation, the higher the average bubble diameter, which is because the turbulence level is high in high saturation ratio with enough bubbles resulting the sizeable average bubble diameter. On the contrary, there is not enough bubbles in low saturation ratio to participate in the collision and coalescence, even though the turbulence level is high.

In order to validate the trend found in Figure 4.7, another series of tests is conducted at different experimental conditions. Figure 4.9 illustrates the relationship between the average bubble diameter and the water flow rate at 2.2 absolute bars. In this series of tests, the system water flow rates were set at 800, 900, 1000,1100 and 1150 l/h respectively. The uncertainties of the measurements are represented by the standard error of mean as well, which is shown as the error bars in Figure 4.9. The data of these

uncertainties are presented in Appendix I.

Figure 4.9 shows the relationship between the average bubble diameter and the system water flow rate is in the same trend with Figure 4.7. The average bubble diameter of the bubble diameters at these five water flow rates is around 1.0 mm which is larger than that in Figure 4.7 due to the effect of the system pressure.

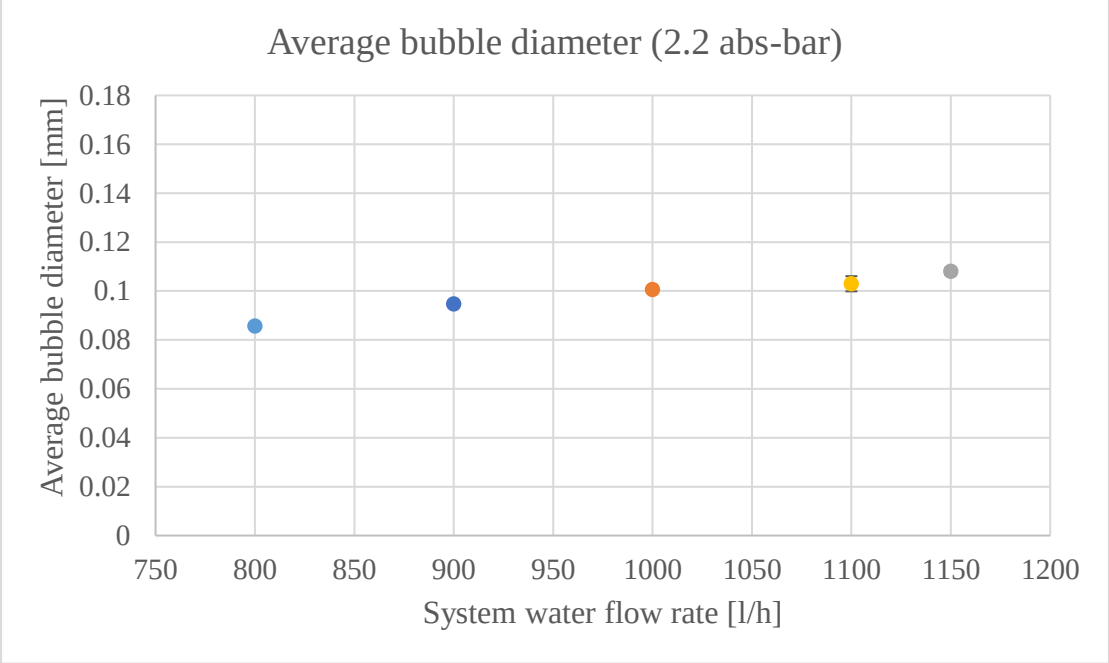

Figure 4. 9 The effect of the water flow rate on the average bubble diameter at 2.2 absolute bar

4.4.3 Effect of system saturation ratio

This section is going to introduce the effect of the system saturation ratio on the average bubble diameter at various water flow rates. Figure 4.10 shows the effect of the system saturation ratio on the average bubble diameter at various flow rates at 2.5 absolute bars. The codes of this series of tests is 6-ES as described in the methodology. The temperature of the supply water is 55 ℃ at the exit of the heat pump, which is controlled by the cooling system as introduced in chapter three.

In this series of tests, the system water flow rates were set at 800, 850, 900, 950 1000 and 1100 l/h respectively. Figure 4.10 shows there is a slight trend that the average bubble diameter increases along with the increase of the saturation ratios. Although, it

is reported by (Shefik, 2015) that the relationship between the average bubble diameter and the saturation ratio is quasi-constant in the gas boiler water heating system, the bubble production sharply increases along with the increase of the saturation ratio in his tests. This trend is observed in heat pump water heating system as well. This trend could be the reason for the larger average bubble diameter at high saturation ratio, because that the high bubble production contributes to the bubble collision and coalescence as discussed in the preceding section.

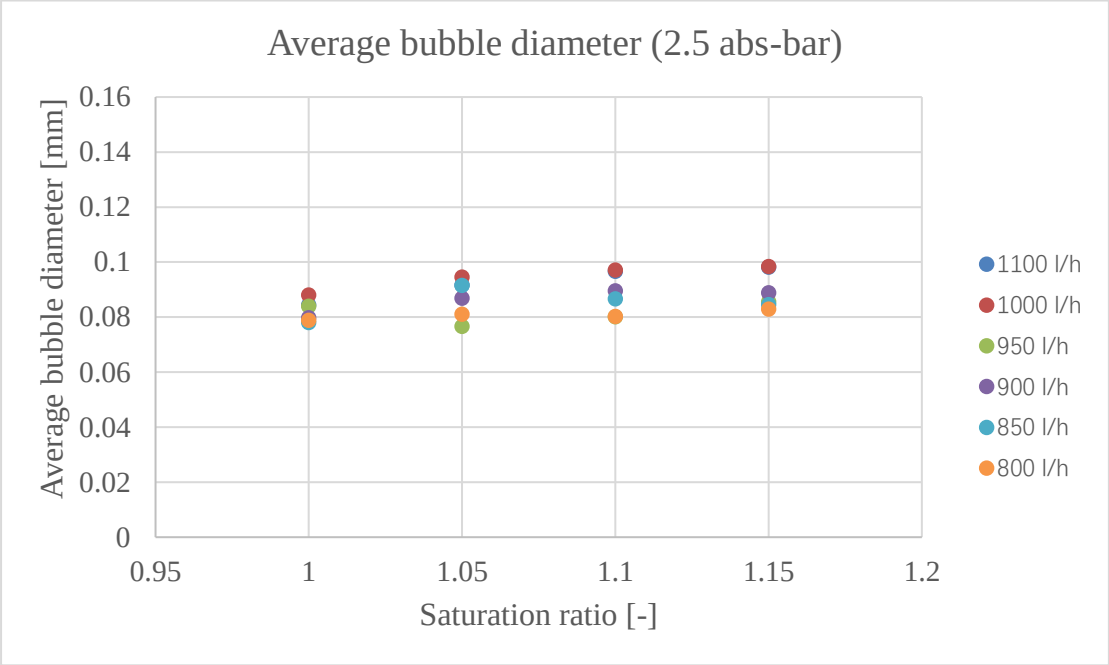

Figure 4. 10 The effect of the system saturation ratio on the average bubble diameter at various flow rates at 2.5 absolute bars

4.4.4 Bubble diameter distribution

This section is going to illustrate the bubble diameters distribution of the bubbly flow at the horizontal heat pump exit. First, the average bubble diameters of different focal plane depths are presented at four different saturation ratios. Four water flow rates, 1100 l/h, 950 l/h, 900 l/h and 800 l/h are presented to introduce the average bubble diameter distributions in the pipe cross-section. Second, a gamma function is introduced to predict the bubble diameter distribution at heat pump exit in the domestic

heat pump water heating system.

4.4.4.1 Average bubble diameter distributions in the pipe cross-section

The average bubble diameter distributions at the cross-section of the pipe have been shown in this section at four various saturation ratios. A good understanding of the distributions of the average bubble diameter provides the insight of the bubbly flow behaviours in the heat pump water heating system.

Figure 4.11 shows the average bubble diameter distributions in the pipe cross-section at saturation ratio 1.15. The trend is clear that the average bubble diameter at 1100 l/h is bigger than that at 800 l/h. Besides, the average bubble diameters of 950 l/h and 900 l/h are similar, which is bigger than that at 800 l/h and smaller than that at 1100 l/h. The average bubble diameters at 1 and 2 DOF are higher than that at the other DOF. This trend is caused by the buoyancy which lifts the big bubbles to the top layers of pipeline in the horizontal flow.

Figure 4.12 shows the average bubble diameter distributions in the pipe cross-section at saturation ratio 1.10. The trend is clear that the average bubble diameter at 1100 l/h is still the biggest amid four water flow rates due to the bubble collision and coalescence as discussed in preceding section. The effect of the water buoyancy is still clear resulting in the average bubble diameters decreases along with the cross-section of the pipe from the top to bottom.

Figure 4.13 shows the average bubble diameter distributions in the pipe cross-section at saturation ratio 1.05. Along with the decrease of the saturation ratio, the bubble number decreases rapidly. The less number of the bubbles, compared to saturation 1.15 and 1.10, the random error of the average bubble diameter increases leading to the irregular trend of the distribution of the average bubble diameters.

Figure 4.14 shows the average bubble diameter distributions in the pipe cross-section at saturation ratio 1.00. As the saturation ratio is around the lowest saturation ratio that this system can achieve, the gas bubble numbers are extremely small, which leads to the irregular trend of the distributions of the gas bubbles at different water flow rate. There are no bubbles found at lower DOFs at 800 l/h. The reason of the absence of bubbles at lower DOFs at low water flow rate is that gas bubbles have enough to be lift to upper DOFs by the water buoyancy.

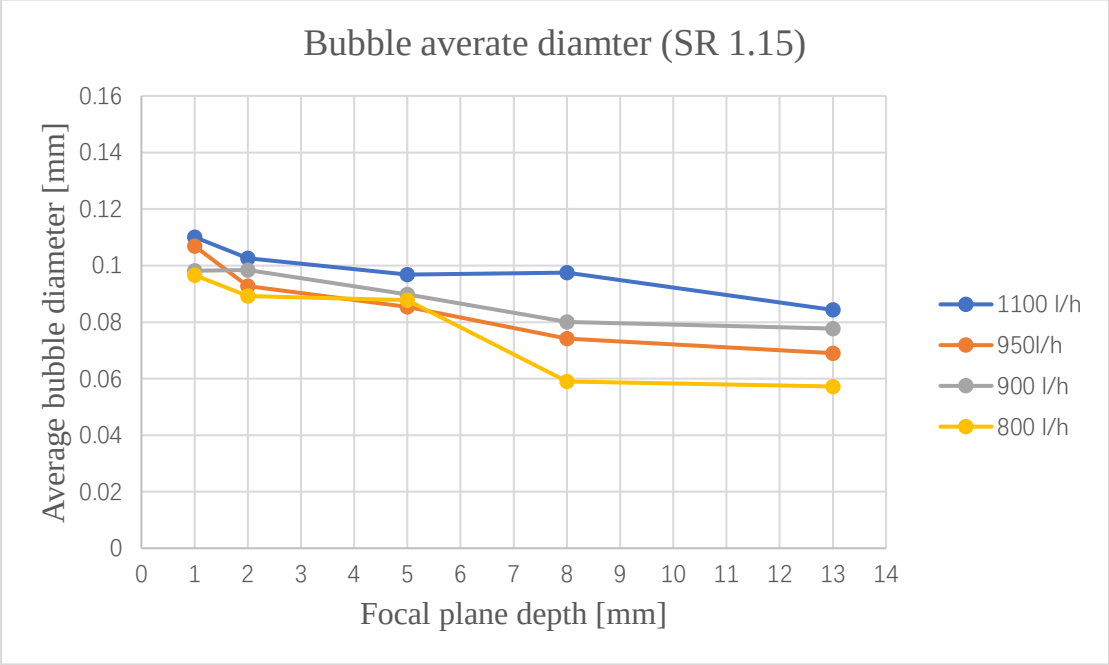

Figure 4. 11 Average bubble diameter distributions in the pipe cross-section at saturation ratio 1.15

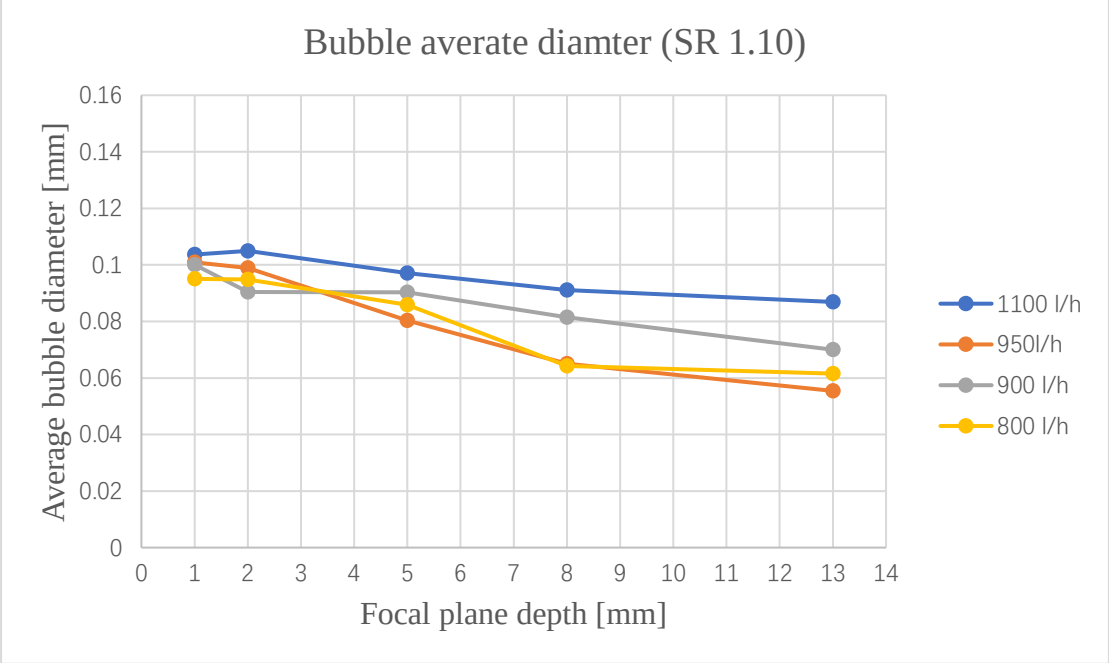

Figure 4. 12 Average bubble diameter distributions in the pipe cross-section at saturation ratio 1.10

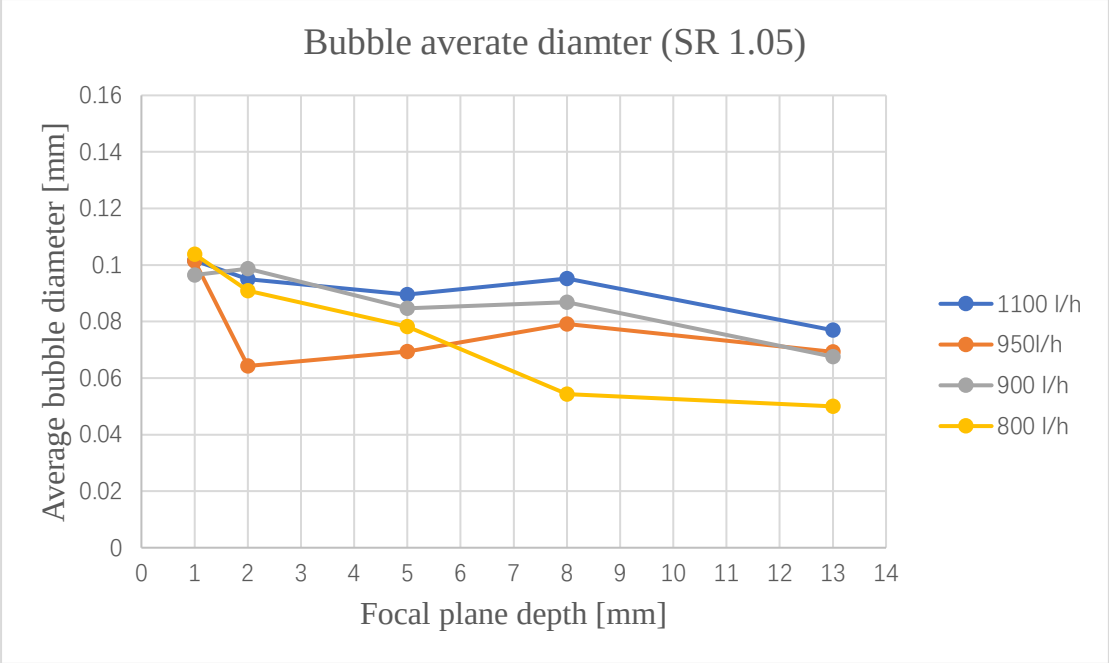

Figure 4. 13 Average bubble diameter distributions in the pipe cross-section at saturation ratio 1.05

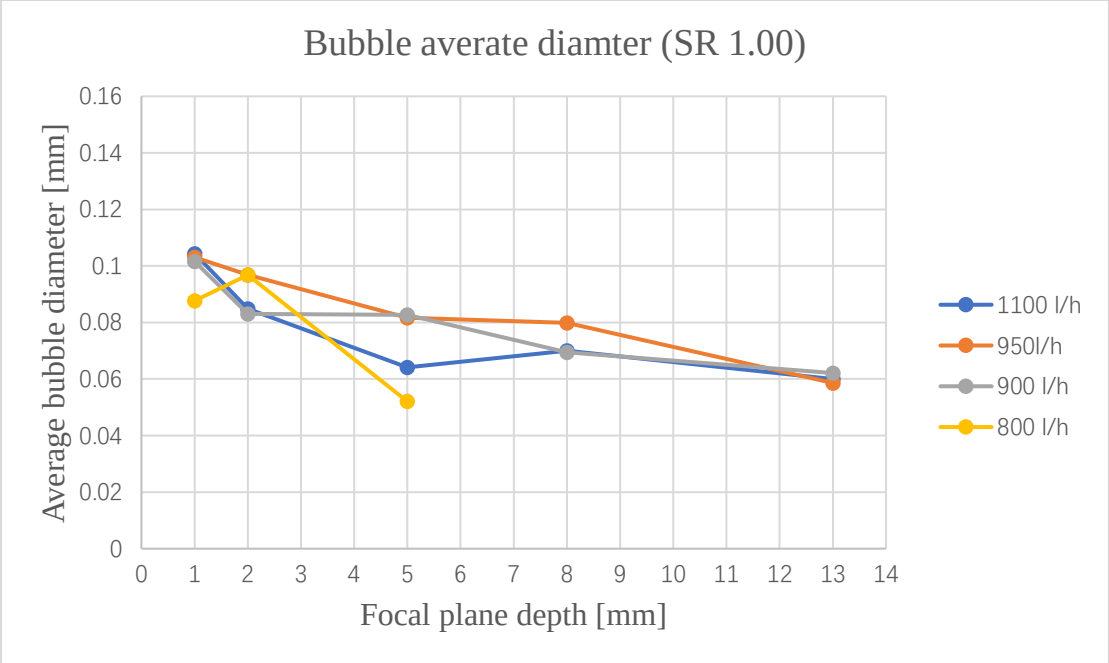

Figure 4. 14 Average bubble diameter distributions in the pipe cross-section at saturation ratio 1.00

4.4.4.2 Prediction of bubble diameter distribution at a focal plane

The sight-glass is installed horizontally near the plate heat exchanger exit as shown in Figure 3.1 to investigate the bubble behaviours due to the sub-cooled boiling. For each test, 5400 images were captured by the camera in 3 minutes. A large number of images ensures the accuracy of the experiment to illustrate the possibility of the bubble diameter distributions. This experiment investigated four parameters which may affect bubble diameters in a domestic heat pump water heating system. There were 104 tests have been conducted at various experimental conditions during this series. It is found that most results of the tests obey the Gamma probability density function as shown in Figure 4.15 and Figure 4.16. Based on the experimental data, the following three parameters Gamma probability density Equation 4.1 is proposed.

$$f(x,\alpha,\beta,\mu) = \frac{\beta^{-\alpha}}{\Gamma(\alpha)}(x-\mu)^{\alpha-1}e^{-\frac{(x-\mu)}{\beta}} \quad \textbf{(4. 1)}$$

The α is the shape parameter, the β is the scale parameter and the μ is the location parameter. The value of μ is the smallest diameter of bubbles which can be recognized by the camera is 0.046 mm.

The χ^2 test (chi-square test) is used to test whether the bubble diameter distribution obey the Gamma probability density function. 86 of 104 tests, 82.69%, obeys the Gamma probability density function. The reason of those tests does not obey Gamma probability density function is the amount of bubbles is too small. Therefore, it is clear, at most conditions, bubble diameter distributions obey the Gamma probability density function. As illustrated in Figure. 4.17, the increase of water flow rate can result in the increase of parameter α and β. Parameter β increases along with the system pressure increases as shown in Figure 4.18. The system heating load has limited effect on the parameters. Figure. 4.20 shows the bubble diameter distributions based on the Gamma probability density function fitting. The increase of water flow rate can result in the skewness of the distribution curve and the distribution peak decrease. This is because of the turbulent flow and the increase of water flow rate enhanced the bubbles colliding and coalescing.

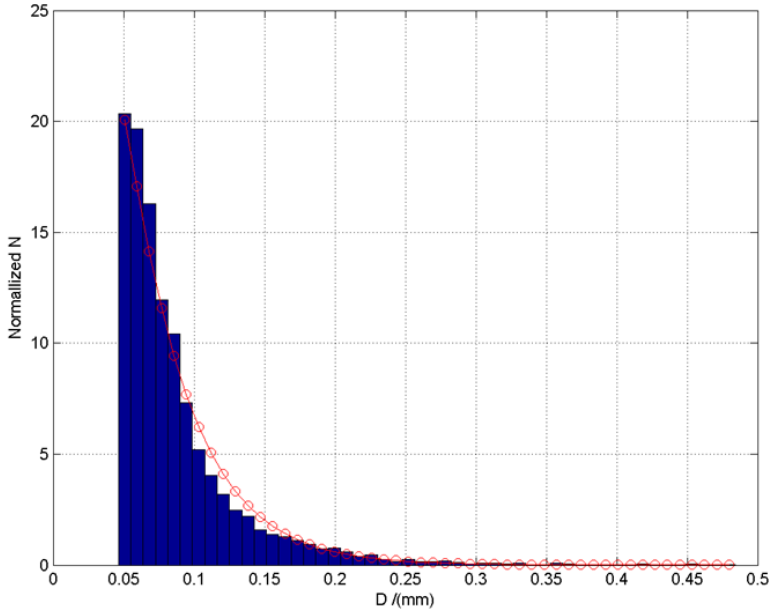

(A)

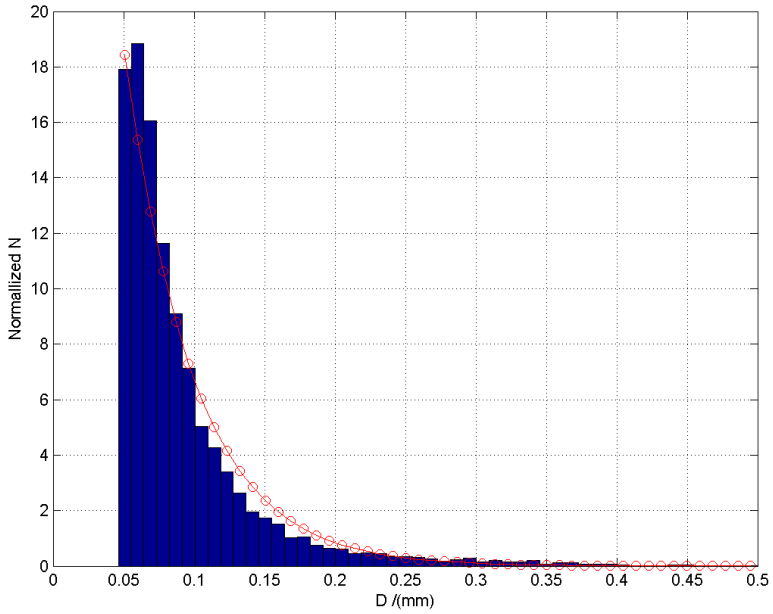

(B)

Figure 4. 15 (A)FR600 l/h, Pressure 2.2 bars, heating load 6 kW; (B)FR 900 l/h, Pressure 2.2 bars, heating load 7.2 kW

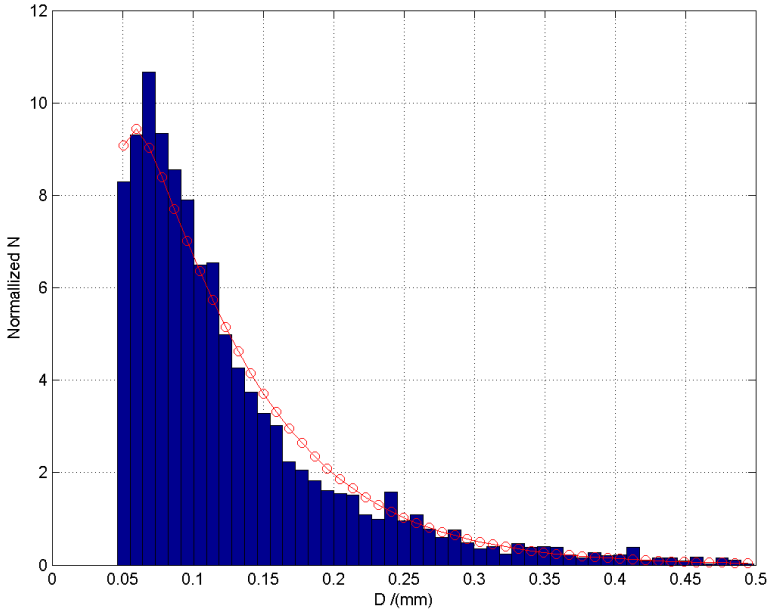

(A)

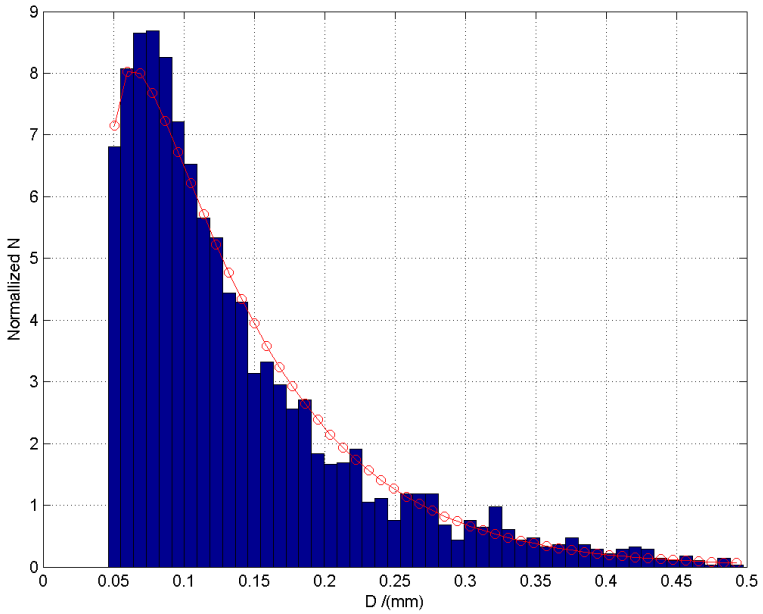

(B)

Figure 4. 16 (A)FR 1000 l/h, Pressure 2.2 bars, heating load 6 kW; (B)FR 1150 l/h, Pressure 2.2 bars, heating load 8 kW

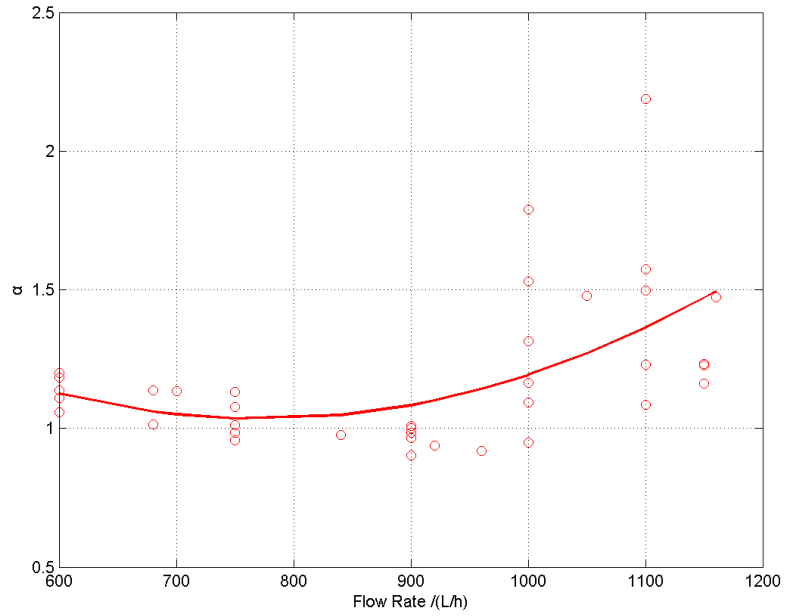

(A)

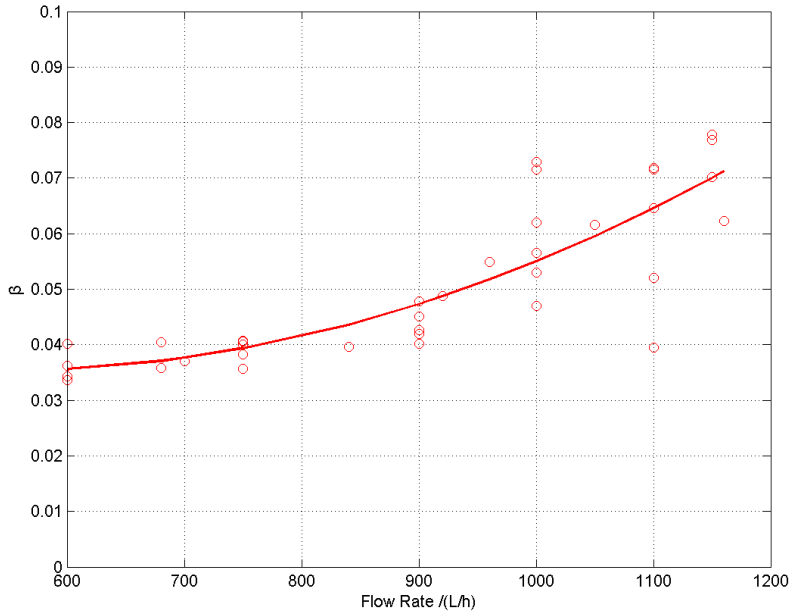

(B)

Figure 4. 17 (A) Gamma parameter α with flowing rate; (B) Gamma parameter β with flow rate

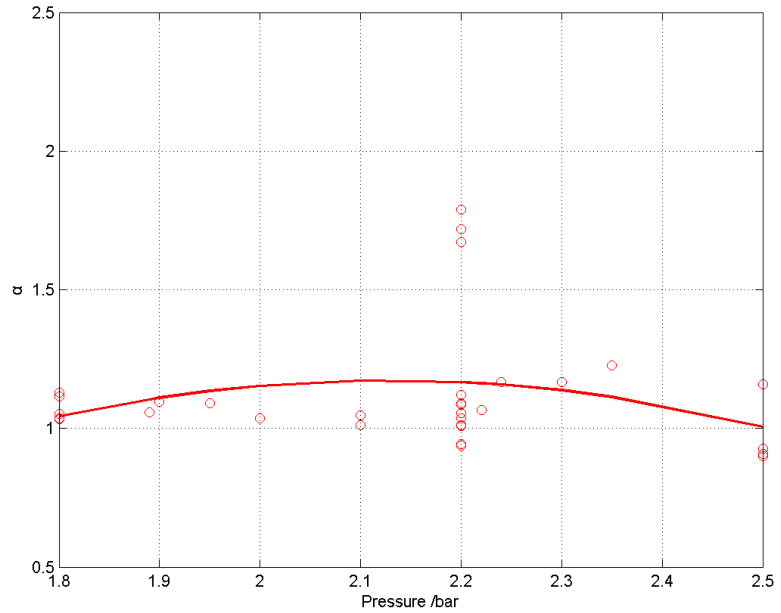

(A)

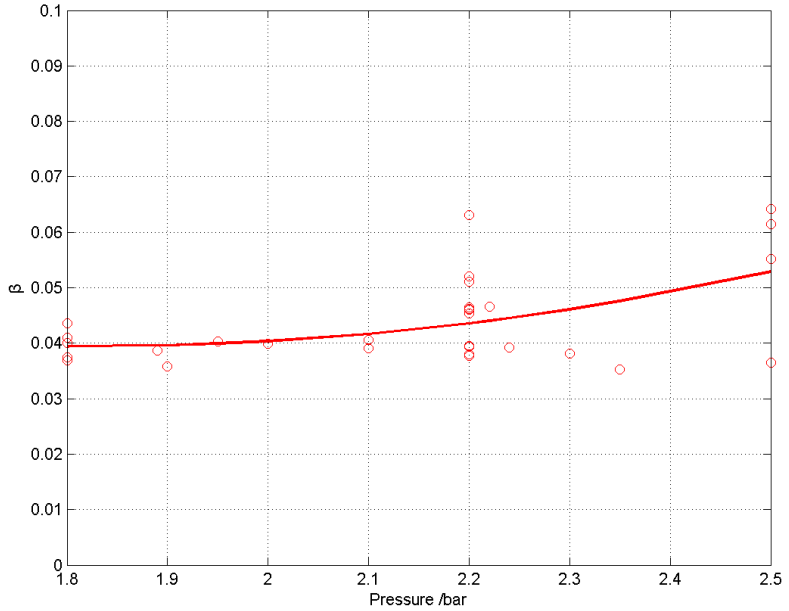

(B)

Figure 4. 18 (A) Gamma parameter α with system pressure; (B) Gamma parameter β with system pressure

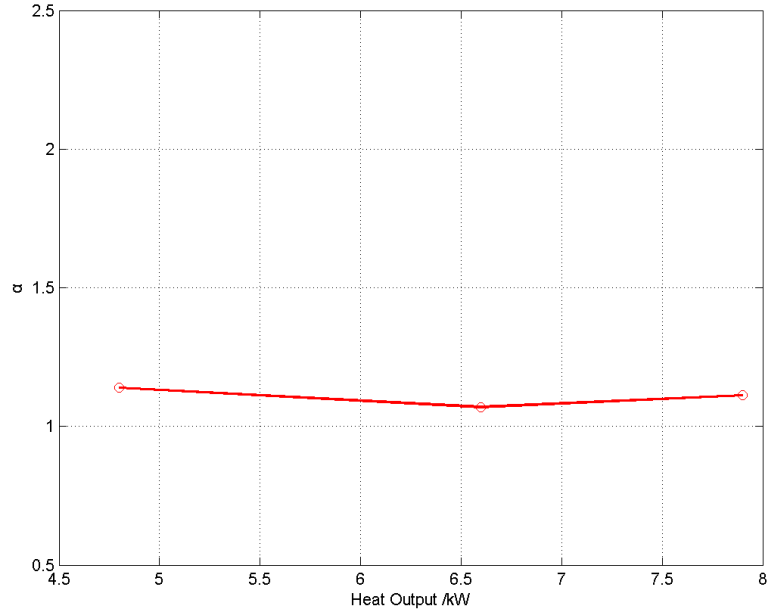

(A)

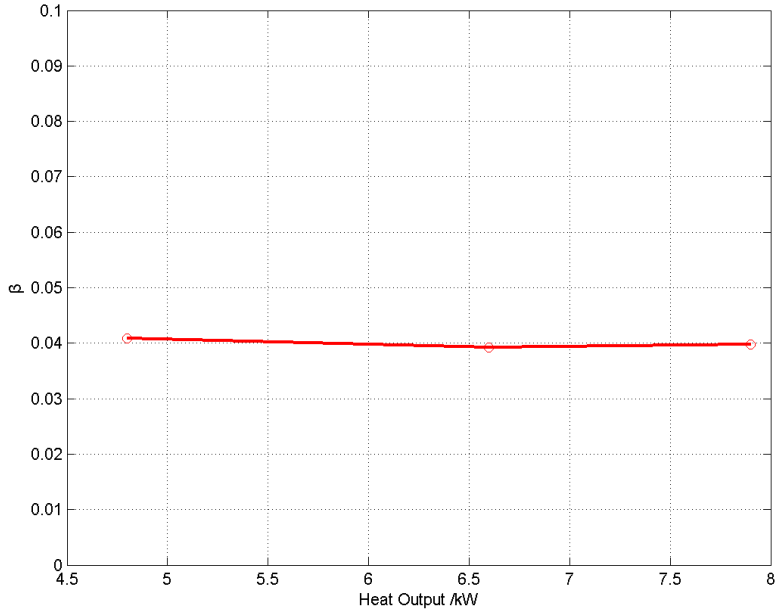

(B)

Figure 4. 19 (A) Gamma parameter α with heating load; (B) Gamma parameter β with heating load

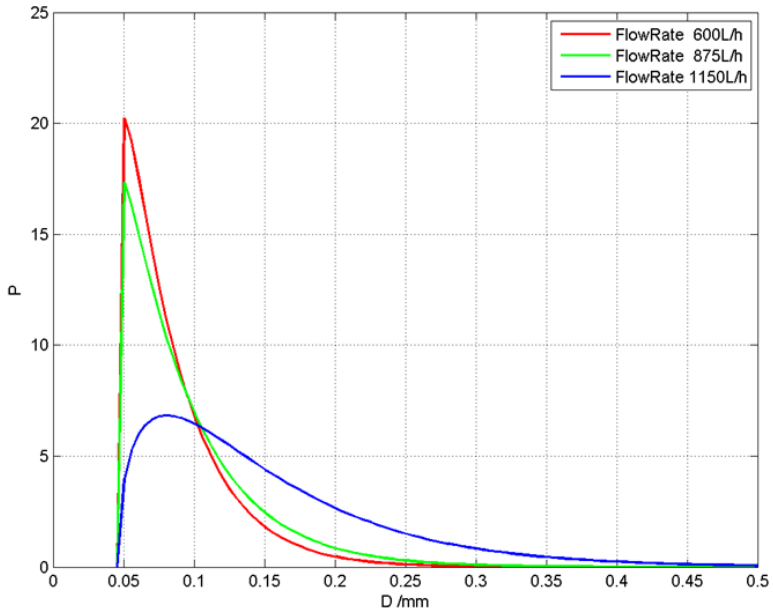

Figure 4. 20 Bubble diameter distributions with water flow rate

4.5 Bubble volumetric void fraction characteristics

This section is going to introduce bubble volumetric void fraction characteristics at the heat pump exit. The code of the test series is 9-VF as introduced in the experimental methodology. Section 4.5.1 presents the effect of system water flow rates and section 4.5.2 illustrates the effect of system saturation ratio. Moreover, section 4.5.3 introduces the effect of system pressure on the bubble volumetric void fraction. Finally, section 4.5.4 introduces the distributions of the bubble volumetric void fraction

4.5.1 Effect of system water flow rate

Table 4.1 shows the experimental conditions has been conducted to study the effect of the system water flow rate on the volumetric void fraction distribution at heat pump exit. The relationship between the system flow rate and the volumetric void fraction was investigated at 2.5 absolute bar. Five water flow rates were covered which are 850 l/h, 900 l/h, 950 l/h, 1000l/h and 1100 l/h respectively. Four saturation ratios were achieved as the preceding tests achieved.

Three test conditions have been shown as follows. Figure 4.21 shows the experimental conditions at 900 l/h. Figure 4.22 presents the experimental conditions at 1000 l/h. Figure 4.23 illustrates the experimental conditions at 1100 l/h. The bubble measurement periods have been marked in the figures.

Table 4. 1 Experimental conditions for the effect of system water flow rate

Flow rate (LPH)	SR (-)	System Pressure (Bar)	Heat Pump exit temp. (°C)	Sight-glass Position
850	1-1.15	2.5	55	Heat pump exit
900	1-1.15	2.5	55	Heat pump exit
950	1-1.15	2.5	55	Heat pump exit
1000	1-1.15	2.5	55	Heat pump exit
1100	1-1.15	2.5	55	Heat pump exit

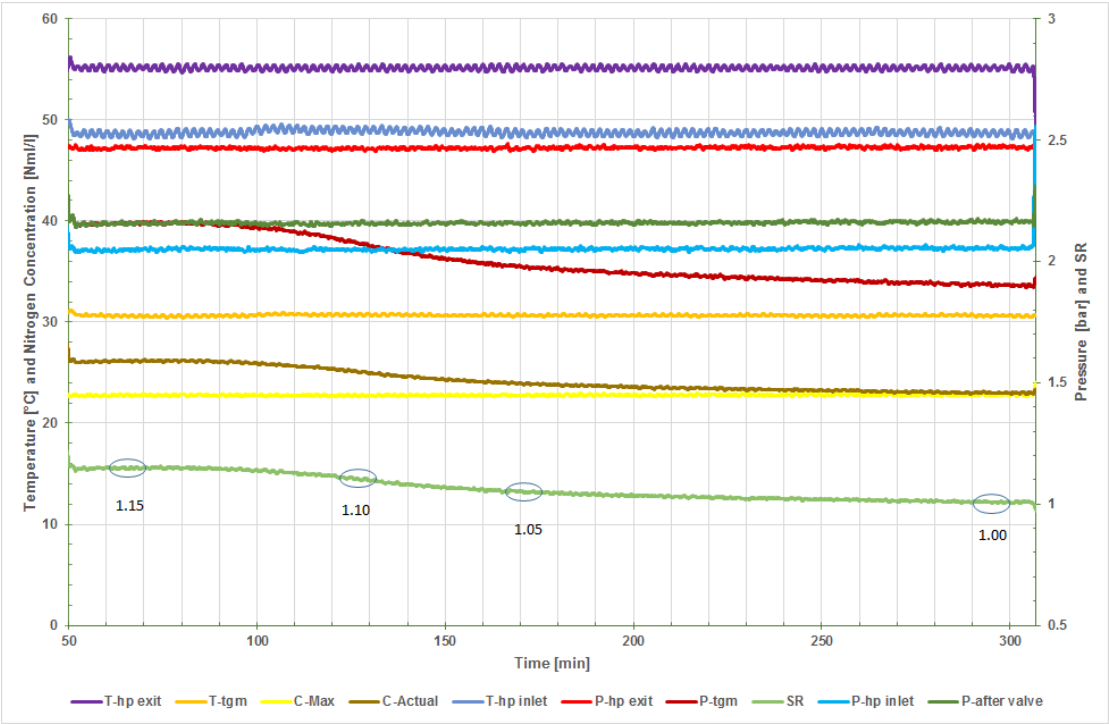

Figure 4. 21 System conditions variation during the measurements at 900LPH

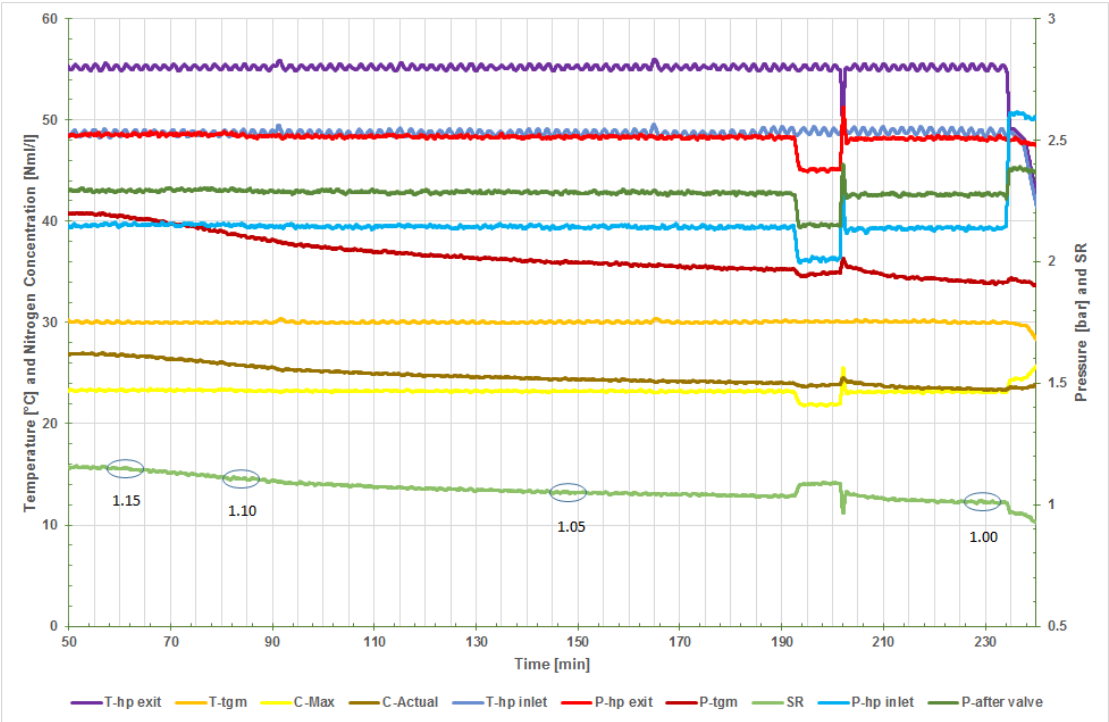

Figure 4. 22 System conditions variation during the measurements at 1000LPH

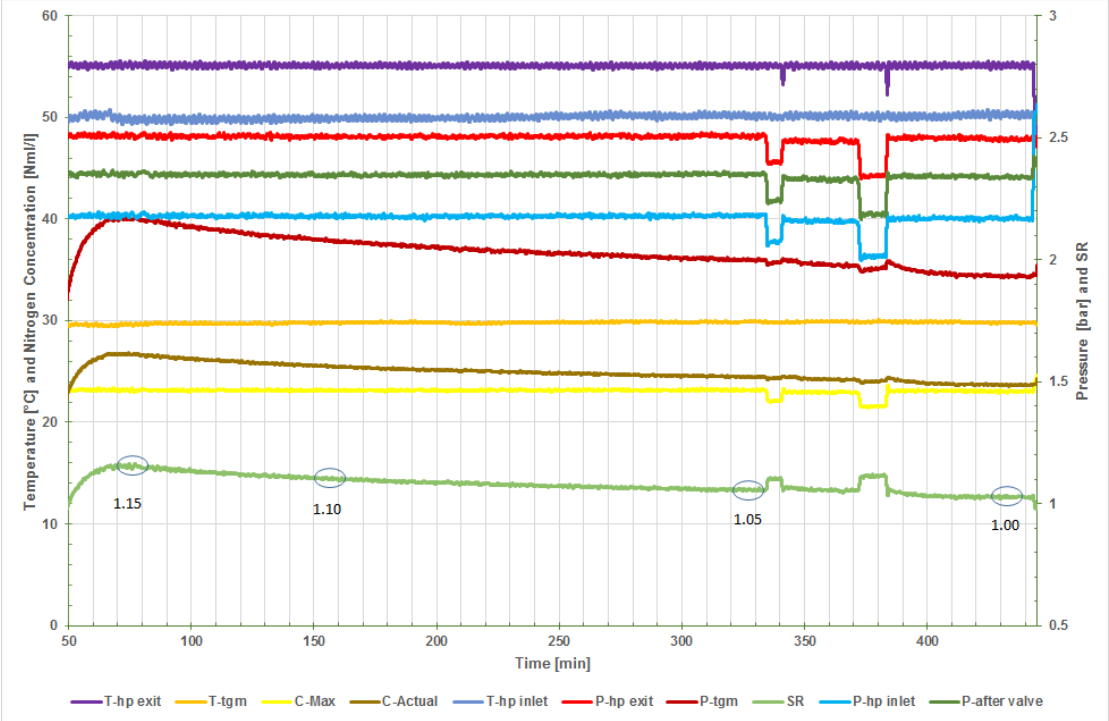

Figure 4. 23 System conditions variation during the measurements at 1100LPH

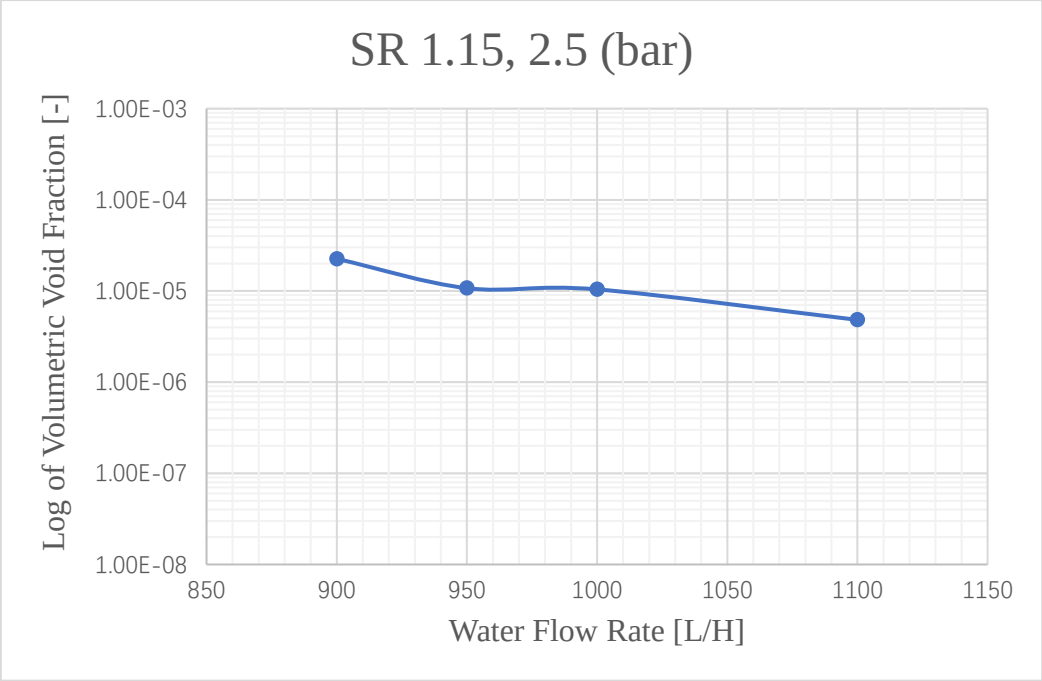

Figure 4. 24 Volumetric void fractions with various water flow rates at heat pump exit at saturation ratio 1.15

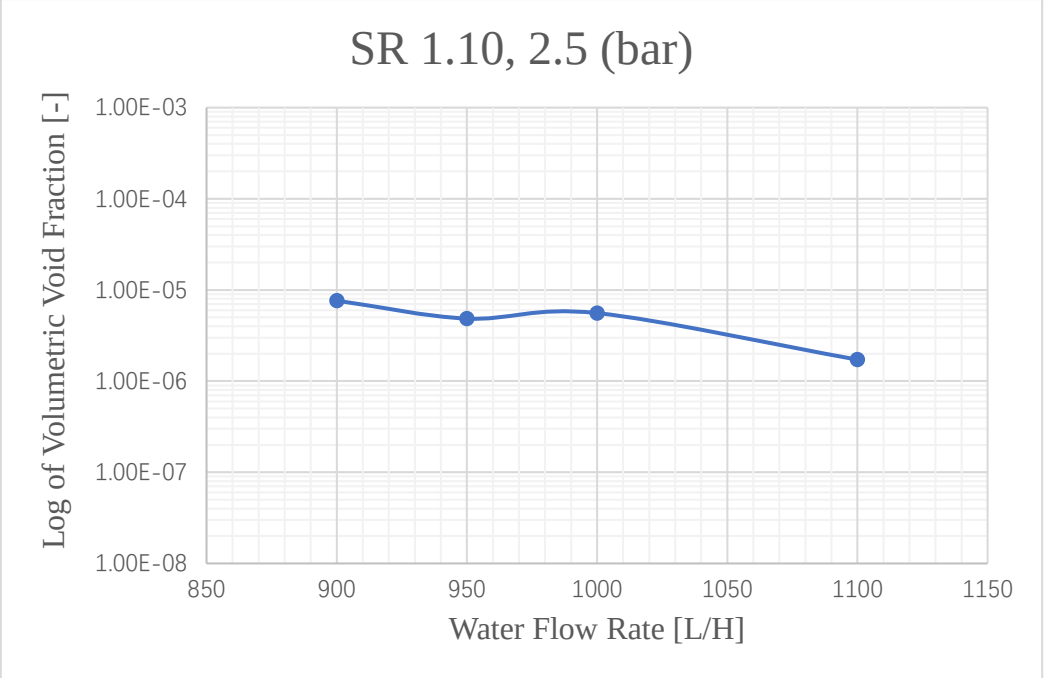

Figure 4. 25 Volumetric void fractions with various water flow rates at heat pump exit at saturation ratio 1.10

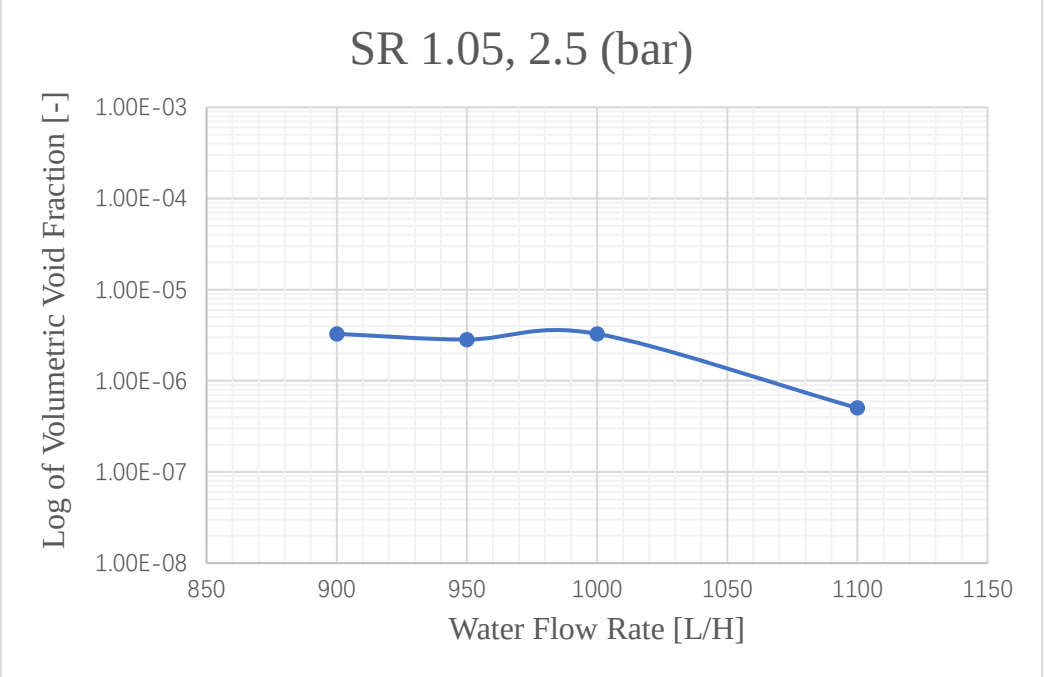

Figure 4. 26 Volumetric void fractions with various water flow rates at heat pump exit at saturation ratio 1.05

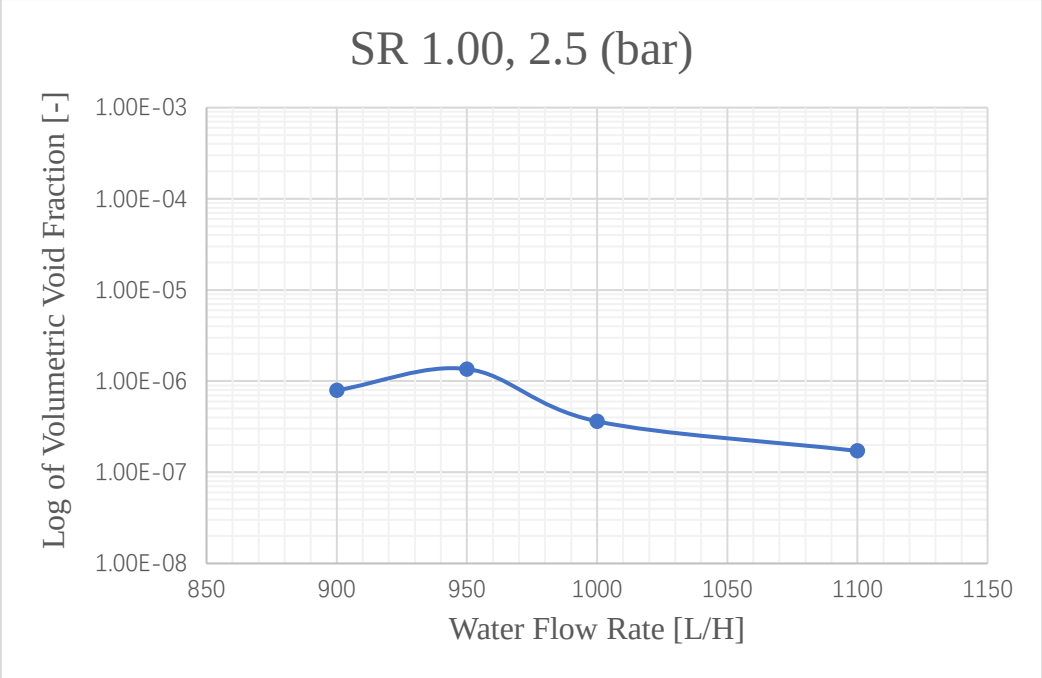

Figure 4. 27 Volumetric void fractions with various water flow rates at heat pump exit at saturation ratio 1.00

The figures present the results for the bubble distribution at heat pump exit (outlet) in a horizontal bubbly two-phase flow. As illustrated in figures, the results are presented through the measured volumetric void fractions with various water flow rates and saturation ratios.

Figure 4.24 shows there is a clear trend that bubble volumetric void fraction decreases along with the increase of the water flow rate. This trend is same with the results of Fsadni (Fsadni, 2012). In the supersaturated two-phase fluid, the bubbles continue to grow up till to breakup. There is an enough long distance between the plate heat exchanger and the sight-glass at heat pump exit for bubble growing. The bubbles with lower flow rate has longer time to reach the sight-glass compared to the bubbles with higher flow rate. Hence, the volumetric void fraction at low water flow rate is higher than that at high water flow rate.

Figure 4.25, Figure 4.26 and Figure 4.27 illustrate the same trend with Figure 4.24 at saturation ratio 1.10, 1.05 and 1.00 respectively. Some data in these figures are not in the trend due to the minor differences of the water flow rates and the bias and random errors. The random errors at saturation 1.00 are higher than the other saturation ratios due to the small number of bubbles at the saturation ratio 1.00.

4.5.2 Effect of system saturation ratio

The gas bubble void fraction at the heat pump exit position is introduced in this section. Bubble measurements are conducted at the heat pump exit position, which was just 920 mm away from the plate heat exchanger exit, as shown in Figure 3.1. The experimental data was analysed, and the following graphs have been presented to show how bubble volumetric void fraction changes with saturation ratios. As the figures indicate, the bubble volumetric void fraction changes along with the various saturation ratio significantly. Table 4.2 shows the experimental conditions achieved for the study of the effect of system saturation ratio.

Table 4. 2 Experimental conditions for the effect of system saturation ratio

Flow rate (LPH)	SR (-)	System Pressure (Bar)	Heat Pump exit temp. (°C)	Sight-glass Position
1000	1-1.15	2.2	55	Heat pump exit
1000	1-1.15	2.35	55	Heat pump exit
1000	1-1.15	2.5	55	Heat pump exit
1000	1-1.15	2.7	55	Heat pump exit
900	1-1.15	2.5	55	Heat pump exit
950	1-1.15	2.5	55	Heat pump exit
1100	1-1.15	2.5	55	Heat pump exit

Figure 4.28 shows the volumetric void fraction at various water flow rates with various saturation ratios. The effect of the saturation ratio in the heat pump water heating system is significant as shown in Figure 4.28. The trend is clear that the bubble volumetric void fraction decreases along with the decrease of the saturation ratio. As the huge differences of the temperatures of the wall of the heat exchangers between the gas boiler water heating system and heat pump water heating system, the majority of the bubble productions are due to the supersaturated condition at the heat exchanger wall without water subcooled boiling. The distance between the plate heat exchanger and the sight-glass is relative long enough for the bubble diameter increasing by the effect of the saturated boiling caused by the supersaturated conditions of the water. Hence, the

saturation ratio is a main factor that affects the volumetric void fraction in the heat pump water heating system.

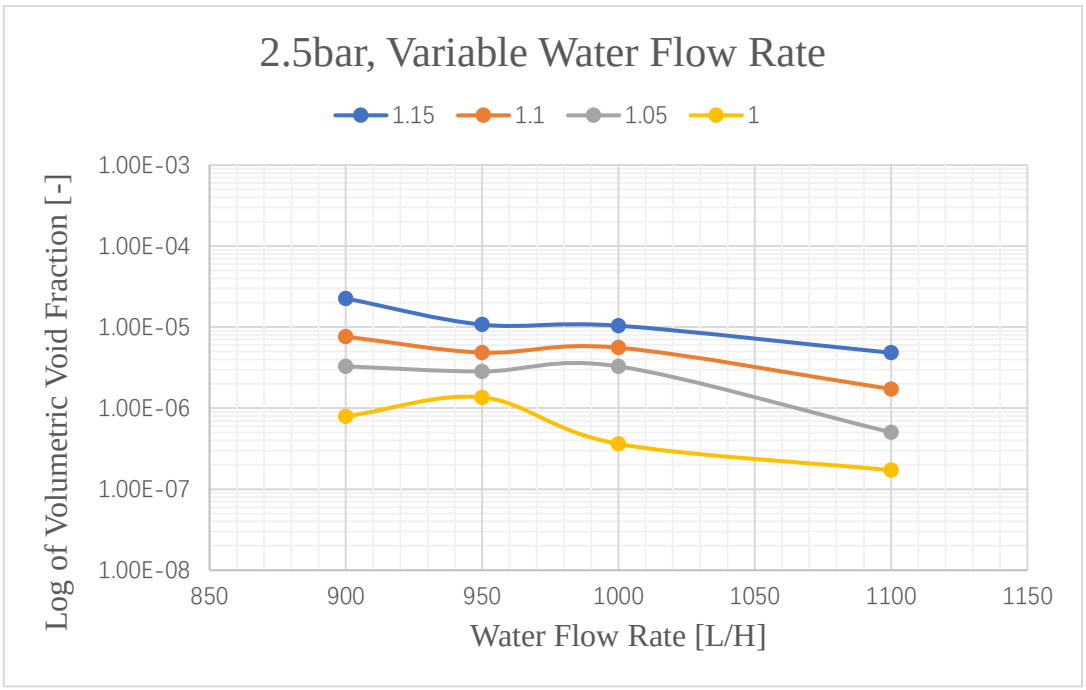

Figure 4. 28 The relationship between volumetric void fraction and saturation ratio at 2.5 bar

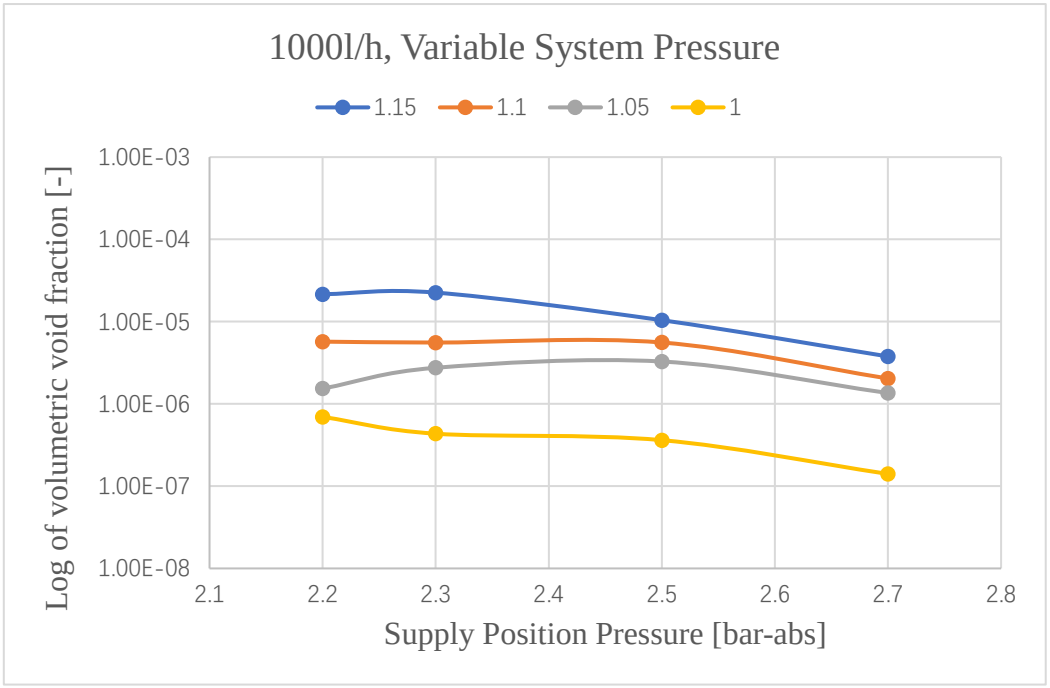

Figure 4. 29 The relationship between volumetric void fraction and saturation ratio at 1000 l/h.

Figure 4.29 shows the relationship between the volumetric void fraction and the

saturation ratio at different heat pump exit pressures. The same trend is found with Figure 4.28.

4.5.3 Effect of system pressure

Table 4.3 shows the experimental conditions has been investigated to study the effect of the system pressure on the volumetric void fraction at heat pump exit. The relationship between the system pressure and the volumetric void fraction was investigated at 1000 l/h. Four system pressures were covered which are 2.2 bar, 2.3 bar, 2.5 bar and 2.7 bar respectively. Four saturation ratios were achieved as well.

Table 4. 3 Experimental conditions for the effect of system pressure

Flow rate (LPH)	SR (-)	System Pressure (Bar)	Heat Pump exit temp. (°C)	Sight-glass Position
1000	1-1.15	2.2	55	Heat pump exit
1000	1-1.15	2.3	55	Heat pump exit
1000	1-1.15	2.5	55	Heat pump exit
1000	1-1.15	2.7	55	Heat pump exit

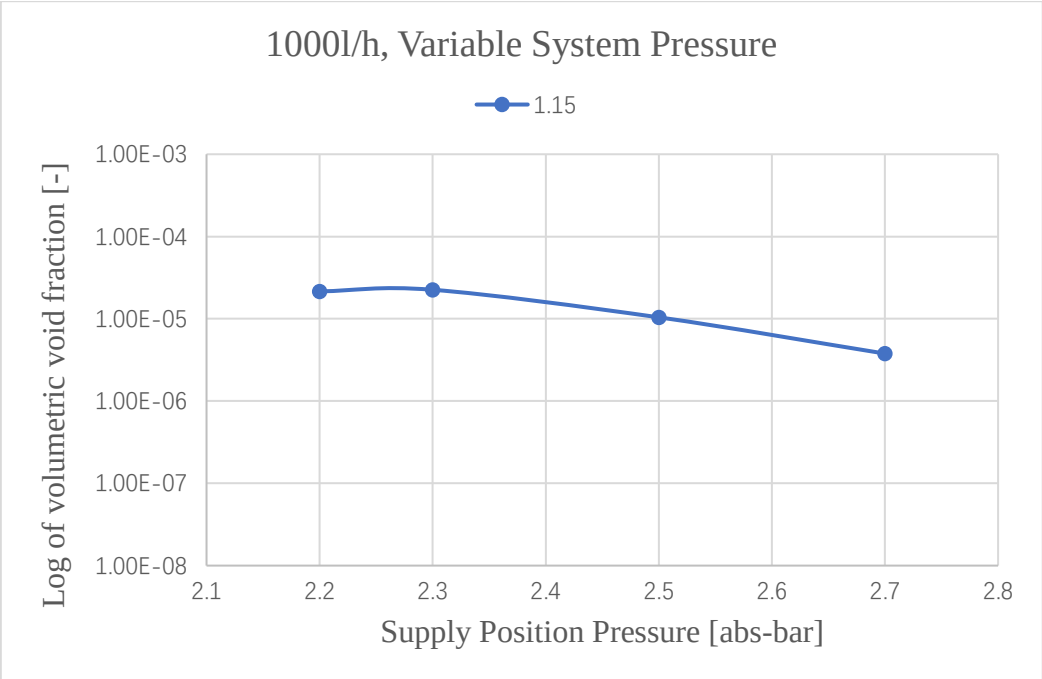

Figure 4. 30 Relationship between volumetric void fraction and system pressure at SR 1.15

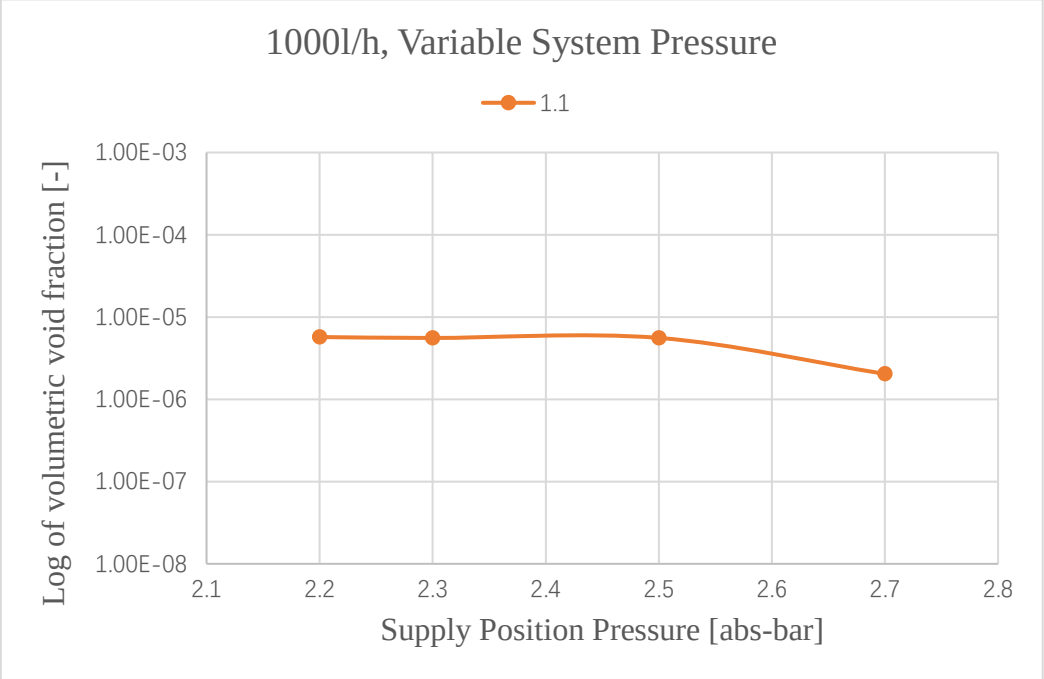

Figure 4. 31 Relationship between volumetric void fraction and system pressure at SR 1.10

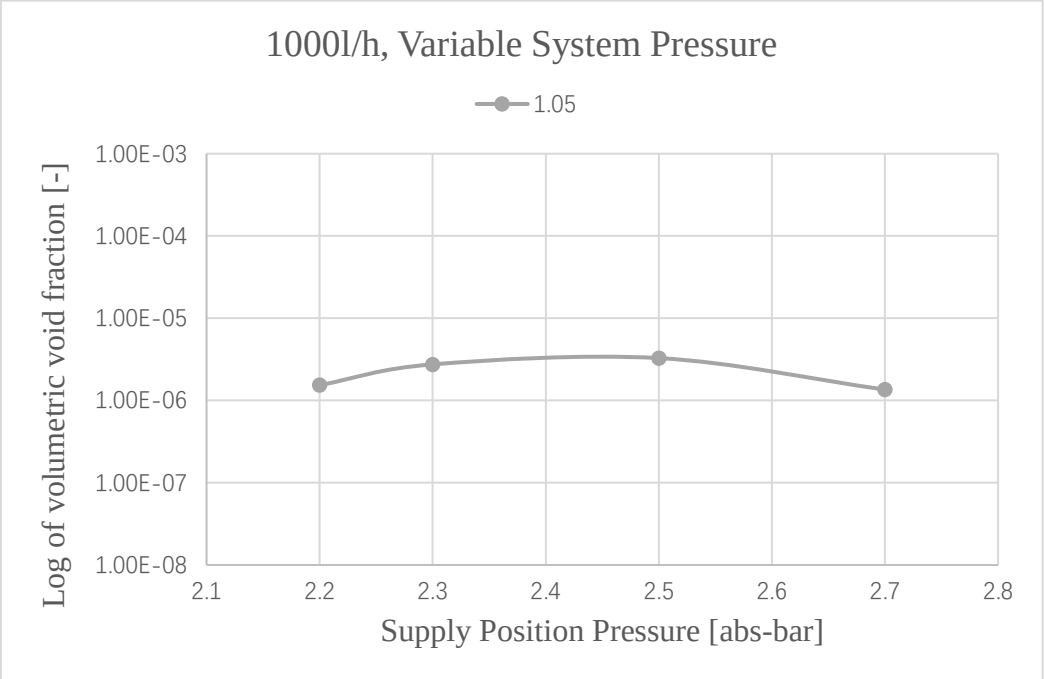

Figure 4. 32 Relationship between volumetric void fraction and system pressure at SR 1.05

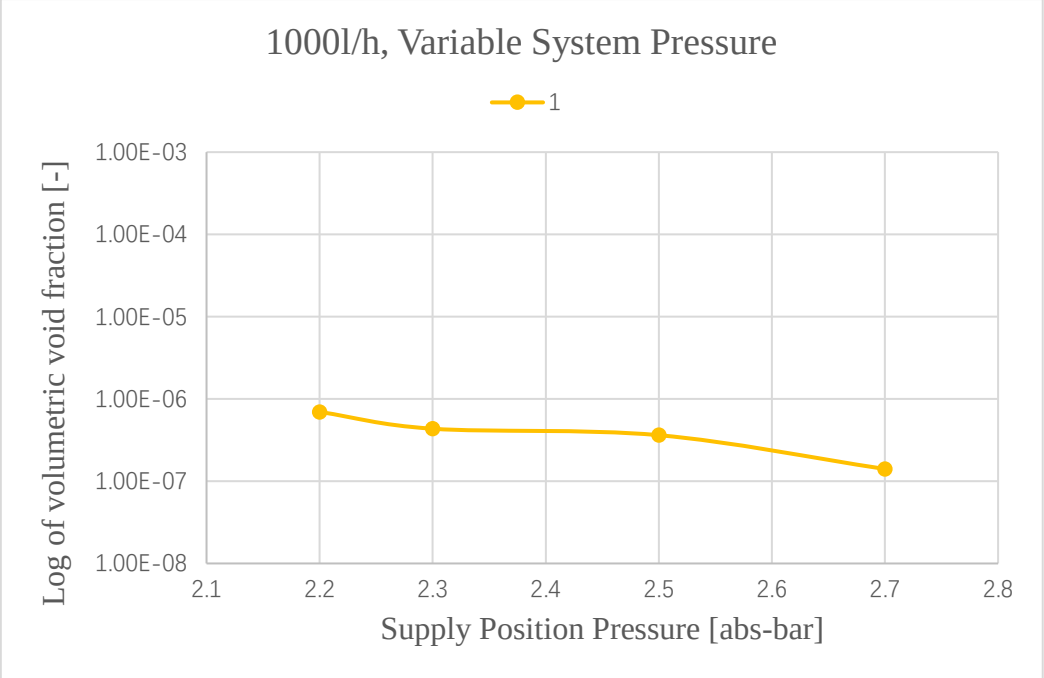

Figure 4. 33 Relationship between volumetric void fraction and system pressure at SR 1.00

Figure 4.31 – Figure 4.33 illustrate the relationships between volumetric void fractions and system pressure at SR 1.15, 1.10, 1.05 and 1.00 respectively. At saturation 1.15, the trend is most evident that the volumetric void fraction decreases along with the increase of the system pressure. In another way, the volumetric void fraction is inversely proportional to the system pressure. This conclusion matches the studies of Shefik and Fsadni (Fsadni, 2012; Shefik, 2015) at gas boiler water heating system. This conclusion indicate that the bubble production is enhanced in low pressure system pressures. Besides, the results match the nitrogen solubility graph. As the nitrogen has lower solubility at low pressures compared to high pressures, the bubbles come off from the water easier at low pressures.

4.5.4 Bubble volumetric void fraction distribution

A thorough understanding of the distribution of the volumetric void fraction is crucial for designing the gas deaerator products. This section is going to present some examples for explaining the distribution of the volumetric void fraction in the heat pump water heating system. This data is presented in relation to the position across the pipe section, from H-apparent 1mm to 14 mm. Four different saturation ratios were tested. The void fraction distribution in horizontal pipes is affected by the buoyancy effect of bubbles thus resulting in a higher void fraction at the upper section of the pipe. Big bubbles go to upper layers of the pipe in the force of water buoyance. This phenomenon causes more big bubbles captured in upper Depth of Focal Planes than lower ones. This trend results in the higher average bubble diameter and void fraction of upper DOF than lower ones.

Figure 4.34 illustrates the volumetric void fraction distribution at pipe cross-section at 1000 l/h, at 2.5 absolute bar. The volumetric void fraction at 1 mm DOF is the highest in all the depth of focal planes measured. This is the result of the effect of the buoyancy of the water. There is a trend that the volumetric void fraction decreases with moving down the depth of focal plane. This conclusion matches the results of Fsadni and Shefik at two-phase bubbly horizontal flow (Fsadni, 2012; Shefik, 2015).

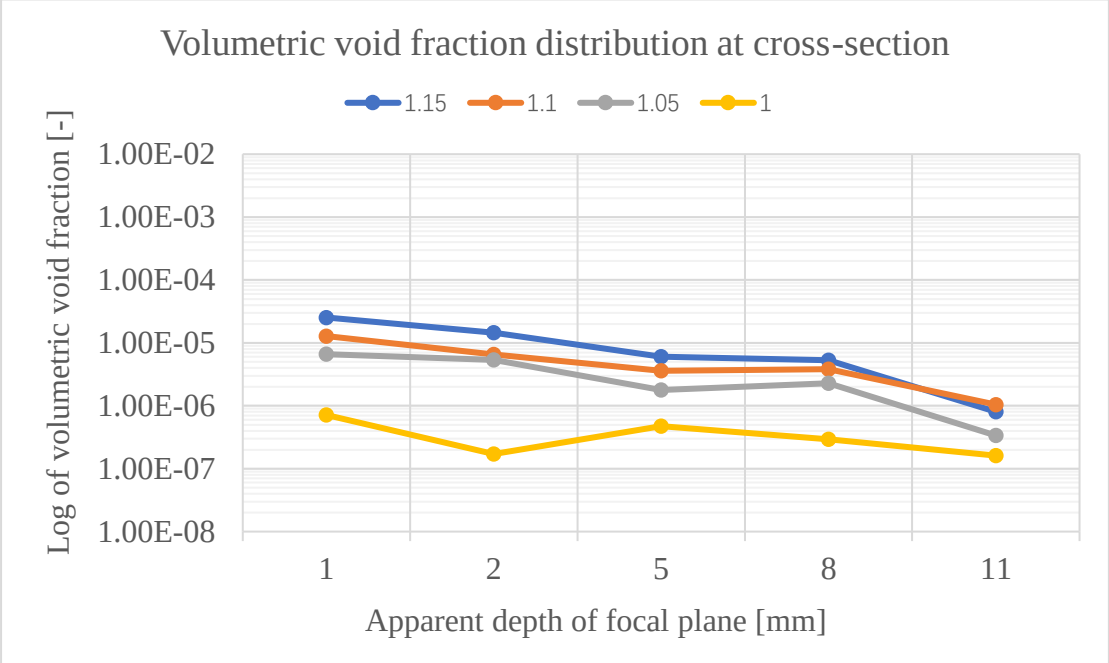

Figure 4. 34 Volumetric void fraction distribution at cross-section at 1000 l/h, 2.5 absolute bar

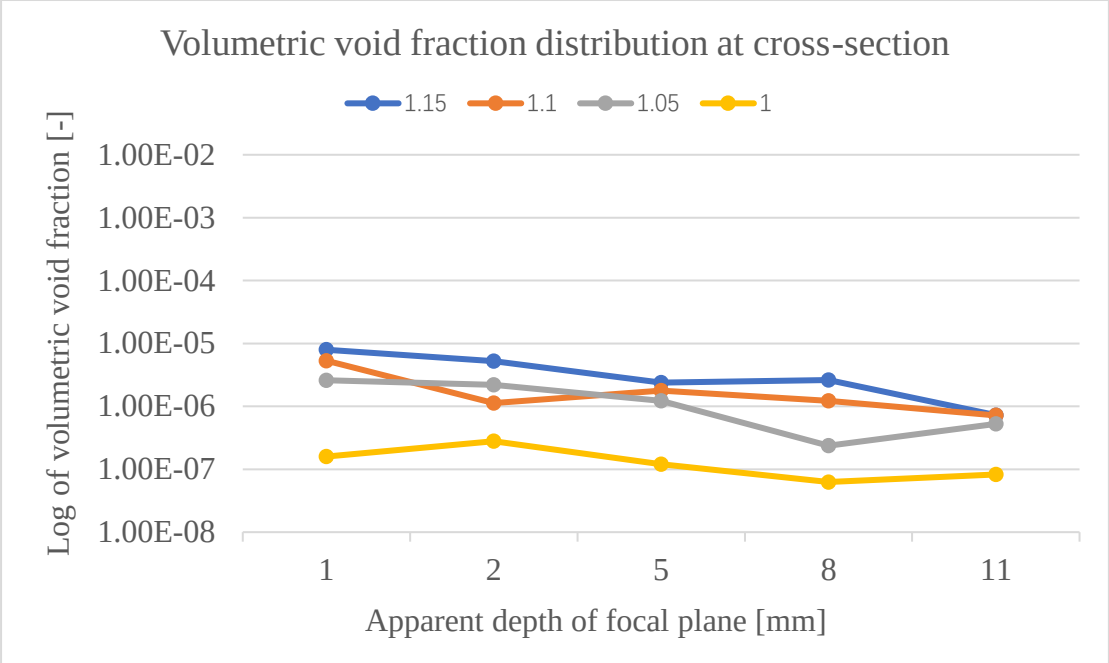

Figure 4. 35 Volumetric void fraction distribution at cross-section at 1000l/h, 2.7 absolute bar

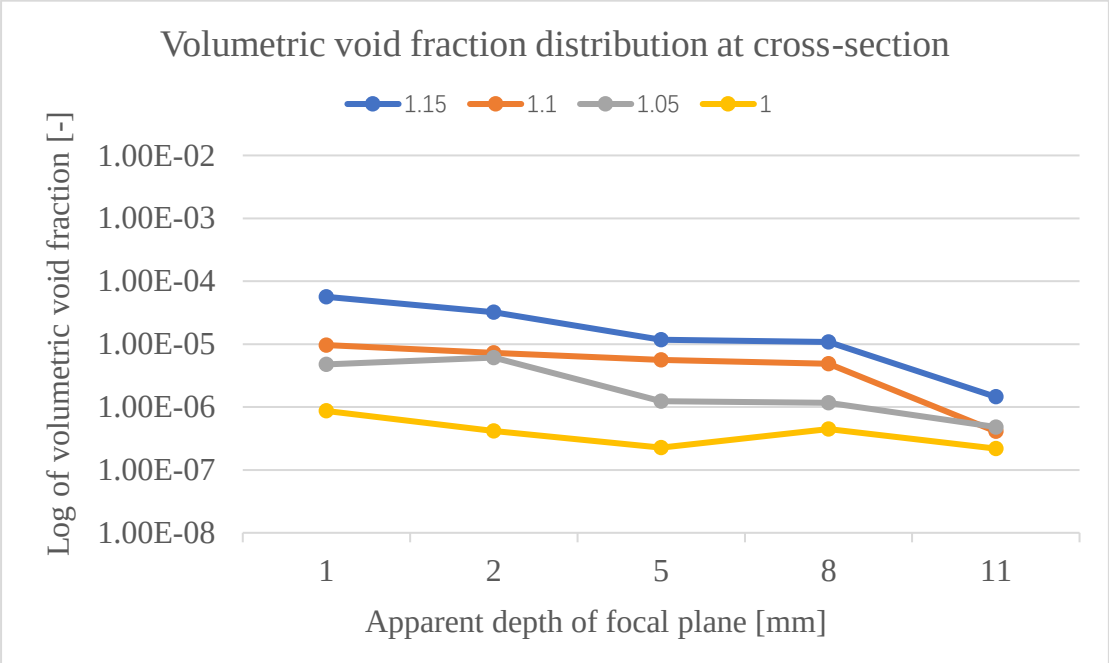

Figure 4. 36 Volumetric void fraction distribution at cross-section at 1000l/h, 2.3 absolute bar

There are relatively more bubbles at higher focal planes in the heat pump exit sight-glass as shown in Figure 4.34 – Figure 4.36. Due to the minor number of bubbles at SR 1.00, the distribution of bubble volumetric void fractions at three figures are not stable.

4.6 Bubble production rate

According to the results of several series of tests, the relationship between the various water flow rate and the bubble number have been found as shown in Figure 4.37. The range of the water flow rate is from 600 l/h to 1160 l/h.

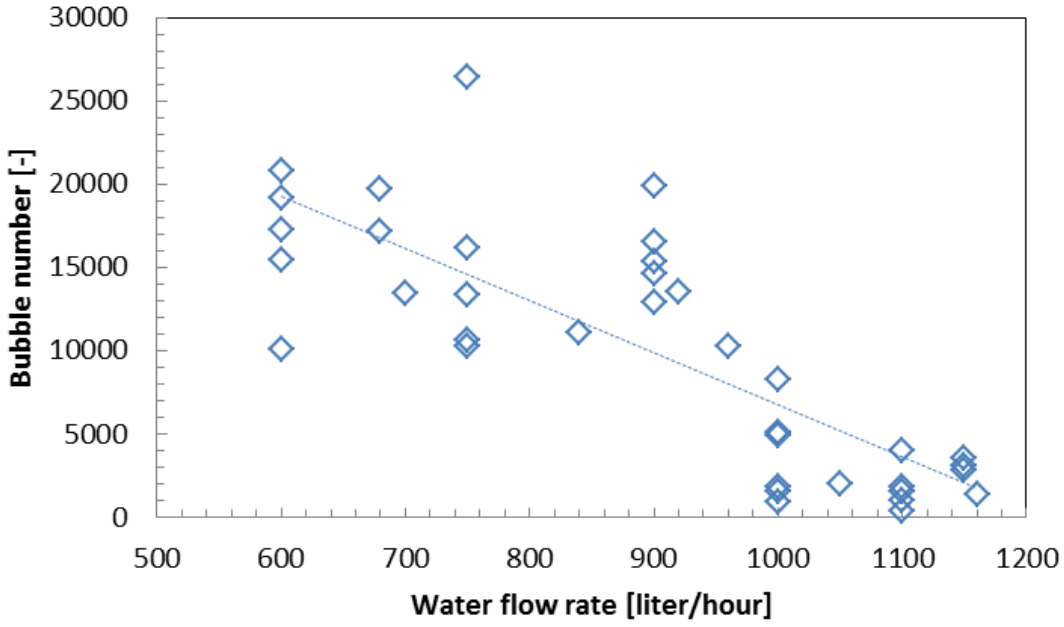

Figure 4. 37 Bubble production rate at various water flow rate

The filming time of each investigation is 3 minutes, which represents there are 5400 frames taken for each investigation. The trend is clear that the bubble numbers decreases along with the increase of the water flow rate.

As the water flow rate is higher than 1000 l/h, the bubble numbers rapidly decreases to less than 5000. This phenomenon is due to the increase of the turbulence level which leads to the bubble collision and coalescence. The explanation is validated by the results of the average bubble diameter which shows the average bubble diameter is larger at high water flow rate than that at low water flow rate.

The flow regime of the bubbly flow changes with the water flow rate increases from 600 l/h to 1160 l/h. Many tests failed at the water flow rate from 600 l/h to 750 l/h due to this flow regime change. The reason is the flow regimes at 600 l/ to 750 l/h are plug flow leading to the big plug covers the sight-glass. In a two-phase flow pipe, some bubbles have coalesced to form larger bubbles, or plugs. In a horizontal pipe, these

plugs flow at the top layer contacted with the inner wall of the pipe.

The plug flow regime is characterized by big elongated gas bubbles, which do not reach the dimension of the full section of the pipe. Therefore, a liquid volume is always presenting in the bottom part of the pipe. The flow regime of plug flow is caused by the high superficial velocity of the gas bubbles. These bubbles merge into the huge plug even though the turbulence level is low. However, the plug flow regime cannot present at high water flow rate with low superficial velocity of gas bubbles, even though the turbulence level is high.

4.7 City main water test

Many bubble behaviours tests, in a heat pump water heating system, have been done during last several years. All those tests are conducted in a supersaturated condition, which is achieved by injecting nitrogen into the buffer vessel. It is curious that what is the highest SR value that can be got without injecting nitrogen into the buffer vessel. A test has been done to find out the result.

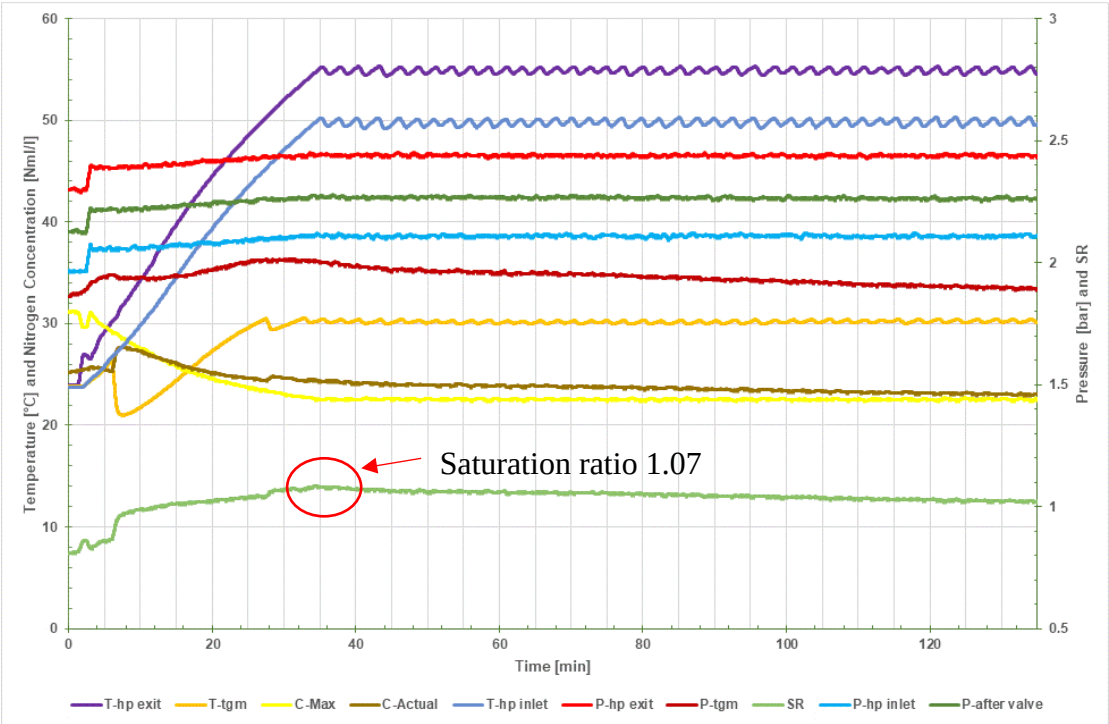

Figure 4. 38 City main water test system conditions

The working fluid comes from the city main water. The conditions of the test are shown in the figure 4.22. The SR value keeps increasing at the beginning of the test till to the value reached 1.07. This period is the first phase. During this phase, the temperature of water keeps increasing and the wall temperature of compressor outlet keeps increasing as well. The highest value of wall temperature of compressor outlet is 96 Celsius degree, at which point the water has the lowest solubility. Then the second phase comes. The nitrogen keeps coming off from the water and the SR keeps decreasing. This process is not going to stop until the actual dissolved nitrogen is no more than the solubility of water. Ant the lowest SR can be achieved in this system is around 0.98 by theoretical calculation.

This test identifies the supersaturated condition happens in the heat pump water heating system. And supersaturated condition means that the gas bubble is going to come off from the water. These gas bubbles are collected in the system such as radiators. This can cause the air block in the heating system and reduce the heating efficiency which ultimately leads to the increase of carbon dioxide equivalent emissions.

4.8 Summary

This chapter introduced and discussed the experimental results of the gas bubble behaviours in the air-source heat pump water heating system. First, the typical experimental conditions achieved is introduced in detail. Second, the bubble diameter characteristics were presented, which comprise four parts. The four parts included the effect of system pressure on the average bubble diameter, the effect of system water flow rate on the average bubble diameter, the effect of system saturation ratio on the average bubble diameter and the bubble diameter distribution at cross-section of the pipelines. A mathematical model to estimate the gas microbubble's diameter distributions, at various operating conditions, is obtained in present research. The conditions include varied system pressures, water flow rates, saturation ratios and heating loads. The 104 experimental tests have been conducted and analysed. The results show the gas microbubble's diameter distributions obey Gamma probability density function. The three parameters are α, β and μ. The values of three parameters are illustrated in figures. The prediction of bubble diameter distribution can help improving the design of deaerators. Furthermore, the bubble volumetric void fraction characteristics were illustrated, in which the effects of system water flow, system pressure and system saturation ratio on the volumetric void fraction were presented. In addition, the bubble production rate along with various system conditions were demonstrated. Finally, the highest saturation ratio of the city main water at specific environmental conditions were introduced. At that environmental temperature, the highest system saturation ratio achieved was 1.07.

Chapter 5 Bubble production in return pipe to the heat pump and pressure drop

5.1 Introduction

This chapter introduces the study of the bubble production in return pipe to the heat pump and the system pressure drops. This study can contribute to the instalment of the air-vents in the heat pump water heating system and understanding the bubble volumetric void fraction behaviours in the system. In this supersaturated two-phase bubbly flow system, bubble production may be generated at the return pipe depending on the system pressure drop. At heat pump inlet position, the pressure drop is the maximum in the system. Hence, it is necessary to study the bubble production at the heat pump inlet in this heat pump water heating system. During the test, the high-speed camera is moved between the sight-glasses at the heat pump inlet and exit.

5.2 Test Conditions

Table 5.1 provides the experimental conditions for this series tests. The water flow rate was 1000 l/h. The saturation ratio was measured at 1.15, 1.10 and 1.05. The system pressure was set at 2.5 absolute bar. The heat pump exit temperature was 55 ℃. The system pressure drop between the heat pump exit and the heat pump inlet was 0.4 bar. Two sight-glasses were installed at the heat pump exit and heat pump inlet respectively.

Table 5. 1 Experimental conditions

Flow rate (LPH)	SR (-)	System Pressure (abs-bar)	Heat Pump exit temp (°C)	Pressure drop (abs-bar)	Sight-glass Position
1000	1.05-1.15	2.5	55	0.4	Heat pump exit
1000	1.05-1.15	2.5	55	0.4	Heat pump inlet

Figure 5.1 and Figure 5.2 have shown the experimental conditions achieved at the pump

exit and the heat pump inlet respectively. An experimental skill has been used during the test, which is reducing the system pressure to boost the dissolved gas coming off from the water. This method can achieve the specific saturation ratio with shorter time.

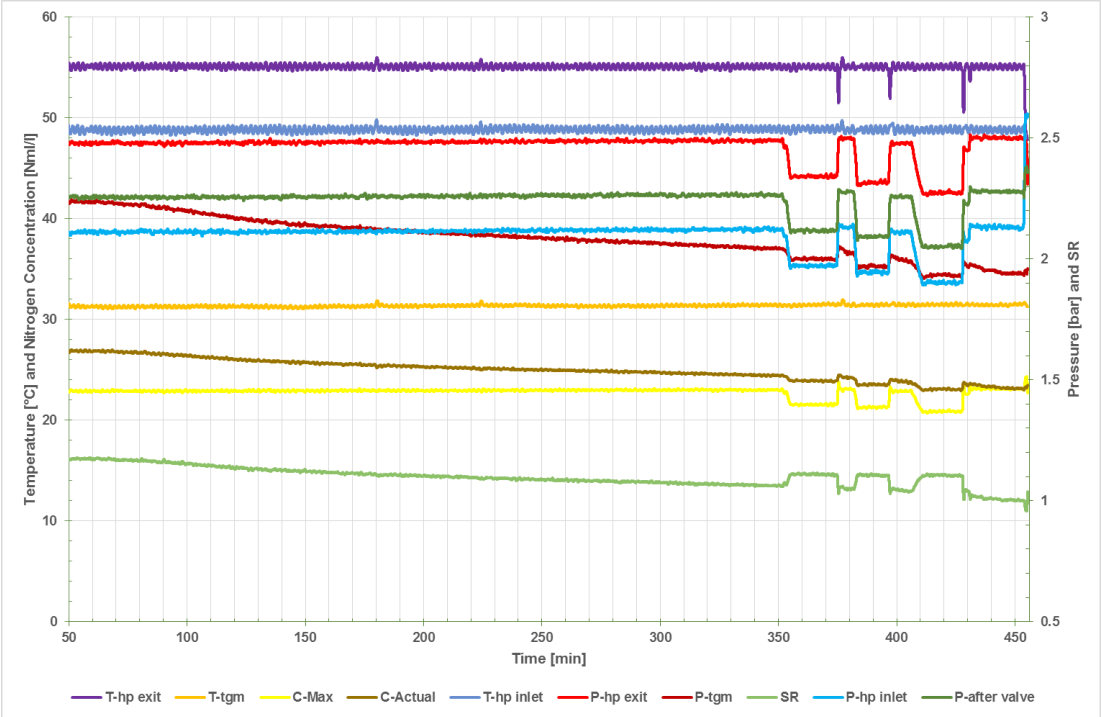

Figure 5. 1 System condition variations during the measurements at supply position

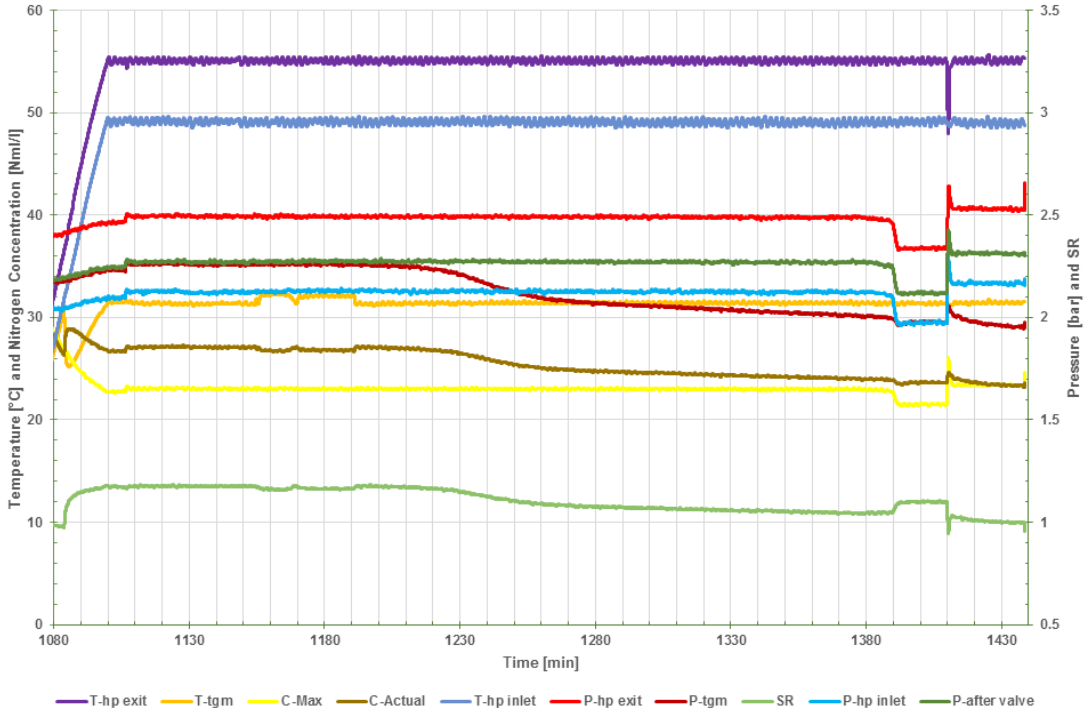

Figure 5. 2 System condition variations during the measurements at return position

5.3 Experimental results

The figures below present the results for the bubble volumetric void fraction distributions at the heat pump exit (outlet) and Return (inlet) positions in a horizontal bubbly two-phase flow. As illustrated in the following figures, the results are presented through the measured volumetric void fractions across the pipe section at different saturation ratio. These data are related to the positions across the pipe section, from H-apparent 1mm to 11 mm. Three different saturation ratios were investigated. In Figure 5. 4 and Figure 5. 5, the void fractions of the Return Positions are 0. Therefore, they are not shown in the figures.

As shown in Figure 5.3, Figure 5.4 and Figure 5.5, the void fraction is higher in upper focal planes than that in lower focal planes, which matches the trend found in preceding sections. The void fraction distribution in a horizontal pipe is affected by the buoyancy effect of bubbles thus resulting in a higher void fraction at the upper section of the pipe. These results are in the same trend with those from previous tests. In another way, the bubble volumetric void fraction distributions are the same between the heat pump exit and inlet.

The saturation ratio has a significant effect on the volumetric void fraction. The higher saturation ratio results in higher volumetric void fraction. These results are in the same trend with those from previous tests as well.

At these three saturation ratios, the SR 1.15 is the only condition that bubble productions are found at the heat pump inlet position as shown in Figure 5.3. There are no bubble productions found at SR 1.10 and SR 1.05 at the heat pump inlet position. This is because the actual dissolved nitrogen in the water is lower than the saturated conditions at SR 1.10 and SR 1.05. Considering the conclusion in section 4.7, which is that the maximum achievable saturation ratio by using city main water is 1.07, there should be no bubble productions at the heat pump inlet in the heat pump water heating system.

Figure 5.4 presents the bubble volumetric void fraction gradually decrease with the depth of focal plane getting deeper. As shown in Figure 5.5, there are most bubble production found at the second focal planes. This can be seen as the random error of the measurement due to the limited bubble numbers at the low saturation ratio.

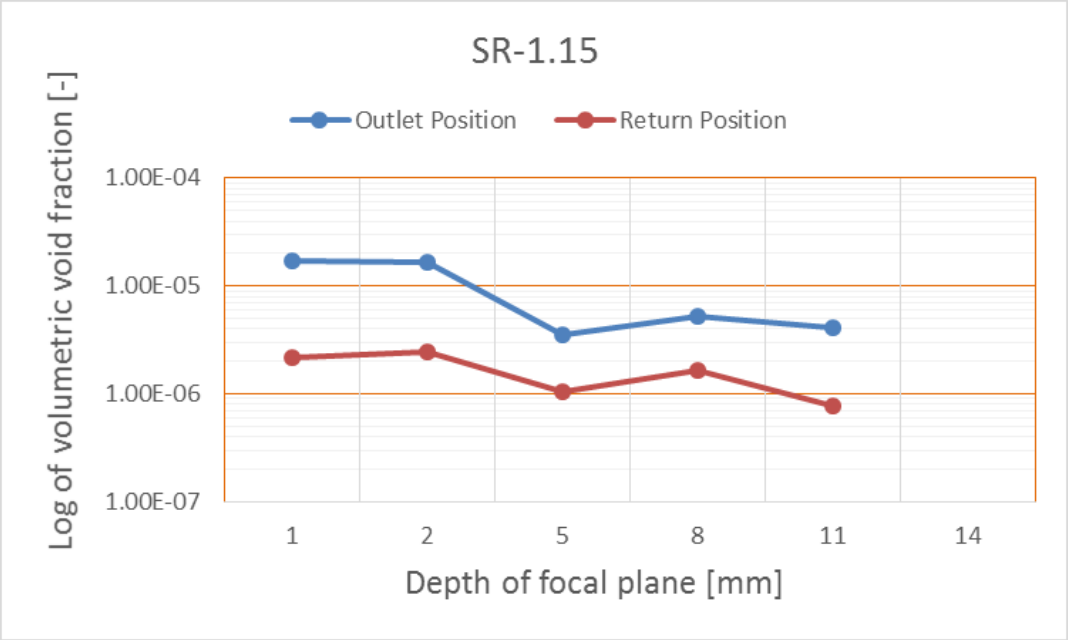

Figure 5. 3 Volumetric void fractions with focal plane depth across horizontal pipe at heat pump exit and inlet with the bulk fluid flow rate at 1000 l/h and saturation ratio at 1.15

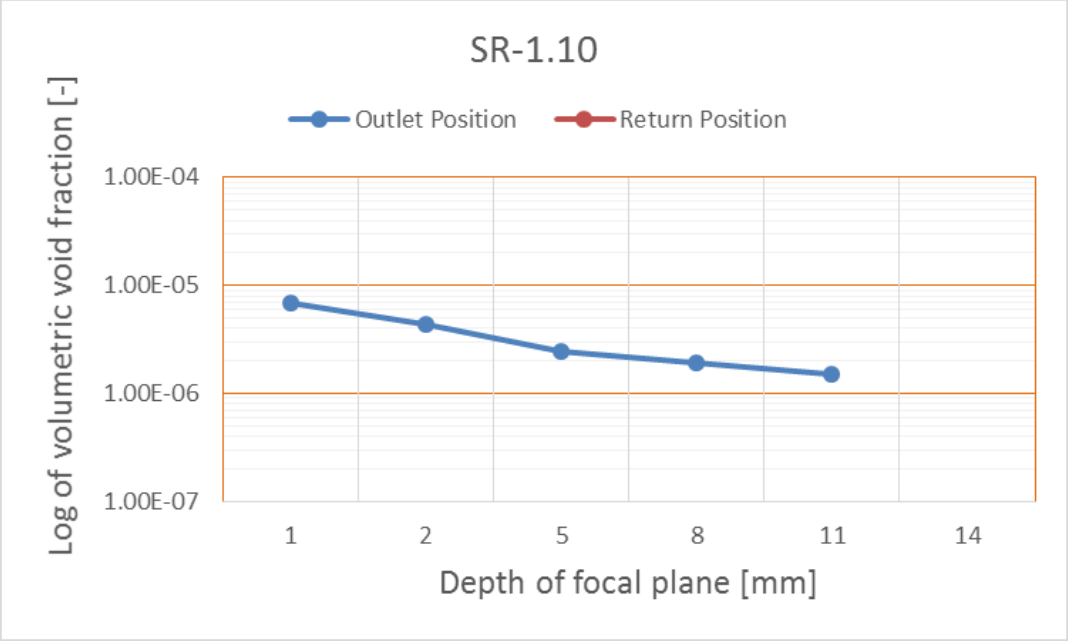

Figure 5. 4 Volumetric void fractions with focal plane depth across horizontal pipe at heat pump exit and inlet with the bulk fluid flow rate at 1000l/h and saturation ratio at 1.10 (No bubble measured at return position)

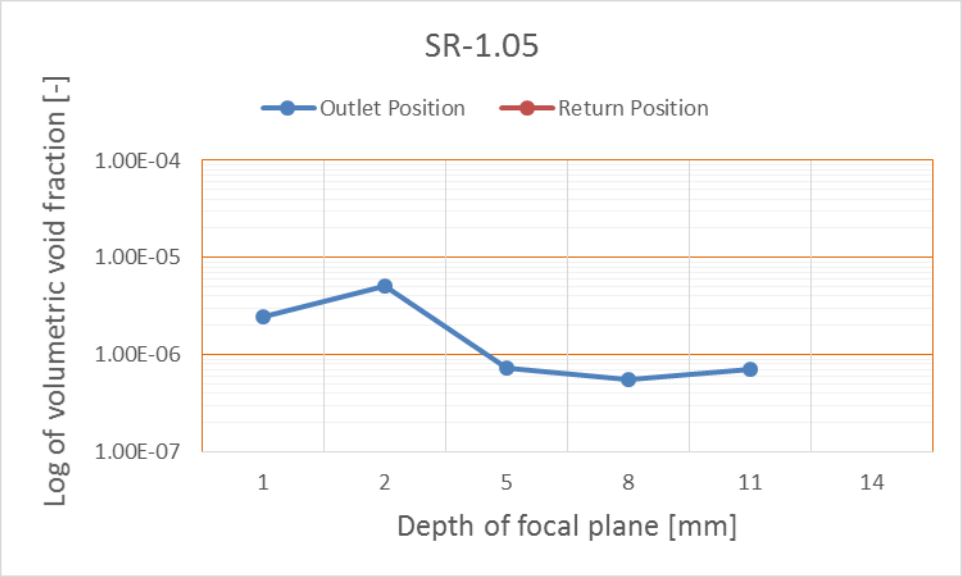

Figure 5. 5 Volumetric void fractions with focal plane depth across horizontal pipe at heat pump exit and inlet with the bulk fluid flow rate at 1000 l/h and saturation ratio at 1.05 (No bubble measured at return position)

5.4 Conclusion

The reasons of there are gas bubble production at the heat pump inlet position are the friction loss leading to the pressure at heat pump inlet position (2.1 bar) is lower than that at heat pump exit (2.5 bar) and the gas bubbles go through the buffer vessel to the heat pump inlet. The water becomes super-saturated at the heat pump inlet.

The higher saturation ratio results in higher volumetric void fraction at the same water flow rate. The void fraction distribution in a horizontal pipe is affected by the buoyancy effect of bubbles thus resulting in a higher void fraction at the upper section of the pipe comparing to that at the lower section of the pipe.

The bubble production is only found at the SR 1.15 at the heat pump inlet position, and there is no bubble found at SR 1.10 and SR 1.05 at the heat pump inlet position. This phenomenon can be interpreted as there is no bubble production at return pipe in the daily use in an air-source heat pump water heating system.

.

Chapter 6 Conclusions

6.1 Conclusions

The experimental investigation of the bubble behaviours in the domestic water heating system was accomplished with the help of Spirotech b.v. and Brunel University London. This project, as a continuous research project, shared a part of the experimental method with preceding researches. However, the difference between the present project and the previous projects are enormous as the temperatures of the wall of the plate heat exchanger in the air-source heat pump is much less than that in the gas boiler. This fundamental difference leads to that gas boiler water heating system has more bubble production. In addition, the geometries of heat exchangers are totally different in gas boiler system and heat pump system. The experimental time of gas boiler system is shorter comparing to the air-source heat pump water heating system.

In the present research, the improvements have been done in many fields. First, a PID control method was developed to control the heat pump exit temperature steadily. Second, a MATLAB programme was developed with the help of Baptiste, which increased the efficiency of analysing the bubble flow video. Thirdly, the total gas measurement equipment was assembled with more precision way by using the torque wrench with 10 NM moment of force. This method helped to increase the accuracy of the measurement of the partial pressure of the gas.

The results of the experimental tests were presented with various sections. The effects of various parameters of the system on the average bubble diameters were introduced. First, the average bubble diameters decrease along with the increase of the system pressures. In another way, there is an inverse relationship between the average bubble diameter and the system pressure. The bubble detachment diameter is affected by the system pressure. There is an inverse relationship between the detachment diameter and the system pressure. Besides, the average bubble diameter increases along with the increase of the system water flow rate. In another way, the average bubble diameter is proportional to the system water flow rate. This relation is caused by the phenomenon of the increase in bubble collision and coalescence with the increase of the turbulence level in the micro-channel of the plate heat exchanger in the air-source heat pump

system. Furthermore, the average bubble diameter slightly increases along with the increase of the system saturation ratio. The higher saturation ratio means more bubble production. Bubble collision and coalescence increases with the increase of bubble production in the micro-channel of the plate heat exchanger. Finally, the bubble diameter distribution was introduced. The big bubbles tend to appear at the upper layers of the depth of focal planes due to the effect of the buoyancy. A prediction equation for the bubble diameter distribution was proposed.

The effects of various parameters of the system on the volumetric void fraction were introduced. First, the effect of the system water flow rate on the volumetric void fraction was presented. The volumetric void fraction decreases along with the increase of the water flow rate. Second, the effect of the system saturation ratio on the volumetric void fraction was illustrated. The volumetric void fraction increases along with the increase of the system saturation ratio. In another way, the volumetric void fraction is proportional to the saturation ratio. This relation is due to the bubble production is proportional to the supersaturation level of the water.

The bubble production rate was introduced that the number of the bubble production decreases with the increase of the water flow rate. This is due to the high turbulence level at the micro-channel with low volumetric void fraction at high water flow rate. The highest city main saturation ratio was achieved at 1.07 at the specific environmental condition. This value depends on the weather, which means the value varies with the weather. In winter, this value could be higher due to the low temperature resulting in the high solubility of air in the system water. The volumetric void fraction was investigated in the heat pump inlet, which shows that there is bubble production at 1.15 and 1.10 saturation ratios caused by the system pressure drop.

6.2 Recommendations for improvements of heat pump system

The present study demonstrates that larger average bubble diameter is at the higher water flow rates at heat pump exit. Large bubbles are known can facilitate passive deaeration process in domestic central water heating system according to the working principle of passive deaerators. Besides, high water flow rates result in lower bubble production. Therefore, higher system water flow rates should lead to improved

deaeration rates to improve energy efficiency of heat pump system. Furthermore, two passive deaerators are suggested to install at the heat pump exit and inlet. Because gas bubbles could generate at return pipes due to the system pressure drops.

In addition, lower supply water temperatures and higher system pressures achieve lower saturation levels, which consequently reducing the bubble production in heat pump water heating system.

6.3 Recommendations for future work

Based on the experience acquired from this experimental investigation, following recommendations are suggested.

- A visualized plate heat exchanger is suggested to make to investigate bubbles' generation, collision and coalescence process.
- A customised heat pump system is suggested to make to investigate bubble behaviours at more conditions.
- Electrical impedance equipment is suggested to use to investigate void fraction. This technique can speed up test speed and result accuracy.

References

Abdelmessih, A. ., Hooper, F. . and Nangia, S. (1972) 'Flow effects on bubble growth and collapse in surface boiling', *International Journal of Heat and Mass Transfer*. Pergamon, 15(1), pp. 115–125. doi: 10.1016/0017-9310(72)90170-6.

Baptiste, C. (2015) *RESEARCH REPORT*.

Battino, R. and Clever, H. L. (1966) 'The solubility of gases in liquids', *Chemical Reviews*, 66(4), pp. 395–463. doi: 10.1021/cr60242a003.

Blander, M. and Katz, J. L. (1975) 'Bubble nucleation in liquids', *AIChE Journal*. Wiley-Blackwell, 21(5), pp. 833–848. doi: 10.1002/aic.690210502.

Bonjour, J., Clausse, M. and Lallemand, M. (2000) 'Experimental study of the coalescence phenomenon during nucleate pool boiling', *Experimental Thermal and Fluid Science*. Elsevier, 20(3–4), pp. 180–187. doi: 10.1016/S0894-1777(99)00044-8.

Cambridge in Colour (2018) *Understanding Depth of Field in Photography*. Available at: https://www.cambridgeincolour.com/tutorials/depth-of-field.htm (Accessed: 20 June 2018).

Chua, K. J., Chou, S. K. and Yang, W. M. (2010) 'Advances in heat pump systems: A review', *Applied Energy*, 87, pp. 3611–3624. doi: 10.1016/j.apenergy.2010.06.014.

Dean, R. B. (1944) 'The Formation of Bubbles', *Journal of Applied Physics*. American Institute of Physics, 15(5), pp. 446–451. doi: 10.1063/1.1707453.

DECC (2013) 'Energy Savings Opportunity Scheme (ESOS)', (July), pp. 1–92.

Desideri, U., Proietti, S. and Sdringola, P. (2009) 'Solar-powered cooling systems: Technical and economic analysis on industrial refrigeration and air-conditioning applications', *Applied Energy*. Elsevier, 86(9), pp. 1376–1386. doi: 10.1016/J.APENERGY.2009.01.011.

Druck (2014) *Sensing & Inspection Technologies PTX 7500 Series*.

EU (2002) *The Kyoto Protocol and climate change - background infromation MEMO/02/120*.

Fogg, P. G. T. (2003) ‘Some Aspects of the Solubility of Gases in Liquids’, *Monatshefte f€ u ur Chemie*, 134, pp. 619–631. doi: 10.1007/s00706-002-0580-x.

Fsadni, A. M. (2012) ‘The fundamentals of two-phase flow in wet domestic central heating systems’, (April), pp. 1–254.

Fsadni, A. M. and Ge, Y. (2012) ‘Micro bubble formation and bubble dissolution in domestic wet central heating systems’, *EPJ Web of Conferences*, 25, p. 01016. doi: 10.1051/epjconf/20122501016.

Fsadni, A. M., Ge, Y. T. and Lamers, A. G. (2011) ‘Experimental analysis of two-phase flow in domestic central heating systems: micro bubble characteristics’, in, pp. 165–176. doi: 10.2495/MPF110141.

Fsadni, A. M., Ge, Y. T. and Lamers, A. G. (2011) ‘Measurement of bubble detachment diameters from the surface of the boiler heat exchanger in a domestic central heating system’, *Applied Thermal Engineering*, 31(14–15), pp. 2808–2818. doi: 10.1016/j.applthermaleng.2011.05.006.

Fsadni, A. M., Ge, Y. T. and Lamers, A. G. (2012) ‘Bubble nucleation on the surface of the primary heat exchanger in a domestic central heating system’, *Applied Thermal Engineering*, 45–46, pp. 24–32. doi: 10.1016/j.applthermaleng.2012.04.016.

Ge, Y. T., Fsadni, A. M. and Wang, H. S. (2013) ‘Bubble dissolution in horizontal turbulent bubbly flow in domestic central heating system’, *Applied Energy*, 108, pp. 477–485. doi: 10.1016/j.apenergy.2013.03.055.

Hefter, G. T. and Tomkins, R. P. T. (Reginald P. T. . (2003a) *The experimental determination of solubilities*. J. Wiley & Sons.

Henry, W. (1803) ‘Experiments on the Quantity of Gases Absorbed by Water, at Different Temperatures, and under Different Pressures’, *Philosophical Transactions of the Royal Society of London*. The Royal Society, 93(0), pp. 29–274. doi: 10.1098/rstl.1803.0004.

Hoang, N. H. *et al.* (2016) ‘A mechanistic model for predicting the maximum diameter of vapor bubbles in a subcooled boiling flow’, *International Journal of Heat and Mass Transfer*. Pergamon, 94, pp. 174–179. doi: 10.1016/J.IJHEATMASSTRANSFER.2015.11.051.

Jones, S. (1999) ‘The cycle of bubble production from a gas cavity in a supersaturated solution’, *Advances in Colloid and Interface Science*, 80(1), pp. 51–84. doi: 10.1016/S0001-8686(98)00075-X.

Jones, S. F., Evans, G. M. and Galvin, K. P. (1999) ‘Bubble nucleation from gas cavities - A review’, *Advances in Colloid and Interface Science*, 80(1), pp. 27–50. doi: 10.1016/S0001-8686(98)00074-8.

Kingspan (2014) *User interface Comfort Series Installation Manual*.

Kong, R. *et al.* (2018) ‘Effects of pipe size on horizontal two-phase flow: Flow regimes, pressure drop, two-phase flow parameters, and drift-flux analysis’, *Experimental Thermal and Fluid Science*, 96, pp. 75–89. doi: 10.1016/j.expthermflusci.2018.02.030.

Lee, S., Devahdhanush, V. S. and Mudawar, I. (2018) ‘Investigation of subcooled and saturated boiling heat transfer mechanisms, instabilities, and transient flow regime maps for large length-to-diameter ratio micro-channel heat sinks’, *International Journal of Heat and Mass Transfer*, 123, pp. 172–191. doi: 10.1016/j.ijheatmasstransfer.2018.02.020.

Leith, W. C. and Thompson, A. L. (1960) ‘Some Corrosion Effects in Accelerated Cavitation Damage’, *Journal of Basic Engineering*. American Society of Mechanical Engineers, 82(4), p. 795. doi: 10.1115/1.3662761.

Liu, C. *et al.* (2018) ‘A high-temperature hybrid absorption-compression heat pump for waste heat recovery’, *Energy Conversion and Management*, 172, pp. 391–401. doi: 10.1016/j.enconman.2018.07.027.

Liu, Q., Wang, W. and Palm, B. (2017) ‘Numerical study of the interactions and merge of multiple bubbles during convective boiling in micro channels’, *International Communications in Heat and Mass Transfer*. pp. 10–17. doi: 10.1016/J.ICHEATMASSTRANSFER.2016.11.009.

Lu, J., Fernández, A. and Tryggvason, G. (2005) ‘The effect of bubbles on the wall drag in a turbulent channel flow’, *Physics of Fluids*. American Institute of Physics, 17(9), p. 095102. doi: 10.1063/1.2033547.

Lubetkin, S. and Blackwell, M. (1988) ‘The nucleation of bubbles in supersaturated solutions’, *Journal of Colloid and Interface Science*. Academic Press, 126(2), pp. 610–

615. doi: 10.1016/0021-9797(88)90161-0.

Miglani, S., Orehounig, K. and Carmeliet, J. (2018) 'Integrating a thermal model of ground source heat pumps and solar regeneration within building energy system optimization', *Applied Energy*. Elsevier, 218, pp. 78–94. doi: 10.1016/J.APENERGY.2018.02.173.

Mohanraj, M. *et al.* (2018) 'Research and developments on solar assisted compression heat pump systems – A comprehensive review (Part A: Modeling and modifications)', *Renewable and Sustainable Energy Reviews*. Pergamon, 83, pp. 90–123. doi: 10.1016/J.RSER.2017.08.022.

Moumouni, Y. and Galupa, N. (2018) 'Experimental evaluation of a wind turbine's energy dependence on air density', *2018 Advances in Science and Engineering Technology International Conferences, ASET 2018*. IEEE, pp. 1–4. doi: 10.1109/ICASET.2018.8376777.

Nassar, A. B. (1994) 'Apparent depth', *The Physics Teacher*. American Association of Physics Teachers, 32(9), pp. 526–529. doi: 10.1119/1.2344102.

National Grid (2014) *UK Future Energy Scenarios UK gas and electricity transmission*. Available at: http://fes.nationalgrid.com/media/1298/2014-fes.pdf (Accessed: 18 June 2018).

National Instruments (2008) 'User Guide and Specifications: USB-6008/6009', *System*, pp. 1–32. doi: 371303L-01 May08.

Nawaz, K. *et al.* (2017) 'Performance optimization of CO 2 heat pump water heater', *International Journal of Refrigeration*. Elsevier Ltd, 85, pp. 213–228. doi: 10.1016/j.ijrefrig.2017.09.027.

Nilpueng, K. and Wongwises, S. (2010) 'Two-phase gas–liquid flow characteristics inside a plate heat exchanger', *Experimental Thermal and Fluid Science*, 34(8), pp. 1217–1229. doi: 10.1016/j.expthermflusci.2010.05.001.

Pamperin, O. and Rath, H.-J. (1995) 'Influence of buoyancy on bubble formation at submerged orifices', *Chemical Engineering Science*. Pergamon, 50(19), pp. 3009–3024. doi: 10.1016/0009-2509(95)00140-Z.

Perry, R. H., Green, D. W. and Maloney, J. O. (1997) *Chemical Engineers ' Handbook Seventh, Society*. doi: 10.1021/ed027p533.1.

Phantom (2007) 'Phantom v5.1', 170, pp. 8–10. Available at: http://www.komiweb.co.kr/data/v51.pdf.

Prodanovic, V., Fraser, D. and Salcudean, M. (2002) 'Bubble behavior in subcooled flow boiling of water at low pressures and low flow rates', *International Journal of Multiphase Flow*. Pergamon, 28(1), pp. 1–19. doi: 10.1016/S0301-9322(01)00058-1.

R.Buckminster Fuller (1968) *A Fuller View - Buckminster Fuller's Vision of Hope and Abundance for All - Buckminster Fuller's Synergy Solutions for Today*. Available at: http://www.buckyfullernow.com/a-fuller-view---buckminster-fullers-vision-of-hope-and-abundance-for-all.html (Accessed: 10 July 2018).

RENSEN, J., LUTHER, S. and LOHSE, D. (2005) 'The effect of bubbles on developed turbulence', *Journal of Fluid Mechanics*. Cambridge University Press, 538(1), p. 153. doi: 10.1017/S0022112005005276.

Shefik, A. (2015) 'INVESTIGATION OF TWO-PHASE FLOW STRUCTURES IN THE PIPEWORK OF WET CENTRAL HEATING SYSTEMS', PhD Thesis, Brunel University London, London.

Shuxue, X. *et al.* (2018) 'Investigation of air-source heat pump using heat pipes as heat radiator', *International Journal of Refrigeration*. Elsevier Ltd, 90, pp. 91–98. doi: 10.1016/J.IJREFRIG.2018.03.025.

Simply Bearings Ltd (2010) *AISI 52100 Chrome Steel Data Sheet*. Available at: https://simplybearings.co.uk/shop/files/52100.pdf (Accessed: 20 May 2018).

Socrates Christidis (2018) *UK heat pump market is growing again*. Available at: https://www.openaccessgovernment.org/uk-heat-pump-market-is-growing-again/44301/ (Accessed: 17 June 2018).

Song, M. *et al.* (2018) 'Review on improvement for air source heat pump units during frosting and defrosting', *Applied Energy*, 211(December 2017), pp. 1150–1170. doi: 10.1016/j.apenergy.2017.12.022.

Staudinger, J. and Roberts, P. V. (1996) 'A critical review of Henry's law constants for

environmental applications', *Critical Reviews in Environmental Science and Technology*. Taylor & Francis Group , 26(3), pp. 205–297. doi: 10.1080/10643389609388492.

Taylor, J. R. (1997) *An introduction to error analysis : the study of uncertainties in physical measurements*. University Science Books.

The European Commission (2016) 'The new Energy efficiency measures'. Available at: https://ec.europa.eu/energy/sites/ener/files/documents/technical_memo_energyefficiency.pdf.

The European Commission (2018) *Heating and cooling - European Commission*. Available at: https://ec.europa.eu/energy/en/topics/energy-efficiency/heating-and-cooling (Accessed: 1 June 2018).

The Renewables First (2018) *Heat Pump Introduction*. Available at: http://www.renewablesfirst.co.uk/water-source-heat-pumps/heat-pump-introduction/ (Accessed: 19 June 2018).

Tsai, Y.-C., Liu, F.-B. and Shen, P.-T. (2009) 'Investigations of the pressure drop and flow distribution in a chevron-type plate heat exchanger', *International Communications in Heat and Mass Transfer*. Pergamon, 36(6), pp. 574–578. doi: 10.1016/J.ICHEATMASSTRANSFER.2009.03.013.

Vlasogiannis, P. *et al.* (2002) 'Air-water two-phase flow and heat transfer in a plate heat exchanger', *International Journal of Multiphase Flow*. doi: 10.1016/S0301-9322(02)00010-1.

Vorushylo, I. *et al.* (2018) 'How heat pumps and thermal energy storage can be used to manage wind power: A study of Ireland', *Energy*. Elsevier Ltd, 157, pp. 539–549. doi: 10.1016/j.energy.2018.03.001.

Wallerand, A. S. *et al.* (2018) 'Optimal heat pump integration in industrial processes', *Applied Energy*, 219, pp. 68–92. doi: 10.1016/j.apenergy.2018.02.114.

Wang, D. *et al.* (2018) 'Heating performance evaluation of a CO2 heat pump system for an electrical vehicle at cold ambient temperatures', *Applied Thermal Engineering*. Pergamon, 142, pp. 656–664. doi: 10.1016/J.APPLTHERMALENG.2018.07.062.

Wilhelm, E., Battino, R. and Wilcock, R. J. (1977) ‘Low-Pressure Solubility of Gases in Liquid Water’, *Chemical Reviews*. doi: 10.1021/cr60306a003.

Winterton, R. H. S. (1972) ‘Sizes of bubbles produced by dissolved gas coming out of solution on the walls of pipes in flowing systems’, *Chemical Engineering Science*. Pergamon, 27(6), pp. 1223–1230. doi: 10.1016/0009-2509(72)80099-X.

Wu, W. *et al.* (2018) ‘Configurations of solar air source absorption heat pump and comparisons with conventional solar heating’, *Applied Thermal Engineering*. Elsevier, 141(October 2017), pp. 630–641. doi: 10.1016/j.applthermaleng.2018.06.024.

Yin, L., Jia, L. and Xu, M. (2015) ‘Experimental investigation on bubble sliding during subcooled flow boiling in microchannel’, *Experimental Thermal and Fluid Science*. Elsevier, 68, pp. 435–441. doi: 10.1016/J.EXPTHERMFLUSCI.2015.05.010.

Zeng, L. Z. *et al.* (1993) ‘A unified model for the prediction of bubble detachment diameters in boiling systems—II. Flow boiling’, *International Journal of Heat and Mass Transfer*. Pergamon, 36(9), pp. 2271–2279. doi: 10.1016/S0017-9310(05)80112-7.

Zhang, A. M. *et al.* (2015) ‘Experimental study on bubble dynamics subject to buoyancy’, *Journal of Fluid Mechanics*. Cambridge University Press, 776, pp. 137–160. doi: 10.1017/jfm.2015.323.

Appendix I Bubble distributions

This section presents some examples of the cumulative bubble behaviours distributions, which were used to analyse the two-phase flow in the heat pump water heating system.

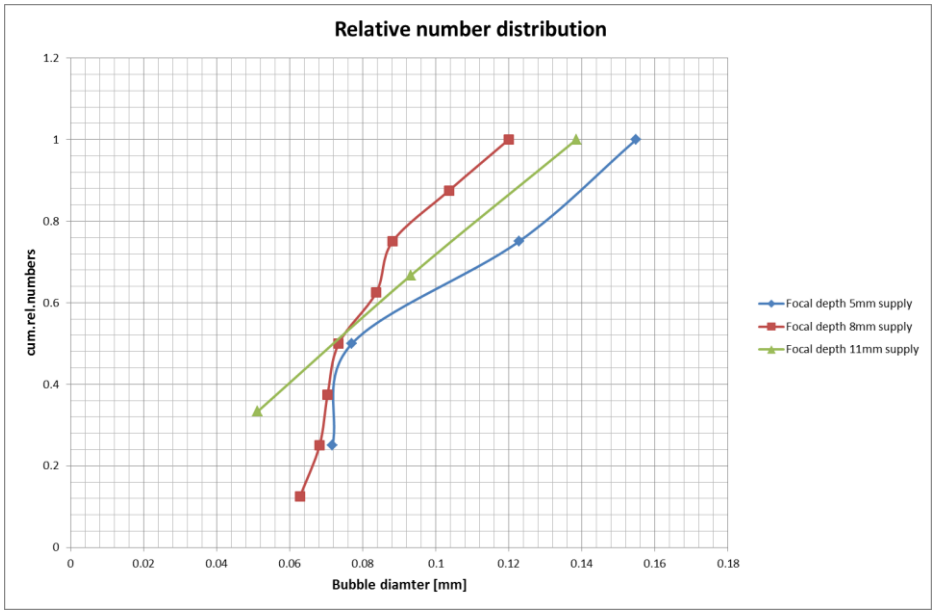

Appendix. 1 Relative number distribution at SR=1.0

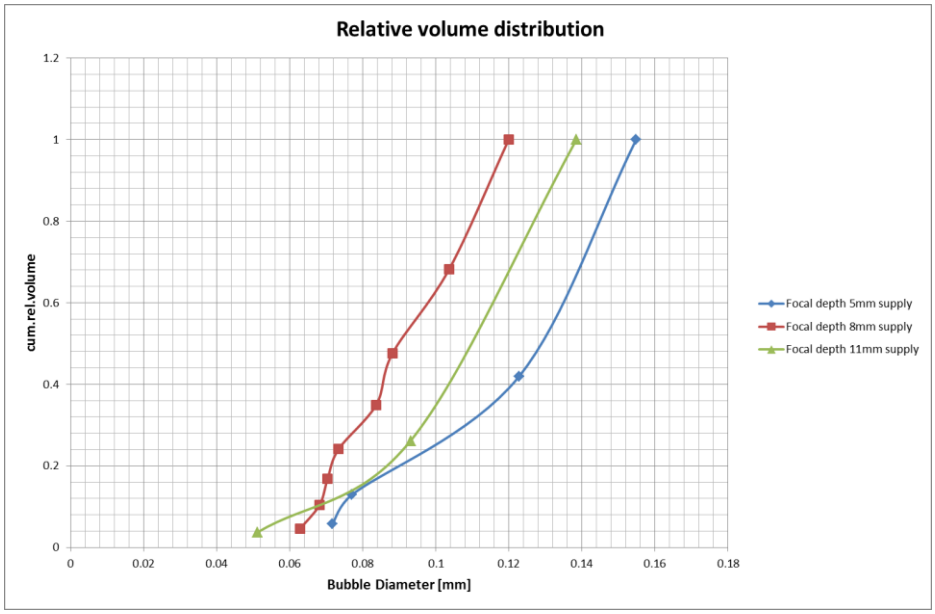

Appendix. 2 Relative volume distribution at SR=1.0

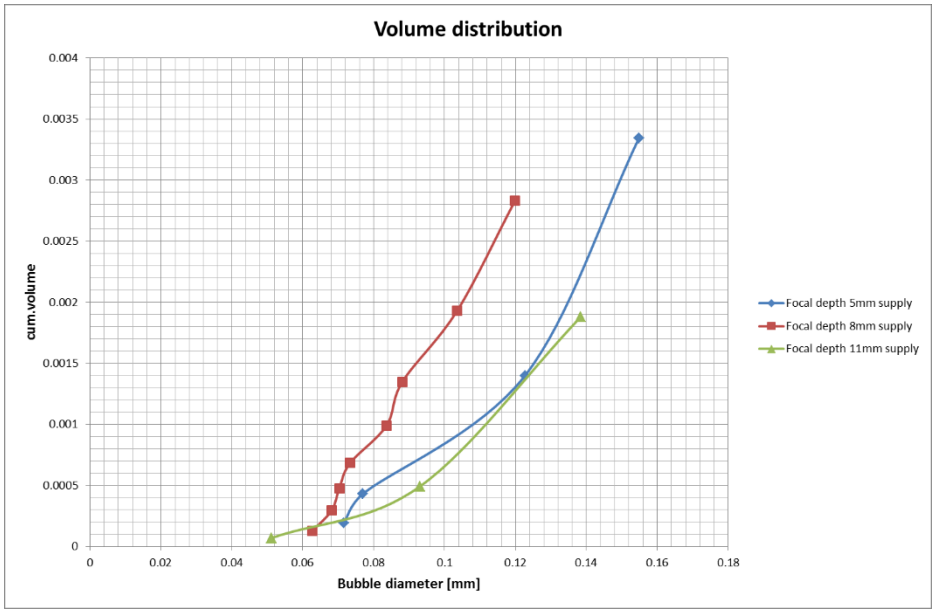

Appendix. 3 Volume distribution at SR=1.0

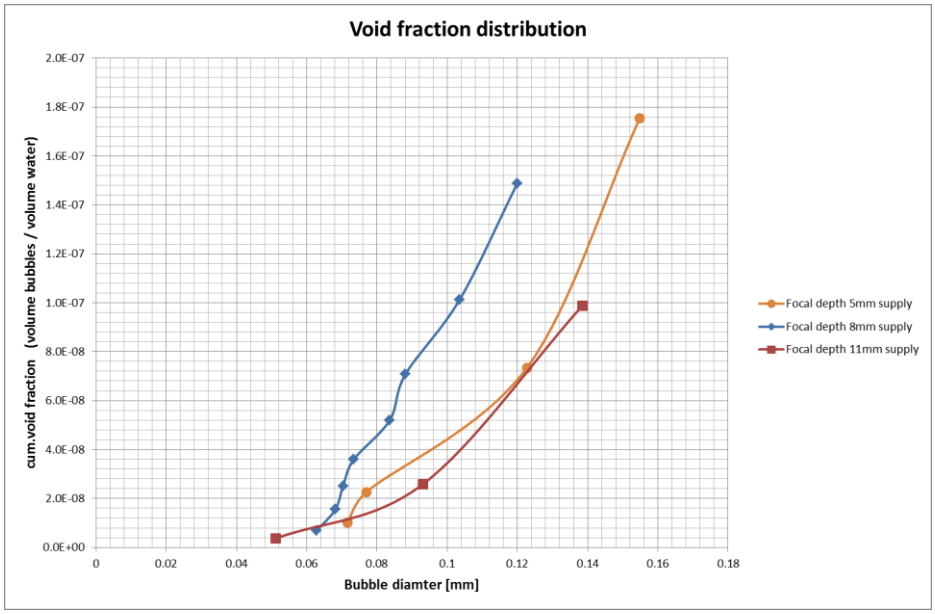

Appendix. 4 Void fraction distribution at SR=1.0

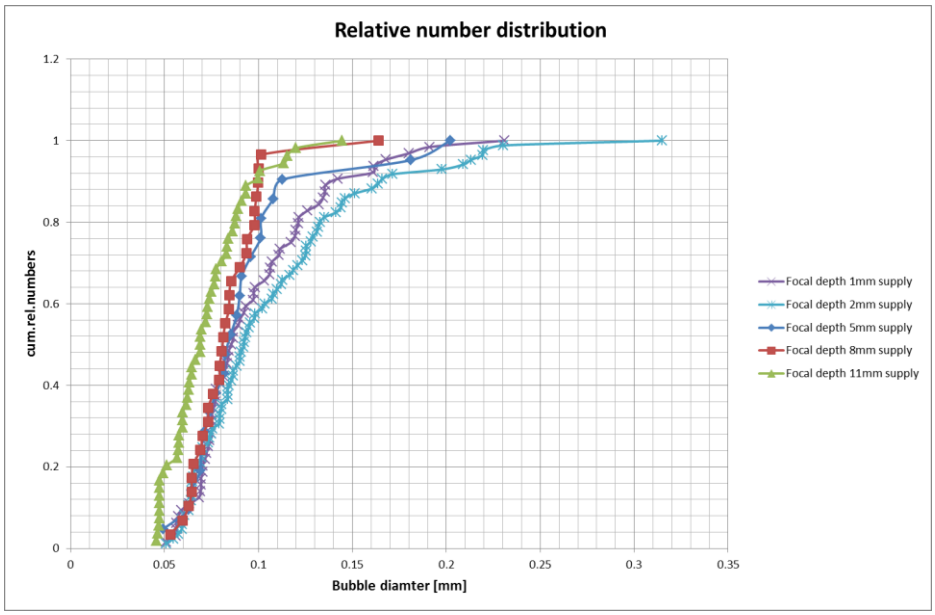

Appendix. 5 Relative number distribution at SR=1.05

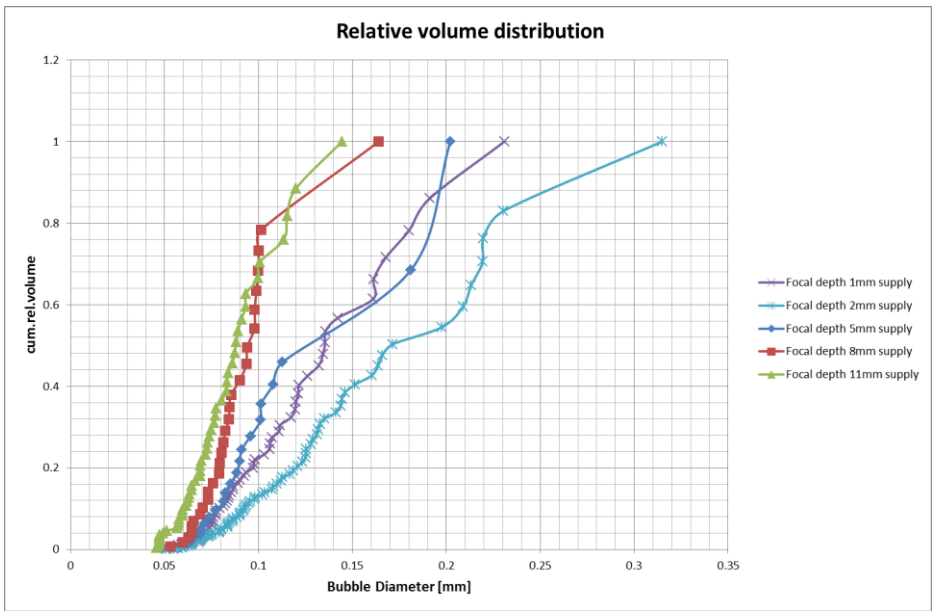

Appendix. 6 Relative volume distribution at SR=1.05

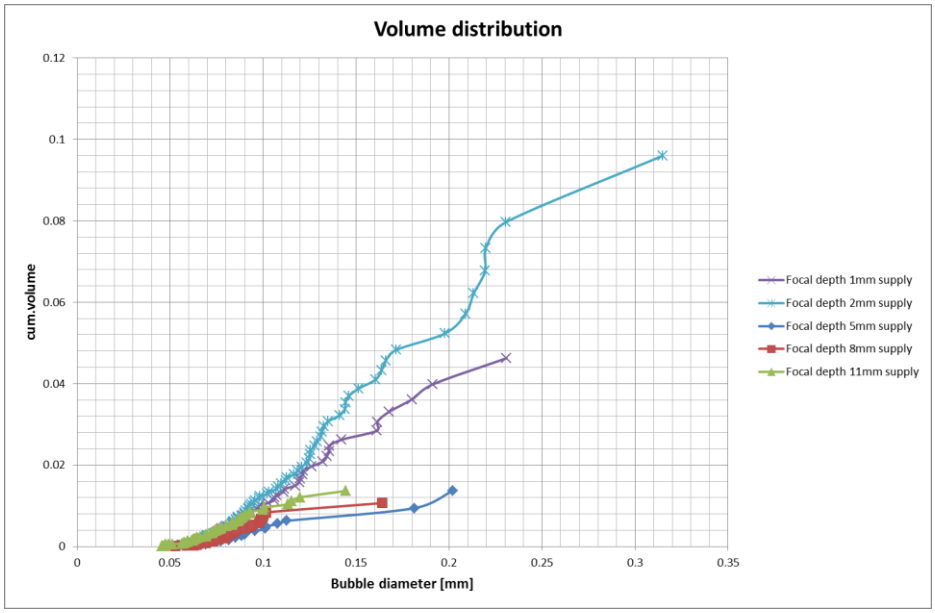

Appendix. 7 Volume distribution at SR=1.05

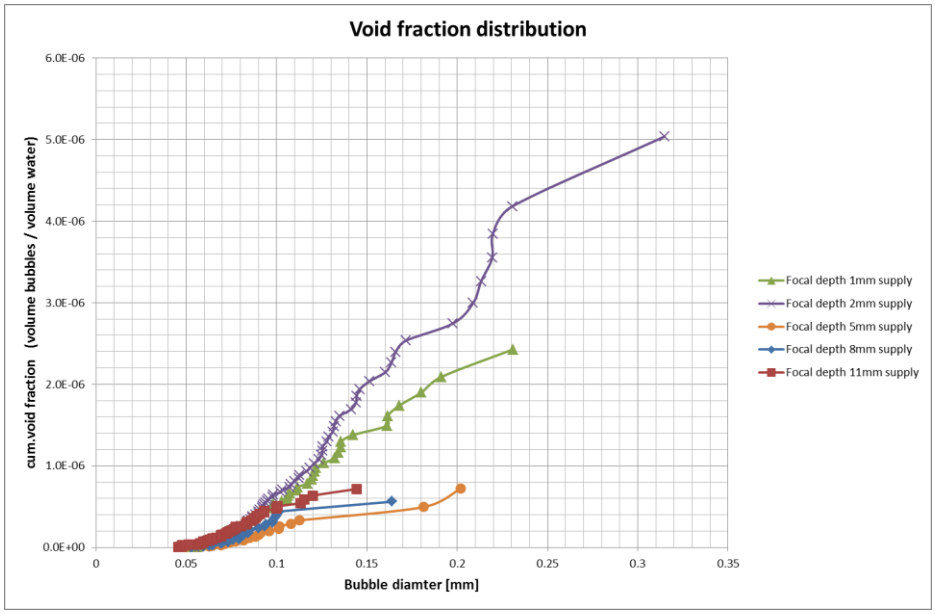

Appendix. 8 Void fraction distribution at SR=1.05

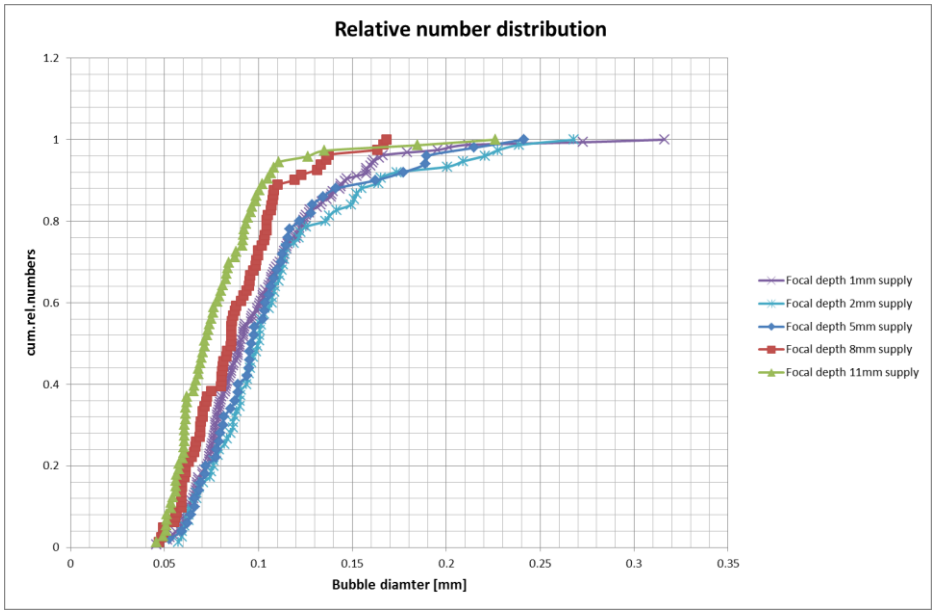

Appendix. 9 Relative number distribution at SR=1.10

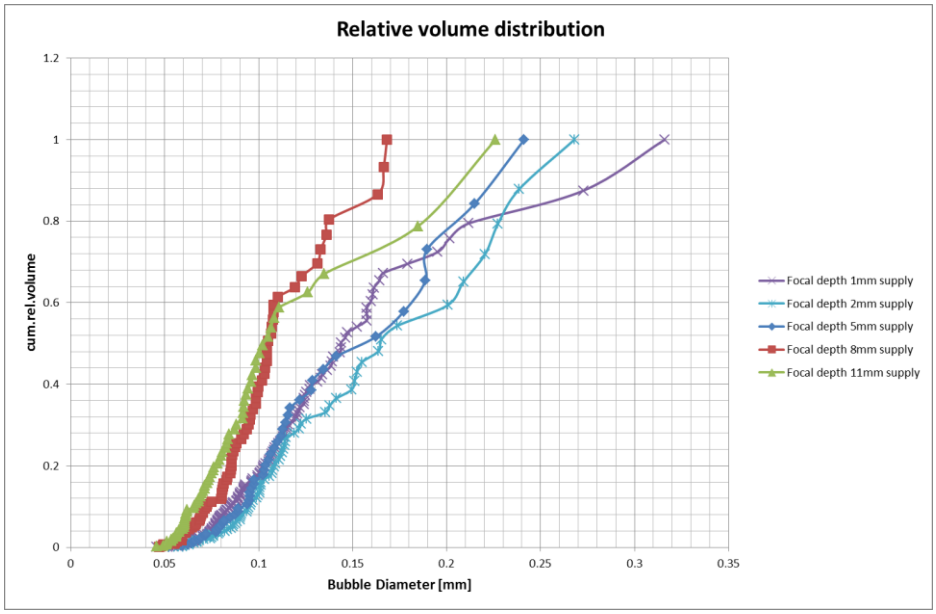

Appendix. 10 Relative volume distribution at SR=1.10

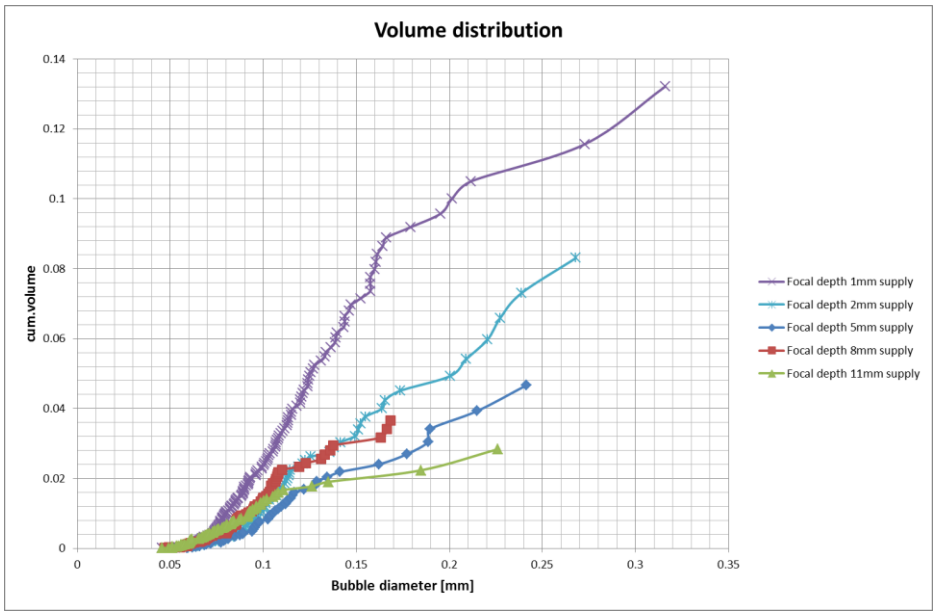

Appendix. 11 Volume distribution at SR=1.10

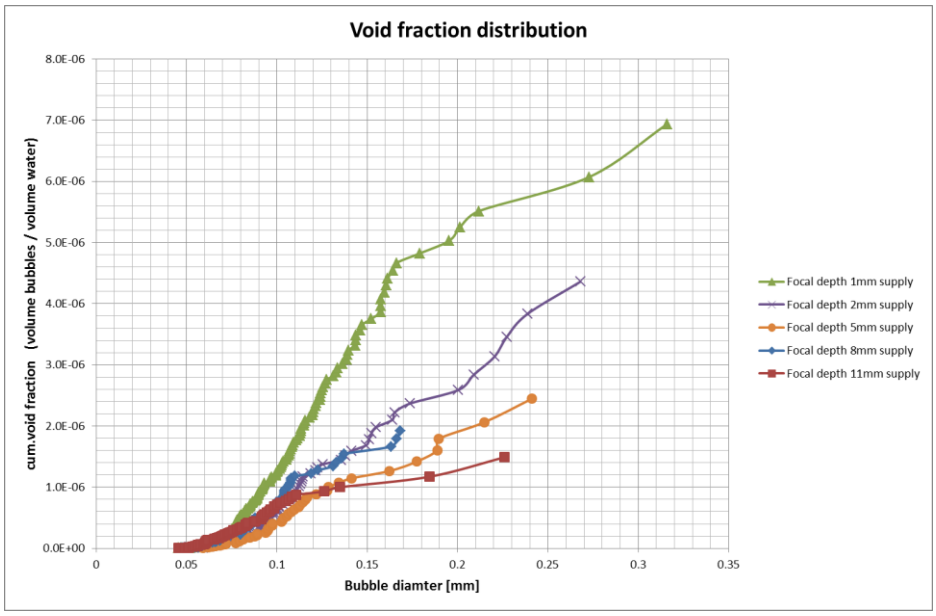

Appendix. 12 Void fraction distribution at SR=1.10

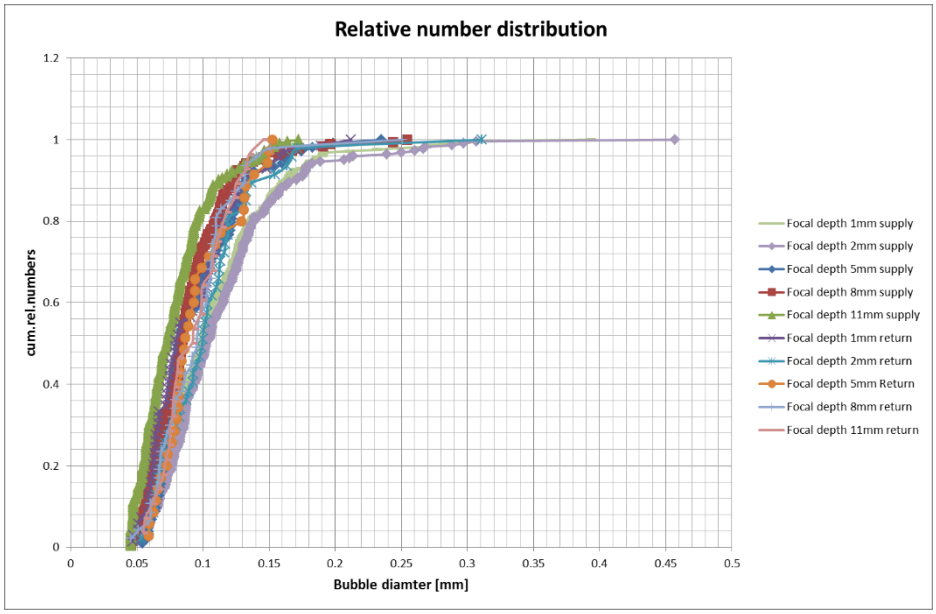

Appendix. 13 Relative number distribution at SR=1.15

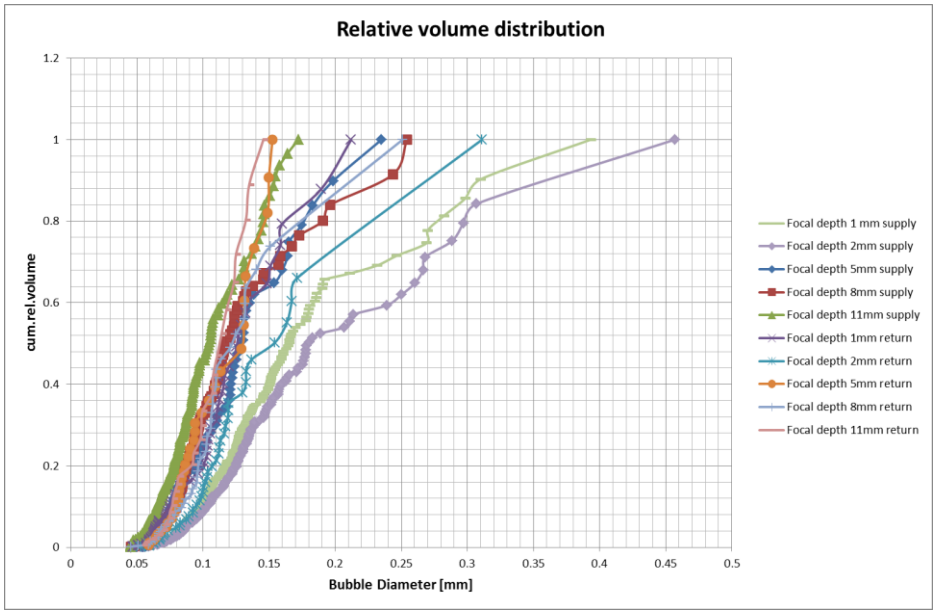

Appendix. 14 Relative volume distribution at SR=1.15

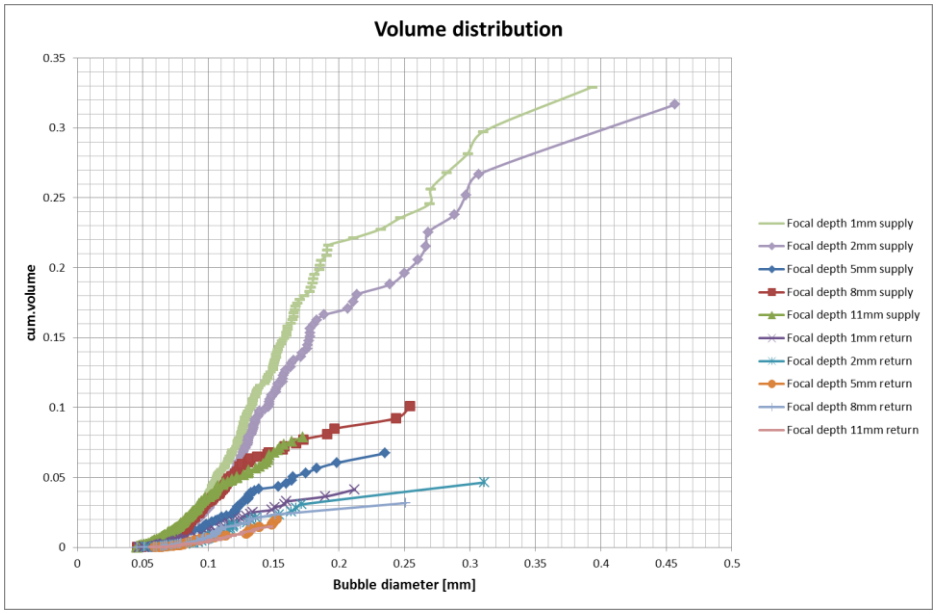

Appendix. 15 Volume distribution at SR=1.15

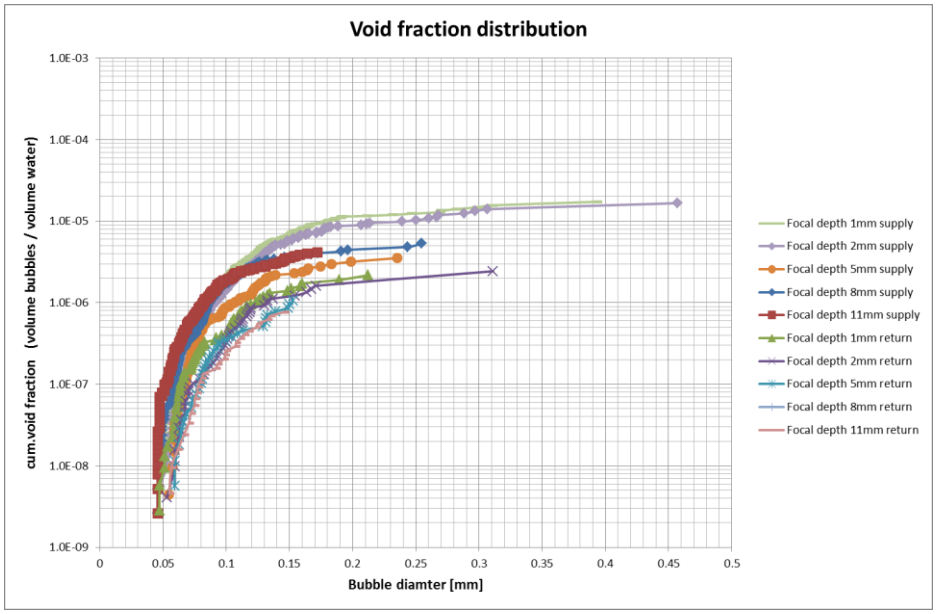

Appendix. 16 Void fraction distribution at SR=1.15

Appendix II LabVIEW programme

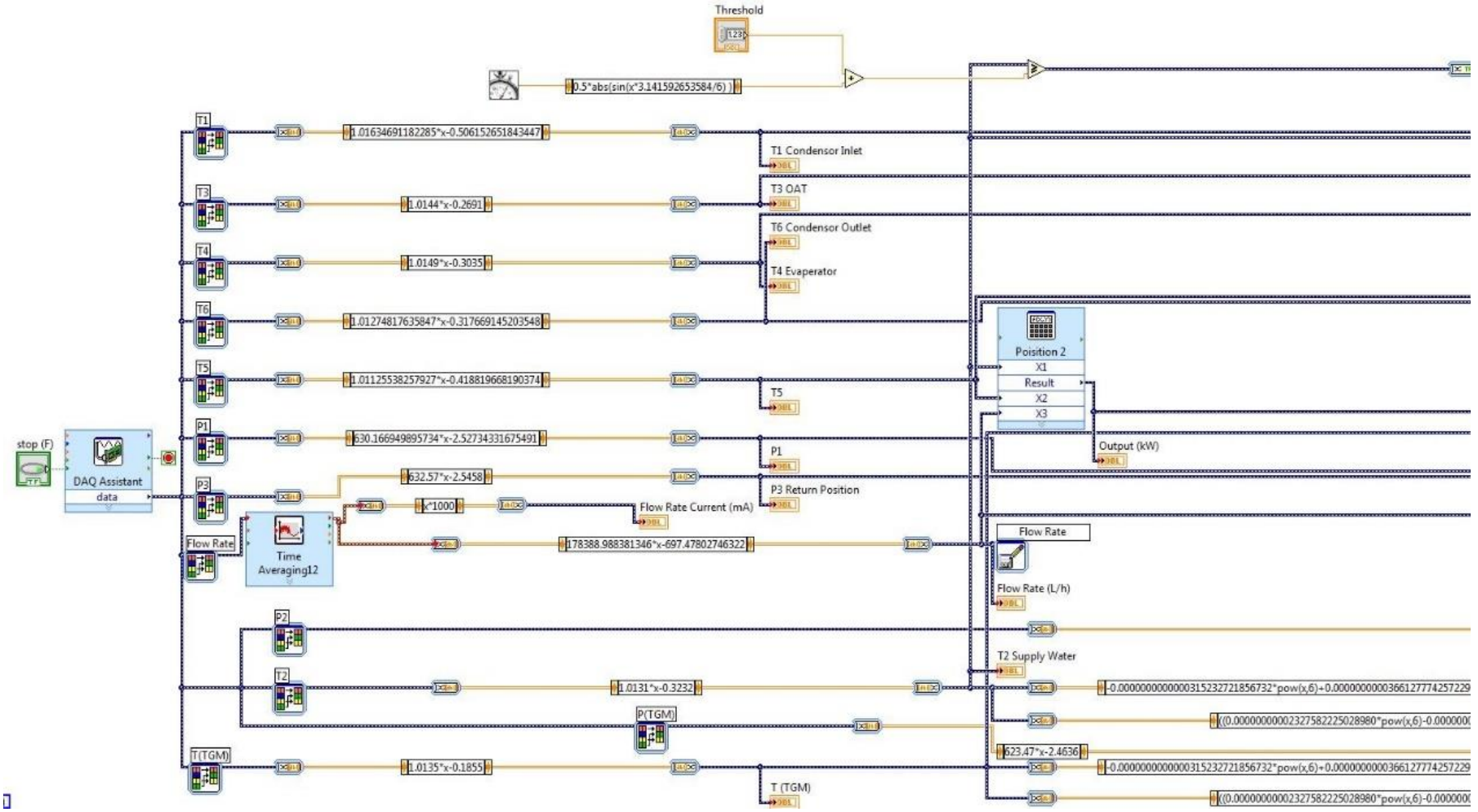

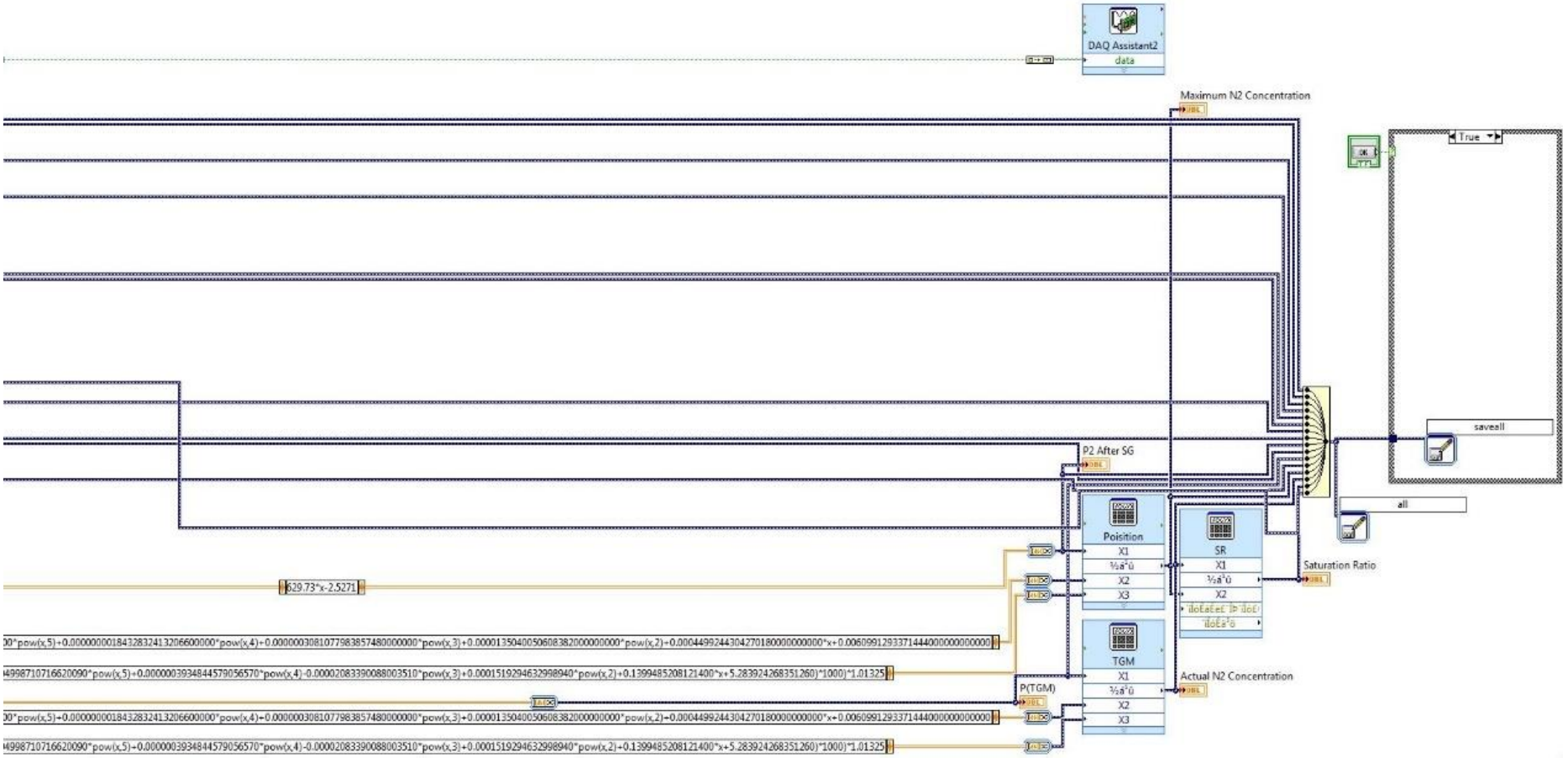

Appendix. 17 LabVIEW block design

Appendix III Calibration equations for sensors

The calibration equations for sensors have been shown as follows.

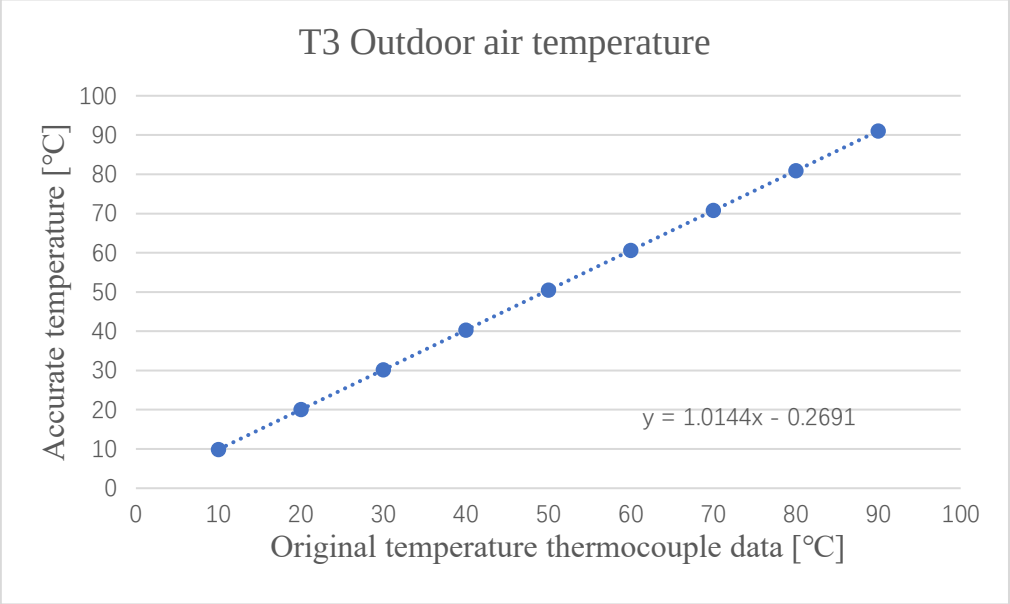

Appendix. 18 Calibration equation for T3 outdoor air temperature

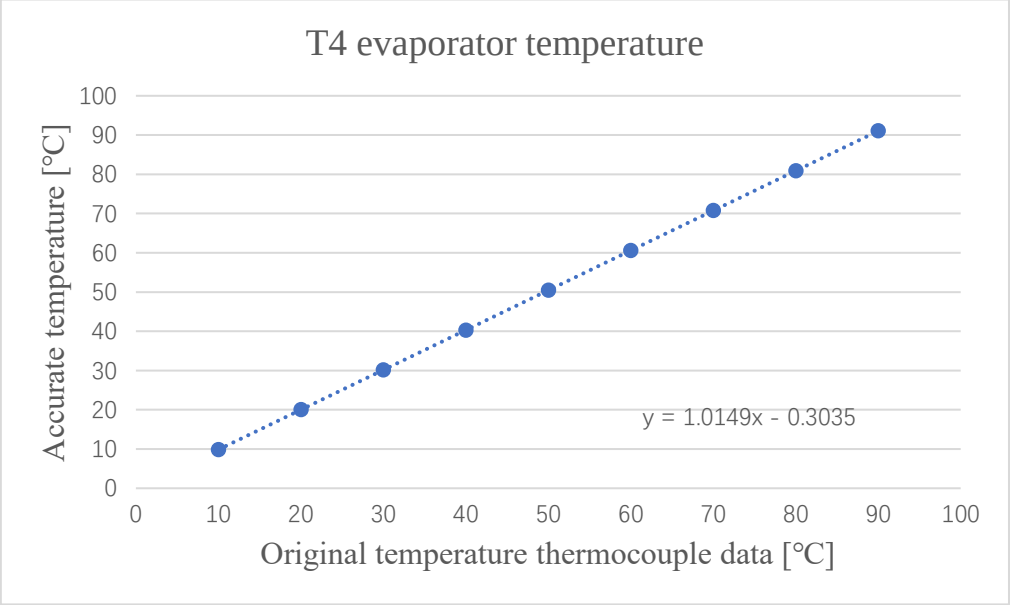

Appendix. 19 Calibration equation for T4 evaporator temperature

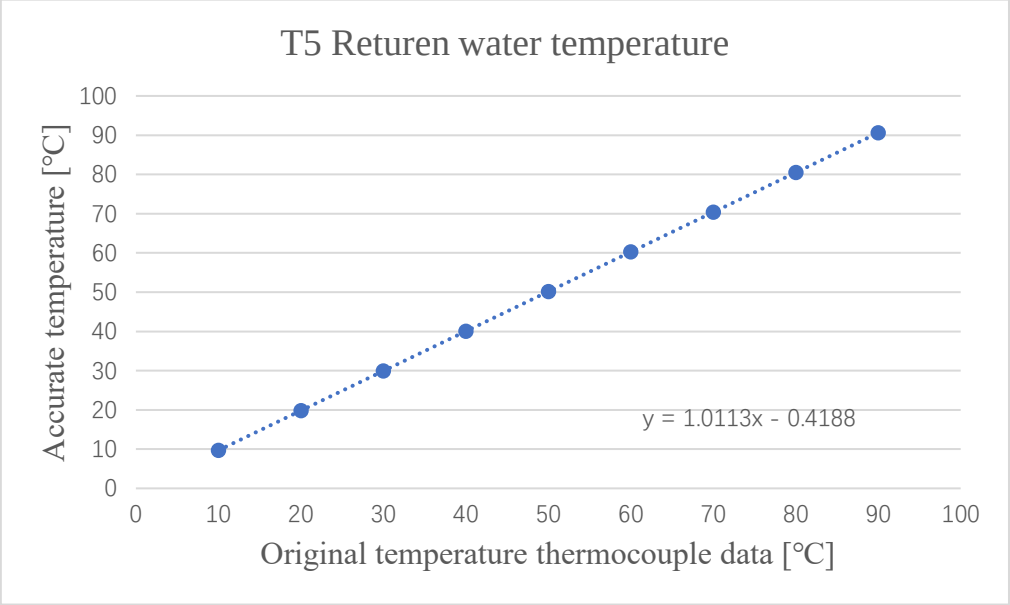

Appendix. 20 Calibration equation for T5 return water temperature

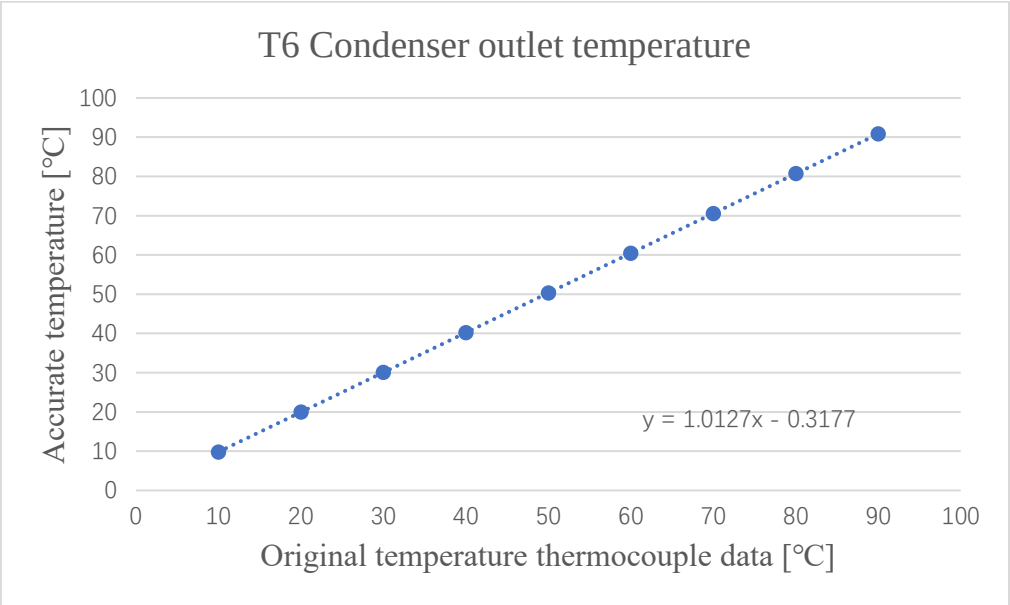

Appendix. 21 Calibration equation for T6 condenser outlet temperature

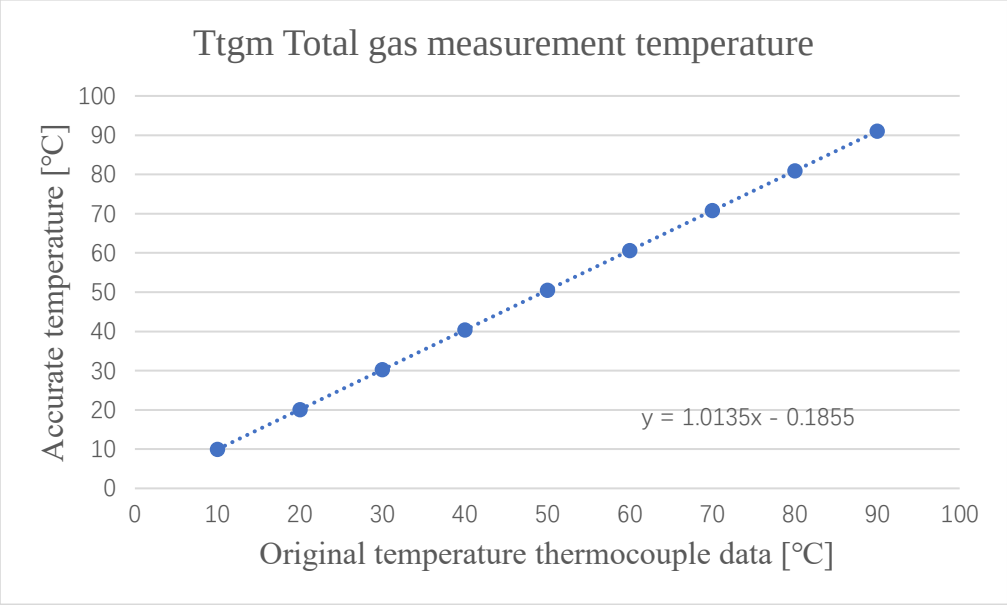

Appendix. 22 Calibration equation for Ttgm total gas measurement temperature

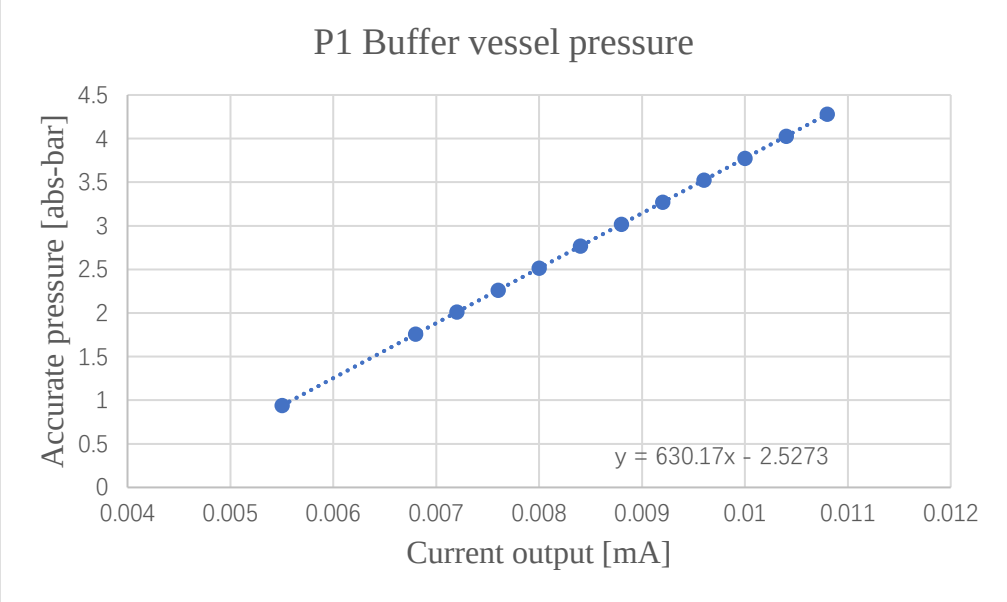

Appendix. 23 Calibration equation for P1 buffer vessel pressure

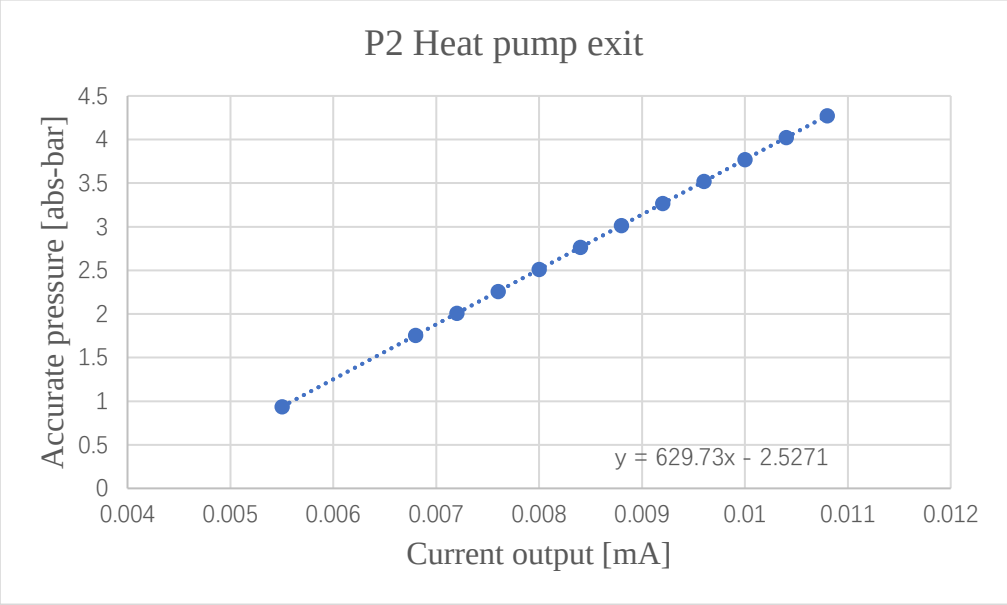

Appendix. 24 Calibration equation for P2 heat pump exit

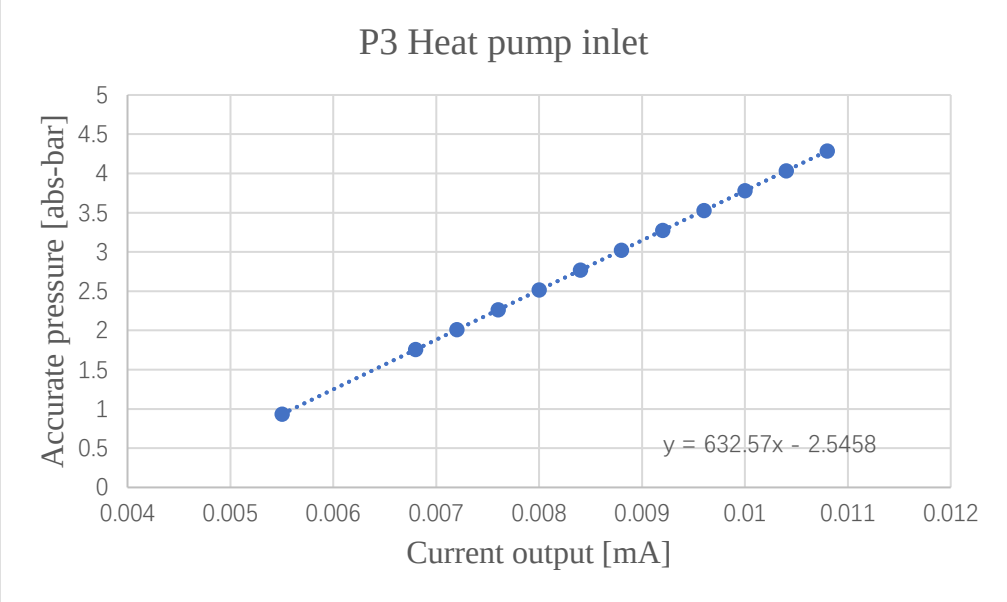

Appendix. 25 Calibration equation for P3 heat pump inlet

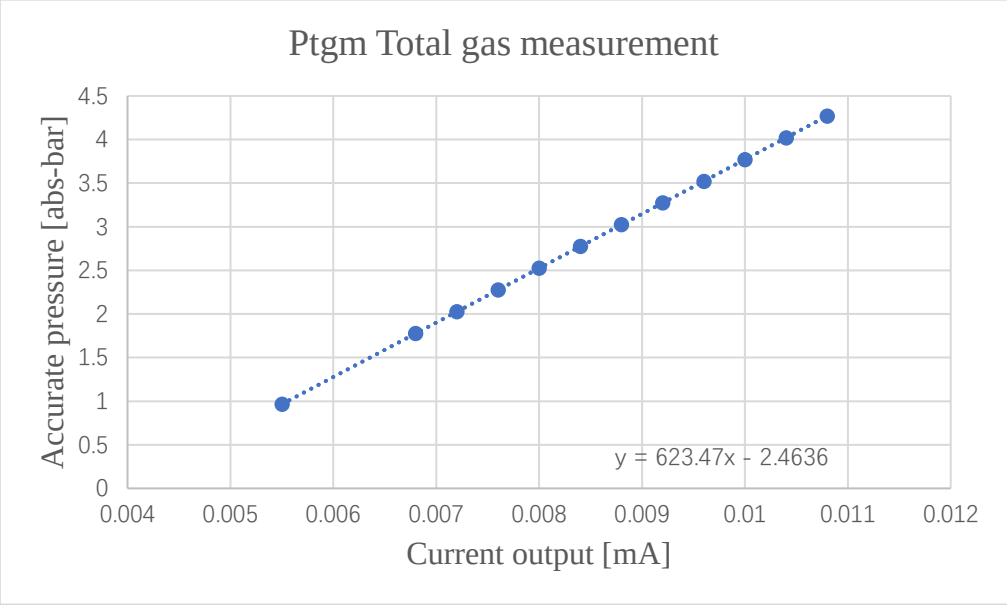

Appendix. 26 Calibration equation for P_{tgm} total gas measurement

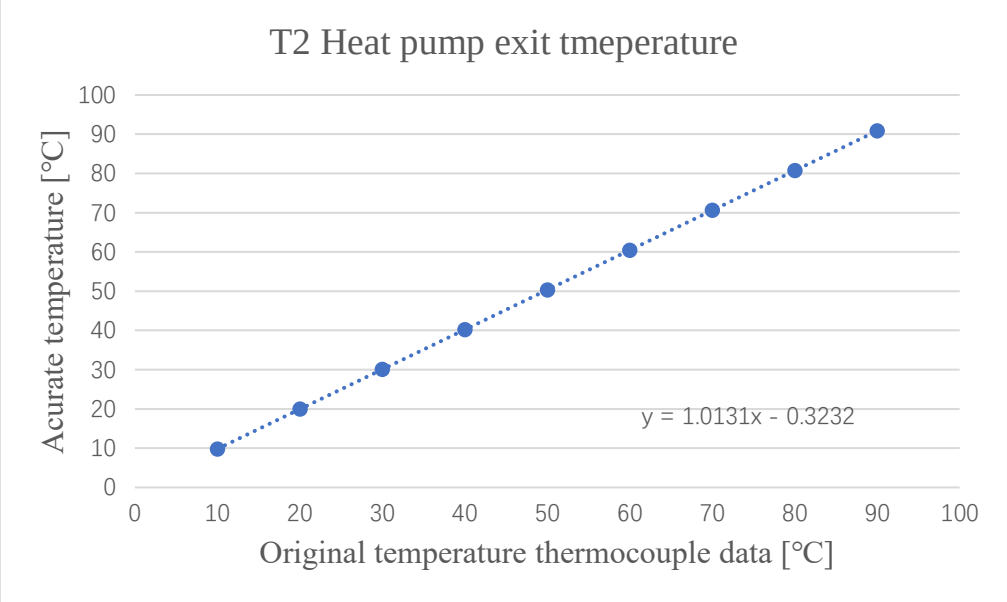

Appendix. 27 Calibration equation for T2 heat pump exit temperature

Appendix IV MATLAB image processing code

This MATLAB code is programmed initially by Collette Baptiste advised by Dr. Hongying Meng, Prof. Yunting Ge, Ali Shefik, Jianbo Qin and Asim Jan. And improved by Xianghua Jiang and Jianbo Qin (Baptiste, 2015). The parts of the code have been shown as follows.

```
close all;
clear all;
clc;

%Options
global applyOtherAlgo postProcess showTracking
global removeBackgroundImage recordEnhancedVideo nameOfVideo newVideo
global showElapsedTime plotAverage plotMin plotMax
global readVideoBeforeEnhancement readVideoAfterEnhancement
global nameWithoutExtension data set
%Enhancement
global doMedian sizeMedian
global doLinear gamma lowIn highIn lowOut highOut
global doAverage sizeAverage
global doWiener sizeWiener
global doHistEqua doWaveletDenoising doSharpening
%Algo display
global writeExcel removeBlurry showUnblurred
global showImageProcessing printImages
%Plots
global framerate pixelToMm ratioImage
global height width depth
global tifdir

global csobel; %jxh
csobel=0.025;

showDebugElapsedTime = 0; %Tells at the end of each process in MATLAB the
time elapsed
nameWithoutExtension = '';

postProcess = 0; %Track the bubbles to show how their size evolves - useless
if done in an image with a low framerate. Will record the video.
showTracking = 0; %Show an image with the bubbles tracked - does not work
with big videos
removeBackgroundImage = 1; %Necessary - removes the noise in the image by
removing the background
recordEnhancedVideo = 1; %Record a video (tif images) with the non blurred
bubbles on a black background
showElapsedTime = 1; %Tells at the end in MATLAB the time elapsed
plotAverage = 0; %Plot the average size of the bubbles
plotMin = 0; %Plot the minimum size of the bubbles
plotMax = 0; %Plot the maximum size of the bubbles
readVideoBeforeEnhancement = 0; %Read the original video
readVideoAfterEnhancement = 0; %Read the video with the non blurred bubbles
on a black background
```

Appendix. 28 MATLAB code 1 of 19

```
% Extra algorithms - not needed, can make the result worse
doMedian = 0; %Apply a median filter
sizeMedian = 3;
doLinear = 0; %Apply a linear gaussian filter
gamma = 0.8;
lowIn = 15;
highIn = 110;
lowOut = 0;
highOut = 255;
doAverage = 0; %Apply an average filter
sizeAverage = 3;
doWiener = 0; %Apply a Wiener filter
sizeWiener = 3;
doHistEqua = 0;
doWaveletDenoising = 0; %Apply wavelet denoising algorithm
doSharpening = 0; %Use unsharp masking

showUI = 1; %Show the GUIDE interface

writeExcel = 1; %Compute an Excel file
removeBlurry = 1; %Do not compute the blurred bubbles
showUnblurred = 0; %Show both the original image and the circles around the
bubbles
showImageProcessing=0; %Trace the evolution of the image
data = {}; %All the names of the videos to be computed
set = {}; %data contains sets of videos.

ratioImage = 2; %Ratio to know which function to call
printImages = 0; %Show graphs about max/mean diameter, (cumulative) void
fraction and bubble distribution
pixelToMm=0.005698; %0.0079; %6.34/800; %1/195=0.0051 for boiler -
6.34/800=0.0079 for heat pump/
framerate=800; %To compute the speed in post_process

%Heat pump
width =4.2; % 6.34; %mm 6.34 for heat pump
height =4.2; % 4.76; %mm 4.76 for heat pump
depth = 0.6; %mm 0.625 for boiler

%Wait for the user to make its choices
if(showUI)
    uiwait(simple_gui())
end

if(showElapsedTime) %tic command if we want to see the time
    tic
end
```

Appendix. 29 MATLAB code 2 of 19

```
%Looks if other algorithms need to be done
applyOtherAlgo = doMedian || doLinear || doAverage || doWiener ||...
    doHistEqua || doWaveletDenoising || doSharpening;

%Data
if(size(set,2)>0)
    set={set};
    data = [data set]; %Push the set
    set = {}; %Clear the set
end

numberSets = size(data,2);
%Initialisation
numberVideosSets = [];
legendFigures = [];
diametersMmAllVideosSets ={};
cumulativeVoidFractionAllVideosSets ={};
cumulativeSizeDistributionAllVideosSets ={};
cumulativeVolumeDistributionAllVideosSets ={};
averageDiameterAllVideosSets ={};
maxDiameterAllVideosSets ={};
voidFractionsAllSets = {};

%Shape inserters to draw circles or disks
if(postProcess)
    shapeInserter =
vision.ShapeInserter('Shape','Circles','Fill',true,'FillColor','White');
else
    shapeInserter = '';
end
if(recordEnhancedVideo)
    shapeInserter2 =
vision.ShapeInserter('Shape','Circles','BorderColor','Custom','CustomBorderCo
lor',[255 0 0]);
else
    shapeInserter2 = '';
end

for nbSet = 1:numberSets %Process each set separately
    set=data{nbSet};
    %Sets
    videoList=char(cellstr(set));
    numberVideos = size(videoList,1);
```

Appendix. 30 MATLAB code 3 of 19

```
    %Plots for all videos
    numberOfBubblesAllVideos = 0;
    diametersMmAllVideos = [];
    averageDiameterAllVideos = [];
    minDiameterAllVideos = [];
    maxDiameterAllVideos = [];
    totalVolumeAllVideos = 0;
    voidFractions = [];

    for nb=1:numberVideos
        %The name of the video is directly taken from data
        %Need to add the absolute path before for it to work
        nameOfVideo=videoList(nb,:)

        %Process the name provided as "nameOfVideo" to automatically create
the
        %name for the new video and for the Excel file if needed.
        %PostProcess also records a video to apply Kalman filtering
        if(writeExcel || recordEnhancedVideo || postProcess)
            filehead=j_extractfilehead(nameOfVideo,0);
%             nameWithoutExtension = strsplit(nameOfVideo,'.');
%             nameWithoutExtension=nameWithoutExtension(1);
            nameWithoutExtension=j_extractfilehead(nameOfVideo,1);
            nameExcel = strcat(nameWithoutExtension,'\',filehead,'.xls');
            nameExcel=char(nameExcel);
            newVideo =
char(strcat(strcat(nameWithoutExtension,'\Enhanced'),'.avi'));
            newVideoPostProcess =
char(strcat(strcat(nameWithoutExtension,'\Recorded'),'.avi'));
        end

        if(~isempty(nameWithoutExtension))    %jxh
            if ~exist(char(nameWithoutExtension))
                mkdir(char(nameWithoutExtension));
            end
            tifdir=char(strcat(nameWithoutExtension,'\tif'));
            if ~exist(tifdir)
                mkdir(tifdir);
            end
        end

        if(showDebugElapsedTime)
            'Process the name of the video'
            toc
            'Read the avi video frame by frame'
            tic
        end
```

Appendix. 31 MATLAB code 4 of 19

```
        %Read .avi video frame by frame
        %Use VideoReader to get the video
        videoObj = VideoReader(nameOfVideo);
        %Width and height of the video
        nFrames=videoObj.NumberOfFrames;
        k = 1;

        if(showDebugElapsedTime)
            toc
            'Remove the background'
            tic
        end

        %To remove the background image, we do an average of all the frames.
        backgroundaveragepix=0;  %jxh
        if(removeBackgroundImage)
            [sizex,sizey,sizez]=size(read(videoObj,1));
            sumImages=zeros(sizex,sizey,sizez); %To have the right size
            for k = 1 : nFrames
                sumImages=sumImages+im2double(read(videoObj,k)); %and the sum
is computed
            end
            %Calculate the background image
            background=im2uint8(sumImages/nFrames); %Background image

            s=size(background,3);
            if(s==3)
                backgroundgray=rgb2gray(background);
            else
                backgroundgray=background;
            end

backgroundaveragepix=sum(sum(backgroundgray))/size(backgroundgray,1)/size(bac
kgroundgray,2);
            x1=95;y1=0.025;x2=70;y2=0.02;
            csobel=-0.03886+0.001287*backgroundaveragepix-6.2e-
06*backgroundaveragepix^2; %(backgroundaveragepix-
0.05)*0.000375;%0.00404813*(backgroundaveragepix-32.1812)^0.439736; %y2+(y1-
y2)*(backgroundaveragepix-x2)/(x1-x2);
%             ratioImage=1;
%             csobel=0.1;
        end

        if(showDebugElapsedTime)
            toc
            'Configure the videowriter'
            tic
        end
```

Appendix. 32 MATLAB code 5 of 19

```
        %Save the video
        if(recordEnhancedVideo)
            writerObj = VideoWriter(newVideo); %New file
            open(writerObj);
        else
            writerObj = '';
        end
        %Save the video for post processing
        if(postProcess)
            writerObj2 = VideoWriter(newVideoPostProcess); %New file
            open(writerObj2);
        else
            writerObj2 = '';
        end

        if(showDebugElapsedTime)
            toc
            'Configure the Excel sheet'
            tic
        end

        %We want to plot the average size, the min and the max size of the
objects
        %on the screen.
        %Those arrays will stay at zero if the booleans for plot are false.
        averageSizes=zeros(1,nFrames);
        minSizes=zeros(1,nFrames);
        maxSizes=zeros(1,nFrames);

        %Matrix used for showing the size of the bubbles in each frame
        %Bubbles are counted by sizes to compute an histogram-like graph
        maxSize=270; %In pixels, the maximum size that can be computed
        lapse=45; %Size of a "bar"
        matrix = zeros(maxSize/lapse+1,nFrames);

        if(writeExcel)
            %Excel manipulation
            Excel = actxserver ('Excel.Application');
            File=nameExcel;
            if ~exist(File,'file')
                ExcelWorkbook = Excel.workbooks.Add;
                ExcelWorkbook.SaveAs(File,1);
                ExcelWorkbook.Close(false);
            end
            try
                invoke(Excel.Workbooks,'Open',File);
```

Appendix. 33 MATLAB code 6 of 19

```
            catch
                Excel.Quit;
                Excel.delete;
                clear Excel;
                Excel = actxserver('Excel.Application');
                invoke(Excel.Workbooks,'Open',File);
            end

            %Write the first line of the Excel file
            xlswrite1(Excel,File,{'Image'},1,strcat('A',int2str(1)));
            xlswrite1(Excel,File,{'Number of
bubbles'},1,strcat('B',int2str(1)));
            xlswrite1(Excel,File,{'Diameters  (mm)'},1,strcat('C',int2str(1)));

            indexExcel=2;
        else
            Excel='';
            indexExcel='';
            File='';
        end

        if(showDebugElapsedTime)
            toc
            'Process frames'
            tic
        end

        %Process each frame individually
        points = {};
        diametersMmWholeVideo = [];
        numberOfBubblesVideo = 0;
        numberOfBubblesLayers=[];
        for k = 1 : nFrames
            image=read(videoObj,k); %Take the frame k
            originalImage=image; %Keep in memory the original image

            if(showImageProcessing) %If we want to see the process, show this
original image
                %figure(1);
                subplot(1,3,1);imshow(image);title('Original Image');
            end
```

Appendix. 34 MATLAB code 7 of 19

```
            %Remove the background image
            if(removeBackgroundImage)
                %If the bubbles appear white in a black background in the
                %original image, put 'image=image-background' here
                image = background - image; %So that the black objects appear
white
            else
                image=255-image;
            end

            if(showImageProcessing) %Show this image without background
                subplot(1,3,2);imshow(image);title('Remove background');
            end

            if(showImageProcessing) %Show the enhanced image - if there was
no enhancement this image will be the same.
                subplot(1,3,3);imshow(image);title('Enhanced image');
            end

            if(removeBlurry) %Remove the blurred objects, plot
min/max/average...
                %Show the non-blurred image to compare
%                 if(showUnblurred)
%                     figure(7);
%                     subplot(1,2,1);imshow(originalImage);hold on
%                 end

                %Process the image - get an image with white bubbles on a
                %black background, the radius of each bubble in the frame,
                %the number of Bubbles in the frame, the matrix with the
                %size of the bubbles, and an image where bubbles are
                %circled.
                %See this function for more information
%                 if(ratioImage==1)
%                     [image, diametersMm, point, numberOfBubbles, matrix,
circlesImage] = processOneImageRatio1(writerObj, image, originalImage,
showUnblurred, matrix, lapse, k, pixelToMm, recordEnhancedVideo,
nameWithoutExtension, applyOtherAlgo, postProcess, 1, shapeInserter,
shapeInserter2);
%                 else %ratio==2
                    [image, diametersMm, point, numberOfBubbles, matrix,
circlesImage] = processOneImageRatio2(writerObj, image, originalImage,
showUnblurred, matrix, lapse, k, pixelToMm, recordEnhancedVideo,
nameWithoutExtension, applyOtherAlgo, postProcess, 1, shapeInserter,
shapeInserter2);
%                 end
```

Appendix. 35 MATLAB code 8 of 19

```
                if(size(point)>0)
                    points{k} = point; %Add the point parameter to the cell
array
                    diametersMmWholeVideo = [diametersMmWholeVideo
diametersMm];
                    numberOfBubblesVideo =
numberOfBubblesVideo+numberOfBubbles;
                else
                    points{k} = [0 0 0];
                end
            end


numberOfBubblesLayers=[numberOfBubblesLayers;numberOfBubbles]; %jxh

            %Record in a xlsx file
            if(writeExcel)
                %File
                %Fill the first column with the number of the image
                xlswrite1(Excel,File,{strcat('image
',int2str(k))},1,strcat('A',int2str(indexExcel)));
                %Fill the second column with the number of bubbles

xlswrite1(Excel,File,int2str(numberOfBubbles),1,strcat('B',int2str(indexExcel
)));
                %Fill the third column with the radius of each computed
bubble,
                %writen in succesive rows of the column C
                for nradii=1:numberOfBubbles

xlswrite1(Excel,File,diametersMm(nradii),1,strcat('C',int2str(indexExcel)));
                    if(nradii<numberOfBubbles)
                        indexExcel=indexExcel+1;
                    end
                end
                %Go to the next line
                indexExcel=indexExcel+1;
            end

            %Save the video with non blurred bubbles
            if(postProcess)
                %Convert to uint8 to record the video
                imageRecord=circlesImage;
                writeVideo(writerObj2,imageRecord);
            end
```

Appendix. 36 MATLAB code 9 of 19

```
    %Plots of min / average / max
    if(plotMin)
        minSizes(1,k) = min(diametersMm);
    end
    if(plotAverage)
        averageSizes(1,k) = mean(diametersMm);
    end
    if(plotMax)
        maxSizes(1,k) = max(diametersMm);
    end
end

delete(videoObj); %jxh

if(showDebugElapsedTime)
    toc
    'Close the open files'
    tic
end

%Close the open files
if(writeExcel)
    %Close Excel
    Excel.ActiveWorkbook.Save;
    Excel.Quit
    Excel.delete
    clear Excel
end

if(recordEnhancedVideo)
    close(writerObj);
end
if(postProcess)
    close(writerObj2);
end

if(showDebugElapsedTime)
    toc
    'Plot min/max/mean sizes'
    tic
end
```

Appendix. 37 MATLAB code 10 of 19

```
        %Plot min/max/mean sizes
        if(plotMin || plotMax || plotAverage)
            figure(2);
            x=1:nFrames;
            plot(x,minSizes,x,maxSizes,x,averageSizes);
            title('Minimum, maximum and average sizes');
        end

        %Plot number of objects from different sizes
        if(plotMin || plotMax || plotAverage)
            figure(3);
            x=1:nFrames; %x axis
            listColor='ymcrgbk'; %7 curves max
            listSymbols='ox+*ox+*'; %Different symbols

            %Plot all sizes in one graph or in different graphs
            plotAll = 0;
            if(plotAll)
                for i=1:maxSize/lapse+1
                    subplot(maxSize/lapse+1,1,i);
                    plot(x,matrix(i,:));%,strcat(strcat(listColor(i),'-
'),listSymbols(i)));
                    titleGraph=strcat('Size between ',int2str(lapse*(i-1)));
                    titleGraph=strcat(titleGraph,' to ');
                    titleGraph=strcat(titleGraph,int2str(lapse*i));
                    %leg{i}=titleGraph;
                    title(titleGraph);
                    hold on;
                end
            else
                leg=cell(maxSize/lapse+1,1);
                for i=1:maxSize/lapse+1
                    plot(x,matrix(i,:),strcat(strcat(listColor(i),'-
'),listSymbols(i)));
                    titleGraph=strcat('Size between ',int2str(lapse*(i-1)));
                    titleGraph=strcat(titleGraph,' to ');
                    titleGraph=strcat(titleGraph,int2str(lapse*i));
                    leg{i}=titleGraph;
                    hold on;
                end
                legend(leg);
            end
            title('Size of bubbles');
        end
```

Appendix. 38 MATLAB code 11 of 19

```
        if(isempty(diametersMmWholeVideo))                          %jxh
            disp(char(strcat('no bubble found in ',nameWithoutExtension)));
            continue;
        end

j_plotcum([],[],numberOfBubblesLayers,diametersMmWholeVideo,20,nameWithoutExt
ension);  %jxh
        vd43=j_GetVD43(diametersMmWholeVideo); %jxh

        if(showDebugElapsedTime)
            toc
            'Bubble tracking'
            tic
        end

        %If we want to track the bubbles. We get a cell array of speeds and
        %one of diameters out of the newVideo (with non-blurred bubbles in a
        %black background
        if(postProcess)
            [ speeds, diameters ] =
post_process(nameWithoutExtension,newVideoPostProcess, points);
        end

        if(removeBlurry)
            %Void fraction for ONE video
%             diametersMmSortedOneVideo = sort(diametersMmWholeVideo);
%             sizeDiametersMmOneVideo = size(diametersMmWholeVideo,2);
%             volumesMm3OneVideo = zeros(size(diametersMmWholeVideo));
%
%             cumulativeVoidFraction = zeros(size(diametersMmWholeVideo));
%              cumulativeSizeDistribution = zeros(size(diametersMmWholeVideo));
%
%             invNumberOfBubbles = 1/numberOfBubblesVideo;
%             totalVolume = nFrames * width * height * depth;
%             depthLocal=depth;
%             for i=1:sizeDiametersMmOneVideo
%                 bubbleDiam = diametersMmSortedOneVideo(i);
%                 if(bubbleDiam<depthLocal)
%                     volumeMmI=pi*(bubbleDiam^3)/6;
%                 else
%                     volumeMmI=pi/6*((6*(bubbleDiam^2)/4)-
(6*(depthLocal^2)/4)+depthLocal^2)*depthLocal;
%                 end
%                 volumesMm3OneVideo(i)=volumeMmI;
```

Appendix. 39 MATLAB code 12 of 19

```
%             end
%             for i=1:sizeDiametersMmOneVideo
%                 if(i==1)
%                     cumulativeVoidFraction(i)=volumesMm3OneVideo(i);
%                     cumulativeSizeDistribution(i)=invNumberOfBubbles;
%                 else
%                     cumulativeVoidFraction(i)=cumulativeVoidFraction(i-
1)+volumesMm3OneVideo(i);
%
cumulativeSizeDistribution(i)=cumulativeSizeDistribution(i-
1)+invNumberOfBubbles;
%                 end
%             end
%             cumulativeVoidFraction=cumulativeVoidFraction/totalVolume;
%             voidFractionVideo =
cumulativeVoidFraction(sizeDiametersMmOneVideo)
%             cumulativeVolumeDistribution =
cumulativeVoidFraction/voidFractionVideo;
%
%
%             fileoutname=char(strcat(nameWithoutExtension,'\r.out')); %jxh
%             fout=fopen(fileoutname,'a');
%             fprintf(fout,'csobel=%g\r\n',csobel);
%             fprintf(fout,'voidFractionVideo=%g\r\n',voidFractionVideo);
%             fprintf(fout,'Volumewise averaged
diameter(DiaPer(con)43)=%g\r\n',vd43);
%             fclose(fout)
%
%             averageDiameterVideo = mean(diametersMmSortedOneVideo);
%             minDiameterVideo = diametersMmSortedOneVideo(1);
%             maxDiameterVideo =
diametersMmSortedOneVideo(sizeDiametersMmOneVideo);

[totalVolume,averageDiameterVideo,minDiameterVideo,maxDiameterVideo,voidFract
ionVideo]=j_GetVoidFraction(diametersMmWholeVideo,nFrames,width,height,depth);
            fileoutname=char(strcat(nameWithoutExtension,'\r.out')); %jxh
            fout=fopen(fileoutname,'a');
            fprintf(fout,'backgroundaveragepix=%g,
csobel=%g\r\n',backgroundaveragepix,csobel);
            fprintf(fout,'N=%g\r\n',length(diametersMmWholeVideo));
            fprintf(fout,'voidFractionVideo=%g\r\n',voidFractionVideo);
            fprintf(fout,'Volumewise averaged
diameter(DiaPer(con)43)=%g\r\n',vd43);
            fclose(fout);
```

Appendix. 40 MATLAB code 13 of 19

```
%Values for all videos
            totalVolumeAllVideos = totalVolumeAllVideos + totalVolume;
            numberOfBubblesAllVideos =
numberOfBubblesAllVideos+numberOfBubblesVideo;
            diametersMmAllVideos = [diametersMmAllVideos
diametersMmWholeVideo];
            averageDiameterAllVideos = [averageDiameterAllVideos
averageDiameterVideo];
            minDiameterAllVideos = [minDiameterAllVideos minDiameterVideo];
            maxDiameterAllVideos = [maxDiameterAllVideos maxDiameterVideo];
            voidFractions = [voidFractions voidFractionVideo];
        end
    end

    if(removeBlurry && printImages)
        %Plot for all videos
        diametersMmAllVideos = sort(diametersMmAllVideos);

        sizeDiametersMmAllVideos = size(diametersMmAllVideos,2);
        volumesMm3AllVideos = zeros(size(diametersMmAllVideos));

        cumulativeVoidFractionAllVideos = zeros(size(diametersMmAllVideos));
        cumulativeSizeDistributionAllVideos =
zeros(size(diametersMmAllVideos));
        invNumberOfBubblesAllVideos = 1/numberOfBubblesAllVideos;

        depthLocal = depth;
        for i=1:sizeDiametersMmAllVideos
            bubbleDiam = diametersMmAllVideos(i);
            if(bubbleDiam<depthLocal)
                volumeMmI=pi*(bubbleDiam^3)/6;
            else
                volumeMmI=pi/6*((6*(bubbleDiam^2)/4)-
(6*(depthLocal^2)/4)+depthLocal^2)*depthLocal;
            end
            volumesMm3AllVideos(i)=volumeMmI;
        end
        for i=1:sizeDiametersMmAllVideos
            volumeMmI = volumesMm3AllVideos(i);
            if(i==1)
                cumulativeVoidFractionAllVideos(i)=volumeMmI;

cumulativeSizeDistributionAllVideos(i)=invNumberOfBubblesAllVideos;
            else

cumulativeVoidFractionAllVideos(i)=cumulativeVoidFractionAllVideos(i-
1)+volumeMmI;
```

Appendix. 41 MATLAB code 14 of 19

```
cumulativeSizeDistributionAllVideos(i)=cumulativeSizeDistributionAllVideos(i-
1)+invNumberOfBubblesAllVideos;
            end

        end

cumulativeVoidFractionAllVideos=cumulativeVoidFractionAllVideos/totalVolumeAl
lVideos;
        voidFractionAllVideos =
cumulativeVoidFractionAllVideos(sizeDiametersMmAllVideos);
        cumulativeVolumeDistributionAllVideos =
cumulativeVoidFractionAllVideos/voidFractionAllVideos;

        %Print plots in png files
        target = strsplit(char(nameWithoutExtension),'\');
        target = target(size(target,2));

        %Plot the cumulative void fraction of all videos
        figure(31);

plot(diametersMmAllVideos,cumulativeVoidFractionAllVideos);title('Cumulative
void fraction');
        xlabel('Diameter (mm)');ylabel('Cumulative void fraction');
        %Print the plot
        targetDia = char(strcat(target,'CumulativeVoidFractionAllVideos'));
        print(targetDia,'-dpng');

        %Plot the size distribution of all videos
        figure(32);

plot(diametersMmAllVideos,cumulativeSizeDistributionAllVideos);title('Cumulat
ive size distribution');
        xlabel('Diameter (mm)');ylabel('Size distribution');
        %Print the plot
        targetDia =
char(strcat(target,'CumulativeSizeDistributionAllVideos'));
        print(targetDia,'-dpng');

        %Plot the size distribution of all videos
        figure(33);

plot(diametersMmAllVideos,cumulativeVolumeDistributionAllVideos);title('Cumul
ative volume distribution');
        xlabel('Diameter (mm)');ylabel('Volume distribution');
```

Appendix. 42 MATLAB code 15 of 19

```
 %Print the plot
        targetDia =
char(strcat(target,'CumulativeVolumeDistributionAllVideos'));
        print(targetDia,'-dpng');
   |
        %Plot the mean diameter for all videos
        figure(41);
        plot(1:numberVideos,averageDiameterAllVideos);title('Average diameter
against plane');
        xlabel('Video');ylabel('Average diameter (mm)');
        %Print the plot
        targetDia = char(strcat(target,'AverageDiameterAllVideos'));
        print(targetDia,'-dpng');

        %Plot the mean diameter for all videos
        figure(42);
        plot(1:numberVideos,maxDiameterAllVideos);title('Maximum diameter
against plane');
        xlabel('Video');ylabel('Maximum diameter (mm)');
        %Print the plot
        targetDia = char(strcat(target,'MaxDiameterAllVideos'));
        print(targetDia,'-dpng');

        %Plot the void fraction for all videos
        figure(43);
        semilogy(1:numberVideos,voidFractions);title('Void fraction against
plane');
        xlabel('Video');ylabel('Void fraction');
        %Print the plot
        targetDia  =  char(strcat(target,'VoidFractionsAgainstPlaneAllVideos'));
        print(targetDia,'-dpng');

        %Data
        numberVideosSets = [numberVideosSets numberVideos];
        legendFigures = [legendFigures;strcat('Set',int2str(nbSet))];
        diametersMmAllVideosSets{nbSet} = diametersMmAllVideos;
        cumulativeVoidFractionAllVideosSets{nbSet} =
cumulativeVoidFractionAllVideos;
        cumulativeSizeDistributionAllVideosSets{nbSet} =
cumulativeSizeDistributionAllVideos;
        cumulativeVolumeDistributionAllVideosSets{nbSet} =
cumulativeVolumeDistributionAllVideos;
        averageDiameterAllVideosSets{nbSet} = averageDiameterAllVideos;
        maxDiameterAllVideosSets{nbSet} = maxDiameterAllVideos;
        voidFractionsAllSets{nbSet} = voidFractions;
    end
end
```

Appendix. 43 MATLAB code 16 of 19

```
if(removeBlurry && printImages)
    %Print plots in png files
    target = 'AllSets';
    listColor='bmcrgyk'; %7 sets max

    %Plot the cumulative void fraction of all videos
    figure(131);
    diametersMmAllVideos = diametersMmAllVideosSets{1};
    cumulativeVoidFractionAllVideos=cumulativeVoidFractionAllVideosSets{1};
    plot(diametersMmAllVideos,cumulativeVoidFractionAllVideos,listColor(1));
    for i=2:numberSets
        hold on
        diametersMmAllVideos = diametersMmAllVideosSets{i};

cumulativeVoidFractionAllVideos=cumulativeVoidFractionAllVideosSets{i};

plot(diametersMmAllVideos,cumulativeVoidFractionAllVideos,listColor(i));
    end
    title('Cumulative void fraction');
    xlabel('Diameter (mm)');ylabel('Cumulative void fraction');
    legend(legendFigures);
    %Print the plot
    targetDia = char(strcat(target,'CumulativeVoidFractionAllSets'));
    print(targetDia,'-dpng');

    %Plot the size distribution of all videos
    figure(132);
    diametersMmAllVideos = diametersMmAllVideosSets{1};

cumulativeSizeDistributionAllVideos=cumulativeSizeDistributionAllVideosSets{1
};

plot(diametersMmAllVideos,cumulativeSizeDistributionAllVideos,listColor(1));
    for i=2:numberSets
        hold on
        diametersMmAllVideos = diametersMmAllVideosSets{i};

cumulativeSizeDistributionAllVideos=cumulativeSizeDistributionAllVideosSets{i
};
```

Appendix. 44 MATLAB code 17 of 19

```
plot(diametersMmAllVideos,cumulativeSizeDistributionAllVideos,listColor(i));
    end
    title('Cumulative size distribution');
    xlabel('Diameter (mm)');ylabel('Size distribution');
    legend(legendFigures);
    %Print the plot
    targetDia = char(strcat(target,'CumulativeSizeDistributionAllSets'));
    print(targetDia,'-dpng');
    %Plot the size distribution of all videos
    figure(133);
    diametersMmAllVideos = diametersMmAllVideosSets{1};

cumulativeVolumeDistributionAllVideos=cumulativeVolumeDistributionAllVideosSe
ts{1};

plot(diametersMmAllVideos,cumulativeVolumeDistributionAllVideos,listColor(1));
    for i=2:numberSets
        hold on
        diametersMmAllVideos = diametersMmAllVideosSets{i};

cumulativeVolumeDistributionAllVideos=cumulativeVolumeDistributionAllVideosSe
ts{i};

plot(diametersMmAllVideos,cumulativeVolumeDistributionAllVideos,listColor(i));
    end
    title('Cumulative volume distribution');
    xlabel('Diameter (mm)');ylabel('Volume distribution');
    legend(legendFigures);
    %Print the plot
    targetDia = char(strcat(target,'CumulativeVolumeDistributionAllSets'));
    print(targetDia,'-dpng');

    %Plot the mean diameter for all videos
    figure(141);
    averageDiameterAllVideos=averageDiameterAllVideosSets{1};
    plot(1:numberVideosSets(1),averageDiameterAllVideos,listColor(1));
    for i=2:numberSets
        hold on
        averageDiameterAllVideos=averageDiameterAllVideosSets{i};
        plot(1:numberVideosSets(i),averageDiameterAllVideos,listColor(i));
    end
    title('Average diameter against plane');
    xlabel('Video');ylabel('Average diameter (mm)');
    legend(legendFigures);
    %Print the plot
    targetDia = char(strcat(target,'AverageDiameterAllSets'));
    print(targetDia,'-dpng');
```

Appendix. 45 MATLAB code 18 of 19

```
    %Plot the mean diameter for all videos
    figure(142);
    maxDiameterAllVideos=maxDiameterAllVideosSets{1};
    plot(1:numberVideosSets(1),maxDiameterAllVideos,listColor(1));
    for i=2:numberSets
        hold on
        maxDiameterAllVideos=maxDiameterAllVideosSets{i};
        plot(1:numberVideosSets(i),maxDiameterAllVideos,listColor(i));
    end
    title('Maximum diameter against plane');
    xlabel('Video');ylabel('Maximum diameter (mm)');
    legend(legendFigures);
    %Print the plot
    targetDia = char(strcat(target,'MaxDiameterAllSets'));
    print(targetDia,'-dpng');

    %Plot the void fraction for all videos
    figure(143);
    voidFractions=voidFractionsAllSets{1};
    semilogy(1:numberVideosSets(1),voidFractions,listColor(1));
    for i=2:numberSets
        hold on
        voidFractions=voidFractionsAllSets{i};
        semilogy(1:numberVideosSets(i),voidFractions,listColor(i));
    end
    title('Void fraction against plane');
    xlabel('Video');ylabel('Void fraction');
    legend(legendFigures);
    %Print the plot
    targetDia = char(strcat(target,'VoidFractionsAllSets'));
    print(targetDia,'-dpng');
end

%The algorithm stops here
if(showElapsedTime)
    toc
end
```

Appendix. 46 MATLAB code 19 of 19

Appendix V Uncertainty (standard error of mean)

Table.apx. 1 Standard error of mean at 2.5 absolute bar

Standard error of mean			
Pressure (bar)	Water flow rate (l/h)	Average bubble diameter (mm)	SEM (mm)
2.5	800	0.0768	0.0044
2.5	850	0.0814	0.0029
2.5	900	0.0852	0.0026
2.5	950	0.0856	0.0036
2.5	1000	0.0945	0.0028
2.5	1050	0.0930	0.0040
2.5	1100	0.0932	0.0027

Table.apx. 2 Standard error of mean at 2.2 absolute bar

Standard error of mean			
Pressure (bar)	Water flow rate (l/h)	Average bubble diameter (mm)	SEM (mm)
2.2	900	0.0947	0.0006
2.2	1000	0.1006	0.0013
2.2	1150	0.1080	0.0016
2.2	1100	0.1030	0.0031
2.2	800	0.0857	0.0004

Table.apx. 3 Standard error of mean at 1000 l/h

Standard error of mean			
Pressure (l/h)	Water flow rate (l/h)	Average bubble diameter (mm)	SEM (mm)
2.2	1000	0.1000	0.0035
2.35	1000	0.0973	0.0038
2.5	1000	0.0945	0.0027
2.7	1000	0.0873	0.0043

Table.apx. 4 Standard error of mean at 850 l/h

Standard error of mean			
Pressure (bar)	Water flow rate (l/h)	Average bubble diameter (mm)	SEM (mm)
1.7	850	0.1006	0.0037
1.9	850	0.0991	0.0036
2.1	850	0.0865	0.0039
2.3	850	0.0890	0.0046
2.5	850	0.0814	0.0029

Appendix VI Representative Processed Images

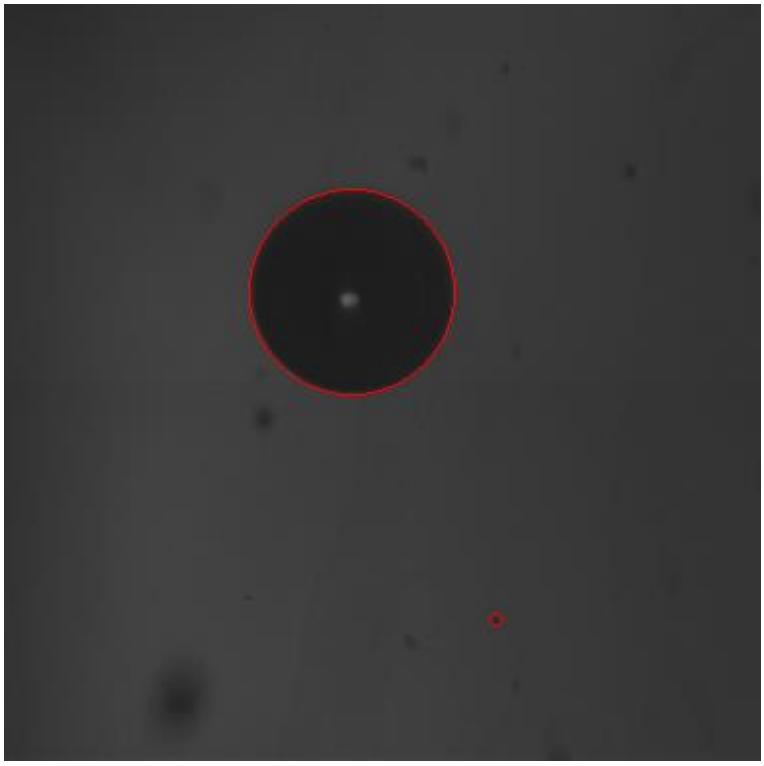

Appendix. 47 Processed Image

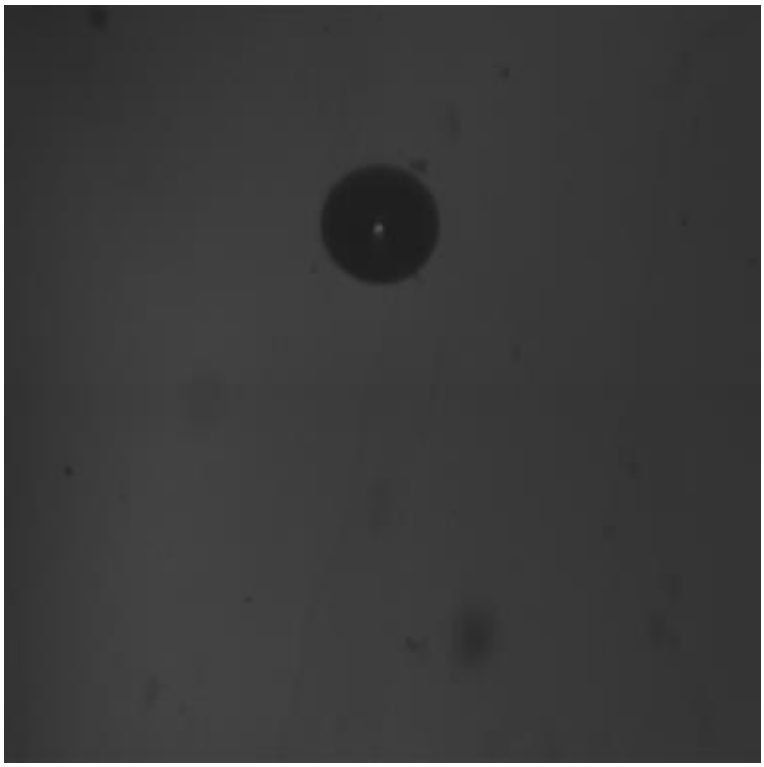

Appendix. 48 Processed Image

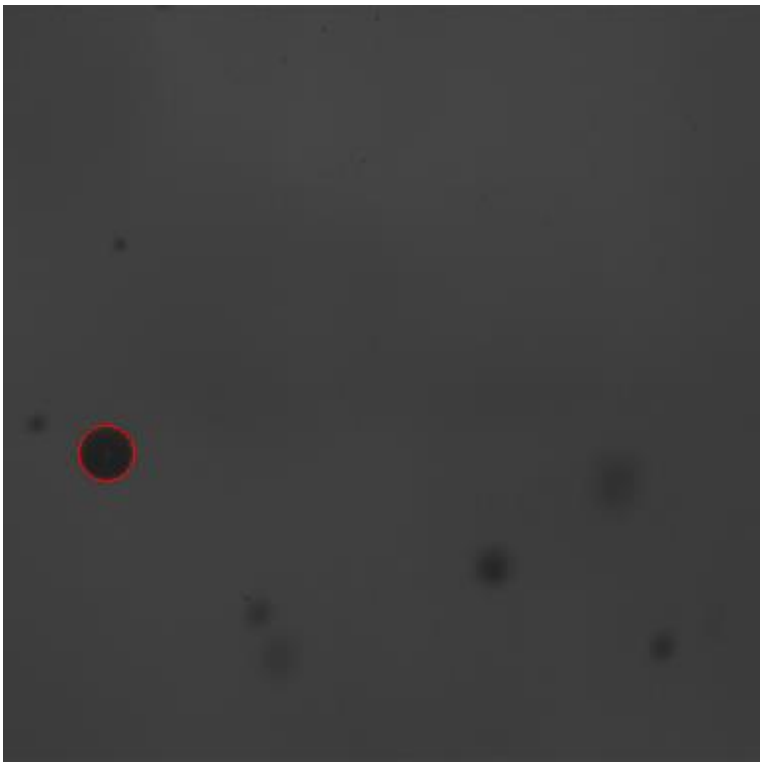

Appendix. 49 Processed Image

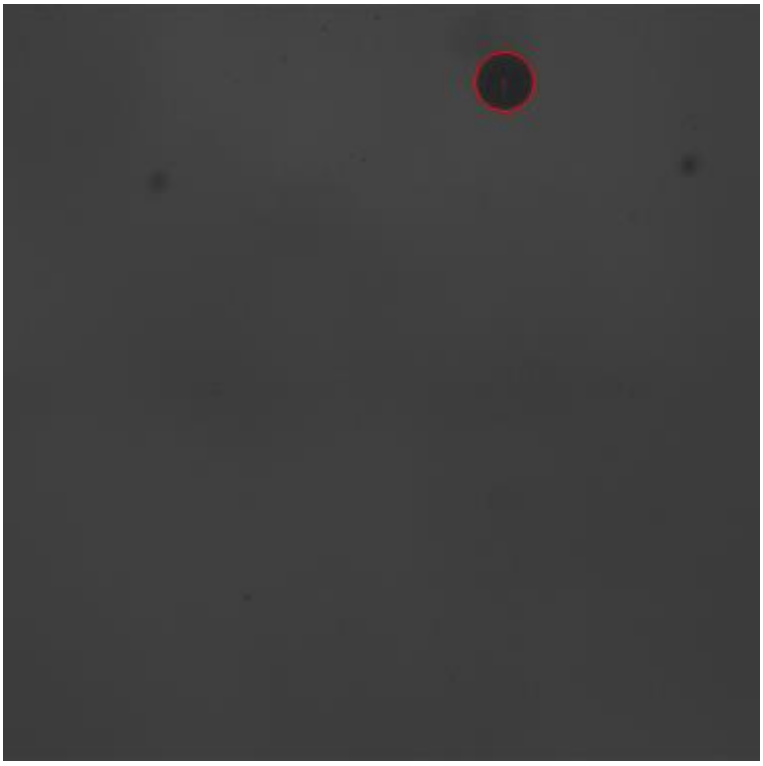

Appendix. 50 Processed Image

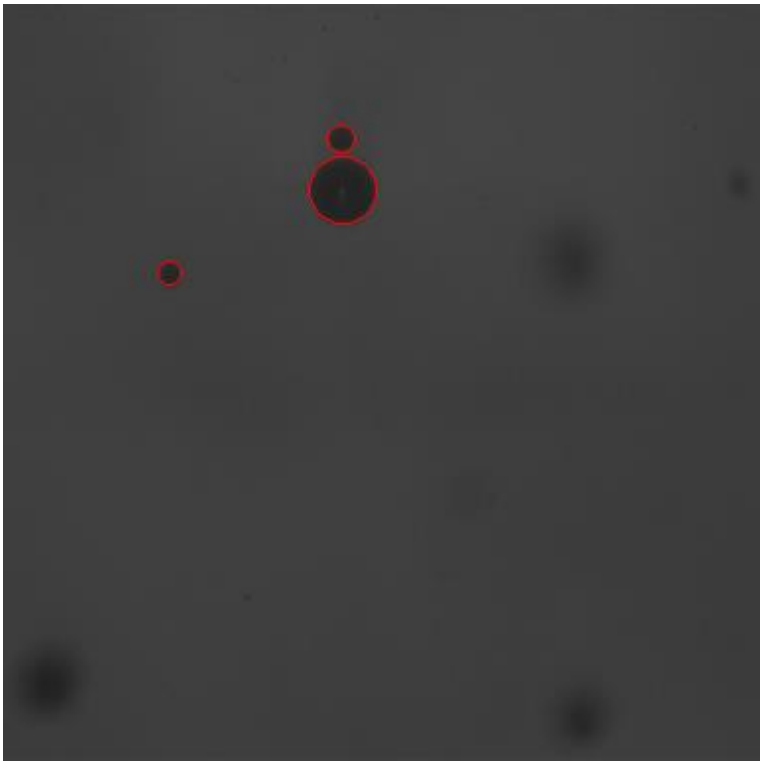

Appendix. 51 Processed Image

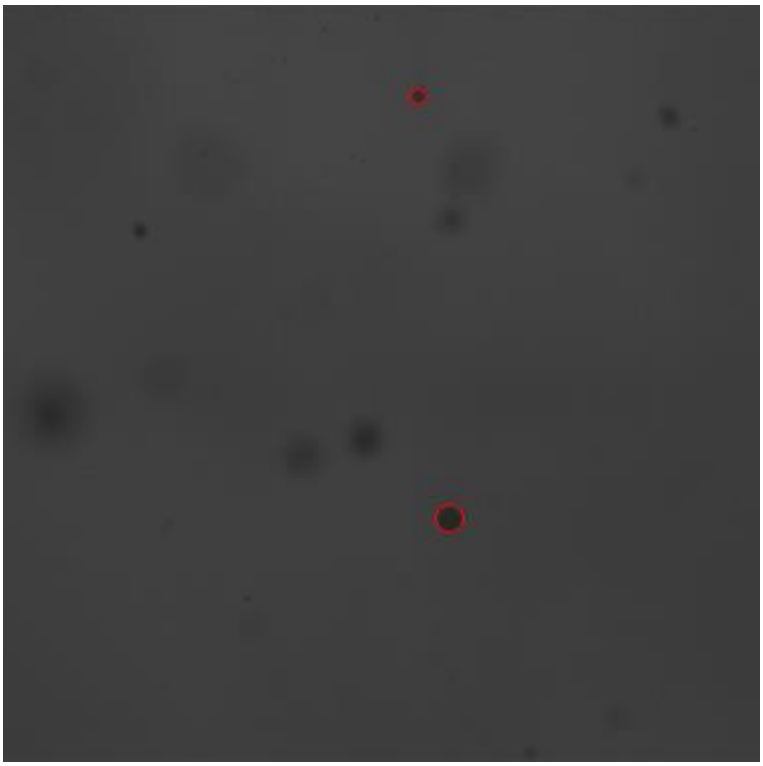

Appendix. 52 Processed Image

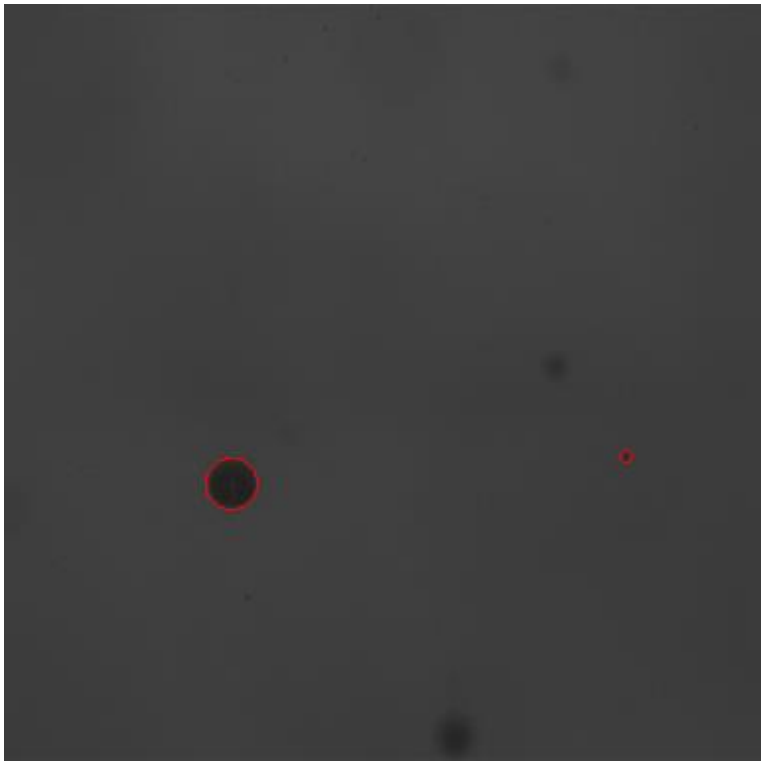

Appendix. 53 Processed Image

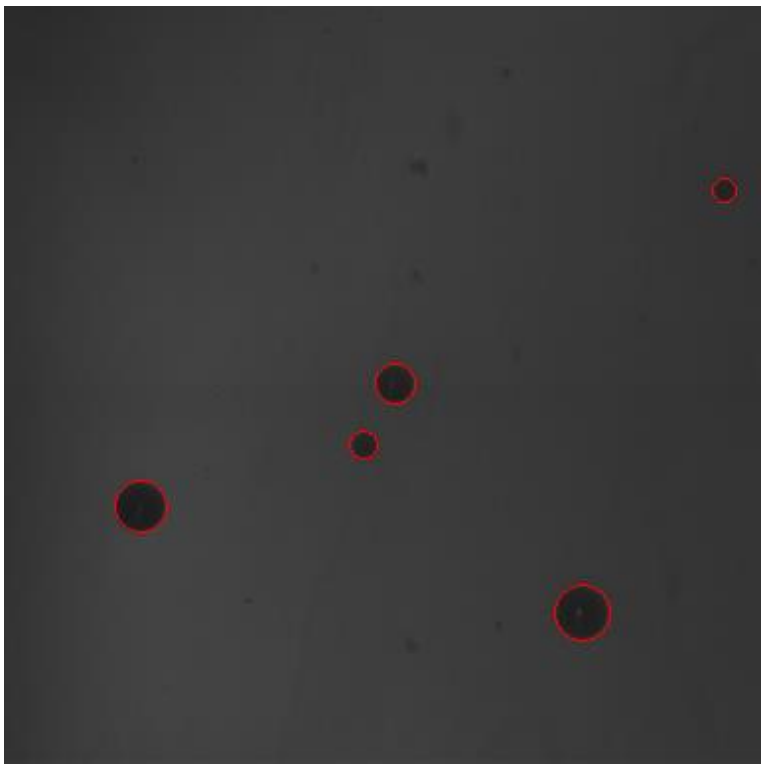

Appendix. 54 Processed Image

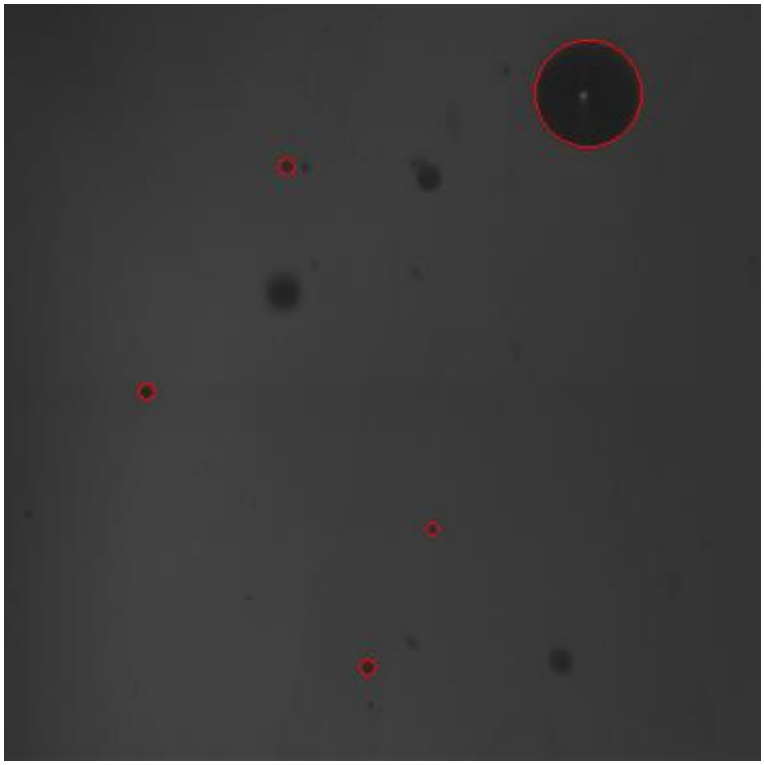

Appendix. 55 Processed Image

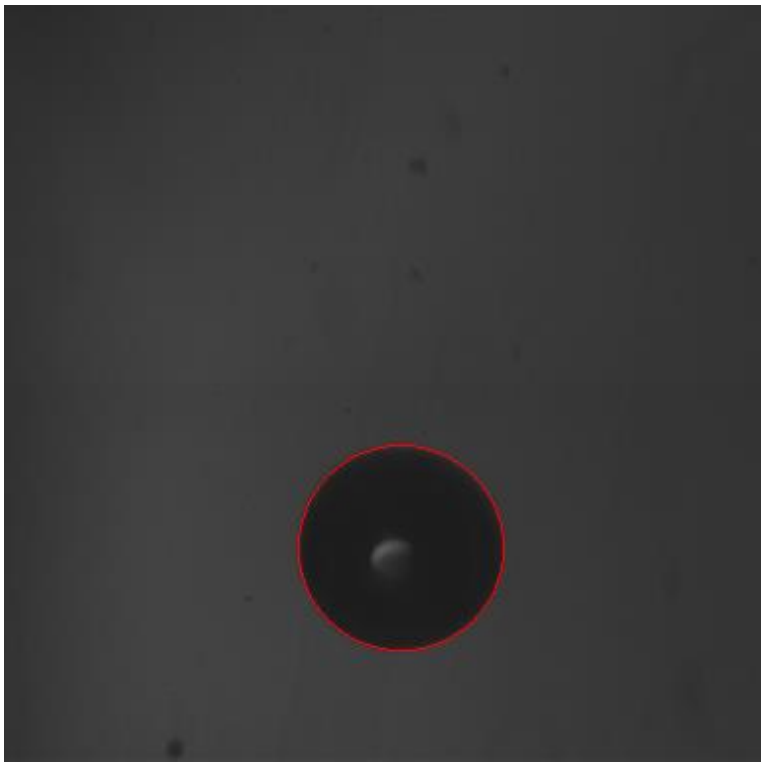

Appendix. 56 Processed Image

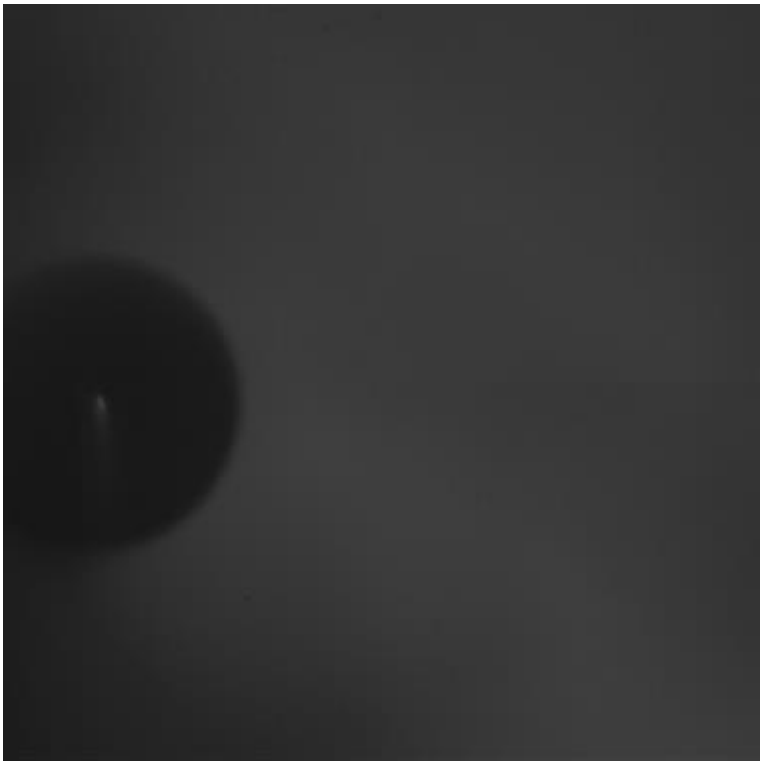

Appendix. 57 Processed Image (out of focus)

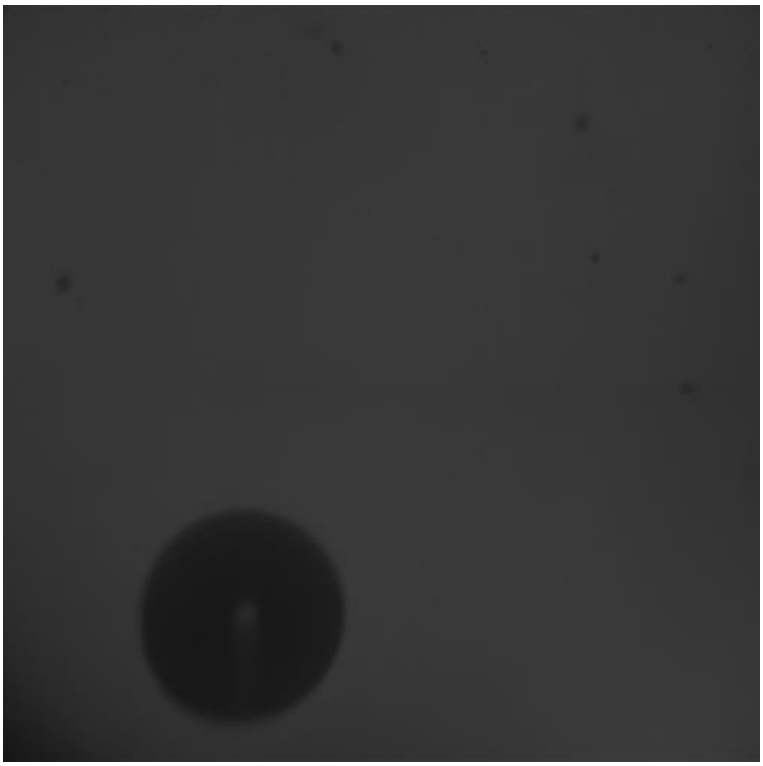

Appendix. 58 Processed Image (out of focus)